The bioenergetic and redox phenotype in human critical illness

Doctor of Philosophy

University College London

Dr Helen McKenna

MBBS, MA (Cantab), MRCP

May 2020

Declaration

I, Helen McKenna, confirm that the work presented in this thesis is my own. Where information has been derived from other sources, I confirm that this has been indicated in the thesis.

The studies presented in this thesis were highly collaborative, involving different institutions across the UK. The role of each of these collaborators, along with a clear outline of the work I performed are detailed below.

Chapter 2

The TIMELORD study was supervised by Dr Daniel Martin at University College London. I led the study at the Royal Free Hospital, and undertook the screening, recruitment and consent process for all subjects. I collected all biological samples, clinical data and follow up data. I performed the statistical analysis of all data.

Chapter 4

I performed all muscle biopsies and carried out respirometry assay for all subjects. Metabolomic analysis and enzyme assays of frozen muscle was performed by Dr Katie O'Brien at University of Cambridge under supervision by Dr Andrew Murray and Dr Julian Griffin. I subsequently analysed the data generated from these assays.

Chapter 5

Collection of whole blood from the subjects was carried out by myself and several members of the Intensive Care research team at the Royal Free Hospital (Helder Filipe, Margaret

McNeill, Manuel Pinto and Christine Eastgate). I carried out analysis of plasma protein content, free thiols, total antioxidant capacity and lipid peroxidation, under supervision from Bernadette Fernandez and Professor Martin Feelisch at the University of Southampton. In order to carry out multiple assays on the first thaw of the samples, I was assisted by Adam Tod (MSc student). Simultaneous plasma nitrite/nitrate analysis was performed by Bernadette Fernandez, and isoprostanes by Laurie Lau. I subsequently analysed the data generated from all assays.

Chapter 6

I performed microcirculatory assessment of all subjects and analysed all the data generated.

Abstract

A multitude of pathologies may progress to a state called ‘critical illness’, the hallmark of which is multiple organ failure. Supportive therapy is based on the hypothesis that organ failure results from bioenergetic collapse but attempts to restore energetic capacity through augmentation of systemic oxygen transport have failed to improve survival. The potential relevance of cellular adaptation for survival in critical illness has not been considered. This thesis explored the hypothesis that survival from critical illness could be related to dynamic changes in cellular bioenergetic and redox phenotype. Instead of bioenergetic collapse, skeletal muscle from critically ill patients demonstrated a profile of modifications consistent with cellular hypoxic adaptation, including: greater coupling efficiency of oxidative phosphorylation; selective reduction in respiratory capacity supported by complex I and fatty acid oxidation (FAO), accompanied by a switch from the tricarboxylic acid cycle towards glycolysis, and downstream impairment in FAO and accumulation of medium and long chain carnitines, in comparison to reference patients. The overall redox status in skeletal muscle was more reduced in in critically ill patients than reference patients, suggesting an enhanced reductive drive. Survivors and non survivors exhibited distinct phenotypes, the nature of which were time-specific. Within 48 hours of developing organ failure, survivors had lower skeletal muscle complex I capacity and lower plasma antioxidant capacity, but 7 days later these differences had resolved, and survivors now demonstrated lower plasma lipid peroxidation than non survivors. Specific bioenergetic modifications in skeletal muscle and plasma redox status in critical illness were related to aspects of microcirculatory function but not systemic indices of oxygenation. Dynamic adaptation in microscopic biological functions, such as bioenergetics, metabolism and redox, may underpin human resilience to life-threatening stress. This work calls for further investigation into cell-based strategies of human life-support.

Impact Statement

The findings in this thesis provide new insights into pathways relevant to human survival during life-threatening illness. These findings may thus contribute to the development of alternative therapeutic approaches to improve clinical outcomes in the sickest patients. This work has the potential to benefit more than 175 000 adults admitted to intensive care units in the UK every year (1). Improving outcomes in this cohort is a priority, as average acute hospital mortality in these patients is greater than 20%, while survivors have a 20% risk of mortality in the first year following discharge and a high incidence of long-term morbidity. Improving the effectiveness of supportive therapy has the potential to extend life, improve quality of life and reduce healthcare costs. Supportive therapy in for multiple organ failure is one of the most expensive aspects of hospital treatment (estimated to cost up to £2000 per day depending on the number of organs involved) (2). The problem is only likely to become more important with time, as demand for intensive care therapy in the UK is projected to continue to increase at a rate of 5% per year (3).

The work in this thesis supports a shift away from the current clinical focus of targeting systemic physiological variables in critical illness, manipulation of which has not been shown to improve survival. The specific features identified in skeletal muscle during critical illness and their similarities to features of hypoxic adaptation suggest a new avenue to explore in the development of supportive therapy in critical illness. Building on these findings to produce clinical benefit for patients will require collaboration between scientists with expertise in identifying the mechanisms underlying cell signalling and hypoxic adaptation as well as intensive care clinicians with expertise in the complex pathophysiological state of human critical illness, and provision of supportive care in this context.

The new insights generated by this thesis emerged as a result of applying an integrated approach to exploring complex processes, through simultaneous assessment of cellular bioenergetics, redox status and microcirculatory function, using complementary techniques, in different compartments at multiple timepoints. Future application of this integrated approach may allow the development of new biomarkers in critical illness, which may be more biologically meaningful than single biomarkers in isolation.

Acknowledgements

This thesis was completed with the support of many remarkable people, whom I am incredibly fortunate to now count as my mentors and friends. Dr Andrew Murray patiently guided me through the labyrinthine world of metabolism and mitochondria and never failed to provide constructive advice. Professor Martin Feelisch provided unparalleled insight into redox biology and it was a privilege to experience his eloquence and passion for the subject. I am grateful to the incomparably bright, efficient and generous Katie O'Brien, who offered her assistance with metabolomic analysis. Bernie Fernandez gave up months of her time to teach and support me through redox analysis, in which I was also kindly assisted by Adam Tod and Magdalena Minnion. Professor Monty Mythen provided wisdom and support at all stages of this process. I could not have carried out this work without financial support from the London Clinic, for whom I worked as a clinical fellow on the intensive care unit throughout my PhD. The intensivist consultants, Dr John Goldstone, Dr Geoff Bellingan and Dr Sara Polhill, supported me with boundless kindness and warmth, as did their entire team of wonderful nurses. Olwen Horsfield and Philip Bradbury provided a home for me for several months, so that I could carry out experiments at Southampton University, and looked after me like family during this time. My own family encouraged my aspirations and listened with patience to my frustrations during this very long journey. The study itself took place at the intensive care unit at the Royal Free Hospital, and my gratitude goes to the entire team of intensive care doctors and nurses, who supported my presence there, at all times of day and night. Most of all, I am forever indebted to the patients themselves, and their loved ones, who agreed to contribute to this study. I was humbled by their desire to help others, even in the face of unimaginably difficult circumstances. This thesis is dedicated to Professor Daniel Martin, who first offered me this opportunity to become a scientist and changed my life forever.

Funding

This study was funded by the Intensive Care Society (through a New Investigator Award) and the Royal Free Charity. I received personal support from The London Clinic Charity.

Table of contents

Table of figures

List of tables

Abbreviations

ADP	Adenosine diphosphate
AMPK	5'AMP-activated protein kinase
APACHE II	Acute Physiology and Chronic Health Evaluation II
ATP	Adenosine triphosphate
AUC	Area under the curve
BMI	Body mass index
CREB	cAMP response element-binding protein
CaO_2	Arterial oxygen content
CO	Cardiac output
cO_2	Oxygen concentration
DAMPs	Damage-associated molecular patterns
DO_2	Systemic oxygen delivery
ETF	Electron transferring flavoprotein
ETS	Electron transport system
FAD; $FADH_2$	Flavin adenine dinucleotide (oxidised and reduced forms)
FAO	Fatty acid oxidation
F_IO_2	Fractional concentration of inspired oxygen
FRAP	Ferric reducing ability of plasma
GDP	Guanosine diphosphate
GLUT1/4	Glucose transporter 1/4
GTP	Guanosine triphosphate
Hb	Haemoglobin
HIF	Hypoxia-inducible factor
HPLC	High performance liquid chromatography

ICU	Intensive Care Unit
Keap1	Kelch-like ECH-associated protein 1
MAP	Mean arterial pressure
MODS	Multiple organ dysfunction syndrome
NAD+; NADH	Nicotinamide adenine dinucleotide (oxidised and reduced forms)
NFE2L2	Nuclear factor erythroid 2 like 2
NF_KB	Nuclear factor kappa-light-chain-enhancer of activated B cells
NIRS	Near infrared spectroscopy
NLR	Nod-like receptor
NO	Nitric oxide
NO_2^-	Nitrate
NO_3^-	Nitrite
O_2	Oxygen
OXPHOS	Oxidative phosphorylation
PAMPs	Pathogen-associated molecular patterns
PaO_2	Arterial partial pressure of oxygen
Pi	Inorganic phosphate
PO_2	Partial pressure of oxygen
PPARA	Peroxisome-proliferator activated receptor alpha
POSSUM	Physiological and Operative Severity Score for the enumeration of Mortality
RCT	Randomised controlled trial
RIG-1	Retinoic acid-inducible gene 1
RNNO	N-nitrosamines
ROC	Receiver operating characteristic

ROS	Reactive oxygen species
RSNO	S-nitrosothiols
RXNO	Total nitroso species (sum of RSNO and RNNO)
SIRS	Systemic inflammatory response syndrome
SIRT1	Sirtuin 1
SpO_2	Peripheral arterial oxygen saturation
SOFA	Sequential Organ Failure Assessment
TCA	Tricarboxylic acid
TBARS	Thiobarbituric acid reactive substances
TLR	Toll-like receptor
VOT	Vascular occlusion test

Chapter 1. Introduction and literature review

'It is not the strongest or the most intelligent that survives. It is the most adaptable to change'. Charles Darwin

1.1. Human survival during extreme physiological stress

1.1.1. Homeostasis, biological stressors and stress

Biological systems within organisms strive to maintain homeostasis, a steady state which represents the ideal conditions for processes essential for function and survival (4). Maintaining conditions at the optimal set point depends upon continuous flux and compensation by biological systems, as the organism is exposed to a changing internal and external environment (5). Stimuli which result in a deviation away from the homeostatic set point are described as 'stressors'. The compensatory response of the organism, as it attempts to restore conditions to the homeostatic set point, is referred to as 'stress'. Physiologist and medical doctor, Hans Selye, was the first to describe the phenomenon of different illnesses, affecting distinct organ systems, eventually manifesting as similar pattern of signs and symptoms. He proposed that this common phenotype, which he referred to as the "*syndrome of just being sick*", was the manifestation of "the non-specific response of the body to any demand placed upon it." (6). Stress has subsequently been redefined as a condition in which "the demand on a system exceeds the natural regulatory capacity of the organism." (7). When a stressor generates a magnitude of physiological stress that exceeds the capacity of the individual to compensate, the risk of rapid deterioration and death increases. Diverse insults, from severe infection, haemorrhage, inflammation, cardiac arrest, burns or trauma (including surgery) can trigger perturbations in human homeostasis that progress to a common pathway

of multiple organ dysfunction and death (8). There is no universal definition of this syndrome in the literature, but in the clinical setting it is generally referred to as 'critical illness'. Empirically, a continuum exists, from the initial homeostatic perturbation triggered by tissue injury or other pathology; the subsequent compensatory responses to it; and progression to widespread cell dysfunction and death.

1.1.2. Critical illness and multiple organ failure

Critical illness, regardless of the primary aetiology, may progress to multiple organ failure, which is characterised by progressive and potentially reversible dysfunction in two or more organ systems (9). Acute risk of mortality increases as degree of organ failure (severity of dysfunction and number of organs affected) increases (10, 11). At the whole-body level, the initial stress response in critical illness is thought to be triggered by a systemic response to danger signals, emitted in response to tissue injury or inflammation (12), which triggers a wide-ranging array of downstream effects on cardiovascular, neuroendocrine, immune and coagulation systems, to produce the so-called systemic inflammatory response syndrome (SIRS)(8, 13). These signals are detected by pattern-recognition receptors, which may be cell surface receptors or within the cytoplasm. Cell surface receptors, such as toll-like receptors (TLR), which detect bacterial components such as lipopolysaccharide (pathogen-associated molecular patterns, PAMPs) or the extracellular presence of intracellular components released by cell injury, such as ATP or mitochondrial DNA (damage-associated molecular patterns, DAMPs). Within the cytoplasm, Nod-like receptors (NLRs) and RIG-1-like receptors (RLRs). Activation of these pattern-recognition receptors results in the activation of a complex molecular transduction network. The response includes translocation of the transcription factor, nuclear factor kappa-light-chain-enhancer of activated B cells (NF_KB), which regulates the transcription of genes responsible for the both the innate and adaptive

immune responses, including chemokines, interleukins and interferons. These cytokines act at cell surface receptors, and modify RNA and protein synthesis. A subset of cytosolic pattern recognition receptors that recognise PAMPs and DAMPs activates the assembly of a multiprotein complex called “the inflammasome”, which activates a pyroptotic inflammatory cascade, resulting in the secretion of pro-inflammatory cytokines (interleukins 1β and 18) and activation of programmed necrotic cell death. Collectively, downstream effects of inflammasome activation include: immune cell activation and recruitment, destruction of stressed cells; increased endothelial permeability, and activation of platelets and coagulation pathways (14). Necrotic cell death releases intracellular content, contributing to a vicious cycle of DAMP-induced inflammation.

Diagnosis of this whole-body inflammatory state (SIRS) was originally made on the basis of the following criteria: body temperature < 36 ºC or > 38 ºC; heart rate > 90 beats per minute; respiratory rate > 20 breaths per minute; white cell count < 4 or > 12 x 10^9/L. Greater than 90% of critically ill patients meet the original criteria for SIRS (15). When these systemic features occur in the context of diagnosed or suspected infection, they are taken to represent “sepsis”, defined as life-threatening organ dysfunction caused by a dysregulated host response to infection (16), and the precise clinical criteria defining this syndrome continue to be refined. There is significant overlap between the systemic physiological derangement and organ dysfunction seen in sepsis, and the systemic inflammatory response to a variety of severe clinical insults. It is not certain how the observable changes in systemic physiology reflect molecular alterations within individual cells to generate the phenotype of multiple organ failure,

1.1.3. The bioenergetic theory of multiple organ failure

The prevailing theory states that the development of multiple organ dysfunction and death result from progressive cellular bioenergetic failure (17, 18). This is a plausible explanation, as ultimately cell function and integrity rely on the adequate production of energy. Within mammalian cells, the free energy required to drive thermodynamically unfavourable reactions is almost exclusively provided by the hydrolysis of adenosine triphosphate (ATP) to adenosine diphosphate (ADP) and phosphate (P_i) (Equation 1). The ratio of ATP to ADP ([ATP]/[ADP]) within the cell is maintained at much higher levels than it would at equilibrium, such that the forward reaction is favoured. In order to maintain this ratio, and the ability of the cell to "do work" (energetics), ATP must be continuously regenerated by the cell. An average adult human uses approximately 40 kg ATP in 24 hours (19). This is achieved through the process of energy metabolism, via the complex network of interconnected pathways summarised in section 1.2. Cellular bioenergetic capacity cannot be measured directly in critically ill patients, and evidence for the putative bioenergetic impairment comes from small observational clinical studies and animal models. An observational study of 28 septic patients with multiple organ failure demonstrated lower skeletal muscle ATP concentrations in the patients who died compared to those who survived (20). A study of 16 patients with multiple organ failure recently admitted to ICU and 10 healthy age-matched patients reproduced this finding of lower ATP concentrations in non-survivors compared to survivors (21). Some animal models of sepsis have shown decreases in ATP concentration after 12 hours (22), but these findings have not been consistent (23). The problem with using skeletal muscle ATP concentrations as a surrogate marker of bioenergetic capacity is that its concentration reflects turnover; both production and consumption. Intracellular ATP production is also highly regulated to maintain ATP at a constant set-point, despite fluctuations in workload. For example, rate of ATP flux

(consumption and supply) increases up to 10-fold in myocardium during exercise, but that actual ATP concentration remains constant (24).

Equation 1. ATP synthesis and breakdown

$$ATP \rightleftharpoons ADP + P_i$$

1.2. Factors influencing bioenergetic capacity

There are two means by which ATP can be synthesised within the cell: via glycolysis in the cytoplasm; or via oxidative phosphorylation within specialised organelles called mitochondria. In contrast to glycolysis, oxidative phosphorylation is an oxygen-dependent process, and it yields 20-times the amount of ATP per glucose molecule (25). Bioenergetic capacity is the end-product of a network of many complex and interacting pathways, such as the mitochondrial electron transport and oxidative phosphorylation machinery and the donation of electrons from the catabolism of macromolecules (carbohydrate, protein, fat) via multiple interweaving metabolic pathways. The output of these pathways will depend on the supply of nutritional substrate and the co-ordination of multiple catalysed steps, which depend upon the activity of receptors, transporters and enzymes, some of which have the potential for reversal when the concentration of their products exceeds that of their substrates. The complexity of these processes, and the enzymes and substrates on which they depend are discussed in turn. Figure 1 summarises how these pathways interact.

Figure 1. Schematic representation of energy metabolism

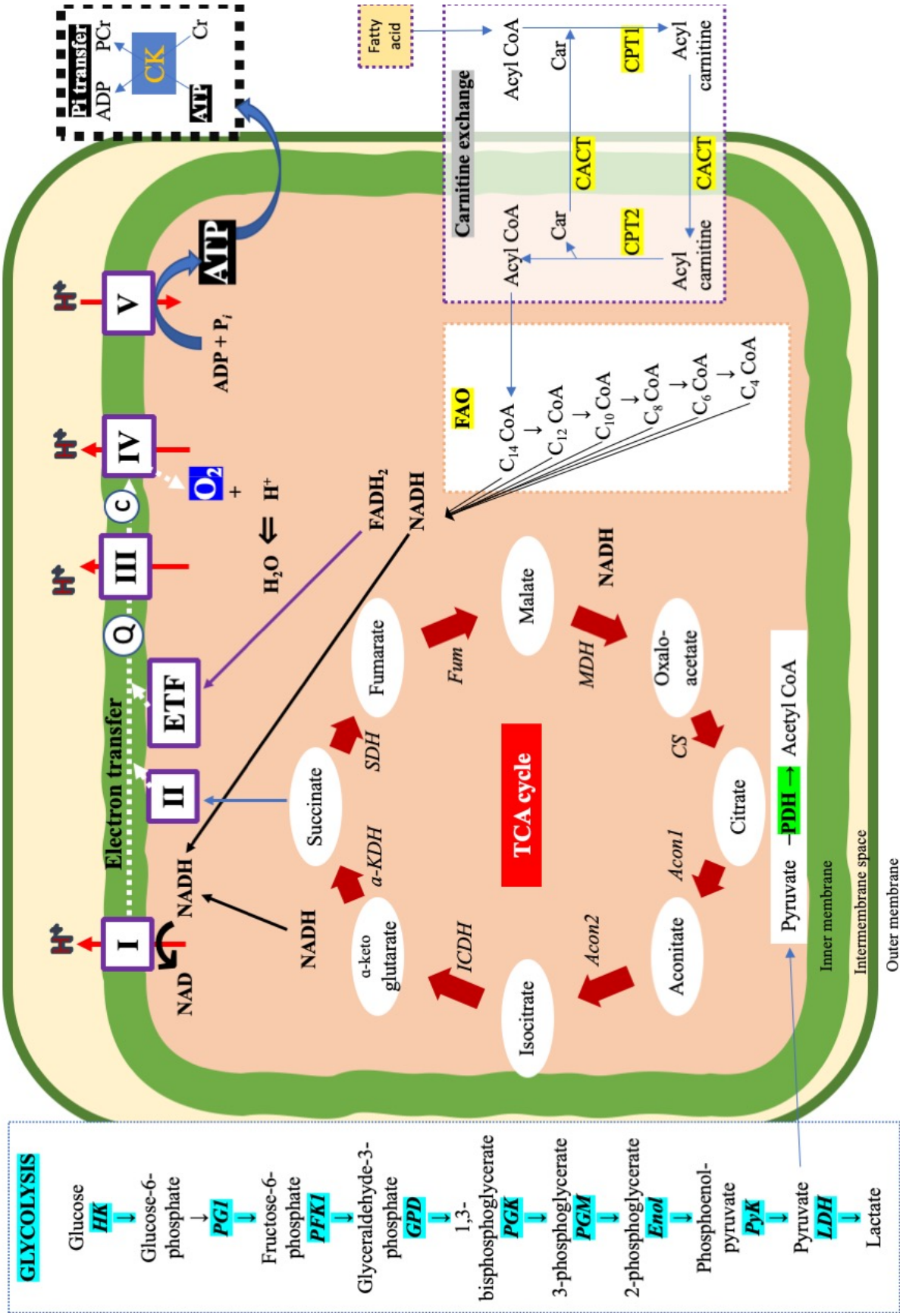

HK: hexokinase; PGI: phosphoglucose isomerase; PFK1: phosphofructokinase-1; GPD: glyceraldehyde 3-phosphate dehydrogenase; PGK: phosphoglycerate kinase; PGM: phosphoglycerate mutase; Enol: enolase; PyK: pyruvate kinase; LDH: lacate dehydrogenase; PDH: pyruvate dehydrogenase; CS: citrate synthase; Acon1: aconitase-1; Acon2: aconitase-2; ICDH: isocitrate dehydrogenase; KDH: ketoglutarate dehydrogenase; Fum: fumarase; MDH: malate dehydrogenase; CPT1: carnitine palmitoyl transferase-1; CACT: carnitine acetylcarnitine translocase; CPT2: carnitine palmitoyl transferase-2; Car: free carnitine; NADH: reduced nicotinamide adenine dinucleotide; FADH2: reduced flavin adenine dinucleotide; I: NADH: ubiquinone reductase; II: succinate-Q-reductase; ETF: electron transferring flavoprotein; Q: coenzyme Q_{10}; III: coenzyme Q:cytochrome *c* reductase; c: cytochrome *c*; IV: cytochrome *c* oxidase; V: ATP synthase; Cr: creatine; PCr: phosphocreatine.

1.2.1. Glycolysis

Glycolysis refers to the breakdown of a 6-carbon (C) sugar molecule, glucose, to generate two pyruvate (3C) molecules, along with NADH and a net yield of 2 ATP molecules. For glycolysis to continue, NAD^+ must be regenerated from NADH (26, 27). Regeneration of NAD^+ depends on the catabolism of the end-product, pyruvate, to lactate (via fermentation), or via the tricarboxylic acid (TCA) cycle. Glycolysis and lactate fermentation can proceed, in the absence of oxygen, within the cytoplasm. Lactate can either be converted back to pyruvate or transported out of the cell and transferred to the liver, where it is converted back to glucose via gluconeogenesis (Cori cycle). Pyruvate can also be transported into the mitochondrial matrix, as a fuel for oxidative metabolism.

1.2.2. Chemiosmosis

Mitochondria transduce energy via chemiosmosis, the process by which electron transfer maintains an electrochemical gradient across the inner mitochondrial membrane, which in turn drives the phosphorylation of ADP to ATP (28). Mitochondria are intracellular organelles, with an outer membrane and a highly folded inner membrane (to form cristae), surrounding a matrix. Within the inner membrane exists a series of protein complexes, along which electrons are transferred, from high to low redox potential. The energy transduced by these redox reactions is used by the complexes to pump protons from the matrix to the intermembrane space. This produces an electrochemical gradient, $\Delta\mu H^+$, across the mitochondrial inner membrane. An ATP synthase enzyme spans the mitochondrial inner membrane. This complex is permeable to protons, and diffusion of protons through a central pore, along their concentration gradient, rotates a molecular motor, which drives the phosphorylation of ADP to ATP. ATP synthesis via chemiosmosis thus depends on (1) the electron transfer system, which couples electron flow to the generation of an electrochemical

gradient, (2) the continuous supply of electrons (from substrates such as carbohydrate and fat) via metabolic pathways which extract electrons from them and donate them to the electron transfer system, and (3) a continuous supply of oxygen to act as a final electron acceptor. A deficit in any one of these components may have an impact on the ability of the system to produce ATP.

1.2.3. The electron transfer system

Th electron transfer system consists of a series of enzyme complexes (I – IV) within the inner mitochondrial membrane, and two soluble transporters (ubiquinone and cytochrome c) within the intermembrane space. There are three entry points for electron transfer into the inner mitochondrial membrane electron transport system. Complex I (NADH: ubiquinone oxidoreductase) accepts electrons from the reduced equivalent of the nicotinamide adenine dinucleotide carrier, NADH. Complex II (succinate: ubiquinone oxidoreductase) accepts electrons from the reduced equivalent of the flavin adenine dinucleotide carrier, $FADH_2$. Electrons released during fatty acid oxidation (FAO) are transferred from $FADH_2$ to another respiratory complex, called the electron transferring flavoprotein (ETF). Ubiquinone (or Coenzyme Q) accepts electrons from all three of these entry points and donates them to cytochrome c via complex III (ubiquinol: ferricytochrome c oxidoreductase). Complex IV (cytochrome c oxidase) transfers electrons from cytochrome c to the terminal electron receptor, molecular O_2, to form water. Electron transfer at complexes I, II and IV is coupled to the transfer of protons into the intermembrane space, which generates the electrochemical gradient used to drive ATP production by the ATP synthase (complex V).

1.2.4. Proton leak and uncoupling

During oxidative phosphorylation, not all of the pumped protons flow through the ATPase to drive ATP production; some "leak" back across the inner membrane. Oxygen consumption that is not coupled to ATP production is referred to as "leak respiration", and increases approximately exponentially with the proton gradient, $\Delta\mu H^+$, across the mitochondrial inner membrane (29). Total proton leak is thought to result from both unregulated basal leak (unregulated) and inducible leak, which is under the control of specific proteins in the mitochondrial inner membrane (30). The molecular basis of basal proton leak is not understood (31), but inducible leak is thought to require activation of carriers, including the adenine nucleotide transporter (ANT) and uncoupling proteins (UCPs). The extent to which substrate oxidation is coupled to ATP production (coupling efficiency), will depend on the permeability of mitochondrial inner membrane to protons, which can be modulated by the expression and activation of UCPs (32). For example, minimising proton leak has been shown to preserve ATP production in mammalian liver cells in which substrate oxidative capacity was reduced by low temperatures (33). In contrast, increased uncoupling is a mechanism for thermogenesis, and is thought to be involved in the regulation of redox state (discussed in 1.5.2) (30). Administration of uncoupling agents (protonophores), increase the rate of respiration, reduce the mitochondrial membrane potential and decrease the production of reactive oxygen species (ROS) in isolated mitochondria (34). Mitochondrial uncoupling also generates heat, in a manner that has been shown to be under regulation by cellular, peripheral and central (thyroid hormones and catecholamines) pathways (35). Fever is a ubiquitous feature of systemic inflammation and its relevance for survival remains under investigation.

1.2.5. Intermediary metabolism

Chemiosmosis depends on the transfer of electrons and protons to the ultimate electron acceptor, molecular oxygen (O_2). The oxygen is provided by the oxygen delivery system, via a combination of convective and diffusive transport (outlined later in section 1.2.11). The electrons and protons are derived from the catabolism of organic macromolecules, carbohydrate, fat and protein. Thus, chemiosmosis depends on availability of these nutritional substrates and the metabolic pathways involved in their degradation. These include the tricarboxylic acid cycle and fatty acid oxidation, both of which occur in the mitochondrial matrix.

1.2.6. The tricarboxylic acid cycle

The tricarboxylic acid (TCA) cycle describes a series of reactions used by all aerobic organisms to release protons and electrons from organic macromolecules (carbohydrates, fats and proteins), to drive ATP synthesis by chemiosmosis. The starting point of the TCA cycle is the 2C molecule, acetyl CoA, which can be provided through the catabolism of carbohydrate, fat or protein. For example, the end-product of glycolysis, pyruvate, can be transported to the mitochondrial matrix, where it is converted to acetyl CoA (2C) by pyruvate dehydrogenase. Acetyl CoA may also be generated from the β-oxidation of fatty acids (fatty acid oxidation, FAO). In the TCA cycle, a series of reactions, catalysed by eight enzymes, results in the complete oxidation of the acetyl group of acetyl CoA to form two molecules of carbon dioxide and two molecules of water. The first step of the TCA cycle is the condensation reaction of acetyl CoA (2C) with the 4C compound, oxaloacetate, to form citrate (6C). Via a series of dehydrogenation and decarboxylation reactions, oxaloacetate is regenerated from citrate, so that the cycle may continue on donation of a fresh acetyl CoA molecule. The reactions also release protons and electrons from the intermediates, which are

accepted by carriers, nicotinamide adenine dinucleotide (NAD^+) and flavin adenine dinucleotide (FAD) to produce the reduced versions, NADH and $FADH_2$. The net yield of the cycle is three reduced equivalents of NADH and one $FADH_2$, which are subsequently used to drive electron transfer in mitochondrial chemiosmosis. For every NADH and $FADH_2$ produced by the TCA cycle, 2.5 and 1.5 ATP molecules are generated in oxidative phosphorylation respectively. The TCA cycle also results in the phosphorylation of guanosine diphosphate (GDP) to guanosine triphosphate (GTP). Many intermediates of the TCA cycle are also used as precursors for the biosynthesis of other molecules, such as proteins, DNA, fatty acids and haem. Intermediates drawn off for biosynthesis must be replenished to allow the TCA cycle to continue. Because it is a cycle, it can be replenished by the generation of any of the intermediates (anaplerosis). For example, if oxaloacetate is converted to amino acids for protein synthesis, the flux through the TCA cycle will decrease, as acetyl CoA must condense with oxaloacetate to enter the cycle, and acetyl CoA levels will rise. In response, carboxylation of pyruvate to replenish oxaloacetate and the TCA will occur.

1.2.7. Fatty acid oxidation

Electrons for chemiosmosis are also derived from fat catabolism. Fatty acids, in the form of acyl CoA esters, undergo β-oxidation in the mitochondrial matrix. Transfer into the matrix involves a carnitine shuttle. Acyl CoA must first be converted to acyl carnitine by carnitine transferase-1. Carnitines can then enter the mitochondrial matrix via the carnitine: acylcarnitine translocase. Within the matrix, acyl carnitine is then converted back to acyl CoA via carnitine palmitoyl transferase-2. FAO involves the successive removal of acetyl groups from the acyl coA, until only two acetyl CoA molecules remain. Each step of this iterative process releases one acetyl CoA for the TCA cycle and an acyl CoA ester that has

been shortened by two carbon atoms. The process also liberates two electrons. One electron is passed to NADH, which donates electrons to complex I, and the other electron to $FADH_2$, which donates electrons to the electron transferring flavoprotein (ETF). FAO consists of four enzymatic reactions (dehydrogenation, hydrations and thiolysis), which are performed by enzymes that are specific to the length of the fatty acid chain (short, C4, medium C 6 – C12 and long chain C14 – C18) acyl CoA dehydrogenases. FAO is a critical source of energy in a variety of cell types, including the heart, where it provides 60 – 70% of the ATP required for contraction. During periods of high energy demand, such as fasting or endurance exercise, fat stores are broken down for metabolism.

1.2.8. Amino acid oxidation

The majority of electrons for ATP production are derived from carbohydrate and fat, but oxidation of amino acids (derived from protein) can also contribute significantly to the generation of energy. This pathway is particularly important during starvation and insulin insufficiency or insensitivity. Amino acids undergo oxidative deamination to α–keto acids and ammonium compounds (NH_4^+), in the mitochondrial matrix (example in Equation 2). The α–keto acid may enter the TCA cycle (Figure 2), and the ammonium compound is ultimately either excreted as urea or used in the synthesis of amino acids, nucleotides and other amines. Degradation of the carbon skeletons of the 20 common amino acids yields one of 7 intermediates: pyruvate, oxaloacetate, α–ketoglutarate, succinyl CoA and fumarate can all serve as precursors for glucose synthesis (glucogenic), whilst acetyl CoA and acetoacetate serve as precursors for fatty acid or ketone synthesis (ketogenic). Amino acids can also undergo transamination, in which the amino group is transferred to α–ketoglutarate to form glutamate, which can then enter biosynthetic pathways or be converted to ammonia. Transamination occurs in the cytosol and is catalysed by aminotransferase enzymes

(Equation 3). Ammonia is highly toxic and is converted to glutamine, catalysed by glutamine synthetase (Equation 4). In the liver, glutamine is converted back to glutamate by glutaminase, and urea is a byproduct of this process.

Equation 2. Oxidative deamination of glutamate

$$glutamate \rightarrow \alpha\ ketoglurate + NH_4$$

Equation 3. Transamination reaction

$$\alpha\ ketoacid_2 + amino\ acid_1 \leftrightarrow \alpha\ ketoacid_1 + amino\ acid_2$$

For example: α–ketoglutarate + alanine produces pyruvate and glutamate.

Equation 4. Conversion of ammonia to glutamine

$$glutamate + NH_4 \rightarrow glutamine$$

Figure 2. Amino acids which replenish the TCA cycle

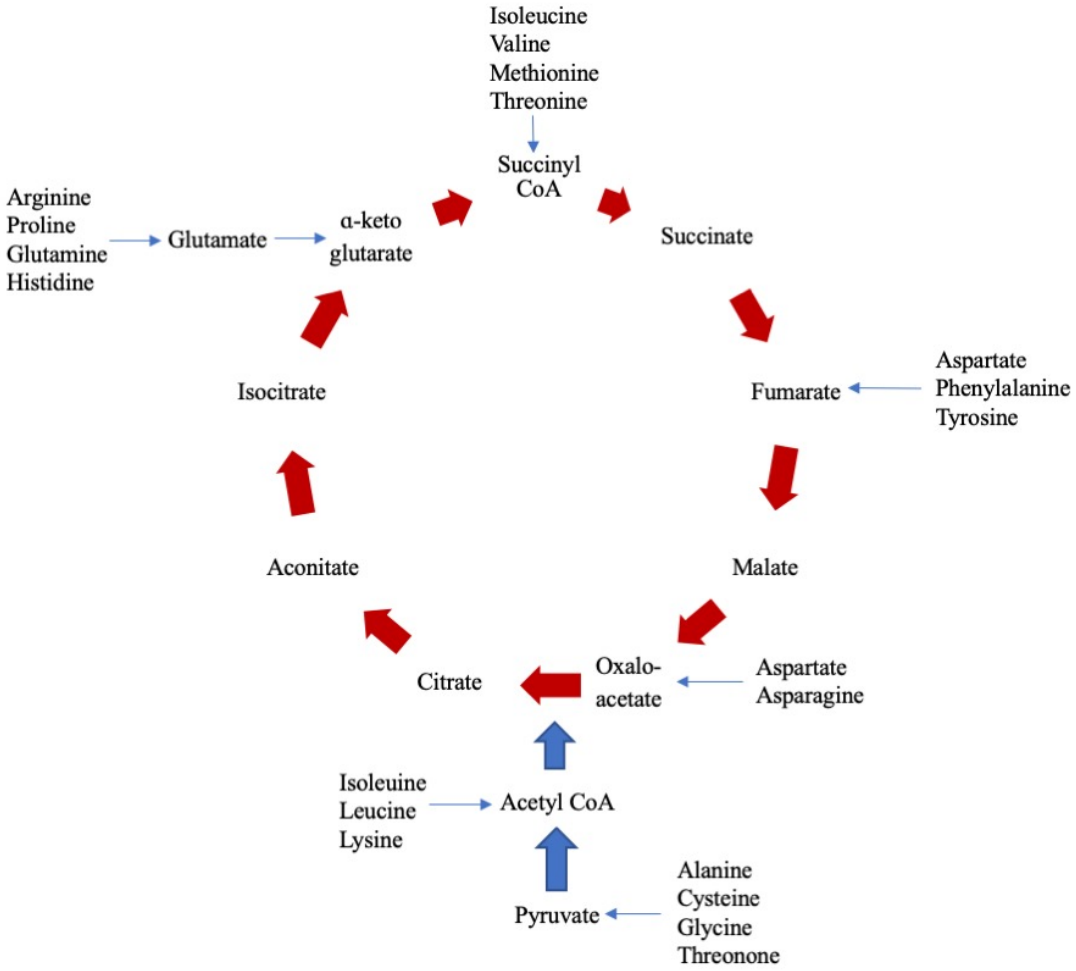

1.2.9. ATP transport

ATP is transported out of the mitochondrion in exchange for ADP by the adenine nucleotide transporter (ANT). In the matrix and cytoplasm, the high energy phosphate group is transferred from ATP to creatinine, to produce phosphocreatine (PCr), which serves as an energy reserve molecule in some tissues, such as muscle.

1.2.10. The relationship between bioenergetic capacity and substrate utilisation

Different substrates (carbohydrates, fats, and proteins) have different effects on electron transfer, ATP yield, oxygen consumption and carbon dioxide production. Glycolysis results in the net production of two molecules of ATP, per molecule of glucose (6C). For every NADH and $FADH_2$ produced by the TCA cycle, 2.5 and 1.5 ATP molecules are generated in oxidative phosphorylation respectively (the theoretical maxima are 3 and 2 respectively, but this is not achieved). Per molecule of acetyl CoA, the TCA cycle produces: 2 NADH and 1 $FADH_2$ (as well as 1 ATP), and therefore a net yield of 10 ATP. So, for one molecule of glucose (6C), 2 ATP are produced by anaerobic glycolysis, and 2 NADH are produced with the conversion of 2 pyruvate to acetyl CoA, from which are derived 2 molecules of acetyl CoA, which produce 20 ATP via the TCA cycle. Each β-oxidation cycle produces 1 NADH, 1 FADH2 and 1 acetyl CoA (approximately 14 ATP). An even-numbered saturated fat (C_{2n}) may undergo $n-1$ oxidations, with the final step yielding an additional acetyl CoA. Two ATP are lost during the activation of the fatty acid, so the net yield of ATP is described by Equation 5. Thus, for the equivalent number of carbons as glucose (6C), which produces 22 ATP through glycolysis and the TCA cycle; FAO of a 6C fatty acid produces 36 ATP. FAO of unsaturated fatty acids changes the ATP yield due to the requirement of two additional enzymes. The transfer of NADH generated from glycolysis into the matrix requires ATP. In the liver, this occurs via a malate-aspartate shuttle (the electrons are actually transferred to

intermediates that are transported into mitochondria and NADH is regenerated). In skeletal muscle, this occurs via the glycerol-3-phosphate shuttle, which regenerates only $FADH_2$ in the mitochondria from the NADH produced in the cytosol, such that overall, less ATP is produced from chemiosmosis.

Equation 5. Net yield of ATP from FAO of an even-numbered fatty acid

$$Net\ yield\ of\ ATP = 14\,n - 6$$

n: number of carbon atoms

1.2.11. Oxygen availability

Almost 98% of human energy requirements are provided through the process of oxidative phosphorylation in mitochondria (17) which relies on a continuous supply of oxygen. The rate of respiration in cells within a given medium remains constant until the partial pressure of oxygen (PO_2) falls to a critically low level (0.7-0.9 kPa), representing the point at which oxygen availability limits mitochondrial electron transport (36). At this point, further decreases in PO_2 cause greater decreases in oxygen consumption. When this experiment is repeated with isolated mitochondria, the rate of oxygen consumption becomes oxygen dependent at 0.4 – 0.7 kPa. Of all the factors influencing bioenergetic capacity outlined in this section, oxygen availability has been the focus of intervention on the ICU. It is thought that cellular oxygen limitation is a common feature of critical illness, resulting in bioenergetic impairment, organ dysfunction and death. It is not possible to measure cellular oxygenation directly in the clinical setting (37). Elevated plasma lactate levels have been taken to represent increased glycolysis due to failure of oxygen-dependent mitochondrial oxidative phosphorylation (38), but such concentrations also depend on the rate of hepatic lactate metabolism (39).

1.3. Oxygen delivery in critical illness

1.3.1. Systemic oxygen delivery in critical illness

Both the triggering pathology and the body's response to critical illness can compromise the delivery of oxygen to the cells. In humans, a combination of convective and diffusive transport delivers oxygen from the atmosphere to the mitochondria. The movement of oxygen across a series of physiological barriers, referred to as the oxygen cascade, is summarised in Table 1. The driving force for the diffusion of oxygen is the gradient of oxygen partial pressure (PO_2), which is maintained by the continuous consumption of oxygen by the mitochondria (the "oxygen sink"). Oxygen is transferred from the atmosphere to the lungs, via the active process of ventilation. In the lungs, oxygen diffuses along its concentration gradient, across the alveolar membrane and pulmonary capillary endothelium, into the blood, where it binds to haemoglobin within erythrocytes, and a small proportion dissolves in the plasma. Arterial blood oxygen content (CaO_2) is determined by Equation 6. Oxygenated blood is transported to cells along a successive branching network of blood vessels. The contractile function of the heart actively drives the convective transport of oxygen, contained within large arteries, to different organs. This mass flow of oxygenated blood from the heart to the aorta is referred to as the "macrocirculation". The volume of oxygen leaving the left ventricle of the heart every minute (referred to as systemic oxygen delivery, DO_2) is calculated according to Equation 7.

Common triggers of critical illness can disrupt oxygen flux at different steps in the cascade, sequentially reducing the availability of oxygen to the mitochondria. For example, direct damage to lung parenchyma, from pneumonia, inflammatory diseases or trauma; or pulmonary oedema from cardiac failure or fluid overload, impairs gas exchange between the

alveoli and the pulmonary capillaries. Haemoglobin concentration is decreased by haemorrhage, haemolysis and other causes of anaemia. Cardiac contractility may be reduced by arrhythmia, coronary ischaemia or infarction, valvular dysfunction or myocarditis. Hypovolaemia, from dehydration or acute haemorrhage, will also reduce cardiac output through diminished left ventricular preload. In addition to these primary insults, systemic oxygen delivery may be impaired by the systemic inflammatory response itself. Exposure to systemic inflammatory mediators can trigger pulmonary inflammation (adult respiratory distress syndrome) (40) and inhibit intrinsic myocardial activity (41). The systemic inflammatory response is also responsible for uncontrolled vasodilatation (vasoplegia) and increased capillary permeability, which contributes to reduced cardiac output through reduced preload (42).

Table 1. The oxygen cascade

The O_2 cascade	**PO_2 (kPa)**
Dry atmospheric air (at sea level)	21
Humidified air within the trachea	20
Alveolar gas	14
Arterial blood	13.3
Capillary blood	6-7
Mitochondria	< 1

Equation 6. Arterial oxygen content

$$CaO_2 = (PaO_2\ x\ s) + ([Hb]\ x\ SO_2\ x\ H)$$

CaO_2: arterial oxygen content (ml/l); PaO_2: arterial partial pressure of oxygen (kPa); S: the solubility coefficient for oxygen in blood, [Hb], the concentration of haemoglobin; SaO_2: arterial oxygen saturation of haemoglobin; H: the oxygen-binding capacity of haemoglobin, or Huffner's constant; which is 1.34 - 1.39 ml/g).

Equation 7. Systemic oxygen delivery, DO_2.

$$DO_2 = CO\ x\ CaO_2$$

DO_2: systemic O2 delivery (ml/min); CO: cardiac output (L/min); CaO_2: arterial oxygen content (ml/L).

1.3.2. Local oxygen delivery by the microcirculation in critical illness

Beyond the aorta, blood is selectively directed via arteries to tissues according to their relative oxygen requirement. Arteries branch up to 8 times on entering an organ, to become arterioles. Each arteriole branches 2-5 times before transitioning to capillaries, which have a diameter of 10-15 μM and represent the lowest cross-sectional diameter within the circulation. Distal to these, venules transport blood away from the tissues. Together, arterioles, venules and capillaries create a network of the smallest vessels (diameter <100 μM), which directly supply tissues and are referred to collectively as "the microcirculation". The microcirculation is the site of transfer of molecules between blood and the tissues, which occurs via diffusion along concentration gradients. Oxygen diffuses from the saturated haemoglobin within erythrocytes, into the plasma of the microcirculation, and from there to the cells and ultimately to the mitochondria, which continuously consume oxygen.

The important determinants of oxygen flux within the microcirculation are capillary density and capillary blood flow. Capillary density determines the vascular surface area across which oxygen can diffuse to the tissue; and will also influence the maximum diffusion distance from the capillary to the cell. The total thickness of the capillary wall is 0.5 μM, to facilitate rapid diffusion of molecules between the plasma and the cells. Capillaries form networks within tissues; with more metabolically active tissues having denser capillary networks. The flow of blood into capillary networks is regulated by smooth muscle tone in arterioles and pre-capillary sphincters. Arteriole walls are muscular, and their diameter changes dramatically to alter the blood flow through capillaries (and create the majority of vascular resistance within the circulation). Full relaxation can double the radius of the arteriole, whilst maximal contraction can close the entrance to the downstream capillary network. However, beyond the arterioles, capillary flow is determined by physical laws of

fluid motion (Poiseuille's law and viscosity). The capillaries can be bypassed by arteriovenous shunts, which directly link an arteriole to a post-capillary venule.

The primary factor influencing local microcirculatory flow is the metabolic rate of the tissue, along with a degree of pressure autoregulation and influence from neurohumoural mediators. The processes by which this microscopic coupling between local microcirculatory flow and the metabolic demand of cells is incompletely understood. The arteriolar muscle responds to local and systemic neurohumoural signals. Catecholamines, such as adrenaline and noradrenaline, tend to cause vasoconstriction via α_1-adrenergic receptors. Decreases in local PO_2 induces vasodilation; except in the pulmonary circulation, where it results in vasoconstriction. In cardiac and skeletal muscle, they induce vasodilation via β-adrenergic receptors. It is thought that local mediators produced by the endothelium, such as the vasodilator nitric oxide (NO), are involved in the coupling of blood flow to tissue demand.

Under normal conditions, tissues are supplied by a dense network of capillaries, most of which are perfused, and flow is coupled to changes in systemic haemodynamic variables (haemodynamic coherence). In pathologies associated with critical illness, such as sepsis, trauma and cardiogenic shock, microcirculatory blood flow is altered and this coherence is disturbed (43, 44). As part of the systemic inflammatory response, vasoplegia results in a decrease in the mean arterial pressure (MAP), reducing the perfusion gradient which drives blood into the microcirculation. Blood flow to organs such as the heart and brain is preserved at the expense of blood flow to the muscle and gastrointestinal tract (45, 46). As mentioned earlier, systemic inflammation also leads to increased microvascular permeability, which can result in interstitial fluid accumulation and increases the diffusion distance for oxygen to reach the cells from the capillaries. Capillaries may become obstructed by platelets and

leucocytes, and blood flow diminished by impairment of erythrocyte deformability. For example, sepsis is associated with a decrease in capillary density, and an increase in the heterogeneity of perfusion, with non-perfused capillaries adjacent to perfused capillaries (47). The consequence of these microcirculatory alterations is increased diffusion distance from oxygen from the blood to the cell, which has shown to result in reduced tissue oxygenation and increased levels of HIF-1α and its downstream targets in a rat model of sepsis (48). Furthermore, correction of systemic haemodynamics does not translate into improved tissue perfusion (49). Under these circumstances, areas of tissue may become hypoxic despite normal systemic oxygen delivery and mean arterial pressure (50).

1.4. Cellular adaptation to variations in oxygen supply

All multicellular organisms have the capacity to sense and respond to a decline in cellular oxygen availability (51). Under hypoxic conditions, an oxygen-sensitive transcription factor (HIF), selectively promotes the expression of an array of genes to generate a phenotype with enhanced tolerance to hypoxia (52). Downstream targets of HIF include proteins responsible for increasing systemic oxygen transport via elevation of haemoglobin concentration (erythropoietin) (53) as well as proteins which promote local microcirculatory blood flow through angiogenesis (vascular endothelial growth factor) (54) and vasodilation (nitric oxide synthase) (55). However, cellular models have demonstrated a crucial part of the HIF response involves intracellular modifications, which alter the utilisation of oxygen. These include upregulation of oxygen-independent means of ATP production (glycolysis) (26); modifications to promote the efficiency of mitochondrial oxidative phosphorylation (56); and suppression of energy expenditure (57).

1.4.1. Bioenergetic adaptations to hypoxia

A key metabolic modification promoted by HIF is the upregulation of ATP production by oxygen independent pathways. HIF mediates a switch away from oxidative phosphorylation and towards glycolysis, via the upregulation of glucose transporters and glycolytic enzymes (58), in conjunction with an increase in lactate dehydrogenase and pyruvate dehydrogenase kinase 1 expression, which regenerates the NAD^+ required to permit glycolysis to continue, by shunting the end-product of glycolysis, pyruvate, away from the TCA cycle and towards lactate production (26, 57). A second important bioenergetic adaptation to hypoxia mediated by HIF is the enhancement of the efficiency of mitochondrial oxidative phosphorylation with respect to oxygen consumption. One mechanism by which it may achieve this is through substrate switching. Respiration supported by fatty acid oxidation (FAO) produces fewer ATP molecules per mole of oxygen consumed, compared with carbohydrate oxidation (59). It is estimated that the oxidation of fat, which is highly reduced, requires 11-12% more oxygen to produce the same amount of ATP as the oxidation of glucose (60). Cells can alter their metabolic fuel to optimise efficiency in response to reduced oxygen availability. One of the downstream targets of HIF is another transcription factor, peroxisome proliferator-activated receptor-alpha (PPARα), which regulates the expression of genes involved in FAO as well as inflammatory mediators (61). Via suppression of this pathway, HIF-1α mediates a substrate switch away from FAO, and thus improves the efficiency of respiration. Another means by which HIF optimizes the efficiency of respiration is by increasing the coupling efficiency of mitochondrial electron transport (and oxygen consumption) to ATP production. There is evidence that HIF promotes the coupling efficiency of oxidative phosphorylation (56); and one of the downstream targets of PPARα is an uncoupling protein (UCP3) (62) Exposure to hypoxia also reduces energy expenditure, at least in part through the active suppression of protein synthesis, which falls dramatically (63). In particular, HIF may preserve

tolerance to hypoxia is through a reduction in mitochondrial number. Mitochondrial autophagy relies on the HIF-dependent expression of BNIP3 and has been argued to minimise cell damage and death from exposure to oxidative stress generated by hypoxic mitochondria (64).

1.4.2. Evidence for cellular hypoxia adaptation in human skeletal muscle

Aspects of this adaptive phenotype, shown to be elicited by the HIF pathway in cell models, have also been observed in human conditions associated with hypoxia (65) or disruption of the HIF-signalling pathway (66). For example, during acclimatization to hypobaric hypoxia on ascent to high altitude, lowlander skeletal muscle undergoes a metabolic shift towards glycolysis, in conjunction with the depletion of some TCA cycle intermediates and enzymes, reflecting a switch from oxygen-dependent respiration towards oxygen-independent ATP production (67). Such lowlander subjects also exhibit a trend towards increased coupling efficiency as well as a decrease in capacity for respiration supported by FAO and decreased expression of FAO enzymes (68). Mitochondrial bioenergetic machinery in skeletal muscle is also depleted, with decreases in components of the electron transport system (complexes I and IV) (69) as well as an overall reduction in mitochondrial volume density and downregulation of electron transport capacity (68). It has been argued that this represents a temporary protective strategy to reduce the generation of mitochondrial reactive oxygen species (ROS) that occurs during low oxygen conditions (70). In another study, exposure to 28 days of hypobaric hypoxia triggered bioenergetic changes independent of mitochondrial content, including specific inhibition of complex I-supported respiration and FAO, along with an increase in coupling efficiency (71). Complex I is thought to one of the major sources of ROS (and thus its reduced capacity at high altitude could be argued to represent a protective cell modification to hypoxia. Himalayan Sherpas, thought to have been exposed to extreme environmental hypoxia for 300 generations, combine an unparalleled functional tolerance to

hypoxia with a skeletal muscle phenotype that is distinct from other populations (72). Compared to acclimatised lowlanders, native Himalayan Sherpas display greater glycolytic capacity, lower skeletal muscle capacity for FAO and enhanced coupling efficiency, associated with increased incidence of a putatively-adaptive haplotype of *PPARA* (encoding PPARα), which has been proposed to underpin their superior cellular energetics and performance at high altitude (68). Whilst downregulation of FAO in lowlanders creates a metabolic bottleneck, resulting in an increased ratio of long-chain to total carnitines (68), considered to represent accumulation of lipotoxic intermediates (73) does not occur in Sherpas. Avoidance of this toxicity may be a crucial discriminator between the Sherpa and lowlander hypoxic phenotype. Although the mechanism is unclear, it may involve non-mitochondrial FAO via omega-oxidation (74, 75). Sherpa muscle exhibit lower levels of oxidative stress at altitude, compared to lowlanders. This finding, together with their lower maximum oxidative phosphorylation capacity and lower mitochondrial volume density supports the concept that reduced mitochondrial capacity in hypoxic conditions may be protective against ROS production.

1.4.3. Hypoxic adaptation in human cardiac muscle

The developing fetal heart thrives in the hypoxic intrauterine environment through appropriate substrate selection (76). It relies exclusively on glycolysis, with suppression of oxidative pathways until after birth (77). The metabolic phenotype is achieved by the action of a transcription factor, Hand1, which specifically represses the expression of proteins involved in FAO and the TCA cycle, by directly binding to and repressing the promoters of the relevant genes. Hand1 is under direct transcriptional control by HIF1. It is abundant in fetal cardiomyocytes but undergoes a sharp drop soon after birth (78). The Hand1-triggered substrate switch demonstrates the potential survival benefit from upregulating oxygen-independent pathways for ATP production, and downregulating oxygen-dependent pathways

when oxygen availability is limited. It also highlights the importance of being able to switch back when oxygen becomes available, as after birth, failure to deactivate Hand1 results in rapid death. Expression of a foetal gene programme can be induced in adult hearts during hypoxia (76). Substrate reprogramming, with a switch away from FAO, is also inducible in adult cardiac muscle in response to cellular hypoxia (60). In animal models of adult heart failure, including pressure overload hypertrophy, PPARα is deactivated and downregulated, resulting in reduced expression of its downstream targets, which include FAO enzymes (79). Clinical benefit from FAO downregulation relies on a compensatory increase in carbohydrate metabolism and is abolished in the absence of glucose (80, 81). In a mouse model of pressure overload-induced ventricular hypertrophy, upregulation of the glucose transporter (GLUT1) prevented the decline in contractile function (82), and preserved mitochondrial function (83). Mutant adult hearts overexpressing Hand1 show enhanced tolerance to acute ischaemic insults and its expression and resulting fetal phenotype can be induced in adult hearts by chronic exposure to hypoxia. Chronic reduction in coronary blood flow reduces resting energy consumption and downregulation of mitochondrial electron transport chain proteins (84). These chronic changes are accompanied by the depletion of contractile elements and contractile function, but also a reduced cellular demand for oxygen and substrate. The downregulation is initially reversible, but when prolonged, can result in inflammation, fibrosis and remodelling (85). Inhibition of complex I has previously been shown to reduce oxidative damage during myocardial ischaemia (86), and thus its reduced capacity at high altitude is consistent with a protective cell modification to hypoxia.

1.4.4. Features of hypoxic adaptation observed in critical illness

Elevated levels of intramuscular HIF1 have been demonstrated in a group of 23 critically ill patients, along with decreasing concentrations of FAO enzymes from day 1 to 7 of ICU

admission, and decreasing markers of mitochondrial biogenesis (87). A relative reduction in whole-body oxygen consumption has been demonstrated in patients with organ impairment compared with those with uncomplicated infections (88). The incubation of healthy human cells in serum from septic patients suppresses their respiration rate, suggesting a generalised cellular metabolic response to infection, which may be coordinated systemically (89). Rapid and severe muscle wasting is a well-known feature of critical illness, associated with decreased protein synthesis (90), mirroring the suppression of this energy-expending process in cell models of hypoxia (91) and in healthy humans ascending to high altitude (92). Although these findings have previously been proposed to support the concept of bioenergetic collapse in organ failure, they mirror many aspects of the cellular response to hypoxia, known to be coordinated by the HIF pathway.

1.5. Redox status, bioenergetics and cellular adaptation

1.5.1. The reactive species interactome

It has been proposed that electron exchange (redox) processes play a central role in sensing stressors and bringing about the necessary responses to enable the continuation of cell integrity and function (93). A complex series of redox interactions between different bioactive species, across multiple compartments within the body, may be responsible for the integration of stress signalling, cellular bioenergetics, intermediary metabolism and inflammation. All biomolecules can act as either electron donors (oxidants) or electron acceptors (reductants), and their redox activity will depend on their atomic constituents and the chemical properties of the set of molecules with which they interact (their redox environment). The simplest redox molecules include small gases (such as H_2, H_2S, NO, O_2, CO_2) and metal ions (iron, copper), but these constitute only a small proportion of redox active compounds. These molecules react with each other, and with other biomolecules (such as protein thiols) and modulate the function of biological targets, such as ion channels, enzymes and transcription factors, influencing mitochondrial function and metabolic activity (94, 95). Each redox reaction has the potential to generate new redox active molecules which, in turn, react with many others. Redox reactions are propagated over time and across space, generating a system of interconnected, dynamic interactions across multiple compartments within the body: the redox interactome (96). Changes in one compartment may result in increases or decreases in redox state in other compartments so that overall redox state of the organism as a whole is maintained.

1.5.2. Relationship between bioenergetic and redox status

The processes underpinning cellular bioenergetics are intimately linked with electron exchange (redox) changes; as chemiosmosis itself is driven by redox reactions. Reactive

oxygen species (ROS) are generated during chemiosmosis, when a single electron is transferred to molecular oxygen from the electron transfer system, to form a superoxide radical ($O2^{\cdot -}$). The dismutation of two superoxide molecules to form hydrogen peroxide (H_2O_2) can be catalysed by the enzyme superoxide dismutase. Mitochondrial superoxide production may occur at complex I, II or III, through the escape of electrons from reduced iron-sulphur groups, flavin-containing proteins, or from the free radical ubisemiquinone in the Q cycle of complex III. When electron flux along the electron transfer system is limited, for example by low PO_2, the half life of the intermediate free radical ubisemiquinone increases. In the inner mitochondrial membrane, oxygen can capture the spare electron from ubisemiquinone, and the probability of this event increases with increasing half-life of ubisemiquinone. ROS avidly interact with cellular components, including lipids, proteins and DNA, altering the structure and function of important machinery, such as cell membranes, mitochondria, and enzymes. In this manner, they play an important role in signalling, and have been proposed as crucial oxygen-sensors in the adaptive response to hypoxia (97–99). Tightly controlled production of redox molecules with specific targets, within a constrained space, allows for selective redox signalling, but excessive, prolonged or uncontrolled production of redox molecules (oxidants or reductants) might interfere with these adaptive processes by acting in an untargeted fashion, at unintended locations. Many different pathological states have been attributed to an imbalance between oxidants and reductants in favour of the oxidants ("oxidative stress"). Uncontrolled oxidation causes irreversible damage to lipids (altering membrane properties and functions), proteins (ion channels, enzymes) and DNA (100). Oxidative stress is thought to be due to excessive production of reactive oxygen species (ROS), as well as reactive nitrogen and sulphur species (RNS, RSS), including NO, which are also generated by the mitochondrial electron transport chain. These reactive species also react with each other, according to their relative

abundance, to produce other toxic compounds, for example NO and superoxide anion yield peroxynitrite, which has been associated with cellular toxicity (101). It has been reported that 1-2% of the oxygen consumed during electron transport is converted to ROS; and ROS production increases with the rate of energy production (102). As a major cellular source of ROS, and an important target, mitochondria represent an interface between bioenergetics and redox signalling and stress. Both ROS signalling and propensity to cause damage will be influenced by a network of agents with reducing capacity (antioxidants), including enzymes such as such as superoxide dismutase (SOD) and molecular antioxidants such as glutathione and Vitamin C. If the capacity of the antioxidant network to compensate is overwhelmed, there will be an indiscriminate shift towards oxidation.

The major regulator of cytoprotective responses to ROS and other electrophiles is the Keap1-NFE2L2 pathway (103). Nuclear factor-erythroid 2-related factor 2 (NFE2L2) is a redox-sensitive transcription factor that regulates both the basal and inducible expression of cytoprotective genes, including antioxidants by binding to the antioxidant response element (ARE) in the regulatory regions of target genes. Under normal conditions, nuclear levels of NFE2L2 are low, as it is targeted for degradation by the ubiquitin proteasome pathway, via binding of the repressor protein Keap1 (Kelch ECH associating protein 1). Redox modifications to the Keap1 cysteine residues in response to ROS alter its conformation, and allows nuclear translocation of NFE2L2 and subsequent target gene expression (104). These include enzymes involved in the glutathione and thioredoxin based antioxidant systems.

Another means by which cellular bioenergetics, metabolism and redox processes are linked is through complex intracellular pathways activated in response to energy stress. Increased energy demand or low energy state will alter the NAD^+/NADH ratio and mitochondrial

matrix redox potential, which directly affects the production of ROS by complex I (105). Peroxisome proliferator activated receptor-γ coactivator (PGC-1α) is a transcriptional coactivator, which is induced in response to a multitude of stimuli indicating high energy demand or low energy status, such as exercise, fasting and cold exposure, and has roles in both orchestrating antioxidant defenses; enhancing mitochondrial electron transport and biogenesis; and promoting glucose transport and FAO(106). It regulates these programmes by binding to and activating a variety of nuclear receptors and transcription factors, to form transcriptional complexes (107).

PGC-1α activity is controlled at the translational and post translational level, in a tissue-specific manner. Transcription of PGC-1α occurs through the activation of the cAMP response element-binding (CREB), through tissue specific means (108). For example, in skeletal muscle, CREB is activated by the rise in intracellular calcium levels in response to exercise; in liver, CREB is activated by glucagon in response to fasting; and in adipose tissue CREB is activated by cold-induced cAMP signalling. Post-translational activation of PGC-1α can occur, for example in low energy states, an increase in the cellular NAD^+/NADH ratio triggers the activation of Sirtuin 1 (SIRT1), a nuclear histone deacetylase, which activates PGC-1α by deacetylation. However, when energy levels increase in cells, PGC-1α is acetylated and inhibited by a different enzyme. The function of PGC-1α can also be modulated by ROS and RNS. For example, mitochondrially-generated ROS oxidises cysteine residues in the energy sensor, AMPK, resulting in its activation and phosphorylation of PGC-1α.

Promotion of PGC-1α target gene expression results in: increased hepatic gluconeogenesis (109), increased levels of certain TCA cycle genes (110) and increases muscle GLUT4

expression and glucose utilisation. PGC-1α interacts with the nuclear receptor, PPARα, the master regulator of FAO, promoting expression of nuclear genes encoding FAO enzymes. Activation of PGC-1α also promotes mitochondrial biogenesis, VEGF and other angiogenic factors in response to hypoxia and nutrient deprivation. PGC-1α also regulates redox regulation through the expression of mitochondrial antioxidant genes, such as catalase, manganese superoxide dismutase, periredoxins, thioredoxins and uncoupling protein 2, as well as activating NFE2L2.

There is some overlap between the cytoprotective effects and activation of PGC-1α pathways in response to energy stress, and those of the HIF response to hypoxia. SIRT1, which responds to perturbations in the ratio of oxidised NAD^+/reduced NADH, and therefore represent cellular redox sensors, have also been shown to modulate HIF activity (111). Upregulation of PGC-1α has been found to increase the expression of a battery of genes regulated by HIF-1α, through increasing mitochondrial oxygen consumption and consequent cellular hypoxia (112). During inflammation, low levels of PGC-1α result in diminished mitochondrial antioxidant levels, oxidative stress and NF_KB activation, exacerbating inflammation.

1.6. "Life support" strategies in critical illness

During the past 50 years, modern medicine has developed strategies to support homeostasis during life-threatening stress, which aim to preserve organ function and promote survival. These interventions are grouped under the umbrella term of "organ support" and are delivered on intensive care units (ICUs) or high dependency units (HDUs). The Intensive Care National Audit and Research Centre, which collects information from 251 adult intensive care units (ICUs) in England, Wales and Northern Ireland reported a total of

175,700 admissions to adult general ICUs in the year 2017-2018, for whom there was an acute hospital mortality of 20% (1). The avowed aim of almost all supportive therapy on the ICU is to bolster cellular bioenergetic capacity, based on the presumption that cell function, survival and repair will depend on the ability to produce sufficient energy. Clinicians target the supply end of the bioenergetic equation through augmentation of convective oxygen transport and mean arterial pressure to support tissue perfusion gradients. Arterial oxygen content is increased by supplementing inspired oxygen concentrations, manipulating mechanical ventilation settings and giving blood transfusions to correct low haemoglobin levels. Cardiac output is increased by a combination of methods, including the correction of hypovolaemia and administration of inotropes, which enhance myocardial contractility. In vasoplegic states, vasopressors, such as noradrenaline, are infused with the aim of increasing mean arterial pressure, with the intention of increasing perfusion pressure and tissue blood flow. Supportive therapy also involves delivering parenteral or enteral nutrition to meet normal energetic requirements.

1.6.1. Limitations of intensive care interventions

Multiple randomised controlled trials in intensive care have demonstrated that manipulating systemic oxygen delivery in critically ill patients, to target typical parameters seen in health, does not improve survival. Recent randomised controlled trials have not demonstrated survival benefit from early goal-directed therapy (113, 114) or augmentation of systemic oxygen delivery (115); and others have shown these interventions to be associated with harm (116, 117). In a large randomised controlled trial of older critically ill patients with vasoplegic hypotension, targeting a lower than normal mean arterial pressure did not increase mortality (118). Similarly, randomised controlled trials have demonstrated neither survival benefit from delivering nutrition to meet calculated energy requirements (119), nor harm for

significant underfeeding (120). Even with the provision of artificial life-support strategies on the ICU, acute mortality for patients with dysfunction in 4 or more organs was >65% (1), indicating the inadequacy of the current approach. Intensive care interventions are limited to manipulations of systemic physiology, and potential reasons for lack of survival benefit include (1) failure to correct cellular oxygenation, (2) failure to restore bioenergetic capacity, (3) failure to support other survival processes or (4) unintended harm from the systemic interventions, such as disruption of redox homeostasis or survival signalling. These will be considered in turn.

Failure to correct cellular oxygenation

It is possible that correction of the systemic measures of oxygen delivery described above may not translate into restored tissue oxygenation, which we cannot currently measure directly in the clinical setting, and which depends on the properties of the network of the smallest vessels which directly supply tissues: the microcirculation. Microcirculatory blood flow and tissue or cellular oxygenation are not measured in the clinical setting. Attempts to improve tissue perfusion by systemic administration of vasopressor agents has the potential to worsen tissue blood flow despite increased mean arterial pressures, by closing off capillary networks (121).

Failure to correct bioenergetic function

Bioenergetic capacity does not depend on oxygen availability alone but is the end-product of a network of many interacting pathways, described in section 1.2. Many of these factors may be altered during critical illness, such that correction of oxygen delivery in isolation may be insufficient to improve bioenergetic capacity. Exposure to hypoxia, reactive oxygen species (ROS) or inflammatory mediators, may influence the expression or activity of critical

enzymes which catalyse rate-limiting steps in intermediary metabolism; the activity of respiratory enzyme complexes, the coupling efficiency of oxidative phosphorylation, or the balance between mitochondrial degradation (autophagy) and generation (biogenesis)(17, 122).

Failure to account for innate survival responses

The network of factors that influence bioenergetic capacity is also subject to reprogramming in response to stress, such as hypoxia, exercise and starvation (123). In response to oxygen limitation, cells can implement oxygen-independent ATP production and modulate bioenergetic efficiency, by altering metabolic fuel preference and "tuning down" mitochondrial proton leak, in a highly regulated manner. They may also suppress energy expenditure (by reducing non-essential processes such as protein synthesis), and downregulate mitochondrial number and activity, to limit exposure to mitochondrially-generated ROS. Thus far, supportive therapy on ICU has neglected to consider the potential relevance of innate cellular adaptive responses to hypoxia, or how to support their expression.

Unintended harm from systemic interventions

Artificial methods to support systemic oxygen delivery may be harmful to critically ill patients, with evidence accumulating that these patients benefit from minimising intervention (the "less is more" approach) (124). Attempts to artificially increase cellular oxygen delivery in this context may have unintended consequences: perhaps circumventing innate adaptive signalling, or disturbing delicate redox homeostasis and imposing oxidative damage. It has been argued that intensive care therapy itself imposes a novel pathophysiological state, not previously encountered during human evolution: 'chronic critical illness" (55).

1.7. Summary

Despite the heterogeneity in triggering insults, critical illness manifests as a recognisable phenotype: with derangements to systemic physiology and widespread organ dysfunction. It is not clear how to support survival during this life-threatening condition. Oxygen availability is important for bioenergetic capacity, but fixation on targeting indirect measures of arterial oxygenation and pressure within the circulatory system does not reliably translate into improved cellular function or survival. Such indices are based on convenience rather than physiological importance. Currently, tools do not exist to monitor how much oxygen is reaching the mitochondria, nor is it understood what represents the optimum value for oxygenation in this pathological context. During the precipitating phase of critical illness, preventing hypoxia may prevent deterioration into organ failure, but once organ dysfunction if underway, it may be more appropriate to support cellular strategies to improve hypoxia tolerance, at least until the triggering disease process can be resolved. Review of hypoxic adaptation in different contexts has highlighted the existence of specific survival pathways, but it is not known if these are activated in critically ill humans, and if so, how they are coordinated from subcellular to higher-level physiology. A more comprehensive understanding of bioenergetic regulation in the context of human critical illness is required, and there is a need for relevant biomarkers to guide supportive therapy. This is not an easy task, given the heterogeneity of pathologies contributing to critical illness, inter-individual variation in the systemic inflammatory response, and the different requirements for each organ. Currently, the manner in which metabolism and mitochondrial function alter during the different phases of critical illness, and how this influences outcomes, is not well understood. Greater understanding of this cellular phenotype during the stress of critical illness may assist in the development of alternative strategies to support cell function without causing harm. To develop life support beyond manipulations of systemic physiology, it will

be necessary to investigate the relationships between organ failure and (1) the network determining cellular bioenergetic capacity, (2) the redox interactome, and (3) microcirculatory blood flow.

1.8. Hypothesis

This thesis explores the alternative hypothesis that survival in critical illness may also depend on changes in intracellular bioenergetic, metabolic and redox phenotype, rather than indicators of systemic oxygen transport alone. It is predicted that such changes will relate to local oxygen delivery by the microcirculation.

The first hypothesis was that critically ill patients will demonstrate a different cellular phenotype compared to reference patients (who do not have acute organ dysfunction). A critical illness phenotype may encompass both dysfunction and potential adaptive modifications due to stress.

The second hypothesis was that survivors of critical illness will demonstrate a different bioenergetic-metabolic-redox phenotype compared to non survivors. Again, differences in phenotype between these groups may reflect different degrees of stress and/or different capacity for adaptive modification.

1.9. Aims

- Determine whether or not there is a particular phenotype, encompassing cellular bioenergetics, metabolic function and redox status, that distinguishes critical illness from health (Figure 3).

- Undertake an integrated approach in real patients exposed to complex stressors triggering critical illness.
- Explore multiple pathways thought to be relevant to bioenergetic capacity and fundamental to survival, including mitochondrial respiration, substrate provision by metabolic pathways, local oxygen delivery by the microcirculation, as well as cellular and systemic redox architecture.
- Determine whether changes in any aspects of this complex bioenergetic phenotype could explain the phenomenon of resilience in eventual survivors (Figure 4) and explore their utility as alternative biomarkers to predict death from critical illness.
- Determine whether or not a relationship exists between these fundamental cellular functions and the systemic measures of oxygenation and haemodynamics that are currently used as therapeutic end points.

Figure 3. Potential components of the cellular phenotype in critical illness

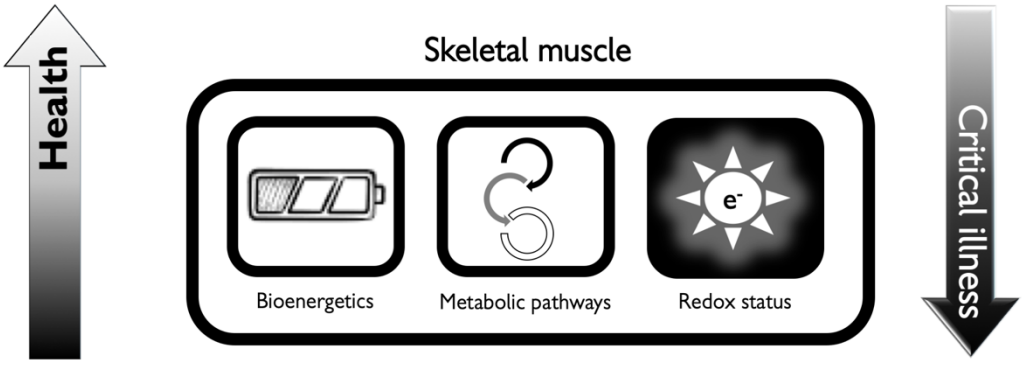

Schematic to represent aspects of the cellular phenotype under investigation in this thesis, including bioenergetic capacity, metabolic pathways and redox status in skeletal muscle, in reference patients without acute organ failure and in critically ill patients.

Figure 4. Potential components of a survival phenotype in critical illness

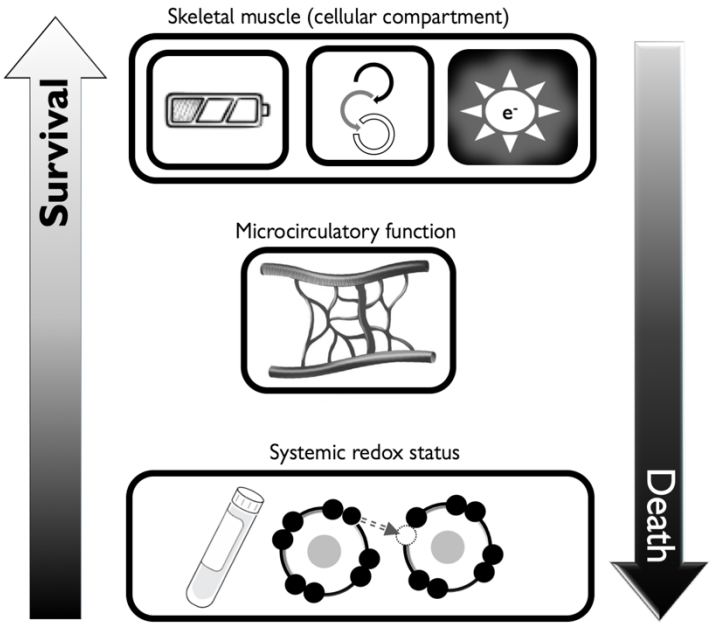

Schematic to represent aspects of the phenotype under investigation in survivors and non survivors of critical illness, including skeletal muscle bioenergetic-metabolic-redox phenotype; microcirculatory function and plasma indicators of systemic redox status.

1.10. Objectives

- Review current literature to determine the best methods to measure the following aspects of tissue and cell physiology:

(i) bioenergetics, metabolic pathways and redox status in cells within solid end-organs

(ii) circulating markers of redox status and nitric oxide activity

(iii) microcirculatory function

- Develop an integrated approach to simultaneously assess multiple aspects of the bioenergetic-redox-microcirculatory phenotype in patients.
- Define the cellular phenotype in human critical illness, by carrying out an observational case-control study, comparing measures of cellular bioenergetics, metabolic pathways and redox status in a group of critically ill patients with multiple organ failure to a reference group, not suffering from organ failure.
- Define the survival phenotype in human critical illness, by carrying out an observational prospective cohort study in critically ill patients, undertaking measures of (i) cellular bioenergetics and metabolism, (ii) circulating plasma redox status and (iii) microcirculatory function at multiple timepoints during the first week of critical illness.
- Describe the relationship between traditional clinical measures of systemic oxygen transport or organ failure and the experimental measures listed in 4.

1.11. Thesis plan

Chapter 2 outlines the conduct of two interrelated studies to characterise the bioenergetic, metabolic, redox phenotype in critically ill patients. Chapter 3 summarises the methods used and the rationale and evidence behind the chosen methodology. In Chapter 4, assessment of intact mitochondrial respiration was combined with metabolomic, lipidomic and redox

profiling in skeletal muscle, in a reference patient cohort is compared to that of a cohort of patients at two timepoints within the first week of developing acute organ failure. In Chapter 5, different aspects of redox status assessed in the central compartment (plasma) at multiple timepoints were compared between survivors and non survivors in the same cohort of critically ill patients. In Chapter 5, skeletal muscle oxygenation and microcirculatory function was compared in survivors and non survivors of critical illness, and the potential relationship between microcirculation and the bioenergetic-redox phenotype was explored.

2. Chapter 2. The TIMELORD study

2.1. Overview

The TIMELORD (**Ti**ssue **me**tabolism and b**l**ood flow in c**r**itical **d**isease) study was a combination of two inter-related observational studies. The first arm was a case-control study of skeletal muscle bioenergetic, metabolic and redox function in patients with acute organ failure compared to reference subjects. The second arm was a prospective cohort study investigating the relationship between clinical outcomes in critical illness and measures of cellular bioenergetic, metabolic and redox function, the microcirculation and systemic redox status. The purpose of this chapter is to provide a brief overview of the aims and conduct of these two inter-related studies. Details of each component of the study, including background, rationale, methodology and analysis will be considered individually in subsequent chapters, which are dedicated respectively to cellular bioenergetics, metabolic pathways, circulating redox status and microcirculatory function.

2.2. Aims and objectives

The general aims and objectives of this thesis are as outlined in the Introduction (section 1.9 and 1.10).

2.3. Study design and ethical approval

The TIMELORD study comprised two arms: a prospective observational cohort study, and a case-control study. It was conducted at a single centre: a tertiary referral teaching hospital in London, UK (the Royal Free Hospital). The conduct of these two interrelated studies will be outlined separately. Protocols received ethical approval from the Camden and Islington NHS Research Ethics Committee (cohort study in critically ill patients), and the East of England

Cambridge South Research Ethics Committee (case-control study), and local site approval from the Royal Free Hospital Research and Development Department.

2.4. Skeletal muscle phenotype in critical illness: a case-control study

2.4.1. Aims

The primary aim was to compare cellular bioenergetics, metabolic pathways and redox status, within a solid end organ, in patients with acute onset, severe physiological derangement resulting in multiple organ failure (cases), to a reference group of patients (controls) in order to determine whether there is a specific cellular phenotype that distinguishes acute critical illness from health. The secondary aim was to assess the relationships between this cellular profile and traditional clinical markers of oxygenation, haemodynamics and degree of organ failure.

2.4.2. Subject selection

This was an observational case-control study in critically ill patients. All participants were recruited from a tertiary referral teaching hospital in London (the Royal Free Hospital). Critically ill patients (cases), were defined as adults with acute onset, severe physiological impairment from any primary cause, requiring at least two forms of organ support, and were studied during the first week of their ICU admission. They were recruited from a mixed surgical and medical intensive care unit (ICU). Reference subjects (controls), were a comparable group of patients, of similar age, undergoing elective hip replacement under general anaesthesia. This group was selected as a reference, as these subjects were likely to share many of the same exposures as the critically ill group, such as mechanical ventilation, supranormal fractional concentrations of inspired oxygen, immobility, and intravenous

medications such as sedatives, analgesia, muscle relaxants and antibiotics and crystalloid fluids. They were recruited from the operating theatres at the Royal Free Hospital.

2.4.3. Screening

Critically ill patients (Cases)

All patients on the ICU were screened daily against the inclusion and exclusion criteria outlined below.

Inclusion criteria:

1. Age $\geq$ 18 years
2. Unplanned (emergency) admission to the ICU
3. Admitted to ICU for < 48 hours
4. Current requirement for at least 2 forms of artificial organ support (e.g. mechanical ventilation, vasopressor or inotropic support or renal replacement therapy).
5. Expected to remain on the ICU for > 5 days (based on clinical judgement).

Exclusion criteria:

1. Severe coagulopathy, defined as platelets < 50 x 10^9/L or International Normalised Ratio (INR) > 1.5
2. Receiving therapeutic anticoagulation or thrombolysis
3. Therapeutic immunosuppression
4. Disseminated cancer
5. Primary neuromuscular pathology
6. Diagnosed mitochondrial disorder

Reference group (controls)

Potential participants for the reference group were identified by screening elective operation lists against the following inclusion criteria, while the exclusion criteria were the same as for the critically ill group.

Inclusion:

1. Age > 18 years
2. Undergoing elective hip replacement surgery under general anaesthetic

Elective hip replacement is carried out at the Royal Free under general anaesthesia, which involves induction of anaesthesia with intravenous opiates (usually fentanyl) and propofol, muscle relaxation using atracurium or rocuronium, and placement of an endotracheal tube for mechanical ventilation and maintenance of anaesthesia with volatile agents such as isoflurane, sevoflurane or desflurane. An audit carried out at this centre, along with 28 other hospitals in England, during the time of the study, demonstrated the administration of a consistent fractional concentration of oxygen of 0.5 throughout surgery, which corresponded to a measured mean partial pressure of O_2 (PaO_2) of 25 kPa in patients with an arterial catheter (125).

2.4.4. Consent and enrolment

Patients deemed to be eligible, according to the inclusion/exclusion criteria, were approached by the research team to request informed consent for participation in the study. For the reference group, eligible patients were provided with a participant information sheet prior to their operation and written, informed consent was provided on the morning of their planned operation. Due to the nature of critical illness and use of sedative medications on the ICU,

critically ill patients meeting the inclusion criteria invariably lacked capacity to provide informed consent to participate in the study. If an eligible patient lacked the mental capacity to provide informed, written consent, proxy consent was initially sought from a personal consultee: either the next of kin, or an appointed legal representative. If an appropriate personal consultee could not be identified, proxy consent was sought from a professional consultee: the intensive care physician responsible for the patient's care on that day. Information was provided in the form of a patient or consultee information sheet, and the consent process carried out, in person or via telephone, in line with the Good Clinical Practice guidelines and the Mental Capacity Act (2005). If a patient recovered capacity following enrolment in the study, their consent was sought prior to continuation of the study, and retrospective consent was required to use data already collected. When necessary, translation was performed by hospital translators.

2.4.5. Sample and data collection

Study-specific measures

Following enrolment, skeletal muscle samples (*vastus lateralis*) were taken from all participants (cases and controls) and subsequently analysed to quantify multiple aspects of cellular bioenergetics (section 3.2), metabolic pathways and redox status (section 3.3). All study-specific methods are outlined in full in Chapter 3 (General Materials and Methods) and referred to in their dedicated chapters. For the critically ill patients (cases), muscle biopsies were performed less than 48 hours after admission to the ICU (baseline) and repeated after 5-7 days. For the reference group (controls), *vastus lateralis* muscle was sampled by the surgeon, immediately following planned exposure of the muscle, during the early stages of their operation, and prior to insertion and cementing of the joint prosthesis.

Clinical data collection

In addition to the study-specific measures, baseline patient characteristics and contemporaneous clinical data were collected from the patients' notes and ICU or anaesthetic charts and recorded in the Case Report Form. Information regarding demographics and pre-existing co-morbidities were collected from all participants, including age, sex, height and weight (from which body mass index (BMI) was calculated according to Equation 8.

Equation 8. Calculation of body mass index, BMI

$$BMI = \frac{weight}{(height)^2}$$

Weight (kg); height (m).

For the critically ill patients, the primary diagnosis or diagnoses resulting in critical illness were also recorded. Severity of critical illness on admission was characterised using two approved scores: the Acute Physiology and Chronic Health Evaluation (APACHE II) score and Sequential Organ Failure Assessment (SOFA) score. These scores use a number of different indices to estimate mortality and morbidity and are validated for patients in the intensive care unit. APACHE II is a severity of disease classification system, calculated from a patients age, previous health status (recent surgery, immunocompromise or history of severe organ insufficiency) and 12 routine physiological measurements measured within the first 24 hours of admission to the ICU, to give an integer value between 0 and 71, with higher scores corresponding to more severe disease and a greater risk of death (126). The SOFA score is used to determine the extent of organ function, based on scores for six different systems, one each for respiratory, cardiovascular, hepatic, coagulation, renal and neurological systems (127). For the reference group, APACHE II and SOFA can be assumed to equal

zero, and the specific risk of death from their operation was calculated using the P-POSSUM physiology score, which estimates the morbidity and mortality related to surgical procedures based on twelve physiological indices, including age, cardiac, respiratory, renal, cerebral and immune function (128).

2.4.6. Statistical analysis

Sample size calculation

The determination of sample size was based on several competing factors. The aim of the study was exploratory: to detect potential aspects of a complex cellular phenotype in critically ill patients, compared to reference patients, by simultaneous assessment of cellular bioenergetic capacity, intermediary metabolism and redox status, using complementary assays. In an exploratory study, the priority must be to optimise sensitivity to detect potential differences, for further investigation in future studies. Greater sample size increases the power (the ability to detect a difference between groups when a difference exists), but the limit to sample size was ultimately determined by the capacity of a solo researcher to recruit and test critically ill and reference patients meeting the inclusion/exclusion criteria, in a single site, within the available timeframe. Given the paucity of published deep phenotyping studies in critically ill patients, in particular, using the multifaceted approach planned in this thesis, it was difficult to perfom a single statistical assessment to ensure adequate power to detect differences between the groups, using all of the assays. The approach chosen to determine a minimum sample size, was to base the calculation on the most important variables of interest. Given that this was a study of potential bioenergetic adaptation, the capacity for respiration supported by proton leak (later defined as $LEAK_{FAO}$) and fatty acid oxidation ($OXPHOS_{FAO}$), and the specific activity of the HADH enzyme (representing the capacity of the FAO metabolic pathway) were chosen to represent the three most important

aspects of a putative bioenergetic and metabolic phenotype in critical illness. "Normal" values for these variables, in a cohort of healthy volunteers at sea level, have previously been determined by our own research group, using identical assays and protocols planned for this thesis. The distributions of these variables were also determined in a population of Himalayan Sherpas, taken to represent an important phenotype of bioenergetic-metabolic adaptation to hypoxic stress. The differences in these variables demonstrated in Sherpas compared to lowlanders may have (1) whole-body functional significance, as Sherpas demonstrate enhanced hypoxic tolerance, and (2) mechanistic plausibility, as they theoretically increase the efficiency of cellular energy production.

Sample size calculations were performed using these values (taken from the data repository for this study (68) and an online power calculation tool (https://clincalc.com/stats/samplesize.aspx) was used, based on two independent samples and a continuous endpoint. An alpha value of 0.05 was chosen (representing a 5% probability of a type I error; the false positive rate, or probability of detecting a difference between the critically ill and reference groups when it does not exist); and power of 80% was selected, as a standard threshold typically considered to represent an acceptable risk of type II error (or false negative rate) in clinical studies. Assuming an enrolment ratio of 1:1, the minimum sample sizes for the three assays are summarised in Table 2. A greater degree of variation was expected in the critically ill cohort than these cohorts (given the variation in expected stress, age, comorbidity and medications), and so these sample sizes were used to represent a minimum target for recruitment. The upper limit target was set by pragmatic considerations related to the capacity of a solo researcher to carry out the recruitment and testing in the 2-year timeframe for data collection. Recruitment of critically ill patients was prioritised over reference patients, at an enrolment ratio of 2:1, in order to allow exploration of differences

between survivors and non survivors in the critically ill group. Thus, at the outset, the aim was to recruit 30 critically ill and 15 reference patients.

Table 2. Sample size estimation for three important aspects of bioenergetic-metabolic phenotype

Critical variables	Anticipated values for reference cohort		Threshold of difference to detect in critically ill cohort	Sample size
	Mean	Standard deviation	Mean	
$LEAK_{FAO}$ (pmol/s/mg)	10.06	1.774	7.038	10 (5 per group)
$OXPHOS_{FAO}$ (pmol/s/mg)	23.6	7.13	15.6	26 (13 per group)
HADH activity µmol/min/mg	0.39	0.09	0.28	24 (12 per group)

Anticipated values for reference cohort based on healthy lowlanders at sea level; threshold of difference to detect in critically ill cohort based on Sherpa values (representing putative hypoxia adaptation).

Data analysis

All data were first tested for normality using the D'Agostino and Pearson omnibus normality test. Parametric continuous data were described using mean and standard deviation (SD); and non-parametric data using median and interquartile range (IQR). Frequency counts and percentages were used to describe categorical variables. Critically ill patients (cases) and reference subjects (controls) were compared using the Mann-Whitney test for independent data with non-parametric distributions. Bivariate correlations between different skeletal muscle measures or clinical measures, were assessed using two-tailed Spearman's test. All statistical analyses were carried out using GraphPad Prism 8 software (GraphPad Software, Inc), as two-tailed, and p values of <0.05 were considered statistically significant.

2.4.7. Results

In total, 21 critically ill patients and 12 reference patients were recruited to the study. The demographic, co-morbidity and clinical information for the subjects in both groups are summarised in this chapter, and subsequently referenced in the subsequent chapters which compare specific measures of bioenergetic, metabolic and redox status in the two groups.

Study cohorts

The baseline demographic and clinical characteristics of the critically ill patients and the reference group are summarised in Table 3. The subjects of the critically ill group all exhibited severe physiological derangement and organ dysfunction. The median severity of illness on admission (calculated as the APACHE II score) predicted an approximate mortality of > 55%, and the actual in-hospital mortality was 57%. All patients in this group were mechanically ventilated, with fractional concentrations of inspired O_2 (F_IO_2) > 21%. A significant proportion met the criteria for adult respiratory distress syndrome ($PaO_2/F_IO_2 < 40$

kPa) (129). All patients had a significant requirement for continuous intravenous vasopressor support (noradrenaline) to artificially support their mean arterial pressure (MAP), and 29% had arterial lactate concentrations greater than the cut-off associated with increased mortality from sepsis (> 2.5 mmol/L) (130). Approximately a quarter of the patients also required renal replacement therapy (haemofiltration) for renal failure. The primary pathologies of the critically ill patients are summarised in Table 4. It is important to note that many of the patients had multiple presenting pathologies and co-morbidities, reflecting the heterogeneity of critically ill patients typically treated on ICU. Almost all the critically ill patients were being treated with intravenous antibiotics for presumed or known infection.

Table 3. Baseline characteristics of critically ill and reference cohorts

Subject characteristics	Acute organ failure < 48 h ICU admission (n=21)	Reference group (n=12)
Age, y median (range)	62 (31-85)	64 (29-83)
Female sex, n (%)	8 (38)	7 (58)
Male sex, n (%)	13 (62)	5 (42)
Height, m median (IQR)	1.75 (1.66-1.77)	1.73 (1.67-1.77)
Weight, kg median (IQR)	70.6 (63.8-90)	78.0 (65.7-96.8)
BMI, kg/m^2 median (IQR)	24.2 (22.0-29.5)	25.4 (22.3-31.9)
Organ insufficiency prior to admission, n (%)	3 (14)	0 (0)
Independent prior to hospital admission, n (%)	20 (95)	12 (100)
Co-morbidities n (%)		
Hypertension	11 (54)	1 (8)
Ischaemic heart disease/arrythmia	6 (29)	1 (8)
Respiratory	6 (29)	2 (17)
Diabetes	4 (19)	0 (0)
Chronic renal impairment	3 (14)	0 (0)
Mechanically ventilated n (%)	21 (100)	12 (100)
Intravenous antibiotic therapy n (%)	19 (90)	12 (100)
Propofol administered n (%)	11 (52)	12 (100)
Muscle relaxant within previous 24 hours n (%)	9 (43)	12 (12)
Nutrition within previous 6 hours n (%)	13 (62)	0 (0)

Table 4. Primary diagnoses in the critically ill cohort

Primary pathology	n (%)
Infection	14 (67)
Haemorrhage	3 (14)
Coronary ischaemia/arrhythmia/ cardiogenic shock	8 (38)
Respiratory	10 (48)
Acute liver impairment	2 (9)
Acute renal impairment	3 (14)
Gastrointestinal/intra abdominal	8 (38)

2.4.8. Discussion

The strengths and limitations related to subject selection and recruitment are common to all subsequent related chapters and will be discussed here to avoid repetition.

Sample size

The small study size meant there was an increased risk of type II error in comparison to study with a larger number of patients. Fewer subjects were recruited to the study during the time frame for subject recruitment (18 months) than the predetermined target of 30 critically ill patients and 15 control patients. This was due to fewer subjects than expected meeting the inclusion/exclusion criteria, with co-existent coagulopathy or therapeutic anticoagulation being the most common cause of exclusion. Enrolment of eligible patients was also lower than anticipated, and the barriers most frequently expressed by personal consultees who did not consent to patient enrolment in the study included (1) the invasive nature of the muscle biopsy in the context of critical illness with no possibility of therapeutic benefit, (2) the narrow time window to make the decision to consent (< 48 hours following admission to the ICU), (3) lack of certainty regarding what the patient themselves would have wanted, and (4) the high stress of their situation (attending a relative suffering from critical illness). Another barrier to recruitment was related to the logistical requirements involved in measuring skeletal muscle mitochondrial respiration. This required the immediate onsite preparation and real-time analysis of fresh tissue, using a complex protocol. Patients could be tested only on days when the operator was available. Although the ultimate sample size was smaller than expected, the number of subjects was still comparable to previous studies in similar patient groups that have successfully demonstrated differences between critically ill patients and controls in related aspects of bioenergetic (131) and redox function (132). The study also

represents the largest study to date of direct measurements of intact mitochondrial respiration in skeletal muscle from patients with acute, severe critical illness.

The critically ill cohort

The critically ill cohort was highly heterogenous, in terms of age, co-morbidity, medications, prior nutrition, as well as primary pathology (or pathologies) and degree of organ dysfunction on admission. All of these factors may influence the bioenergetic and redox variables measured in subsequent chapters. However, the heterogeneity and overlap of conditions seen in this study is typical of the patients treated on the ICU, where multiple pathologies and syndromes often co-exist, rather than existing in isolation. The aim of the case-control study was to identify whether the physiological state of multiple organ failure *per se* (rather than specific diseases or aspects of physiology, such as arterial oxygenation, in isolation) results in measurable differences in cellular bioenergetics and redox status. The purpose was to identify whether any bioenergetic or redox features were *common* to these diverse patients as a result of the magnitude of the stress experienced. Although the heterogeneity of the group increases the noise and makes it more difficult to distinguish any clear differences between groups, if such differences are identified, they must be considered as potentially important aspects of cellular physiology during critical illness and multiple organ failure. In the field of intensive care medicine, pragmatic trial design, which tests the effectiveness of interventions under real-life conditions, are considered to be valuable because of their generalisability of any results to such a highly heterogenous cohort (133). In contrast, an explanatory trial design, which attempts to control for all known biases and confounders, is a better design to explore if and how an intervention actually works.

The reference cohort

The reference group was intended to represent patients of similar age, sex, body mass characteristics, co-morbidity, physical activity and nutritional status as the critically ill patients, to minimise any additional systematic differences between the two groups, other than the condition under investigation (organ impairment as a result of life-threatening stress). The reference group was well-matched to the critically ill group in terms of several important factors known to influence mitochondrial function. These included: age, as mitochondrial capacity is known to decline with advancing age (134, 135) and BMI. Although it was not possible to fully control for the variation in exercise and immobility between the groups, also known to result in remodelling of mitochondrial function (136, 137), arguably the reference group represented adequately comparable pre-existing activity levels, as patients who would not have been subject to extreme remodelling from highly active lifestyle. Both groups were studied in the supine position, without activity of the affected muscle in the previous hour. However, by the first timepoint, critically ill patients had been immobile for up to 48 hours. It was not possible to control for the effects of drugs, as this was an observational study. However, the reference subjects were also exposed to many of the drugs administered to the critically ill patients at the time of the biopsy, including antibiotics, propofol, opiates, benzodiazepines, muscle relaxants, and the groups shared exposure to mechanical ventilation and supplemental inspired oxygen concentrations. At the first timepoint, all patients in both cohorts were mechanically ventilated. Patients undergoing elective arthroplasty must fast for at least 6 hours prior to general anaesthetic. The nutritional intake of the critically ill patients could not be controlled, but a significant proportion at the first timepoint were also in the fasting state at this early phase of critical illness, prior to establishment of a feeding route (insertion of nasogastric tube or central venous access for parenteral nutrition), or due to a failure to absorb enteral feed, a common

finding in critical illness. Although none of these exposures could be controlled for in either group in this clinical context, several important features were similar between critically ill patients and the reference surgical cohort. This commonality diminished, but did not eliminate, the potential confounding effects of mechanical ventilation, drugs, mobility and nutrition on the bioenergetic, metabolic and redox variables measured in subsequent chapters. Surgery and general anaesthesia also represent a form of acute physiological disturbance, but the risk of in-hospital mortality for elective hip replacement surgery is < 0.15%, and all reference subjects were discharged from hospital alive.

2.5. The survival phenotype in critical illness: a prospective cohort study

2.5.1. Aims

The primary aim was to study patients with acute onset, severe physiological derangement resulting in multiple organ failure, during the first week of critical illness, to determine whether changes in cellular bioenergetics, local microcirculatory function and systemic redox status differed between eventual survivors and non survivors. The secondary aim was to assess whether or not there is any relationship between bioenergetic, metabolic, redox and microcirculatory variables, or between these experimental measures and the degree of organ failure.

2.5.2. Subject selection

This was an observational prospective cohort study in critically ill patients. Cellular bioenergetics, microcirculatory function and systemic redox status were studied in cohort of critically ill patients with multiple organ failure, at three different timepoints during the first week of critical illness and followed up to determine mortality at hospital discharge. The cohort was made up of the critically ill patients (cases) recruited for the case-control study (outlined in section 2.4.2).

2.5.3. Screening, consent and enrolment

Screening, consent and enrolment of the critically ill patients were undertaken as previously described in the relevant sections of the case-control study (sections 2.4.3 and 2.4.4 respectively).

2.5.4. Timepoints of sample and data collection

Following enrolment, study measures were taken at three timepoints. Baseline measurements were taken within 48 hours of admission to the ICU (taken to represent the time of diagnosis of critical illness and onset of organ failure). In order to determine whether or not changes occurred within subjects within during the first week of critical illness, repeat measures were undertaken 3-4 days after the baseline measurements, and again at 5-7 days after the baseline measures.

2.5.5. Study-specific measures

A brief overview of the study measures undertaken at each timepoint is summarised in Figure 5. All study-specific methods are outlined in full in Chapter 3 (General Materials and Methods) and referred to in their dedicated chapters. Skeletal muscle (*vastus lateralis*) was sampled for analysis of cellular bioenergetics (section 3.2), metabolic pathways and redox status (section 3.3). Systemic redox status was assessed in plasma, using multiple complementary assays, in both venous and arterial plasma (section 3.5). Skeletal muscle oxygenation and microcirculatory function was assessed in the thenar eminence using near infrared spectroscopy with a vascular occlusion test (section 3.6).

Figure 5. Study schedule

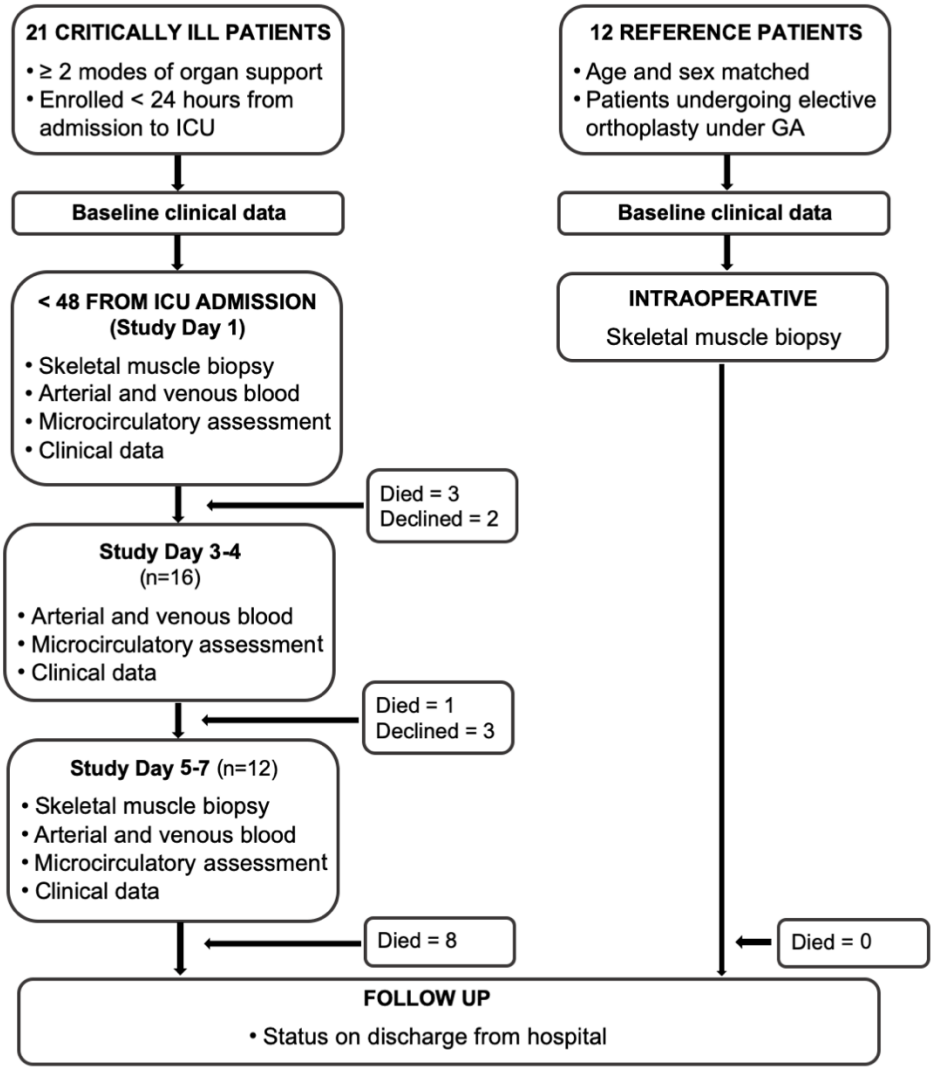

2.5.6. Clinical data collection

In addition to the study-specific measures, baseline patient characteristics and clinical data were collected from the patients' notes and ICU charts and recorded in the Case Report Form (Appendix 6). Collection of baseline characteristics for the critically ill patients has been described in section 2.4.5. A large number of contemporaneous physiological and biochemical measures, routinely undertaken on the ICU, were also recorded at the same timepoints as the study specific measures (< 48 hours, days 3-4 and days 5-7). Relevant clinical variables included the degree of organ support required, and indices used by physicians on the ICU to estimate: the adequacy of systemic oxygenation; global haemodynamics; and dysfunction of specific organs (including renal, respiratory, cardiovascular, renal, hepatic, haematological systems). These variables are described below.

Organ support

Organ supportive interventions were recorded, including mechanical ventilation, administered fractional concentration of oxygen (F_IO_2), dose of vasopressor (such as noradrenaline) or inotropic support, renal replacement therapy or antibiotics.

Measures of oxygenation

Measures of systemic oxygenation included: peripheral arterial oxygen saturation (SpO_2), arterial partial pressure of oxygen (PaO_2), arterial oxygen content (CaO_2), which was calculated using Equation 6. Adequacy of global tissue oxygenation was assessed using the serum lactate concentration. Measures of systemic haemodynamic function included heart rate and blood pressure, along with the required dose of continuous intravenous vasopressor to maintain this.

Respiratory function

Degree of respiratory failure was estimated using the PaO_2/F_IO_2 ratio, calculated according to Equation 9 and value ≤ 39.9 kPa defines acute respiratory distress syndrome (129).

Equation 9. PaO_2/F_IO_2 ratio

$$\frac{P}{F}ratio = \frac{PaO_2}{F_IO_2}$$

PaO_2: arterial partial pressure of oxygen (kPa); F_IO_2: the fractional concentration of inspired oxygen (%).

Liver dysfunction

Liver function was assessed non-specifically using concentrations of substances produced by the liver (albumin, clotting function) to quantify its synthetic function; while the concentration of transaminases, such as alanine aminotransferase and aspartate aminotransferase, act as non-specific markers of liver damage.

Renal dysfunction

Renal function was assessed clinically using serum urea and creatinine concentrations as markers of the renal clearance of these substances Estimated creatinine clearance (ml/min) was also calculated according to the Cockcroft-Gault equation(138), shown in Equation 10. This value can be modified to adjust for BMI. The "weight" in Equation 10 is taken as the actual body weight for patients with BMI <18.5, as the ideal body weight (IBW) for patients with BMI 18.5- 24.9, and as the adjusted body weight (ABW) for patients with BMI ≥ 25 (139, 140). Ideal body weight was calculated using Equation 11 and adjusted body weight was calculated using Equation 12.

Equation 10. Estimated creatinine clearance (Cockcroft-Gault equation)

$$Creatinine\ clearance = \frac{Weight\ \times\ (140 - age)}{72 - serum\ creatinine}$$

Creatinine clearance (ml/min); weight (kg); age (years); serum creatinine (μmol/L). For females, the final value is multiplied by 0.85.

Equation 11. Ideal body weight, IBW (Devine Equation)

$$IBW\ (male) = 50 + (height - 60)$$

$$IBW\ (female) = 45.5 + (height - 60)$$

IBW: ideal body weight (kg); height (inches).

Equation 12. Adjusted body weight, ABW

$$ABW = IBW + 0.4\ \times (actual\ body\ weight - IBW)$$

ABW: adjusted body weight (kg); IBW: ideal body weight (kg)

Inflammation

Degree of systemic inflammation was assessed using body temperature, and circulating markers of inflammation, including white cell count (WCC) and C-reactive protein (CRP).

Nutritional intake

Information about nutritional intake was collected, including: the feeding route (enteral or parenteral); the quantity of calories, lipids, protein (nitrogen), carbohydrate administered in the previous 24 hour period.

Clinical outcomes

Patients were followed up until discharge, to record their clinical outcome (alive/dead) at ICU discharge, hospital discharge and Day 28. The primary outcome variable was survival at hospital discharge.

2.5.7. Statistical analysis

Sample size calculation

Estimation of sample size was described in 2.4.6. All data were first tested for normality and described and presented as described in section 2.4.6. Attrition at later timepoints occurred due to both patient death, and recovery and declining to continue. For parametric distributions, different timepoints of critical illness were initially compared using a mixed effects model (rather than by repeated measures ANOVA, which cannot deal with missing values). However, the mixed model results will only be meaningful if the values were missing for random reasons. Additionally, therefore, secondary analysis was then performed to assess the effect to time using repeated measures ANOVA, including only subjects with complete data at all 3 timepoints (n = 12). If a significant difference was reported, post-hoc pairwise comparisons were carried out using Bonferroni correction for multiple comparisons.

For non-parametric distributions, the effect of time was assessed using Friedman's test (the equivalent of a one-way ANOVA with repeated measures for non-parametric distributions).

If a significant difference was reported, post-hoc pairwise comparisons were carried out using Dunn's correction. Friedman's test cannot take account of missing values, and so only subjects with data completed for all three timepoints were analysed using this technique.

To assess differences in arterial and venous plasma, paired arterial and venous plasma samples were compared at each timepoint using the Wilcoxon signed-rank test. It was not possible to perform a two-way ANOVA, (or a mixed effects model to account for missing values), as these tests are suitable only for parametric data. A non-parametric paired test at each timepoint was considered the best compromise for paired data. For the same reason, survivors and non-survivors were compared at each timepoint using the Mann-Whitney test for independent data with non-parametric distributions. Significance of bivariate correlation was calculated using two-tailed Spearman's correlation, and regression analysis used to plot a line of best fit. All analyses were carried out using GraphPad Prism 8 software (GraphPad Software, Inc.), as two-tailed, and p values of < 0.05 were considered significant.

2.5.8. Results

The critically ill cohort consisted of 21 patients, whose demographic and baseline clinical characteristics have been described previously in Table 3 (section 2.4.7), along with their presenting diagnoses in Table 4. All critically ill patients underwent testing within 48 hours of admission to the ICU. Sixteen of the enrolled patients underwent repeat testing on study days 3-4 (three died prior to this timepoint and two declined further testing), and twelve of these underwent testing at study days 5-7 (a further one patient died and three more declined further participation). The clinical characteristics of the remaining cohort at each of the three timepoints is summarised in Table 5, including relevant medications (such as sedative

infusions, steroids or nitrate) and documented nutritional intake. The baseline (< 48 h) characteristics of survivors and non survivors are compared in Table 6.

Table 5. Clinical characteristics of the critically ill cohort at three timepoints

Clinical characteristics at time of testing	Time after ICU admission		
	< 48 hours (n=21)	Day 3-4 (n=16)	Day 5-7 (n=14)
Females n (%)	8 (38)	5 (31)	4 (29)
Males n (%)	13 (62)	11 (69)	10 (71)
SOFA score median (IQR)	12 (10.5-15)	11.5 (6.5-14.8)	9 (6.5-14.3)
Survival to hospital discharge n (%)	9 (43)	7 (43)	4 (33)
Mechanically ventilated n (%)	21 (100)	13 (81)	11 (79)
F_IO2, % median (IQR)	35 (30-45)	38 (30-44)	38 (30-46)
SpO_2, % median (IQR)	95 (94 -97)	95 (93-97)	96 (93-98)
PaO_2, kPa median (IQR)	11.6 (10.8-12.3)	11.1 (10.0-13.2)	11.5 (10.0-13.1)
CaO_2, ml O_2/100 ml blood median (IQR)	14.6 (11.6-17.1)	11.8 (10.8-14.8)	12.0 (11.0-14.1)
Vasopressor requirement (μg/kg/min) median (IQR)	0.19 (0.07-0.29)	0 (0-0.14)	0 (0-0.08)
Inotrope requirement (μ/kg/min) median (IQR)	0 (0-0.04)	0 (0-0)	0 (0-0.81)
Mean arterial pressure, mmHg median (IQR)	77 (73-81)	83 (80-87)	81 (75-88)
Heart rate, beats per minute median (IQR)	80 (69-100)	83 (68-110)	93 (83-106)
Arterial lactate > 2.5 mmol/L n (%)*	6 (29)	3 (19)	2 (14)
Arterial lactate concentration, mmol/L median (IQR)	1.6 (1.3-3.5)	1.4 (0.9- 2.0)	1.4 (0.9-1.8)
Renal replacement therapy n (%)	5 (24)	4 (25)	4 (29)
Estimated creatinine clearance, ml/min median (IQR)$^{\phi}$	85 (39-116)	100 (79-160)	108 (91-139)
Serum albumin, g/L median (IQR)	28 (22-35)	27 (23-30)	27 (24-30)
Serum bilirubin, μmol/L median (IQR)	10 (5-18)	12 (6-31)	10 (6-19)
Serum ALT, units/L median (IQR)	103 (34-270)	97 (41-1043)	51 (30-191)
Serum AST, units/L median (IQR)	83 (48-315)	79 (43-320)	108 (91-139)
Temperature, °C median (IQR)	36.8 (36.0-37.1)	36.9 (36.6-37.2)	36.8 (36.6-37.2)
White cell count, $x10^9$/L median (IQR)	14 (10.9-18.9)	10.7 (7.9-15)	10.3 (8.8-14.6)
C-reactive protein, mg/L median (IQR)	126 (64-190)	147 (72-190)	181 (87-215)
Intravenous antibiotic therapy n (%)	19 (90)	16 (100)	14 (100)
Steroid therapy in previous 24 hours n (%)	11 (52)	10 (63)	7 (50)
Total steroid dose in 24 hours, mg hydrocortisone equivalents median (IQR)	30 (0-175)	100 (0-200)	160 (100-240)
Intravenous sedation n (%)	20 (95)	10 (63)	8 (57)
Continuous propofol infusion n (%)	11 (52)	0 (0)	1 (7)
Total propofol dose in previous 24 h, mg median (IQR)	495 (0-2365)	0 (0-0)	0 (0-0)

Continuous fentanyl infusion n (%)	20 (95)	11 (69)	7 (50)
Continuous midazolam infusion n (%)	12 (57)	4 (25)	4 (29)
Receiving nutrition at time of biopsy n (%)	13 (62)	14 (87)	14 (100)
Enteral nutrition n (%)	12 (57)	10 (63)	9 (64)
Parenteral nutrition n (%)	1 (5)	4 (25)	5 (36)
Protein administered (g/24 hours) median (IQR)	5 (0-28)	72 (20-83)	75 (75-98)
Carbohydrate administered (g/24 hours) median (IQR)	23 (0-103)	187 (94-225)	187 (187-223)
Fat administered (g/24 hours) median (IQR)	4 (0-22)	56 (15-61)	56 (55-61)
Energy administered (kcal/24 hours) median (IQR)	160 (0-1653)	1580 (510-1689)	1600 (1580-1816)
Muscle relaxant within previous 24 hours n (%)	9 (43)	0 (0)	0 (0)
Continuous nitrate infusion n (%)	0 (0)	0 (0)	0 (0)
Blood glucose, mmol/L median (IQR)	8 (6-10)	9 (7-10)	8 (8-9)
Rate of continuous insulin administered in previous hour, iu/h median (IQR)	0 (0-2.5)	0 (0-2)	0 (0-10)

SOFA: Sequential Organ Failure Assessment (range 0-24), F_IO2: Fractional concentration of inspired oxygen; SpO_2: arterial haemoglobin percentage oxygen saturation determined by pulse oximetry; PaO_2: partial pressure of oxygen dissolved in arterial blood, CaO_2: arterial oxygen content, ALT: alanine aminotransferase; AST: aspartate aminotransferase.

* best threshold to predict acute mortality in patients with sepsis-induced organ failure.

$^{\phi}$ indicates measurements in patients not undergoing renal replacement therapy.

Table 6. Survivors and non survivors of the critically ill cohort

Baseline and clinical characteristics at < 48 h	Survivors (n=9)	Non survivors (n=12)
Age, y mean (95% CI)	55.3 (45.5-65.2)	70.5 (51.5-77.8)
Female sex, n (%)	2 (22)	6 (50)
Male sex, n (%)	7 (78)	6 (50)
Height, m median (IQR)	1.75 (1.69-1.81)	1.73 (1.64-1.77)
Weight, kg median (IQR)	75 (60.8-94.5)	70.3 (63-90)
BMI, kg/m^2 median (IQR)	24.2 (21.4-34.3)	25.3 (21.7 - 29.5)
Severe organ insufficency prior to admission n (%)	1 (11)	2 (16)
Independent prior to hospital admission n (%)	9 (100)	11 (92)
Primary pathology n (%) Infection Haemorrhage Coronary ischaemia/arrhythmia/cardiogenic shock Respiratory pathology Acute liver impairment Acute renal impairment Gastrointestinal/intra abdominal pathology	 6 (67) 1 (11) 2 (22) 5 (56) 2 (22) 1 (11) 5 (56)	 8 (67) 2 (17) 6 (50) 5 (42) 0 (0) 2 (16) 3 (25)
APACHE II score median (IQR)	23 (19-27)	30.5 (29-37)
Admission SOFA score median (IQR)	11 (10-12)	15 (11-17)
F_IO_2, % median (IQR)	30 (30-43)	40 (30-49)
SpO_2, % median (IQR)	96 (95-98)	95 (94-96)
PaO_2, kPa median (IQR)	11.6 (10.8-14.1)	11.6 (10.3-12.0)
CaO_2 (ml/100 ml blood) median (IQR)	15.3 (11.7-17.5)	13.9 (11.4-16.7)
Vasopressor requirement, mcg/kg/min median (IQR)	0.19 (0.05-0.24)	0.25 (0.08-0.52)
Inotrope requirement (mcg/kg/min) median (IQR)	0 (0-0)	0 (0-0)
Mean arterial pressure, mmHg median (IQR)	77 (75-81)	77 (72-83)
Arterial lactate > 2.5 mmol/L n (%)*	1 (11)	5 (42)
Arterial lactate (mmol/L) median (IQR)	1.4 (1.3-1.5)	2.1 (1.7-4.9)
Renal replacement therapy n (%)	1 (11)	4 (33)
Estimated creatinine clearance, ml/min median (IQR) $^{\phi}$	103 (74-136)	43 (20-103)
Serum albumin, g/L median (IQR)	27 (19-38)	30 (24-35)
Serum bilirubin, µmol/L median (IQR)	10 (4-14)	14 (8-39)
Serum ALT, units/L median (IQR)	31 (19-115)	138 (86-575)
Serum AST, units/L median (IQR)	41 (20-140)	126 (69-857)
Temperature, °C median (IQR)	37.1 (36.6-37.6)	36.6 (35.8-36.8)
White cell count, x 109/L median (IQR)	14 (7-20)	14.8 (12.1-18.7)
C-reactive protein, mg/L median (IQR)	142 (49-163)	123 (64-216)
Intravenous antibiotic therapy n (%)	8 (89)	11 (92)
Steroid therapy in previous 24 h n (%)	5 (56)	6 (50)
Total steroid dose in 24 h, mg hydrocortisone equivalents median (IQR)	100 (0-160)	50 (0-188)

Intravenous sedation n (%)	9 (100)	11 (92)
Continuous propofol infusion n (%)	7 (78)	4 (33)
Total propofol dose in previous 24 h, mg median (IQR)	1280 (210-2440)	25 (0-2300)
Continuous fentanyl infusion n (%)	9 (100)	11 (92)
Continuous midazolam infusion n (%)	4 (44)	8 (67)
Receiving nutrition at time of biopsy n (%)	6 (66)	7 (58)
Enteral nutrition n (%)	5 (56)	7 (58)
Parenteral nutrition n (%)	1 (11)	1 (8)
Protein administered (g/24 h) median (IQR)	8.9 (0-39)	2 (0-30)
Carbohydrate administered (g/24 h) median (IQR)	29 (0-117)	13 (0-103)
Fat administered (g/24 h) median (IQR)	0.1 (0-0.4)	0.03 (0-0.4)
Energy administered (kcal/24 h) median (IQR)	200 (0-870)	90 (0-686)
Muscle relaxant within previous 24 h n (%)	4 (44)	5 (42)
Continuous nitrate infusion n (%)	0 (0)	0 (0)
Blood glucose, mmol/L median (IQR)	7 (6-11)	8 (6-10)
Rate of continuous insulin administered in previous hour, iu/h median (IQR)	0 (0-7)	0 (0-2.5)

BMI: Body mass index; APACHE II: Acute Physiology and Chronic Health Score (range 0-100); SOFA: Sequential Organ Failure Assessment range 0-24), F_IO2: Fractional concentration of inspired oxygen; SpO2: arterial oxygen saturation determined by pulse oximetry; PaO2: partial pressure of oxygen dissolved in arterial blood, CaO2: arterial oxygen content; ALT: alanine aminotransferase; AST: aspartate aminotransferase.
* best threshold to predict acute mortality in patients with sepsis-induced organ failure.
$^{\phi}$indicates measurements in patients not undergoing renal replacement therapy.

2.5.9. Discussion

This was a study of human patients, undergoing real life-threatening critical illness and treatment on the intensive care unit. Information gained from studying this cohort is directly applicable to human patients, in contrast to experimental models of stress in animals or cell lines. Within the same cohort of critically ill patients, multiple interrelated aspects of biological function were explored at the same timepoints, including assessment of microcirculatory function and systemic measures of redox status in plasma alongside traditional physiological and biochemical measures of organ function used in the clinical setting. This provides scope for an integrated, systems physiology approach in the future. Assessment of critically ill patients at multiple timepoints (< 48 h, day 3-4 and day 5-7) allowed the dynamics of cell bioenergetics, systemic redox status and microcirculatory function to be explored.

2.5.10. Limitations

The limitations related to subject selection for the prospective cohort study are common to all subsequent related chapters and will be discussed here to avoid repetition. Strengths and limitations relevant to individual aspects of the study will be discussed in the relevant chapter.

These data are from a small group of subjects. There is a risk of type II error, whereby a true difference between groups is not detected. Disease severity, organ function and intensive care medications and interventions varied between patients at baseline, and also varied over the time course of the study, all of which may influence the cellular bioenergetics, microcirculation, and systemic redox status measured in the patients. However, if important differences between survivors and non survivors can be distinguished despite the background

noise in this heterogenous cohort, the difference may represent a relevant aspect of survival physiology. Any of these indices that differ significantly between survivors and non survivors will require further investigation to determine its potential utility as a biomarker for cell stress in critical illness.

Clinical differences in subjects between timepoints

Across the group, average vasopressor requirements were higher and mean arterial pressure lower at the first timepoint than at the subsequent timepoints. This may have been due to resolution of vasoplegia, hypovolaemia or other causes of hypotension following the most acute phase of critical illness. It may also reflect the greater proportion of patients receiving continuous infusions of propofol as a sedative medication at the early time point, compared to the later timepoints. There was biochemical evidence of inflammation at all three timepoints, with supranormal levels of CRP (normal range < 10 mg/L); a non-specific indicator of inflammation. Almost all patients (apart from two at the first time point) received intravenous antibiotic therapy for presumed or proven infections throughout the study. The majority of patients were mechanically ventilated at all timepoints, with supplemental F_IO_2 > 30%. No patients were hypoxaemic in terms of SpO_2 or PaO_2 but calculated arterial oxygen content (CaO_2) was lower than the documented average for 61-80 year olds living in the community (19, IQR 17.9-20.1 ml/dL) in a recent population study of 1018 people (141). At baseline (< 48 h), more patients had arterial lactate concentrations surpassing 2.5 mmol/L, the threshold above which predicted mortality in sepsis increases (130). Roughly one quarter of patients required renal replacement therapy at all timepoints, with higher levels of renal impairment in non-filtered patients noted at the first timepoint.

Baseline differences between survivors and non survivors

Non survivors were, on average, older, with greater severity of critical illness (determined by the APACHE II score), than survivors. Given that this is an observational study, it will not be possible to determine whether differences between survivors and non survivors reflect a greater degree of imposed pathological stress or lower innate resilience in the non-survivors.

Attrition

During the study, there was loss of subjects at later timepoints. Attrition occurred for two reasons: death of the patient prior to completion of the investigations, or patient declining to participate further after clinical recovery. The latter was often due to fluctuating capacity during the narrow timeframe for repeated measurements, which complicated the consent process. As a result of this attrition, important information at the later timepoints was missed. Assessment of change across all three timepoints could be assessed for only 12 subjects, with the ratio of survivors to non survivors decreasing from 9:12 at the first timepoint, to 4: 8 by the final timepoint. Due to this heterogenous attrition, it was difficult to interpret the observed differences between survivors and non survivors at the later time point or in terms of the change over time.

2.5.11. Conclusion

The TIMELORD study generated a comprehensive phenotype based on contemporaneous measurements of numerous aspects of tissue blood flow, cellular bioenergetics, metabolomics and redox status in a cohort of patients undergoing life-threatening stress. From first principles, these aspects of physiology are thought to be fundamental to survival, but they are not currently monitored or targeted by intensive care interventions. Although the measurements were made in a relatively small and heterogenous group, they were all measured at the same timepoints, so that relationships between these complex and interrelated systems could be explored. Each of these aspects of physiology will now be considered individually, to establish if and how they alter as humans respond to critical illness and recover from multiple organ failure.

3. Chapter 3. General Materials and Methods

The methods used throughout the thesis are outlined in this chapter. All protocols received local site approval from the Royal Free Hospital Research and Development Department and ethical approval from either the Camden and Islington NHS Research Ethics Committee (IRAS ID 159977; REC reference 14/LO/1832) or the Cambridge Research Ethics Committee (IRAS ID 208220; REC reference 16/EE/0317).

3.1. Assay precision

The precision of the assays is an important consideration in the interpretation of observations obtained using these methods**.** Precision is not universally defined, but generally refers to "the agreement between independent results of measurements obtained under stipulated conditions" (142). For example, the Clinical and Laboratory Standards Institute describes the protocols for determining the precision of a method: each run in duplicate with two runs per day over 20 days (https://clsi.org/media/1438/ep05a3_sample.pdf). References to the intra- and inter-assay precision, where known from existing product literature and in published manuscripts, have been included in the relevant sections for each assay.

However, precision also depends on the individual operator, the sample volumes and the specific equipment used to run the analyses (which may vary from laboratory to laboratory). This study was not designed to allow evaluation of the operator-specific precision of the various methods used (respirometry, targeted metabolomic analysis, enzyme activity, plasma redox assays, near-infrared spectrosocopy with a vascular occlusion test). The rationale for this decision was that the primary aim of this thesis was to improve understanding of complex, interrelated process by simultaneous assessment of multiple components, in a

cohort of patients with acute life-threatening illness, using previously validated methods. The requirement for multi-component investigation, using limited tissue samples obtainable from unstable patients without causing harm, determined this approach and limited the amount of sample available for repeats. It was decided that the optimal allocation of resources (including operator time, biological sample and experimental costs) did not allow for specific determination of operator precision for all of the assays in this study.

Choice of the particular assays used were therefore based on well-established techniques already shown to demonstrate adequate sensitivity to detect clinically relevant differences between groups in disease states and adequate intra-laboratory reproducibility in existing literature (143, 144) and within the laboratories of my supervisors, with expertise in the respective fields of mitochondrial function (Dr Andrew Murray) and redox assessment (Prof Martin Feelisch) and microcirculatory function (Dr Daniel Martin), all of whom have published data demonstrating the sensitivity and reliability of the techniques (68, 145–147)

3.2. Respirometry

3.2.1. General principles of respirometry

It is possible to undertake direct, dynamic measurements of mitochondrial respiration within cells or tissues, in real-time, using a technique called high resolution respirometry. Respirometry is the measurement of oxygen consumption rates (J_{O2}) in cells, tissues or organisms (148). J_{O2} is a useful functional marker of mitochondrial activity, because the final step in electron flux through the electron transport system is the consumption of O_2. As J_{O2} is indirectly coupled to ATP synthesis, through mitochondrial oxidative phosphorylation, it represents a proxy measure of bioenergetic activity. J_{O2} can more faithfully reflect respiratory flux within the cell, because, in contrast to other putative indicators of

bioenergetic function, including ATP or NAD^+, oxygen is not produced within the cell. The principle relies on the fact the majority of cellular oxygen consumption occurs through respiration, with a very minor proportion consumed as a substrate for xanthine oxidase and nitric oxide synthase enzymes (17). J_{O2} of biological samples can be accurately quantified within a closed chamber containing a polarographic oxygen electrode. Application of specific combinations of substrates, uncouplers and inhibitors, can isolate different respiratory pathways (149). This technique represents an important approach to assessing mitochondrial bioenergetic function (150). It can be used to detect known mitochondrial defects (151) and has been used to identify mitochondrial functional differences in human disorders (152). In this study of critical illness, where cellular hypoxia is proposed to impair bioenergetic capacity (17), J_{O2} is a particularly relevant aspect of metabolic function.

3.2.2. Cell membrane permeabilisation

In this thesis, respirometry was performed in permeabilised cells. Cell membranes were permeabilised using a detergent (saponin), to create pores in the plasma membrane, by interacting with cholesterol, while leaving the mitochondrial membranes intact (153). This allows endogenous substrates, such as ADP, to be flushed out of the cell, and for specific substrates, uncouplers and inhibitors to reach the mitochondria by diffusion. This approach was chosen over the alternatives (studying intact cells or isolated mitochondria) in order to (1) interrogate the activity of specific respiratory pathways and (2) to functionally characterise the entire population of mitochondria within the sample, within their intracellular context, with cytoskeletal interactions between other organelles preserved (149). Studies of isolated mitochondria are limited by the alterations induced in mitochondrial superstructure and unintended selection of specific mitochondrial subpopulations. Studies of intact cells may represent more physiologically relevant conditions, but permeabilisation allows

substrates, uncouplers and inhibitors to enter the cell and mitochondria in a manner that does not limit J_{O2}, and flushes out endogenous substrates, such as ADP, which would permit constitutive activity of the ATP synthase.

3.2.3. The respirometer

Respirometry was carried out using the Oroboros Oxygraph O2K (Oroboros Instruments, Austria). A schematic of the experimental set up is described in Figure 6. This system consists of a chamber containing respiratory medium to which the biological sample is added. The chamber can be sealed from the atmosphere by closing a stopper (composed of oxygen-impermeable polyether ether ketone). A narrow capillary tube within the stopper allows the injection of chemicals to the medium, to alter the respiratory state of the biological sample. To seal the chamber, the stopper is lowered such that the medium within the chamber meets the gas phase within the capillary, to minimise the surface area for gas exchange. The chamber also contains a magnetic stirrer, to optimise the distribution of oxygen and added chemicals within medium. During experiments, the temperature of the medium is strictly controlled at 37°C as temperature is known to have dramatic effects on all chemical reactions (the Arrhenius principle), including respiration rates.

Figure 6. The respirometer

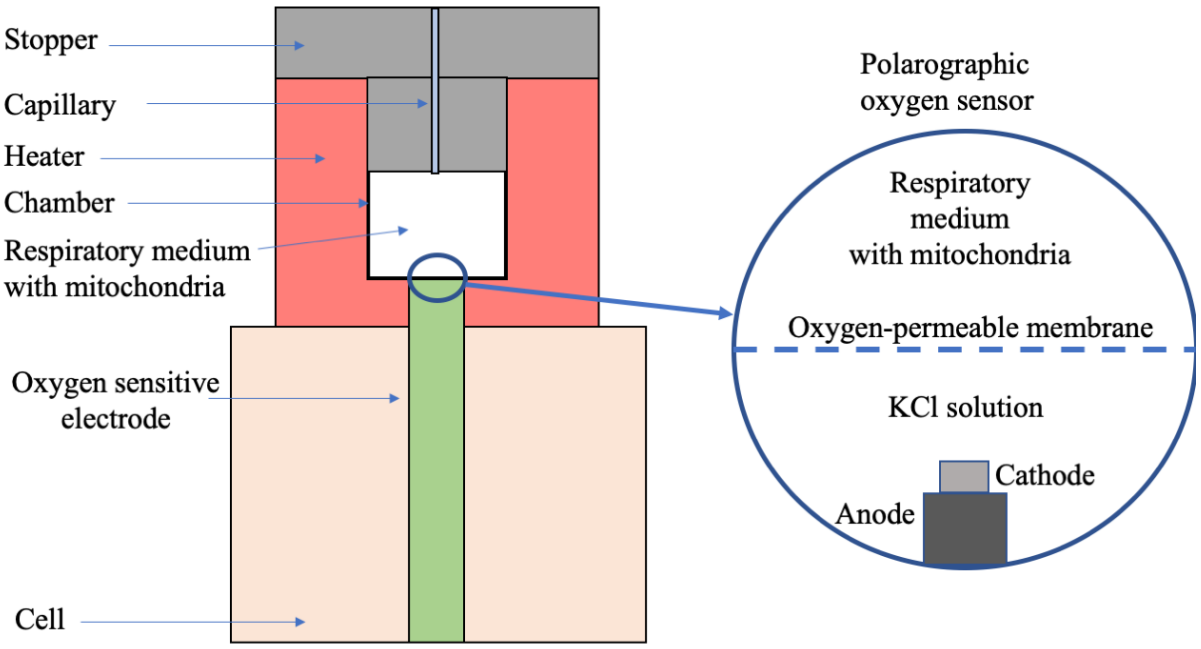

3.2.4. Polarographic oxygen sensing

Oxygen concentration within the chamber is continuously measured by a polarographic oxygen sensor (POS). Polarography is a technique for determining the concentration of specific ions in solution. A potential difference is applied between two sets of electrodes (indicator and reference), connected by an electrolyte. Polarisation occurs, and different anions are discharged at different voltages, and the resulting current is monitored. The graph of current against voltage is used to determine the concentration and nature of the ions. In the POS, the cathode, anode and electrolyte are separated from the analyte medium by an oxygen-permeable membrane. On the passing of a potential difference, oxygen reacts with water at the cathode, while silver in the anode reacts with chloride ions according to Equation 13 and Equation 14. As oxygen is reduced at the cathode, the local oxygen concentration is maintained at zero, and oxygen diffuses from the medium to the cathode resulting in a linear calibration between oxygen partial pressure and electric current.

Equation 13. Reaction at the cathode

$$O_2 + 2H_2O + 4e^- \rightarrow 4OH^-$$

Equation 14. Reaction at the anode

$$4Ag + 4Cl^- \rightarrow 4\mathrm{AgCl} + 4e^-$$

The current generated as a result of these reactions at the anode and cathode varies linearly with oxygen concentration (cO_2), within the experimental range. The measured current can be converted to an estimate of cO_2, using two-point calibration, by measuring the current at two known oxygen concentrations: (1) the oxygen concentration of the medium when in equilibrium with the atmosphere and (2) zero oxygen concentration.

Two-point calibration of the POS

The concentration of oxygen in solution following equilibration with the atmosphere at a given temperature can be calculated using Equation 15. The atmospheric partial pressure of oxygen (PO_2) can be calculated using Equation 16. Using these equations, the cO_2 of distilled water (with known solubility of oxygen, SO_2) allowed to equilibrate with the atmosphere at known barometric pressure and fixed FO_2 (21%) can be calibrated for the first calibration point. For the second calibration point ($cO_2 = 0$), all oxygen is removed, by addition of excess oxygen scavenger (such as sodium dithionite), or metabolically active sample until all oxygen is consumed. Measuring current at the two calibration points and plotting the linear relationship allows the conversion of the measured voltage to cO_2 during experiments. Both the absolute cO_2 and its negative derivative (J_{O2}) are displayed in graphical form in real time using DatLab 6.0 software (Oroboros Instruments, Austria).

Equation 15. Concentration of oxygen in solution, cO_2

$$cO_2 = PO_2 \times SO_2$$

PO_2: partial pressure of O_2 in the atmosphere (kPa); SO_2: solubility of oxygen in solution (a constant, for a given solution at a given temperature).

Equation 16. Atmospheric partial pressure of oxygen, PO_2

$$\boldsymbol{PO_2 = P_{atm} \times FO_2}$$

PO_2: partial pressure of O_2 in the atmosphere (kPa); P_{atm}: barometric pressure (kPa); FO_2: fractional concentration of oxygen (21%).

3.2.5. The substrate-uncoupler-inhibitor titration protocol

J_{O2} of the biological sample was measured during titration of a specific sequence of substrates, uncouplers and inhibitors, added to the chamber at saturating concentrations, to quantity the maximum capacity of different components of mitochondrial respiration. The principles behind the substrate-uncoupler-inhibitor titration (SUIT) protocol are described below.

Leak-supported respiration, LEAK

J_{O2} of the permeabilised cells was first measured in the presence of the respiratory substrates, but in the absence of ADP. Respiratory substrates donate protons and electrons via the TCA cycle (malate, glutamate, pyruvate) and/or FAO (octanoyl carnitine). Redox cofactors, nicotinamide adenine dinucleotide (NAD^+) and flavin adenine dinucleotide (FAD) accept these protons and electrons and donate them to the respiratory complexes. Electron transport along this system, from high to low redox potential, provides energy for the pumping of protons from the matrix into the intermembrane space, generating an electrochemical gradient across the membrane (proton motive force). In the absence of ADP, the ATP synthase is inactive, and protons can only return to the matrix along this gradient by leaking through the membrane itself or slipping through intramembrane proteins (such as uncoupling proteins or the respiratory complexes). Proton leak permits some dissipation of the electrochemical gradient, supporting low level of electron flux through the electron transport system, and oxygen consumption at Complex IV. In this state, J_{O2} is limited by proton leak, and thus reflects oxygen consumption that is not coupled to ATP synthesis. The J_{O2} measured in this state is referred to as "LEAK" and is taken to represent energetically inefficient oxygen consumption (Figure 7).

Figure 7. Schematic representing LEAK respiration

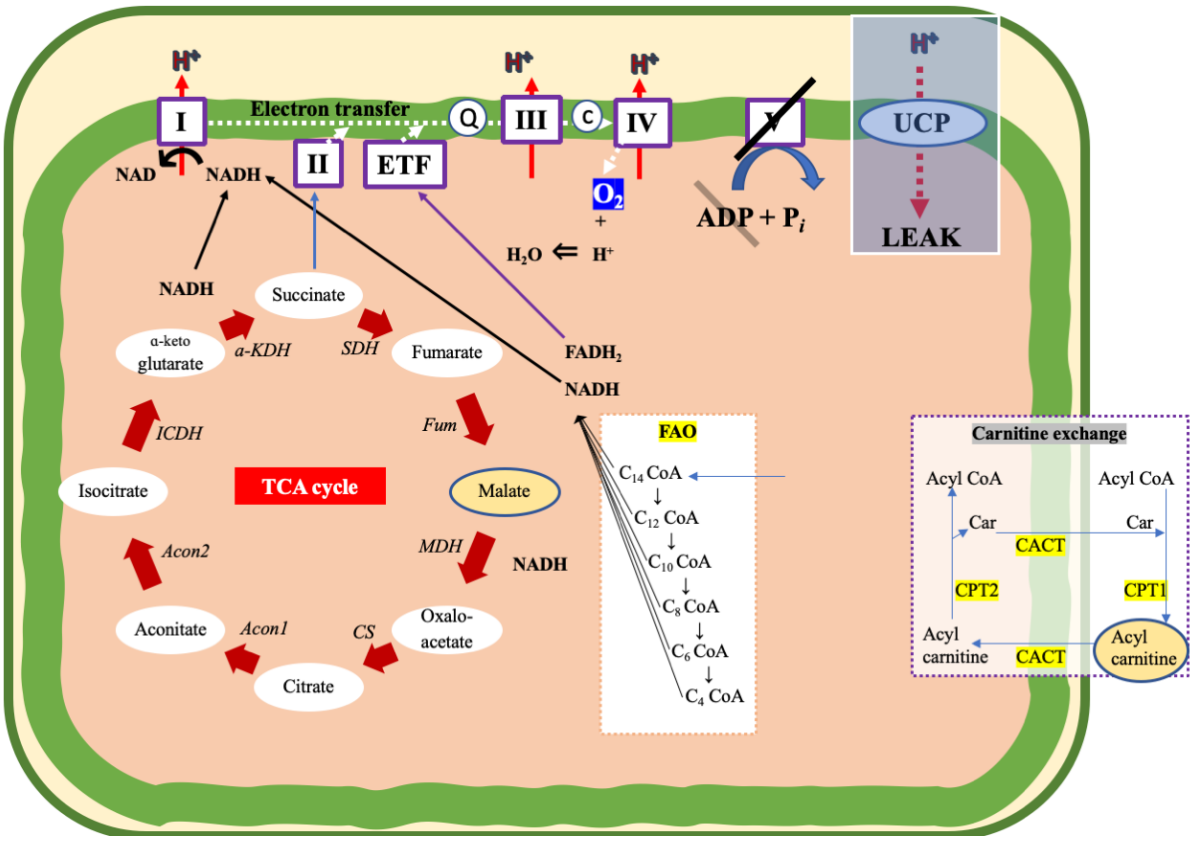

Addition of malate and octanoyl carnitine highlighted in yellow ovals. The process limiting the oxygen consumption rate is demonstrated by the blue box (LEAK). In the absence of ADP, complex V is inactive, and protons re enter the matrix according to the inner membrane permeability, allowing oxygen consumption to continue at a low rate (LEAK respiration).

Oxidative phosphorylation-supported respiration, OXPHOS

Subsequent addition of a saturating concentration of ADP activates the ATP synthase, a path of lower resistance for the return of protons to the matrix. The electrochemical gradient dissipates at a higher rate. Proton leak is no longer the limiting factor to electron flux along the electron transport system and oxygen reduction at Complex IV. In this state, J_{O2} is limited by different components of oxidative phosphorylation (OXPHOS), including (1) electron donation to respiratory complexes, (2) electron flow through the complexes of the electron transport system and/or (3) the capacity of the ATP synthase and nucleotide transporters. The J_{O2} measured in this state is referred to as "OXPHOS" and application of different substrate combinations at saturating concentrations allows us to determine the limitation of OXPHOS exerted by different metabolic pathways and respiratory complexes.

Complex I-supported OXPHOS, $OXPHOS_{CI}$

J_{O2} measured in the presence of saturating concentrations of ADP, malate and glutamate represents OXPHOS supported by electron entry at complex I ($OXPHOS_{CI}$), as shown in Figure 8. Glutamate can enter mitochondria via the electrogenic glutamate/aspartate antiporter, while malate enters through a number of carriers. Malate is driven to produce fumarate, which inhibits complex II by product inhibition. Glutamate can react with oxaloacetate to produce aspartate and alpha-ketoglutarate, which drives the conversion of malate to oxaloacetate, and yielding NADH. The alpha-ketoglutarate is also dehydrogenated to produce further NADH, and NADH is the sole provider of electrons to complex I.

Complex II-supported OXPHOS, $OXPHOS_{CII}$

J_{O2} measured in the presence of saturating concentrations of ADP, succinate and rotenone represents capacity for OXPHOS supported by electron entry at complex II ($OXPHOS_{CII}$), as

shown in Figure 9. Succinate donates electrons to complex II (via $FADH_2$) and rotenone specifically inhibits Complex I.

Fatty acid oxidation-supported OXPHOS, $OXPHOS_{FAO}$

J_{O2} measured in the presence of saturating concentrations of ADP, malate and octanoyl carnitine represents the capacity for OXPHOS supported by β-oxidation of fatty acids ($OXPHOS_{FAO}$), as shown in Figure 10. Octanoyl carnitine is a medium chain (C8) acyl carnitine, which enters the mitochondrion directly via the carnitine-acylcarnitine translocase (CACT). In the matrix, it is converted to acyl CoA by carnitine palmitoyltransferase (CPT2) and undergoes FAO. FAO involves four enzymatic reactions, (dehydrogenation, hydrations and thiolysis), the end products of which are: an acyl CoA ester that has been shortened by two carbon atoms, one acetyl CoA, and two electrons. The process is repeated until only two acetyl coA molecules remain. One liberated electron is passed to $FADH_2$ which feeds into the electron transfer flavoprotein (ETF), and from there to ubiquinone. The other electron is passed to NADH, which feeds into Complex I.

Maximum OXPHOS, $OXPHOS_{MAX}$

J_{O2} measured in the presence of saturating concentrations of malate, glutamate (or pyruvate) and succinate represents the capacity for maximum OXPHOS supported by convergent electron flux from both Complexes I and II ($OXPHOS_{MAX}$), as shown in Figure 11.

Figure 8. Schematic of complex I supported OXPHOS

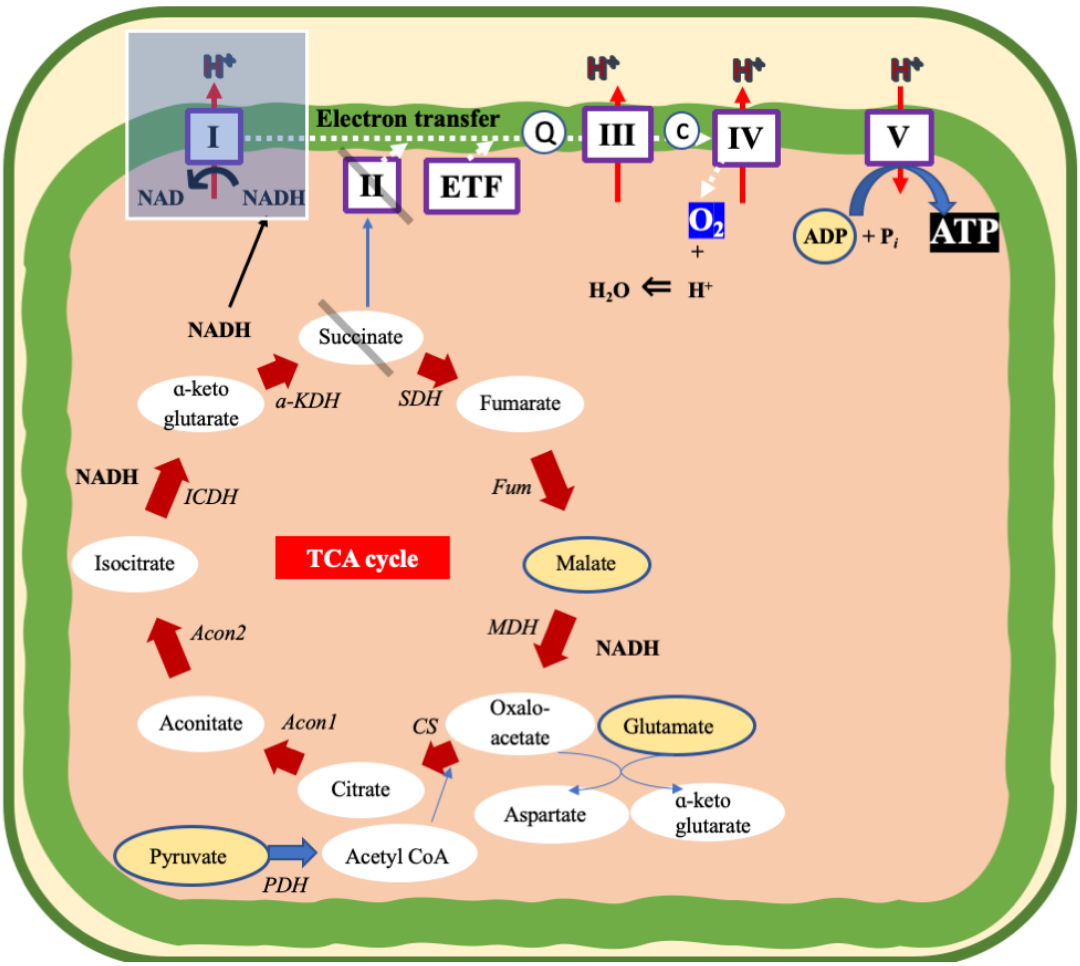

Addition of malate, pyruvate, glutamate and ADP (highlighted in yellow ovals) triggers complex I supported OXPHOS. The process limiting the oxygen consumption rate is demonstrated by the blue box (complex I respiratory capacity).

Figure 9. Schematic of complex II-supported OXPHOS

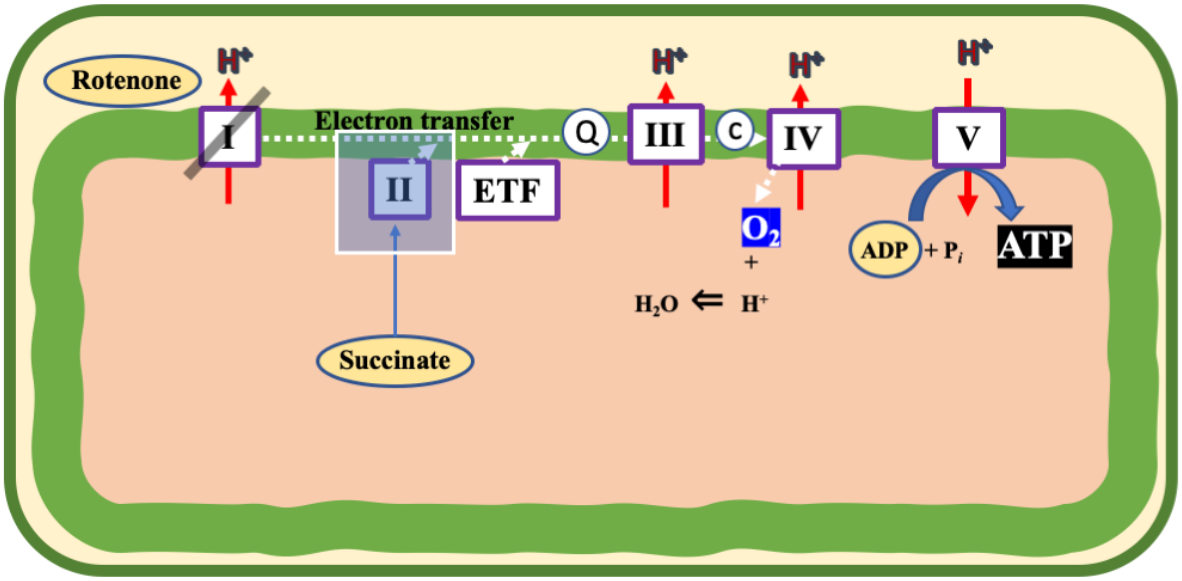

Addition of succinate, ADP and rotenone (highlighted in yellow ovals) triggers complex II supported OXPHOS, whilst inhibiting complex I. The process limiting the oxygen consumption rate is demonstrated by the blue box (complex II respiratory capacity).

Figure 10. Schematic of FAO-supported OXPHOS

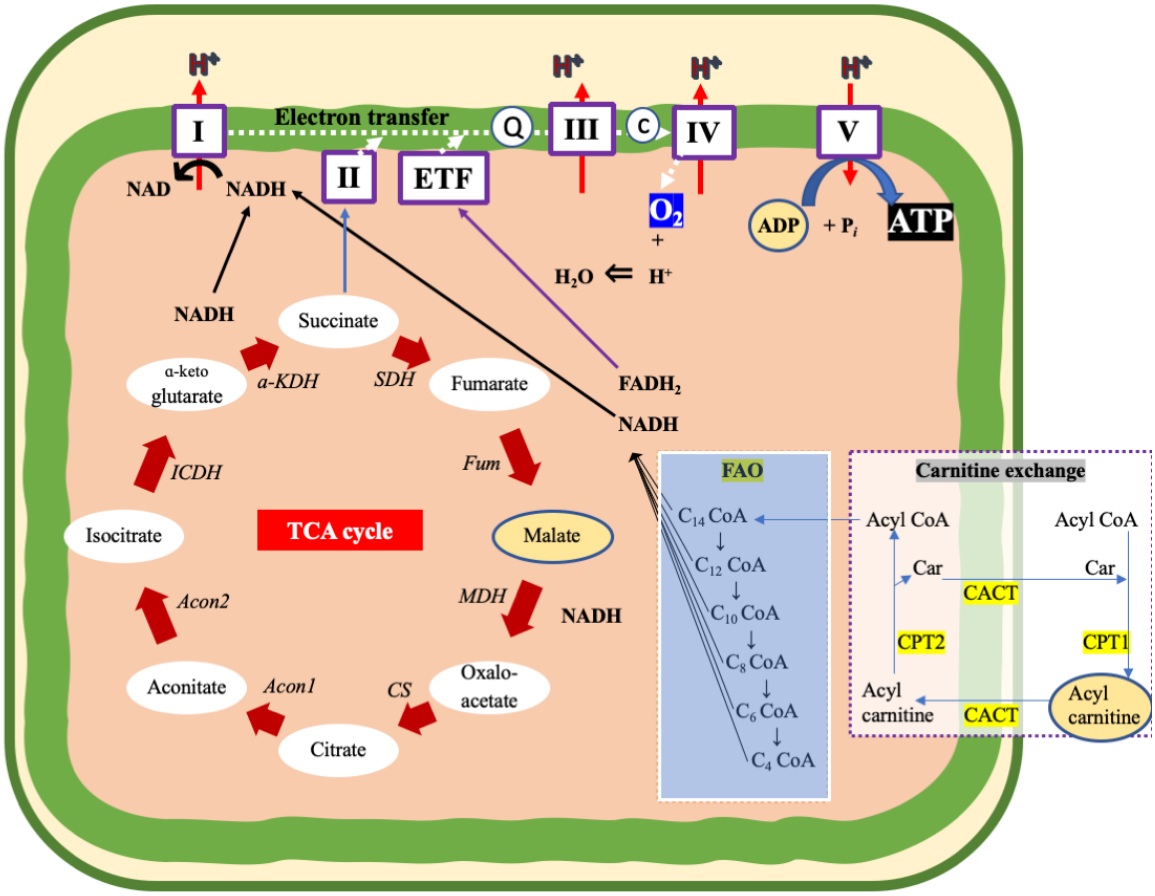

Addition of malate, octanoyl carnitine and ADP (highlighted in yellow ovals) trigger FAO-supported OXPHOS. The process limiting the oxygen consumption rate is demonstrated by the blue box (FAO capacity).

Figure 11. Schematic of maximum OXPHOS

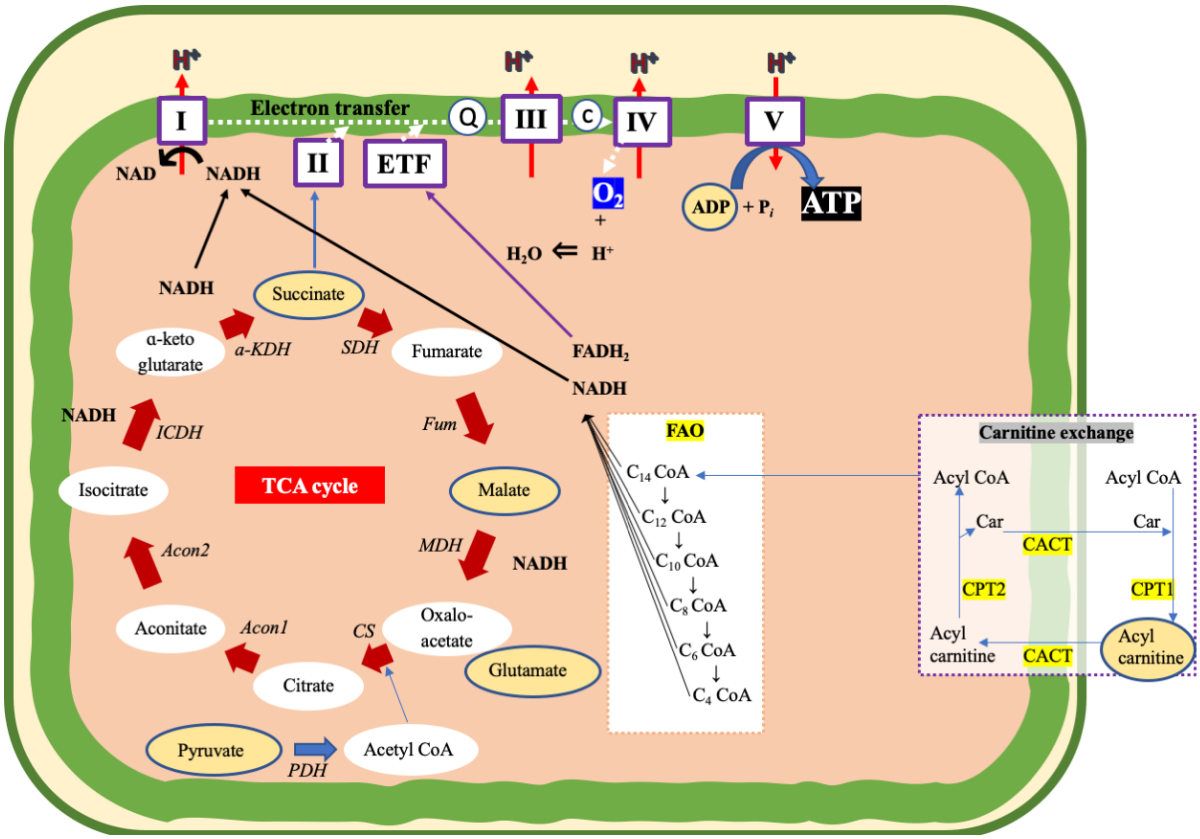

Addition of malate, octanoyl carnitine, pyruvate, glutamate, succinate and ADP (highlighted in yellow ovals) trigger maximum oxidative phosphorylation.

Electron transport system-supported respiration (ETS)

In human muscle, the capacity of the electron transport system to pump protons when Complexes I and II are saturated is greater than the capacity for protons to return to the matrix via the ATP synthase. Addition of a protonophore, carbonyl cyanide p-trifluoro-methoxyphenyl hydrazine (FCCP), allows protons to bypass the ATP synthase. In this state, J_{O2} is limited by electron flux through the electron transport system without limitation from the capacity of the ATP synthase and nucleotide transporters. The J_{O2} measured in this state is referred to as "ETS". ETS supported by individual components (ETS_{CI}, ETS_{CII}, ETS_{FAO}) or maximum capacity supported by complexes I and II together (ETS_{MAX}), can be measured in the presence of the same substrate/inhibitor combinations described for assessing OXPHOS capacities.

Figure 12. Schematic of ETS-supported respiration

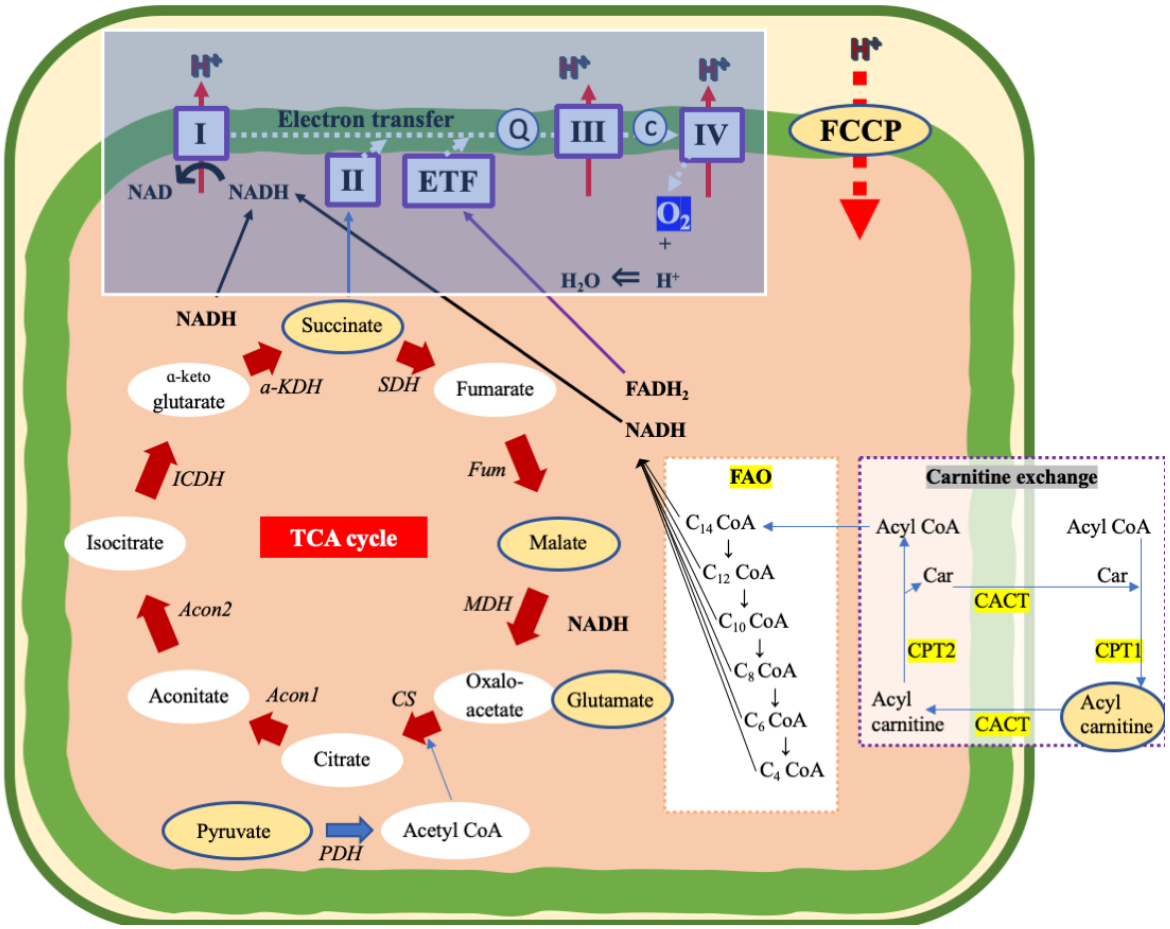

Addition of malate, octanoyl carnitine, pyruvate, glutamate, sucinate and FCCP (highlighted in yellow ovals) trigger maximal electron donation to complexes I, II and the ETF. Protons reenter the matrix via FCCP. Blue box indicates the limiting step for oxygen consumption: the capacity of the electron transport system uncoupled from ATP synthesis.

3.2.6. Study protocol

Sample collection

Biopsies of the *vastus lateralis* muscle were taken from the mid-thigh. In critically ill patients, the biopsy was carried out on the ICU, following local infiltration of local anaesthetic (1mg/kg 1% lidocaine). A 5 mm transverse incision was made in the mid-thigh with a scalpel, and approximately 100 mg of tissue was removed using Tilley-Henkl forceps. Following the biopsy, firm manual pressure was applied to the site for 10 minutes, until haemostasis was achieved. The incision was closed with steristrips and a sterile dressing was applied. In the reference group, the biopsy was performed intra-operatively, a short time after induction of general anaesthetic and following exposure of *vastus lateralis* muscle as part of their planned surgical procedure. Following extraction, the muscle sample was immediately cleared of fat and connective tissue and divided into 4 equal sections using a scalpel. One section (50 mg) was allocated for immediate respirometric analysis and the remaining sections were immediately snap frozen in liquid nitrogen and stored at – 80°C until analysis. The muscle sample for respirometry was immediately placed in ice-cold biopsy preservation medium (BIOPS).

Tissue preparation

Skeletal muscle fibre bundles were prepared from the respirometry-designated sample according to previously described methods (153). The sample of muscle was first separated into fibre bundles, approximately 1 mm in diameter (comprising approximately 6-8 fibres per bundle) Dissection was performed with the muscle tissue submerged in ice-cold BIOPS, under a dissection microscope, using non-metallic dissection forceps (Figure 13). Permeabilisation was achieved by transferring the fibres into ice-cold BIOPS containing 50 μg/ml saponin (Sigma S 7900, prepared fresh) and rocking on ice at 20 rpm for 20 minutes. A quality control test of mitochondrial membrane integrity following this permeabilisation

was carried out during the respirometry protocol (described later). Following permeabilisation, the fibres were washed for by rocking the fibre bundles in 2 ml ice-cold respirometry medium (MIR05) for 5 minutes, in a step that was repeated three times. The permeabilisation and washing steps result in all endogenous substrates (including ADP) being flushed out and replaced with the MIR05 buffer. Following the washing step, 1 to 3 fibre bundles were blotted dry with filter paper, wet weight measured using a microbalance (Mettler-Toledo), before they were added to the Oxygraph chamber.

Figure 13. Mechanical separation of muscle tissue into uniform fibre bundles

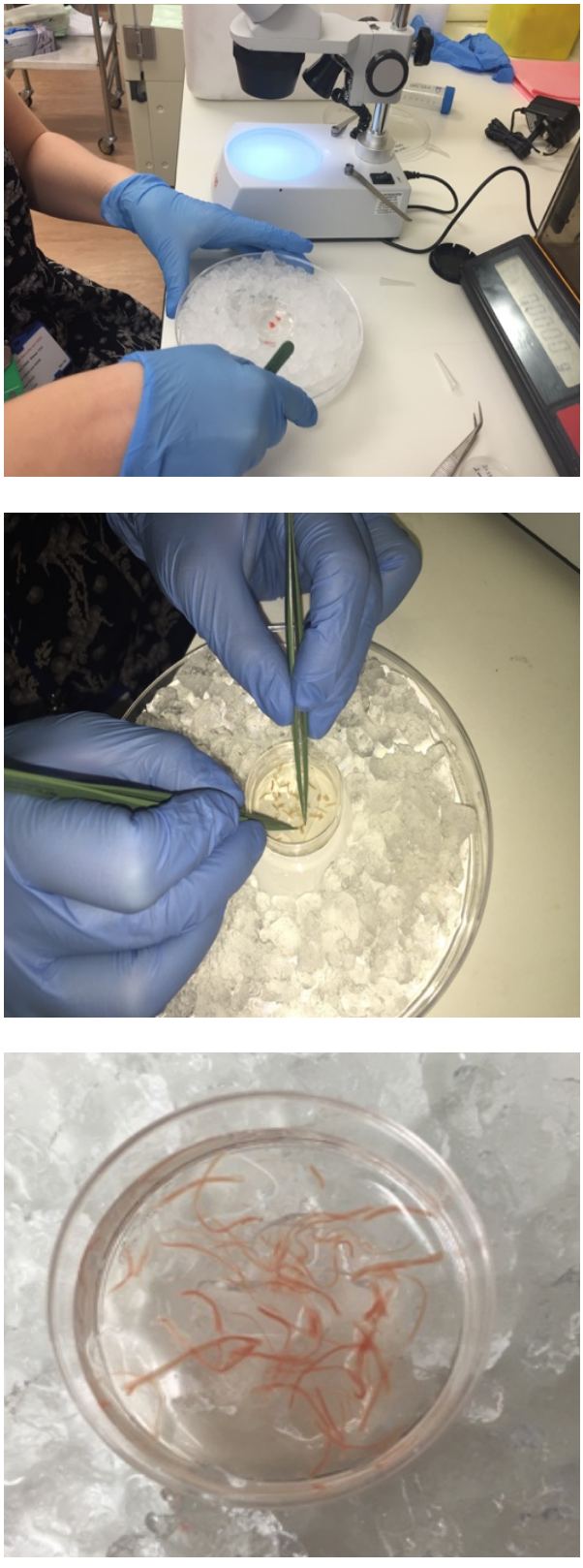

Respirometry set up

The experimental set up is illustrated in Figure 14. Respiration of fibre bundles was measured in mitochondrial respiration medium (MiR05) containing EGTA (0.5 mM), $MgCl_2 \bullet 6H_2O$ (3 mM), K-lactobionate (60 mM), taurine (20 mM), KH_2PO_4 (10 mM), Hepes (20 mM), sucrose (110 mM) and defatted BSA ($1 g.L^{-1}$) at pH 7.4. A volume of 2 ml of MIR05 was added to the chamber, followed by a weighed sample of muscle fibres (1.5-6 mg wet weight). The chamber was then sealed, by closing the stopper, and the oxygen concentration measured continuously and displayed on a laptop screen (blue trace), using the Datlab 6 software (Oroboros Instruments, Innsbruck, Austria). In this closed-system, J_{O2} was calculated by the software as the negative time derivative of the oxygen concentration (red trace). During the experiments, the temperature of the medium was strictly controlled at 37°C. The oxygen concentration of the medium was maintained between 250 and 450 μM throughout the experiment in order to prevent the effect of oxygen diffusion limitation in skeletal muscle. Oxygenation of the medium was achieved by opening the stopper to introduce a gas phase above the medium, into which pure oxygen gas was injected, until the desired concentration was reached and the chamber was closed. J_{O2} was corrected for the background rate of change in oxygen concentration the absence of tissue, which was primarily due to diffusion of oxygen out of the chamber at high medium concentrations.

Figure 14. Respirometry set up

Substrate uncoupler inhibitor titration (SUIT) protocol

Oxygen flux (J_{O2}) of the permeabilised muscle fibres was measured in the presence of a specific sequence of substrates, uncouplers and inhibitors, to quantify the maximum capacity of different components of mitochondrial respiration. The particular protocol used was based on previously reported protocol used to demonstrate changes in human mitochondrial function on acclimatisation to hypobaric hypoxia (68). Individual components of the bioenergetic machinery were isolated, e.g. complex I, II and FAO-supported pathways of electron flow; and leak (LEAK), oxidative phosphorylation (OXPHOS) and uncoupled electron transfer system (ETS) respiratory states.

Saturating concentrations of chemicals were added to the respirometry medium, by injection using dedicated Hamilton microsyringes (Oroboros Instruments, Innsbruck, Austria), in the order shown in Table 7, which also indicates the final concentration of each chemical in the 2 ml chamber. Following injection of each chemical, the J_{O2} was recorded when steady state was reached. All J_{O2} measurements were initially corrected to the wet weight of the sample added to the chamber, and reported as pmol/s/mg. An example trace generated by this protocol is demonstrated in Figure 15.

Malate (2 mM, Sigma M1000) and octanoyl carnitine (0.2 mM, Tocris 0605) were initially added to the respiration medium to simulate the leak-limited respiration (LEAK). This leak-limited respiration was supported by fatty acid oxidation substrates and referred to as $LEAK_{FAO}$. Subsequent addition of ADP (10 mM, Sigma A2754), also at saturating concentration, generated J_{O2} which supported ATP synthesis, but limited by fatty acid oxidation, $OXPHOS_{FAO}$. Addition of pyruvate (20 mM, P2256) and glutamate (10 mM, Sigma G1626) saturated electron entry to complex I ($OXPHOS_{CI}$), and addition of succinate

(20 mM, Sigma S2378) saturated convergent electron flow via complex I and II to the Q-junction ($OXPHOS_{MAX}$). Cytochrome c (10 μM) addition was used as a quality control to confirm outer mitochondrial membrane integrity; all assays with an increase in O_2 consumption of > 15% following cytochrome c addition were excluded from further analysis. Carbonyl cyanide-*p*-trifluoromethoxyphenylhydrazone (FCCP) was used (stepwise titration of 0.5 μM, Sigma C2920) to uncouple oxidative phosphorylation and investigate ETS capacity (ETS_{MAX}). Finally, rotenone was added (0.5 μM, Sigma C2920) to inhibit complex I [and thus FAO] and isolate succinate-linked ETS capacity (ETS_{CII}).

Table 7. SUIT protocol

Respiratory capacity	Isolation of respiratory pathway supporting oxygen flux	Reagents added to chamber
$LEAK_{FAO}$	Proton leak from intermembrane space to matrix, supported by electron entry via fatty acid oxidation, but in the absence of ADP	Malate, 2 mM Octanoyl carnitine, 0.2 mM
$OXPHOS_{FAO}$	Oxidative phosphorylation supported by electron entry via fatty acid oxidation	ADP, 10 mM
$OXPHOS_{CI}$	Oxidative phosphorylation supported by saturating electron entry at complex I	Pyruvate, 20 mM Glutamate, 10 mM
$OXPHOS_{MAX}$	Oxidative phosphorylation supported by convergent electron flow to the Q junction via complexes I and II	Succinate, 10 mM (further addition of ADP to ensure saturation)
Quality control	Test for mitochondrial outer membrane integrity Data discarded if > 15% increase in *JO2*	Cytochrome c, 10 μM
ETS_{MAX}	Electron transfer system uncoupled from ADP phosphorylation, supported by convergent electron flow to the Q junction via complexes I and II.	FCCP (stepwise titration 0.5 μM until inhibitory effect observed)
ETS_{CII}	Electron transfer system, uncoupled from ADP phosphorylation, supported by electron entry via complex II, following inhibition of complex I	Rotenone, 0.5 μM

Figure 15. Representative Oxygraph trace generated by permeabilised muscle fibres during the SUIT protocol

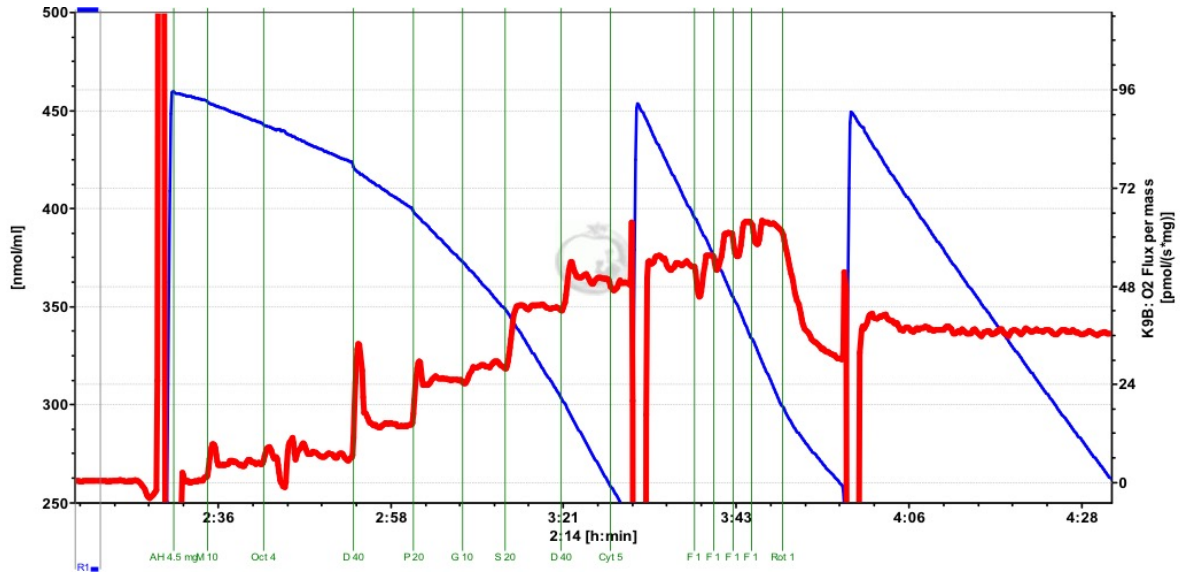

Blue trace indicates the oxygen concentration within the closed chamber (cO_2, nmol/ml on displayed on left X-axis). Red trace indicates the rate of oxygen consumption by the tissue within the chamber (J_{O2}, pmol/s/mg, right X-axis). Green vertical markers indicate the addition of chemicals: M10: malate; Oct4: Octanoyl carnitine; D40: ADP; P20: pyruvate; G10: glutamate; D40: ADP; Cyt5: cytochrome c; F1: titrations of FCCP; Rot1: rotenone. Numbers indicate volume (µL) added to the respirometry chamber to give the desired final concentration noted in Table 7.

Quality control

A single investigator performed all biopsies, preparation and respirometry assays to ensure consistency in technique. All experiments were performed in duplicate, and the results averaged, unless one trace failed to meet the standard for quality control. Confirmation that permeabilisation was successful in removing endogenous substrates, such that their contribution to respiration was negligible, was demonstrated by the observation that muscle fibre respiration rate, prior to addition of exogenous substrates was zero (Figure 16; representative Oxygraph trace). Furthermore, during the SUIT protocol, respiration rates subsequently increased in the manner expected when exogenous substrates were added back in at saturating concentrations. The integrity of the mitochondrial outer membrane following permeabilisation was determined by measuring the increase in respiration rate following the addition of cytochrome c (10 μM); < 15% increase in J_{O2} was taken to demonstrate intactness of the mitochondrial membrane. During the study, only two samples, in one of the two experimental chambers, did not meet this criterion for quality control. The respirometry variables for these samples taken forward for analysis were taken from the single chamber (which did meet this criterion for quality control), rather than averaging the duplicates.

Precision

Precision of the assay, using a similar SUIT protocol with human skeletal muscle, has been reported previously, using six groups and respirometers, using biopsies taken from the same healthy volunteer on three consecutive days (reported as median 100, IQR 90-130) (154). The variation within a group of healthy controls has also been reported previously by my supervisor's group, using an identical protocol to that used in this thesis (68). However, resource allocation (in terms of time, available biological sample, experimental costs) during this thesis did not allow the specific operator precision to be assessed according to the

standards required to validate the reproducibility of the technique (142). In particular, the number of simultaneous experimental runs using the same muscle sample would not feasible for one operator using high resolution respirometry. Within the laboratory, there was only one Oxygraph, with two chambers, such that only two assays can be run at a time. Assays require the continuous presence of an operator, to establish when steady-state oxygen consumption rates have been achieved and inject the subsequent chemical in the SUIT protocol, and the protocol may take 2-3 hours. Cleaning and recalibrating the instrument between runs requires an additional 2 hours, to ensure that inhibitors are completely removed between experimental runs. It has been shown that this amount of time *ex vivo* muscle alters the respirometry findings (149). Within the field of high resolution respirometry, collaboration is ongoing to establish the inter-laboratory reproducibility of this technique (155). In line with the aims of this thesis, high resolution respirometry was chosen as a technique to allow exploration of individual components of respiration.

Normalisation of skeletal muscle J_{O2} to mass of muscle fibres

J_{O2} was first corrected to the wet mass of the muscle fibres added to the chamber to assess respiratory capacity per mass (pmol/s/mg tissue). Thus, oxidative phosphorylation capacity and electron transfer system capacity were expressed per mg tissue ($OXPHOS_{MAX}$ and ETS_{MAX} per mg, respectively).

Flux control ratios

Flux control ratios were calculated to estimate the proportional contribution of various components of the mitochondrial system to total respiratory capacity. In this thesis, J_{O2} measured in each respiratory state was divided by the maximum uncoupled respiratory

capacity (ETS_{MAX}), with ETS_{MAX} taken to represent a functional marker of mitochondrial density.

Oxphos coupling efficiency

Oxphos coupling efficiency (OCE) is used as a measure of the extent of coupling of O_2 consumption to ATP synthesis (see section), where OCE = 1 for a fully coupled system (156). OCE is calculated as the ratio of free to total OXPHOS capacity, where free OXPHOS capacity represents the maximum OXPHOS capacity after correction for LEAK respiration (Equation 17).

Equation 17. Oxphos coupling efficiency, OCE

$$OCE = OXPHOS_{MAX} - LEAK_{FAO}/OXPHOS_{MAX}$$

3.3. Characterisation of related metabolic pathways

In order to further characterise cellular bioenergetics, interdependent metabolic pathways in the muscle were also investigated, in a section of the muscle sample snap frozen at the time of the biopsy, to allow contemporaneous assessment alongside the direct measurements of mitochondrial respiratory capacities.

3.3.1. Enzyme activities as markers of flux through specific metabolic pathways

Adjustment of enzyme activity levels can alter the rate or efficiency of a specific metabolic pathway, and also regulate the extent to which that pathway is used. Previous studies have demonstrated that metabolic enzyme activities can be modified by exposure to cellular hypoxia (157). In this study, citrate synthase activity was assessed as a marker of TCA cycle flux, and the β-oxidation enzyme, 3-hydroxy acyl dehydrogenase (HADH) as a marker of FAO flux.

Citrate synthase activity

Citrate synthase acts a pacemaker enzyme in the TCA cycle as it catalyses the first reaction: the condensation of acetyl CoA and oxaloacetate to form citrate. Citrate synthase is inhibited by high ratios of ATP:ADP and NADH:NAD, which indicate energy supply is high for the cell. It is also inhibited by succinyl-CoA, which acts as a competitive inhibitor to acetyl CoA, and a non-competitive inhibitor to oxaloacetate. Citrate synthase activity was thus measured as an indicator of flux through the TCA cycle.

Mitochondria are dynamic organelles, constantly undergoing fission and fusion such that determination of their number or volume per sample is difficult or even impossible. Citrate synthase is localised in the mitochondrial matrix and is therefore commonly used as a

putative marker for the content of intact mitochondria (158). In pathological states associated with increases in mitochondrial number, citrate synthase activity per cell has been shown to increase, and when citrate synthase activity is expressed per mitochondrial protein or respiratory capacity, it remains constant (159). However, citrate synthase is encoded by the nucleus, and synthesised in the cytoplasm before being transported to the mitochondria, and its reliability as an indicator of mitochondrial density has been questioned in a number of contexts, including studies of the effects of physical training (160), cardiac disease (161) and aging (162). It has been proposed that cellular or tissue respiration may be expressed per citrate synthase activity under specific circumstances (163) (164). In this study, in addition to normalising skeletal muscle fibre J_{O2} to mass of tissue, and to ETS_{MAX} (as a marker of functional mitochondria density), J_{O2} was also expressed relative to the mass-specific citrate synthase activity in a sample of muscle from the same biopsy.

3-hydroxy acyl dehydrogenase

The enzyme, 3-hydroxy acyl dehydrogenase (HADH) has been used as an indicator of FAO capacity (157). HADH is an oxidoreductase enzyme which catalyses the third step in β-oxidation, the oxidation of L-3-hydroxyacyl CoA by NAD^+ to produce 3-ketoacyl CoA, NADH and H^+ (165). This enzyme contributes to several important metabolic pathways, including FAO and degradation of branched chain amino acids (valine, leucine and isoleucine).

3.3.2. Spectrophotometry

Enzyme activity was assessed by quantifying changes in the absorbance of light at specific wavelengths over time using a spectrophotometer (Evolution 220; Thermo Scientific). Samples were added to the assay buffer and warmed to 37 °C for 3 minutes and the

absorbance of light at the wavelength at the wavelength of interest measured every 5 s for 3 minutes (the background rate). The reaction was then initiated and the rate of change of absorbance recorded once the reaction had reached steady state. The background rate was then subtracted from the reaction rate to calculated the enzyme-dependent rate of absorbance change. Enzyme activity was then calculated using Equation 18.

Equation 18. Calculation of enzyme reaction rates from rate of absorbance change

$$J = \frac{r(A)\ x\ V}{L\ x\ \varepsilon}$$

J: rate of reaction (μmol min^{-1}); r(A): rate of absorbance change (min^{-1}); V: reaction volume (ml); L: light path length (cm); ε: extinction coefficient (ml $\mu mol^{-1}cm^{-1}$). The extinction coefficients for DTNB and NADH were 13.6 and 6.22 ml $\mu mol^{-1}cm^{-1}$ respectively.

Homogenisation of tissue for enzyme assays

Approximately 10 mg of the vastus lateralis muscle sample from each individual was homogenized with an Eppendorf pestle in an Eppendorf tube homogenisation buffer containing Hepes (20 mM), EDTA (1 mM), and Triton X-100 (0.1% vol/vol). The samples were then centrifuged (380 × *g*, 30 s, 4 °C), and the supernatant was collected. This supernatant was centrifuged again (380 × *g*, 30 s, 4 °C), and the resulting supernatant was collected to obtain a homogeneous suspension.

3.3.3. Citrate synthase assay

Citrate synthase activity was measured as described previously (166). The assay uses the following reactions to assess the activity of the citrate synthase enzyme:

Reaction 1: $Acetyl\ co-SH + Oxaloacetate + H_2O \rightarrow coA-SH + Citrate$

Reaction 2: $coA-SH + DTNB \rightarrow TNB\ coS-S-TNB^{2-}$

Reaction 1 is catalysed by citrate synthase, and its rate is dependent on the citrate synthase activity of the sample. Reaction 1 is coupled to Reaction 2, which is irreversible, and results in the production of TNB^{2-}. This is quantified by measuring the change in absorbance of light at a wavelength of 412nm. The assay was performed in a spectrophotometer (Evolution 220, ThermoScientific) at 37°C in a reaction volume of 1ml. The muscle homogenate was added at a volume of 5 µl to a quartz microcuvette, containing a micro-stirrer, to which was added (925 µl) citrate synthase assay buffer containing 20 mM Tris (Fisher BP152-1), 0.1 mM 5,5'-dithiobis-nitrobenzoic acid (DTNB) and a saturating concentration (0.3-0.6 mM) of acetyl CoA (Sigma A2056) at pH 8.0. The mixture was warmed to the reaction temperature of 37 °C. After 3 min, baseline absorbance was measured over 180 s (absorbance set to 412 nm, with 3 rate calculations, 0 – 60 s, 60-120 s, 120 – 180 s, intervals set to 5 s). A baseline rate was recorded for 3 minutes, before the reactions were initiated by addition of 0.5 mM oxaloacetate (Sigma 04126), and the absorbance change was measured after 10 s at a wavelength 412 nm. To check saturation was reached, an extra 50 µl oxaloacetate was added for the first few samples. No improvement in absorbance was observed, therefore only one addition was used for the remaining samples. This value was corrected to the protein concentration of the homogenate measured using the Quick Start protein assay (Bio-Rad), to give the specific activity of citrate synthase.

3.3.4. 3-hydroxy acyl dehydrogenase assay

Activity of the β-oxidation enzyme, 3-hydroxy acyl dehydrogenase (HADH) was assayed as described previously (69). This assay uses the reaction in Equation 19 to assess the activity

of the HADH enzyme, as this reaction is catalysed by HADH, and thus the rate of consumption of NADH is dependent on the HADH activity of the sample.

Equation 19. The reaction catalysed by HADH

$$Acetoacetyl\ coA + NADH + H^{+} \rightarrow 3 - hydroxyacyl\ CoA + NAD^{+}$$

The rate of consumption of NADH is quantified by measuring the absorbance change at a wavelength of 340 nm. The assay was performed in a spectrophotometer (Evolution 220, ThermoScientific) at 37°C in a reaction volume of 1ml. A 20 µl volume of the homogenate was added to a quartz microcuvette, containing a microstirrer and 960 µl HADH assay buffer containing 50 mM imidazole (Sigma 56750), 0.15 mM NADH (Sigma N8129) and Triton X-100 (0.1% v/v) at pH 7.4. The reaction was initiated through the addition of 0.1 mM acetoacetyl coA (Sigma A1625) and absorbance change measured at a wavelength of 340 nm. To check saturation was reached, an extra 0.1 mM acetoacetyl coA was added to the first few samples. No improvement in absorbance was observed therefore only one addition was used for subsequent samples. The absorbance value was corrected to the protein concentration of the homogenate measured using the Quick Start protein assay (Bio-Rad), to give the specific activity of HADH.

3.3.5. Protein quantification using the Bradford assay

The protein concentration was measured using the Quick Start Bradford protein assay (Bio-Rad). This assay works on the principle that Coomaisse Blue is deprotonated in the presence of proteins, leading to a detectable colour change with a maximal absorbance at 595nm. Eight standard protein concentrations of bovine serum albumin (BSA) were made (from 0 to 2 mg/ml) by dilution in homogenisation buffer. The skeletal muscle homogenate was diluted

by placing 1 µl in 19 µl of homogenisation buffer. A volume of 200 µl Bradford quickstart dye reagent (Bio-rad) was added to each well of the 96 well plate. To this, 5µl of the standards or samples were added to each well, in duplicate. The plate was incubated at room temperature for 5 min before absorbance was read using a microplate spectrophotometer (ELx800, BioTek). The protein concentrations of the samples were then calculated using the equation generated from the linear line of best fit through the readings from the standard curve. The enzyme activity levels in the two enzyme assays were then corrected to this protein concentration, to give specific activity levels, the final output reported in the results.

3.3.6. Data processing

All enzyme activity assays were performed in duplicate. If the difference between the first and second runs was greater than 15%, a third run (second repeat) was performed. A number of factors contribute to the calculation of activity, including: rate, light absorbance wavelength, sample dilution and protein concentration.

Precision

The operator specific inter- and intra-assay precision for the enzyme and protein assays technique were not demonstrated in this thesis, due to restrictions on time, availability of biological sample and experimental costs. The techniques themselves have previously been validated and widely used in published literature (68, 69, 166).

3.4. Metabolomic profiling in skeletal muscle

To further characterise the effects of adjustments in mitochondrial respiratory capacity and metabolic enzyme activity, the intermediates of specific metabolic pathways were also assessed in the tissue, including: glycolysis, the TCA cycle, FAO and amino acid oxidation. Individual intermediates, and their ratios to each other can influence mitochondrial and enzyme function. Relative changes in the levels of related intermediates can give an indication of flux through metabolic pathways, or specific bottlenecks within them. Targeted metabolomic analysis of skeletal muscle was carried to quantify the following metabolic intermediates.

Energetic markers

Mitochondrial oxidative phosphorylation converts ADP to ATP, which is temporarily converted to phosphocreatine (PCr) by creatine kinase, in order to buffer ATP concentrations within the cell. Levels of ATP and PCr have been used as indicators of the bioenergetic status of the cell. The ratio of [PCr]/[ATP] was used as a marker of the phosphate transfer activity of creatine kinase, while the [ATP]/[ADP] ratio was used as a marker of oxidative phosphorylation. GTP is synthesised from GDP by succinyl CoA synthetase of the TCA cycle. The [GTP]/[GDP] ratio was also used as a measure of energetic status. Energy charge (an estimate of energy flux (167)), was calculated according to Equation 20.

Equation 20. Energy charge

$$Energy\ charge = [ATP] + \frac{0.5\ [ATP]}{[ATP] + [ADP] + [AMP]}$$

Redox status

Reduced glutathione (GSH) and methionine (Met) residues are known to scavenge reactive oxygen species (ROS) such as hydrogen peroxide, resulting in the generation of their oxidised counterparts, oxidised glutathione (GSSG) and methionine sulfoxide (MetSO), as shown by Equation 21 and Equation 22. The ratios of the oxidised form to the reduced form of these antioxidants: [GSSG]/[GSH] and [MetSO]/[Met], were used as indicators of cellular oxidative stress.

Equation 21. Oxidation of glutathione by hydrogen peroxide

$$2GSH + H_2O_2 \rightarrow GSSG + 2H_20$$

Equation 22. Oxidation of methionine by hydrogen peroxide

$$A - (CH_2)_2 - S - CH_3 + H_2O_2 \rightarrow A - (CH_2)_2 - SO - CH_3 + H_2O$$

A: the basic amino acid structure

Glycolytic intermediates

Levels of the following intermediates of glycolysis were measured: glucose-6-phosphate, fructose-6-phosphate, dihydroxyacetone phosphate, 2- and 3-phosphoglycerate combined, pyruvate. The sum of all glycolytic intermediates was used as an indicator of glycolytic flux.

TCA cycle intermediates

Levels of the following TCA intermediates were measured: citrate, aconitate, isocitrate, α-ketoglutarate, succinate, fumarate, malate and oxaloacetate.

Amino acids

Levels of the following amino acids were measured: ornithine, glutamine, glutamate, proline, aspartate, asparagine, as well as the branched chain amino acids (BCAAs); valine, isoleucine and leucine.

Acyl carnitines

Levels of acyl carnitines and free carnitine (carbon chain length, C = 0), were measured. Carnitines were then grouped into free carnitine, short chain (carbon chain length (C1-6), medium chain (C7-15) and long chain (C > 15). The sum of the levels of the carnitine groups was then expressed as a ratio to the sum of the level of total carnitines (total acyl plus free).

3.4.1. Ultra-high performance liquid chromatography mass spectroscopy

Metabolite analysis was carried out using ultra-high performance liquid chromatography mass spectrometry as described previously (168, 169). Mass spectrometry works on the principle of ionising a sample, accelerating the resultant fragments and subjecting them to a magnetic field. The deflection of the fragments within this field is proportional to their mass/charge ratio (*m/z*), and the relative abundance of compounds is quantified against *m/z.* Spectra generated from metabolites of interest are collected together with standards, such that peaks at a given *m/z* can be identified. The identification of metabolites is based on the *m/z* and retention times of metabolites in (listed in Appendix 2). These protocols had previously been optimised by James West for the detection of the metabolites in question, by infusing standards of every analyte of interest, from which *m/z* and retention times were determined. Reproducibility within the run was determined by multiple additions of stable labelled internal standard, to demonstrate consistency over time; as well as assessing the consistency of the internal standards over time. A chloroform/methanol extraction was performed on

snap frozen skeletal muscle (~30mg) as described previously (68), followed by ultra-high performance liquid chromatography mass spectrometry (168, 169). The aqueous phase was analysed using normal and reverse phase analysis. The aqueous and organic fractions were combined for carnitine analysis. The protein pellet was re-suspended in RIPA buffer (Thermo Scientific) containing protease inhibitor (Roche) and protein concentration determined using a bicinchoninic acid (BCA) assay (BCA1-1KT, Sigma). Data were processed using the Vendor software and normalized to the intensity of internal standards.

3.4.2. Extraction protocol

For mass spectroscopy of the skeletal muscle, a chloroform/methanol extraction protocol (Folch extraction) was performed (170). Samples were kept cold throughout, on dry ice, with utensils cooled in liquid nitrogen. First 20 – 90 mg of the frozen skeletal muscle was weighed out and added to a 2 ml cryovial, and 600 µl ice cold chloroform:methanol (2:1) was added followed by a cooled metallic (silver) bead. Samples were lysed in a tissue lyser (Quagen, 10min, 10 s^{-1}) and sonicated for 15 min. The process was repeated until complete lysis was achieved. The metallic bead was removed prior to the addition of 200 µl chloroform and 100 µl distilled water (1:1). Samples were thoroughly vortexed and then centrifuged (13 000 rpm/ 20, 000 x *g*) for 7 min, resulting in clear separation of an upper aqueous phase, a middle protein pellet and a lower organic phase. The aqueous and organic fractions were extracted using a positive displacement pipette and transferred to separate Eppendorf tubes. For the protein pellet remaining, a double extraction was subsequently performed to ensure full metabolite recovery. This process involved repetition of the extraction steps described above with the same solvent volumes. The separate fractions were added to the original fractions. The aqueous fraction was dried using a vacuum centrifuge (Brake off, mode V-AQ for 2 hours at a time). The organic fraction and protein pellet were

dried under nitrogen and stored at – 80 °C until further processing. This was then reconstituted in 10 mM ammonium acetate (NH_4OAc) in the following volumes:100 µL for less than 30 mg wet weight; 200 µl for 30-60 mg; 300 µl for greater than 60 mg, and vortexed. Extraction efficiency has previously been established using this method by the laboratory, by spiking raw sample with labelled internal standards and determining percentage recovery. These protocols had been optimised by James West, demonstrating the recovery of metabolites close to 100% for a double extraction.

3.4.3. Aqueous metabolite analysis

Reverse phase analysis was performed as described previously (168). Before the analysis, samples were reconstituted in 0.1mL of a 10mM ammonium acetate water solution containing a mixture of 8 internal standards at the concentration of 10µM (Proline, Valine D8, LeucineD10, Lys U13, Glutamic acid C13, Phen D5, Succinic acid D3, Serotonine D4). Normal phase analysis was performed using a Thermo scientific $UHPLC^+$ series coupled with a TSQ Quantiva mass spectrometer (Thermo fisher scientific, Waltham, Massachusetts, United States) was used with an ESI source, operated in positive and negative ion mode at the same time. The electrospray voltage was set to 3500 V for the positive ionisation and to 2500 V for the negative ionisation. Nitrogen at 48 mTorr and 420 °C was used as a drying gas for solvent evaporation. The organic phases were analysed with a BEHAmide (150 x 2.1 mm 1.7µm) column. The column was conditioned at 30°C. The mobile phase consisted of: (A) a 0.1% of ammonium carbonate water solution and (B) an acetonitrile solution. The mobile phase was pumped at a flow rate of 600 µL/min programmed as follows: initially stayed at 20% of A for 1.50 min, then was subjected to a linear increase from 20% to 60% of A in 2.5 min and kept at this percentage for one minutes and then brought back to initial condition after 0.1 min. Xcalibur software (Thermo fisher scientific, Waltham, Massachusetts, United

States) was used for data acquisition. Putative recognition of all detected metabolites was performed using a targeted MS/MS analysis. Before the analysis, samples were reconstituted in 0.1mL of a acetonitrile:10mM ammonium carbonate water solution (7:3 v/v) containing a mixture of 3 internal standards at the concentration of 10µM (Glutamic acid C13, Succinic acid D3 and AMP).

3.4.4. Carnitine analysis

Samples were prepared as described previously (68). A Thermo scientific UHPLC^{+} series coupled with a TSQ Quantiva mass spectrometer (Thermo fisher scientific, Waltham, Massachusetts, United States) was used with an ESI source, operated in positive and negative ion mode at the same time. The electrospray voltage was set to 3500 V for the positive ionisation and to 2500 V for the negative ionisation. Nitrogen at 48 mTorr and 420 °C was used as a drying gas for solvent evaporation. The organic phases were analysed with an ACE Excel 2 C18 PFP (100A. 150 x 2.1 mm 5µ) column. The column was conditioned at 30°C. The mobile phase consisted of: (A) a 0.1% of formic acid water solution and (B) a methanol solution. The mobile phase was pumped at a flow rate of 0.450 µL/min programmed as follows: initially stayed at 0.5% of B for 1. min, then was subjected to a linear increase from to 100% of A in 9 min and kept at this percentage for two minutes and then brought back to initial condition after 0.1 min. Thermo Scientific Xcalibur software was used for data acquisition. Putative recognition of all detected metabolites was performed using a targeted MS/MS analysis. Before the analysis, samples were reconstituted in 0.1mL of a methanol: water solution (4:1 v/v) containing a labelled carnitine standard set B mix solution (CN, C2, C3, C4, C5, C8, C14, C16).

3.4.5. Protein quantification using Bichnoninic acid assay

The concentration of protein in the sample pellet remaining after extraction was assessed using the BCA protein assay kit (Sigma BCA-1KT). Peptide bonds in protein reduce Cu^{2+} to Cu^{+} in a concentration dependent manner. Single Cu^{+} ions are chelated by BCA, producing a water-soluble complex which absorbs light at a wavelength of 562 nm, measured using a spectrophotometer. The dried sample pellet was reconstituted in a reagent made from 50 ml of RIPA buffer (Thermofisher 89900) with a protease inhibitor tablet (Complete Protease Inhibitor Cocktail, Roche) in a falcon tube. The volume of this solution added depended on the weight of the pellet (300 µl for < 30mg; 450 µl for 30-60 mg; 600 µl for > 60 -75 mg; 750 µl for 75-90 mg and 900 µl for > 90 mg). The mixture was vortexed and sonicated for 15 min at a time until reconstituted. A volume of 25 µl of this sample, or one of 9 standard protein concentrations (from 0 to 1000 µg/ml), was added to 175 µl of the working reagent (50:1 Reagent A:B). The mixture was placed on a plate shaker for 20 minutes at room temperature, until colour change was observed. Absorbance was measured at a wavelength of 562 nm. Each standard and sample was performed in duplicate. Sample protein concentrations were then generated from the linear line of best fit through the readings from the standard curve across a range of concentrations from 0 – 2 mg/ml.

3.4.6. Data processing

Data were processed using the Xcalibur (Vendor) software. The factor taken forward for analysis is the peak area ratio for the metabolite in question. The location of the peak was confirmed though the use of internal standards. Correct peak selection was then confirmed manually. BEH-amide column and C18 columns were used for analysis of particular analytes, depending on their chemical composition. The peak area ratio was then corrected to

sample weight, and to protein concentration of the sample pellet. The latter was then presented as a ratio to control.

3.5. Plasma redox status

A complementary approach was used to determine composite measures of oxidative stress and reductive capacity in plasma samples. The following assays quantified different aspects of plasma redox status using spectrophotometric methods. All samples and standard solutions were assayed under identical conditions, in triplicate, and the mean and covariance were calculated, to determine the reproducibility of the data.

3.5.1. Plasma antioxidant capacity

Antioxidant capacity of plasma was quantified using the ferric reducing ability of plasma (FRAP) assay, which has been described previously (171). This assay is based on the principle that the reduction of ferric (Fe^{3+}) to ferrous (Fe^{2+}) ions at low pH results in the formation of an intense blue-coloured ferrous-tripyridyltriazine complex with a maximum absorption at 593 nm, according to Equation 23.

Equation 23. Reduction reaction for FRAP assay

$$[Fe^{3+}(TPTZ)_2]^{3+} \rightarrow [Fe^{+}(TPTX)_2]^{2+}$$

FRAP in the biological sample is quantified by comparing the absorbance of the reacted sample at 593 nm with a calibration curve plotting the absorbances of standard solutions of different known concentrations of ferrous ions. The standards were measured in the same plate as the samples.

Preparation of reagents and samples

The FRAP reagent was prepared by addition of stock solutions of 2,4,6-Tris(2-pyridyl)-s-triazine (TPTZ, 10 mM), iron (III) chloride ($FeCl_3$, 20 mM) and sodium acetate trihydrate

buffer (300 mM, pH 3.60) in a volume ratio of 1:1:10. Preparation of the reagents and stock standard solution is described in Table 8. Plasma samples were spun at maximum speed in a high speed centrifuge (Eppendorf Centrifuge 5415D) for 5 minutes to ensure all particles were pelleted at the bottom of the tube. A volume of 10 μL of the clear supernatant (the sample solution) was then diluted in 30 μL of ultrapure water.

Preparation of standard solutions

The linearity of response for iron (II) sulphate has been demonstrated from 50 to 700 μM. Standards of the following concentration were prepared from the stock solution of 10 mM iron (II) sulphate heptahydrate, according to the protocol in Table 9.

Table 8. Preparation of reagents for FRAP assay

Reagent	Components	Amount added to solvent
HCl 40 mM	Hydrochloric acid, 37%	330 mL in 770 ml ultrapure water
TPTZ 10 mM	2,4,6-Tris (2-pyridyl)-s-triazine	0.0062 g in 2 ml 40 mM HCl
Acetate buffer 300 mM (pH 3.6)	Sodium acetate trihydrate ($C_2H_3NaO_2.3H_2O$)	3.1 g in 16 ml glacial acetic acid (Fisher Scientific) and made up to 1 L in ultrapure water
Iron (III) chloride solution 20 mM	$FeCl_3$	0.0065 g in 2 ml acetate buffer
FRAP reagent	TPTZ, 10 mM $FeCl_3$, 20 mM Acetate buffer, 300 mM (pH 3.6)	Added together according to the volume ratio 1:1:10
Iron (II) heptahydrate standard 10 mM	$FeSO_4.7H_2O$	0.0056 g in 2 ml ultrapure water

Table 9. Preparation of standard solutions for the FRAP assay

Standard concentration $[Fe^{2+}]$ (μM)	Volume of stock solution (10 mM $FeSO_4.7H_2O$) (μL)	Volume of ultrapure water (μL)
0 (blank)	0	1000
50	5	995
100	10	990
150	15	985
200	20	980
250	25	975
300	30	970
350	35	965
400	40	960
500	50	950
600	60	940
700	70	930

FRAP assay

To each well of the flat bottom 96 well plate was added 15 μL ultrapure water, and 5 μL of either (1) sample solution, (2) a standard solution or (3) ultrapure water (blank). Finally, 150 μL of the FRAP reagent was added to each well. The plate was placed immediately in the plate reader and incubated at 37°C for 30 minutes, before the absorbance was read at 593 nm. The kinetics of the reaction for blanks, standards and samples are different, therefore the reading was taken at exactly the same time duration for all the samples. All samples and standard solutions were performed in triplicate and the mean and covariance were calculated.

Plotting the calibration curve

To plot the standard curve, the corrected absorbance for each standard concentration (mean absorbance minus mean absorbance of the blank well containing ultrapure water) was plotted against the corresponding concentration (Figure 16). The line of best fit was determined using linear regression and standard curve was accepted if $r^2 > 0.99$. The intercept and slope of this line can be used to calculate the FRAP concentration of all sample solutions, according to Equation 24. In this instance, dilution factor was 4, to account for sample dilution with water.

Figure 16. Standard calibration curve for the determination of FRAP

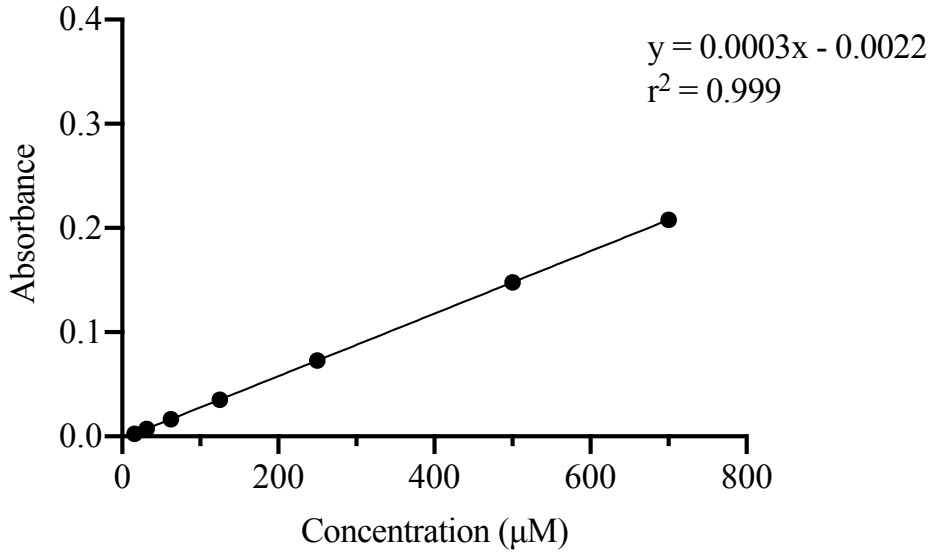

Known [Fe^{2+}] concentration (µmol) of a range of standards plotted against measured absorbance at 593 nm.

Equation 24. Calculation of sample concentration

$$Sample\ concentration = DF \times [sample\ absorbance - blank\ absorbance - \frac{intercept}{slope}]$$

Sample concentration (μM); blank absorbance: mean absorbance for water wells; intercept (m) and slope (c): obtained from the standard curve, y = mx + c; DF: the dilution factor for the sample.

3.5.2. Quantification of lipid peroxidation

The thiobarbituric acid reactive substances (TBARS) assay is used to quantify lipid peroxidation (172). A breakdown product of lipid peroxides, malondialdehyde (MDA), within a biological sample reacts with thiobarbituric acid, under a high temperature and acidic conditions to form a 1:2 MDA-TBA adduct. This adduct can then be measured either colorimetrically (at 532 nm) or fluorometrically (at an excitation wavelength of 530 nm and emission wavelength of 560 nm, cut off at 550 nm. In this thesis, the colorimetric method was chosen, due to the advantage of its greater reliability in detecting a high abundance of TBARS in the critically ill patients. (The fluorometric technique is more useful when there is a low abundance in the tissue, requiring a greater sensitivity, at the cost of reduced reliability). TBARS values in the samples were obtained by comparing the absorbance at 532 nm in the sample with a standard curve of the measured absorbances of solutions of known concentration of MDA (standards). The standards were measured in the same plate as the samples.

Preparation of reagents and samples

Reagents were prepared as described in Table 10. Plasma samples were treated with acid prior to the assay, in order to (1) deproteinise the samples by precipitating most proteins out of solution, while the rest are removed by centrifugation, and (2) to catalyse the TBARS reaction. A volume of 300 μL of TBARS acid reagent and 300 μL of plasma was added to a microcentrifuge tube and incubated at room temperature for 15 minutes, and then centrifuged at > 12,000 g for 4 minutes. The supernatant was then removed, and the prior steps repeated, if necessary, to remove any particulate matter.

Preparation of standard solutions

The absorbance of MDA at 532 nm has been shown to be linear between the concentrations of 16.7 to 0.26 μM. Standard solutions of the following known concentrations were prepared fresh on the day, according Table 11.

Table 10. Preparation of reagents for TBARS assay

Stock solution	Compound	Amount added to solvent
20% acetic acid	Glacial acetic acid	40 ml added to 160 ml ultrapure water
TBARS colour reagent	Thiobarbituric acid	0.26 g dissolved in 50 ml 20 % acetic acid
TBARS acid reagent 0.6 N	Trichloroacetic acid 6 N	10 ml in 90 ml ultrapure water
MDA solution 500 µM	1,1,3,3 tetramethyl hydroxypropanone	41 µL added to 500 ml ultrapure water for at least 30 mins (hydrolysis time)
Final MDA working standard solution 167 µM (acidified)	MDA stock 500 µM	100 µL added to 200 µL 0.6 N trichloroacetic acid

Table 11. Preparation of standard solutions for TBARS assay

Standard concentration [MDA] (µM)	Concentration of acidified MDA stock solution (µM)	Volume of stock solution (µL)	Volume of ultrapure water (µL)
16.7	167	100	900
8.35	16.7	500	500
4.18	8.35	500	500
2.09	4.18	500	500
1.04	2.09	500	500
0.52	1.04	500	500
0.26	0.52	500	500
0 (blank)	nil	nil	1000

TBARS assay

A volume of 150 μL TBARS colour reagent was added to cryovials containing 300 μL of either (1) ultrapure water (or trichloroacetic acid), (2) the final obtained supernatant from the sample solution or (3) a standard solution of known concentration. The cryovials were incubated in a block heater at 100 °C for 1 hour, and then cooled in an ice bath for 10 minutes. A volume of 200 μL of each of these solutions (standards, blanks and samples) were added to a well of a 96 well microplate and the absorbance was read at 532 nm using a spectrophotometer. All samples and standard solutions were performed in triplicate and the mean and covariance were calculated.

Plotting the calibration curve

To plot the standard curve, the corrected absorbance for each standard concentration (mean absorbance minus mean absorbance of the blank well containing ultrapure water) was plotted against the corresponding concentration. The line of best fit was determined using linear regression and standard curve was accepted if $r^2 > 0.99$. The intercept and slope of this line can be used to calculate the MDA concentration of all sample solutions, according to Equation 24. In this instance, the dilution factor was 2, to account for the sample dilution with acid.

3.5.3. Quantification of free thiol groups

The assay to quantify the total thiol status of plasma is based on the reaction of free sulfhydryl groups in the biological sample with dithionitrobenzoic acid (DTNB) to produce a mixed disulphide and 2-nitro-5-thiobenzoic acid (TNB), a yellow-coloured product, which can be measured using a spectrophotometric detector, with peak absorbance at 412 nm.

Preparation of reagents and samples

Reagents for the assay were prepared as described in Table 12. Plasma samples were spun at maximum speed in a high speed centrifuge (Eppendorf Centrifuge 5415D) for 10 minutes to ensure all particles were pelleted at the bottom of the tube. A volume of 100 μL of the clear supernatant (the sample solution) was then diluted in 300 μL of 0.1M Tris pH 8.2 buffer.

Preparation of standard solutions

The linearity of absorbance for cysteine has been demonstrated from 0.977 μM to 500 μM. A stock solution of 10 mM of L-cysteine was prepared, by dissolving 0.0121 g L-cysteine in 10 ml Tris 10 mM ETDA pH 8.2 buffer. Serial dilutions of this stock solution of L-cysteine were performed according to Table 13 to create standards of concentration within the range of known linearity.

Table 12. Preparation of reagents for free thiols assay

Reagent	Component	Amount added to solvent
Tris buffer 0.1 M with EDTA 10 mM (pH 8.2)	Tris-HCl 0.5 M EDTA (pH 8.2)	7.8773 g 10 ml dissolved in ultrapure water to make up total volume of 500 ml pH adjusted to 8.2 with NaOH
Tris buffer 0.1 M (pH 8.2)	Tris-HCl	7.8773 g dissolved in ultrapure water to make up total volume of 500 ml pH adjusted to 8.2 with NaOH
Phosphate buffer 0.1 M (pH 7)	Sodium phosphate dibasic (Na_2HPO_4) Sodium phosphate monobasic (NaH_2PO_4)	0.1286 g 009656 g dissolved in ultrapure water to make up total volume of 100 ml pH adjusted to 7
DTNB reagent 1.9 mM	5,5'-dithio-bis (2-nitrobenzoic acid) Phosphate buffer 0.1 M (pH 7)	0.0075 g 10 ml
L-cysteine standard stock solution 10 mM	L-cysteine Tris buffer 0.1 M with EDTA 10 mM (pH 8.2)	0.0121 g 10 ml

Table 13. Preparation of standard solutions for the free thiols assay

Standard concentration [L-cysteine] (µM)	Stock solution used (µM)	Volume of stock solution (µM)	Volume of 0.1 m Tris buffer 0.1 M with 10 mM EDTA (pH 8.2) (µL)
1000	10 *mM*	200	1800
500	1000	1000	1000
250	500	1000	1000
125	250	1000	1000
62.5	125	1000	1000
31.25	62.5	1000	1000
15.625	31.25	1000	1000
7.812	15.625	1000	1000
3.906	7.812	1000	1000
1.953	3.906	1000	1000
0.976	1.953	1000	1000
0 (blank)	0	-	1000

Free thiols assay

To each well of the flat bottom 96 well plate was added 90 μL of either (1) sample solution, (2) a standard solution or (3) 0.1 M Tris 10 mM EDTA pH 8.2 buffer (blank). All bubbles were removed prior to measuring the pre-incubation absorbance at 412 nm and 630 nm. A final addition of 20 μL 1.9 mM DTNB in 0.1 M phosphate buffer pH 7 was made to each well using a multi-channel pipette. The plate was covered and incubated at room temperature on a shaker for 20 minutes. The post-incubation absorbance was read at 412 nm and 630 nm. Absorption of samples and standard solutions were then calculated according to Equation 25.

Equation 25. Calculation of absorption from pre- and post-incubation absorbances at two different wavelengths

$$Absorption = [post\ incubation\ at\ 412\ nm - post\ incubation\ at\ 630\ nm] - [pre\ incubation\ at\ 412\ nm - pre\ incubation\ at\ 630\ nm]$$

Plotting the standard calibration curve

The corrected absorbance of each standard was plotted against their known [L-cysteine] concentration, and the equation of the line of best fit was calculated. The concentrations of [L-cysteine] in each sample were then calculated using the slope and intercept of this standard curve, according to Equation 24. In this instance, dilution factor was 4 to account for the sample dilution with 0.1 M Tris pH 8.2 buffer.

3.5.4. Plasma protein quantification using Coomassie assay

The amount of protein in the plasma samples was quantified using the Coomassie (Bradford) Protein Assay Kit (ThermoScientific, Pierce Biotechnology Illinois, USA). This assay is based on the principle that Coomassie dye binds to protein in an acidic medium, an

immediate shift in absorption maximum occurs from 465 nm to 595 nm, with a concomitant colour change from brown to blue. The sample is combined with the assay reagent, incubated briefly and the absorbance is measured at 595 nm using a spectrophotometer. Protein concentrations were estimated by reference to absorbances for a series of standard protein dilutions. The colour response with Coomassie is non-linear, the standard curve was completed with each assay.

Preparation of samples and standards

Plasma samples were vortexed (Vortex-Geni touch mixer) for 30 seconds to evenly distribute the protein. Standard concentrations of protein (albumin standard, BSA) were prepared according to Table 14. A volume of 5 μL of each plasma sample or standard solution was pipetted into a 96-well microplate. The Coomassie reagent (250 μL) was added to each well, and the plate incubated at room temperature for 10 minutes on a plate shaker. The absorbance was read at 595 nm with the spectrophotometer. The average blank absorbances were subtracted from all other measured absorbances of samples and other standard solutions. A standard curve was plotted using the blank-corrected absorbances for each BSA standard against its known concentration. A best fit curve (four-parameter quadratic) was plotted and used to determine the protein concentration of the samples.

Table 14. Preparation of albumin standard solutions

Standard BSA concentration (µg/ml)	Stock solution concentration (µg/ml)	Volume of stock solution (µL)	Volume of diluent (µL)
2000	2000	300	0
1500	2000	375	125
1000	2000	325	325
750	1500	175	175
500	1000	325	325
250	500	325	325
125	250	325	325
25	125	100	400
0 (blank)	Nil	Nil	400

3.5.5. Isoprostanes

Isoprostanes (8-iso-prostaglandin F2a) were measured using a commercial enzyme-linked immunosorbent assay (ELISA) kit (Cayman Chemicals, Ann Arbor, Michigan) as described previously(173). The assay is based on competition between 8-isoprostane and an 8-isoprostane-acetylcholinesterase conjugate (Tracer) for a limited number of 8-isoprostane-specific rabbit antiserum binding sites. The concentration of the tracer is constant, so the amount that binds to the rabbit antiserum is inversely proportional to the concentration of 8-isoprostane in the well. The 8-isoprostane-specific rabbit antiserum complex (free or tracer) binds to rabbit IgG mouse monoclonal antibody that has been previously attached to the well. The plate is washed to remove unbound reagents. Ellman's reagent containing the acetylcholinesterase enzyme is then added to the well, which catalyses a reaction to produce a

coloured product which absorbs at 412 nm. The absorbance of this produce is determined spectrophotometrically and is proportional to the concentration of the bound 8-isoprostane tracer, and inversely proportional to concentration of 8-isoprostane.

Precision

Precision data was provided by the manufacturers (https://www.caymanchem.com/pdfs/516351.pdf); which quoted % CV 7.2-20% for intra-assay variation and 9.6-24% for inter-assay variation. However, the laboratory and operator specific inter- and intra-assay precision for this assay were not demonstrated in this thesis, due to restrictions on time, availability of biological sample and experimental costs.

3.6. Quantification of circulating nitrogen oxides

3.6.1. Determination of nitrite and nitrate

Rapid degradation of nitric oxide (NO) in biological samples makes it difficult to quantify with a high degree of accuracy. Nitrite (NO_2^-) and nitrate (NO_3^-) are stable end products of NO oxidation, and determination of these compounds can be performed to assess systemic synthesis of NO.

3.6.2. Principles of nitrite and nitrate detection

In this thesis, nitrite and nitrate were determined using High Performance Liquid Chromatography (HPLC) combined with a diazo coupling reaction (the Griess reaction). Nitrate and nitrite are separated from the treated sample by HPLC, with nitrate retained in the column longer than nitrite. Nitrite is detected spectrophotometrically, following its reaction with acidified Griess reagent (closed-source composition, Eicom), within a reducing column, to generate a diazo compound with peak absorbance at 540 nm, according to Equation 26.

Equation 26. Nitrite reacts with Griess reagent to produce pink/red diazo product

$$NO_2^- + sulphanilamide(H^+) \rightarrow X$$

$$X + N - (1 - naphthyl)ethylenediamine \rightarrow diazo\ compound$$

Nitrate is reduced to nitrite by reaction with a cadmium/copper alloy, which is subsequently quantified by the reaction in Equation 26, and measured spectrophotometrically. The response of the detector is transformed to voltage at the analogue output terminal. The concentrations of nitrite and nitrate in the sample are measured by assessing the peak area of

the absorption and comparing it the peak area of the absorption for standards of known concentration.

Preparation of reagents and samples

Reagents were prepared as described in Table 15. Frozen plasma aliquots were thawed on ice, treated with an excess of N-ethylmaleimide (NEM in PBS 10 mM final concentration), and spun (at 10 000 rpm/9 000 x *g*) in a high speed centrifuge (Eppendorf Centrifuge 5415D) for 5 minutes to ensure all insoluble particles were pelleted at the bottom of the tube, and the clear supernatant was used for the assay. A volume of 100 µL of the plasma sample was mixed with 100 µL of methanol in a microcentrifuge tube, and vortexed (Vortex-Genie touch mixer) for 1 minute, prior to centrifugation in a high speed centrifuge at maximum speed at 4°C for 20 minutes. If the measured concentration of nitrite/nitrate was outside the standard calibration curve, this solution was diluted, and the measurement repeated.

Preparation of standards

The linearity of response for nitrite and nitrate has been demonstrated from 0.1 to 30 µM. Standard solutions of known concentration within this range were prepared by dilution of the stock solution in PBS buffer, according to Table 16.

Table 15. Preparation of reagents for HPLC

Reagent	Compound	Amount added to solvent
10% methanol solution	Methanol AR (ACS) reagent grade	100 ml in 900 ml ultrapure water
0.925% HCl in 10% methanol	37% HCl 10% methanol solution	12.5 ml 487.5 ml
Phosphate buffered saline (PBS)	Sodium phosphate dibasic (Na_2HPO_4) Sodium phosphate monobasic (NaH_2PO_4) Sodium Chloride (NaCl)	1.14 g 0.24 g 8.7 g Made up to 1L with ultrapure water (pH adjusted to 7.4)
NEM 10 mM in PBS	Sodium phosphate dibasic (Na_2HPO_4) Sodium phosphate monobasic (NaH_2PO_4) Sodium Chloride (NaCl) N-ethylmaleimide (NEM) > 98% EDTA 0.5 M	1.14 g 0.24 g 8.7 g 1.25 g 5 ml Made up to 1L with ultrapure water (pH adjusted to 7.4)
Carrier solution	Carrier powder EI-NO-CAP3	Dissolved in 1000 ml 10% methanol
Reactor A solution	Reactor A Powder EI-NO-RAP3	Dissolved in 500 ml 0.925% HCl in 10% methanol
Reactor B solution	Reactor B Powder EI-NO-RBP3	Dissolved in 500 ml 10% methanol
Reactor solution	Reactor A solution Reactor B Solution	Volume ratio 1:1
Nitrite and nitrate standard stock solution 120 µM	Sodium nitrite 99.99% (MW 65 g/mol) Sodium nitrate 99.99% (MW 85 g/mol)	0.008 g 0.010 g Dissolved in 1L ultrapure water

Table 16. Preparation of standard solutions of known nitrite and nitrate concentrations

Standard concentration $[NO_2^-]$ and $[NO_3^-]$ (µM)	Concentration of stock solution used (µM)	Volume of stock (ml)	Volume of PBS buffer (ml)
60	120	0.26	0.24
40	120	0.17	0.33
20	40	0.3	0.3
10	20	0.2	0.2
2	20	0.1	0.9
1	10	0.1	0.9
0.2	2	0.1	0.9
0	nil	nil	0.4

High pressure liquid chromatography

All standards and samples were analysed using HPLC, using 20 µL injection volumes (from a total volume of 35 µL aspirated by the autosampler). Fresh carrier and reactor solutions were prepared as described in Table 15. Following treatment, the samples and standards were injected into the HPLC system, an Eicom NOx Analyser (ENO-20), with spectrophotometric detector. The ENO-20 was fitted with a pre-column (NO-PRE), separation column (NO-PAK) and reduction column (NO-RED). The column temperature was 35 °C, and the flow rates of the carrier and reactor pumps were 0.33 ml/min and 0.11 ml/min respectively. The detection wavelength was fixed at 540 nm. The typical retention time for nitrite was 4.7 mins, while for nitrate it was 7.0 minutes. Blank samples were injected at the beginning of the run, followed by the standards and samples. Standard positions were distributed throughout the entire run (beginning, middle and end). The injectate was initially filtered through the pre-column, and then nitrite and nitrate were separated in the analytical separation column, with nitrate being retained longer than nitrite. From this separation column, the nitrite and nitrate then elute into the reduction column. Nitrite passes through the reduction column first, without any reaction, and is mixed with the reactor solution (Griess reagent) at a three-way joint. Nitrite then reacts with the acidified Griess reagent in the reaction coil and generates diazo compounds, which have a pink/red colour. The quantity of diazo compound was measured by absorbance at 540 nm using a spectrophotometric detector. Nitrate is reduced to nitrite by reaction with a cadmium/copper alloy. The derived nitrite undergoes the same reaction described above. The response of the detector is transformed to a voltage which is generated at an analogue output terminal and analysed using PowerChrom software, which displays the absorbance peaks of the samples and standards, and integrates the peaks to produce peak areas (Figure 17). Regression lines of known concentrations versus peak areas for nitrite and nitrate standards were generated

and forced through zero (Figure 18). The slopes of these regression lines were then used to calculate the concentrations of nitrite and nitrate in the analysed samples, according to **Error! Reference source not found.**.

Figure 17. Example of a chromatogram for an individual sample

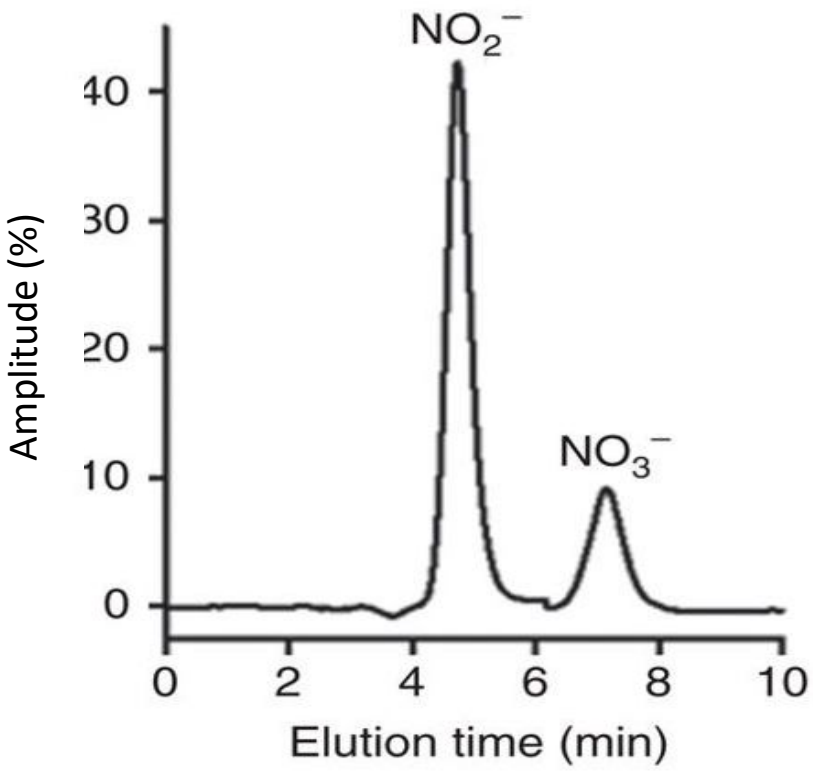

Chromatogram demonstrating the amplitude of the signal generated by the detector (% of full scale reading) over time. The absorbance peak for nitrite peak appears first, whilst the nitrate peak appears second as it must first be reduced to nitrite.

Figure 18. Example calibration curve

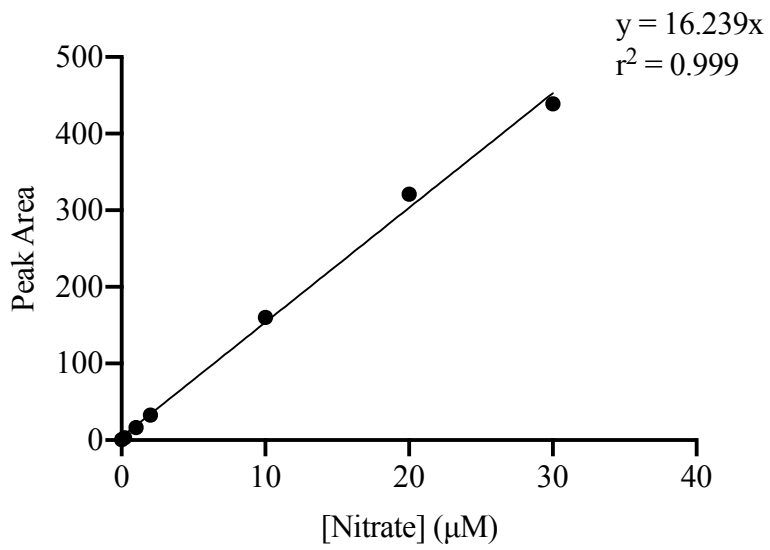

Equation 27. Calculation of sample [nitrate] or [nitrite] concentration

$$Sample\ concentration = DF\ \times \frac{sample\ peak\ area}{slope}$$

Sample concentration (μM); DF: sample dilution factor.

Preparation of the HPLC set up prior to assay

The end of the reactor inlet tube was placed into the bottle containing fresh reactor solution, and 1-2 ml aspirated into the reactor glass tube and then discarded three times to ensure only reactor solution was present in the lines and reactor glass trap, before the reactor glass tube was filled. The end of the carrier inlet tube was placed into the bottle containing fresh carrier solution, and 1-2 ml aspirated into the carrier glass tube, and discarded before the carrier trap

glass tube was filled. To prepare the pre-column, the ENO-20 was switched on, and 2 minutes allowed for the pumps to power up. The pumps were then shut down before opening the unit and detaching the guard column. To avoid drying out of the separation column, a closed-end ferrule (stop fit) was placed at the inlet of the separation column. The guard column was opened using spanners (provided) and the old packaging gel flushed out using a syringe and connector. Both sides of the guard column were flushed with acetone, and its internal surface cleaned with a cotton-tipped applicator to remove residual packing gel. The pressure through both parts of the guard column were checked to ensure the filter was not blocked. The guard column was then refilled with packaging gel. This is prepared by adding 30 ml acetone (AR, ACS reagent grade, Sigma) into a glass bottle containing dry packaging gel and shaking until the powder is suspended in a gel. An aspiration adaptor was connected to the downstream side of the column and a syringe containing 0.5 ml acetone was attached. The guard column was then slowly filled with the packaging gel using a 200 μL pipette whilst simultaneously aspirating acetone from the packaging gel. The step was repeated until the pre-column was filled with gel, then the upstream side was connected and nut fastened. The packed guard column was then flushed with 2-3 ml methanol, followed by 2-3 ml ultrapure water. The guard column was reconnected to the carrier line, with the left side remaining open, and the carrier pump was used to flush the guard column with carrier solution for 3-5 minutes. The guard column was then connected to the separation column and the reactor pump was switched on, and all the connections and columns checked for leaks. The autosampler was checked to ensure no obstructions in the path of the syringe, and the lines were primed to remove bubbles from the coiled line, syringe and lines leading to the 10% methanol reservoir. The injection port was rinsed three times prior to analysis.

3.6.3. Determination of total nitroso-species

Nitric oxide (NO) generation in vivo leads to concomitant formation of nitrosothiols (RSNO), nitrosamines (RNNO) and nitrosylhemes. The sum of nitrosothiols (RSNO) and nitrosamines (RNNO) is treated as total nitroso-species (RXNO). Detection of nitroso species was performed using gas-phase chemiluminescence.

3.6.4. Principles of nitroso species detection

Determination of plasma nitroso species was achieved by determining the concentration of NO released from their reduction, using gas chemiluminescence, as described previously (174). Nitroso species undergo reductive cleavage by an iodide/triiodine-containing reaction mixture, to release NO. The concentration of NO was determined by its chemiluminescent reaction with ozone (O_3) to produce nitrogen dioxide (NO_2) (Equation 28). A proportion of the NO_2 arises in an electronically excited state (NO_2*), which emits light in the near infrared region on decay to its ground state, which is detected by a photomultiplier. Provided O_3 is in excess and reaction conditions are kept constant, the intensity of the emitted light is directly proportional to NO concentration.

Equation 28. Reaction of nitric oxide with ozone to produce nitrogen dioxide

$$NO + O_3 \rightarrow NO_2 * + O_2$$

$$NO_2 * \rightarrow NO_2 + h \cdot v$$

Discrimination between S-nitroso and N-nitroso compounds was achieved by group-specific reagents. Total nitroso species (RXNO) were quantified following pre-treatment of the plasma sample with acidic sulphanilamide. N-nitroso species (RNNO) were quantified after sample incubation with 0.2% mercuric chloride ($HgCl_2$) and acidic sulphanilamide. S-nitroso species (RSNO) were determined by the difference between RXNO and RNNO. The concentration of S-nitrosothiols in these samples was estimated from the difference in NO signal before and after sample pre-treatment with mercuric chloride.

Preparation of reagents and samples

Reagents were prepared as described in Table 17. Frozen plasma aliquots were thawed on ice, treated with an excess of N-ethylmaleimide (NEM 100 mM, 1:10 v/v to the sample), and spun at 10,000 rpm/9000 x *g* in a high speed centrifuge (Eppendorf Centrifuge 5415D) for 5 minutes to ensure all insoluble particles were pelleted at the bottom of the tube, and the clear supernatant was used for the assay. For quantification of RXNO, a volume of 150 μL of the supernatant was incubated for 15 minutes at room temperature with 15 μL of 5% sulphanilamide in 1 M HCl (volume ratio 10:1). For quantification of RNNO, a volume of 150 μL of the supernatant was incubated for 15 minutes at room temperature with 15 μL of 2% $HgCl_2$ (volume ratio 10:1), followed by a second incubation at for 15 minutes at room temperature with 15 μL of 5% sulphanilamide in 1M HCl (volume ratio 10:1).

Preparation of standard

A solution of approximately 1 μM nitrite is used as a standard solution. This is prepared by diluting the stock nitrite solution (prepared as per Table 17) with PBS buffer as shown in Table 18.

Table 17. Preparation of reagents for CLD

Reagent	Compound	Amount added to diluent
NaOH 1M	Sodium hydroxide (NaOH), ACS reagent 99.99%	40 g Dissolved in 1L ultrapure water
HCl 1M	Hydrochloric acid (HCl) 37%	830 µL Made up to total volume of 100 ml with ultrapure water
PBS buffer	Sodium phosphate dibasic (Na_2HPO_4) Sodium phosphate monobasic (NaH_2PO_4) Sodium chloride (NaCl)	1.14 g 0.24 g 8.7 g Made up to total volume of 1L (pH adjusted to 7.4)
PBS buffer with NEM/ETDA	Sodium phosphate dibasic (Na_2HPO_4) Sodium phosphate monobasic (NaH_2PO_4) Sodium chloride (NaCl) N-ethylmaleimide (NEM, >98% HPLC) EDTA 0.5M pH 8 (ultrapure)	1.14 g 0.24 g 8.7 g 1.25 g 5 ml Made up to total volume of 1L (pH adjusted to 7.4)
Iodine/iodide solution	Potassium iodide > 99.5% Iodine > 99.8%	1.08 g 0.38 g Dissolved in 10 ml ultrapure water
Potassium ferricyanide (III) in PBS buffer 0.05 M	Potassium ferricyanide (III) > 99%	1.646 g Dissolved in PBS buffer (pH adjusted to 7.5)
Mercury chloride 2%	Mercury (II) chloride ($MgCl_2$) > 99.5%	0.2 g Dissolved in ultrapure water
5% Sulphanilamide in 1M HCl	Sulphanilamide (>99%)	0.5 g Dissolved in 10 ml 1M HCl
Nitrite standard stock solution 58 µM	Sodium nitrite (>99.8%) MW = 69 g/mol	0.008 g Dissolved in 2L ultrapure water

Table 18. Preparation of nitrite standard solution for CLD.

Standard concentration $[NO_2^-]$ (µM)	Concentration of stock solution (µM)	Volume of stock solution (ml)	Volume of PBS buffer (ml)
10	58	0.17	0.83
1	10	0.1	0.9

Reaction chamber set up

The chemiluminescence detection system (CLD 88, EcoMedics) is illustrated in Figure 19. It consisted of a sealed (with rubber septum), water-jacketed glass reaction chamber. The reaction mixture contained a volume of 13.5 ml glacial acetic acid with 1 ml iodine/iodide solution, continuously bubbled with nitrogen, and kept at a constant temperature of 60 °C by a heating water bath. The reaction chamber was connected to an efficient reflux condenser kept below 0°C by cooling bath containing antifreeze coolant. The outlet of the gas from the reaction chamber was passed through a scrubbing bottle, containing 1M sodium hydroxide, and placed in an ice beaker, in order to trap traces of acetic acid and iodine prior to transfer into the detector (NO-Analyser). The sample tube was connected to the inlet fitting on the NO-Analyser. A pressure gauge is placed between the outlet of the scrubbing bottle and detector inlet for continuous pressure monitoring and adjustment of the purging gas (nitrogen) flow, which was kept constant throughout the measurement cycle in order to minimise noise and optimise consistency of measurements. The response of the detector is transformed to a voltage which is generated at an analogue output terminal and analysed using PowerChrom software, which displays the absorbance peaks of the samples and standards and integrates the peaks to produce peak areas (Figure 20).

Figure 19. Schematic of chemiluminescence detection system

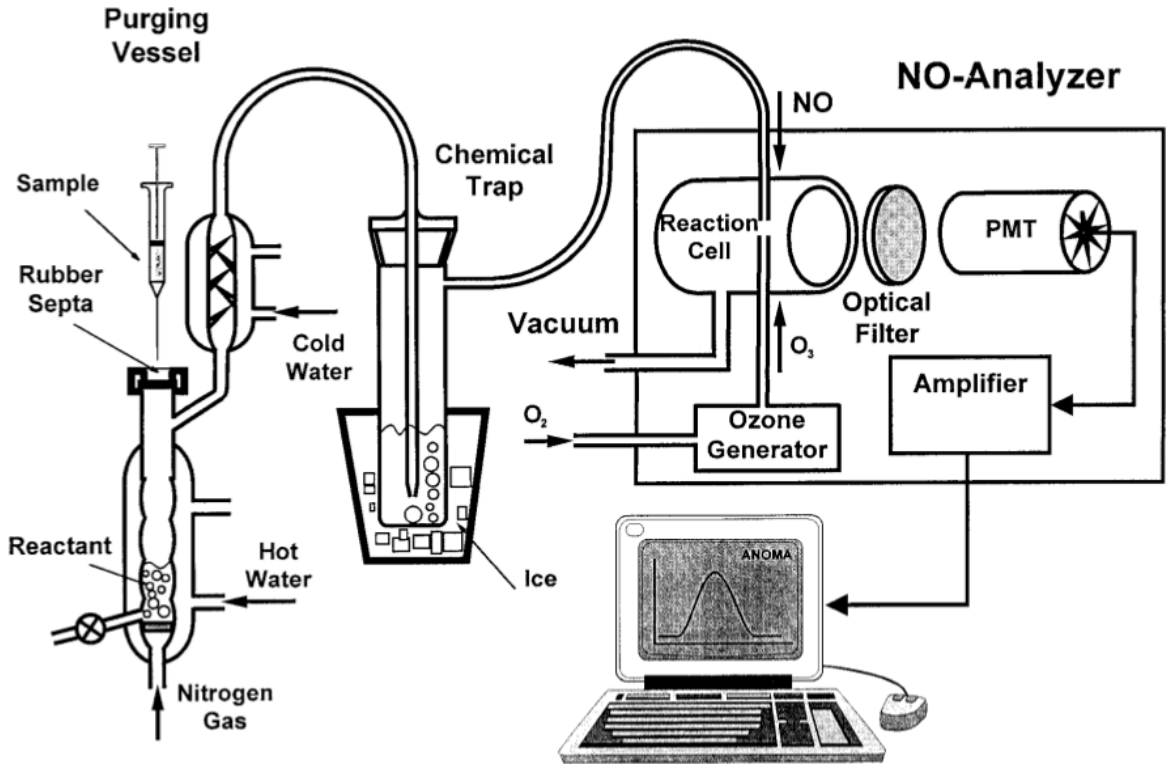

Reproduced from (175).

Figure 20. Example of absorbance peaks of standards and samples

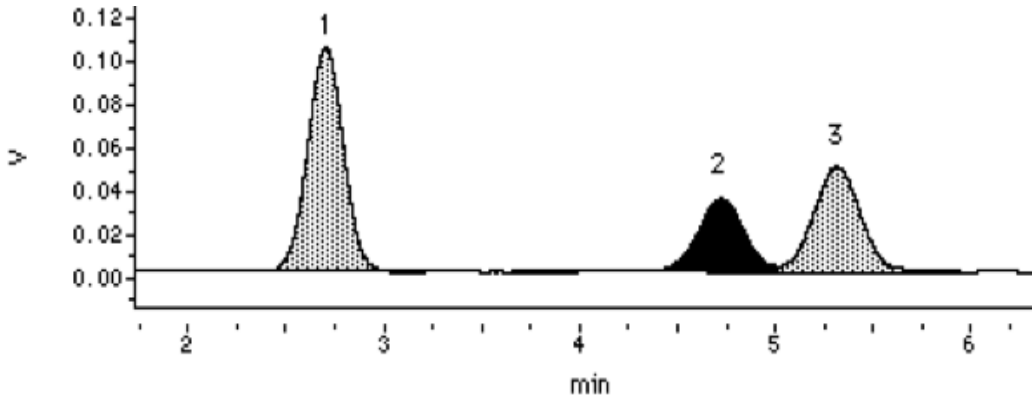

Peak 1 represents a standard of known nitrite concentration; peaks 2 and 3 represent the respective nitrite and nitrate concentrations from plasma samples. The shaded areas represent the peak areas, integrated by the PowerChrom software.

Calculating sample concentrations

The concentration of the analyte in the sample was calculated using Equation 29. Consistency of measurement was determined by calculating the relative standard deviation (%RSD) of the all the peak area values measured for the 1 μM nitrite standard measured during the entire run (Equation 30). Data were considered consistent if %RSD < 10%.

Equation 29. Calculation of analyte concentration

$$Analyte\ concentration = DF \times \frac{sample\ peak\ area\ x\ standard\ injection\ volume\ x\ RF}{sample\ injection\ volume}$$

Analyte concentration (μM); RF: Response factor, concentration of standard (μM) / mean of standard peak areas; DF: dilution factor, volume of sample with added NEM, sulphanilamide or $HgCl_2$)/volume of sample taken for analysis.

Equation 30. Calculation of relative standard deviation for a given standard during a measurement run

$$\%RSD = 100\ \% \times \frac{peak\ area\ standard\ deviation}{peak\ area\ mean}$$

Sample and standard injection and determination

The measurement range of the detector is set to 10, 100 or 1000 parts per billion (ppb), depending on the predicted levels of analytes in the sample, with 100 ppb appropriate for most human samples. The injection volume was also chosen based on the estimated levels of

the analytes in the plasma samples or standards. The usual injection volume for human plasma is 300 μL, while that for the standard solutions is 50 μL. After each injection, the syringe needle was wiped clean with a tissue and rinsed three times with ultrapure water to avoid contamination.

Test of sulphanilamide solution

To test the 5% sulphanilamide in 1M HCl solution , the 1 μM standard solution was incubated with 5% sulphanilamide in 1M HCl solution, in a volume ratio of (10:1), for 15 minutes at room temperature, and then injected into the reaction chamber using a gas-tight Hamilton syringe. If the detector generates a peak, the 5% sulphanilamide in 1M HCl solution must be prepared again.

3.6.5. Cyclic GMP

Concentrations of cyclic GMP in plasma samples were determined by a commercial competitive immunoassay kit (R&D Systems, Abingdon, UK; Biomedica, Vienna, Austria) according to the manufacturer's instructions, and as described previously (146). In this assay, cGMP in the sample competes with a fixed amount of horseradish peroxidase-labelled cGMP for sites on a rabbit polyclonal antibody. During incubation, the rabbit antibody becomes bound to goat anti-rabbit antibody coated onto the microplate. Following a wash to remove both conjugate and unbound sample, a substrate solution is added to the wells, to determine the bound enzyme activity. This produces a coloured compound which absorbs light at 450 nm. The absorbance is inversely proportional to the concentration of cGMP in the sample.

Precision

Precision of the commercial kit in plasma samples was provided by the manufacturers (https://www.rndsystems.com/products/cgmp-parameter-assay-kit_kge003); which quoted a coefficient of variation (%CV) of 5.3-8.1% for intra-assay variation (three samples of known concentration tested on one plate) and 8.2-9.9% for inter-assay variation (three samples of known concentration in separate assays). However, the laboratory and operator specific inter- and intra-assay precision for this assay were not demonstrated in this thesis, due to restrictions on time, availability of biological sample and experimental costs.

Precision of plasma redox assays

Variation within normal populations, and sensitivity to detect changes under experimental conditions using the same protocols used in this thesis are widely reported in published literature: for the FRAP assay (171); TBARS assay (172); free thiols assay (176) and nitrite, nitrate and RXNO (175); and demonstrated within the same laboratory that supervised my experiments (146). For each analyte, all samples were analysed under the same experimental conditions, on the same day, by the same operator; and each sample was run in triplicate and the %CV reported. However, evaluation of the operator-specific precision of the plasma redox assays (using a minimum replicate number of $n > 6$) was not undertaken, due to time and resource restraints. It is therefore not possible to demonstrate the intra-assay reproducibility due to individual operator factors, which may have contributed to the large variation seen in some of the measured variables.

3.7. Assessment of peripheral oxygen oxygenation and microcirculatory function

Several methods have been developed for evaluation of the peripheral microcirculation and its response to treatment. No single method has been universally accepted so far. In this chapter, changes in skeletal muscle tissue oxygenation (StO_2), using near infrared spectroscopy (NIRS) during a vascular occlusion test (VOT), were used to characterise skeletal muscle oxygenation and different aspects of microcirculatory function. This technique was chosen as it is non-invasive; it has been widely used in critically ill patients in the intensive care setting; and its derived values have demonstrated reproducibility. There is evidence that NIRS-derived values correlate with disease severity (177) and clinical outcome (178)in critically ill cohorts. Skeletal muscle of the thenar eminence was investigated because it is minimally susceptible to the confounding effects of tissue oedema and adipose tissue (147).

3.7.1. Principles of near-infrared spectroscopy

When light encounters a tissue surface, it is either absorbed or reflected. The absorption of light passing through a fluid containing an absorptive material depends on three factors, as described by the Beer-Lambert law (Equation 31). Human tissues are comprised of a number of substances with well-defined absorption spectra within near-infrared wavelengths (700 – 1100 nm). Light in the infra-red range of wavelengths can penetrate skin and soft tissue to reach underlying muscle (unlike shorter wavelengths, such as visible light, which are scattered and absorbed by tissue substrates and penetrate only short distances). The absorption of light by tissue chromophores, such as haemoglobin, myoglobin and cytochrome c oxidase, varies according to oxygenation status and the wavelength of light. The absorption spectra of oxygenated and deoxygenated haemoglobin (Hb) in the near-infrared light

spectrum (shown in Figure 21) are sufficiently different to allow differentiation of these compounds by illuminating the tissue with at least two different wavelengths of light, and measuring the differential absorbance.

Equation 31. The Beer-Lambert Law describing the absorption of light by tissues

$$A = e \times b \times c$$

A: absorbance (the ratio of light energy passing through the sample relative to the energy incident upon the sample); e: molar absorptivity of the absorbing material at a specific wavelength (a constant, the optical density of a 1 cm thick sample of given 1 M solution); b: the pathlength of light through the material ; c: the concentration of the absorbing material within the fluid.

Figure 21. Absorption spectra of oxygenated and deoxygenated haemoglobin

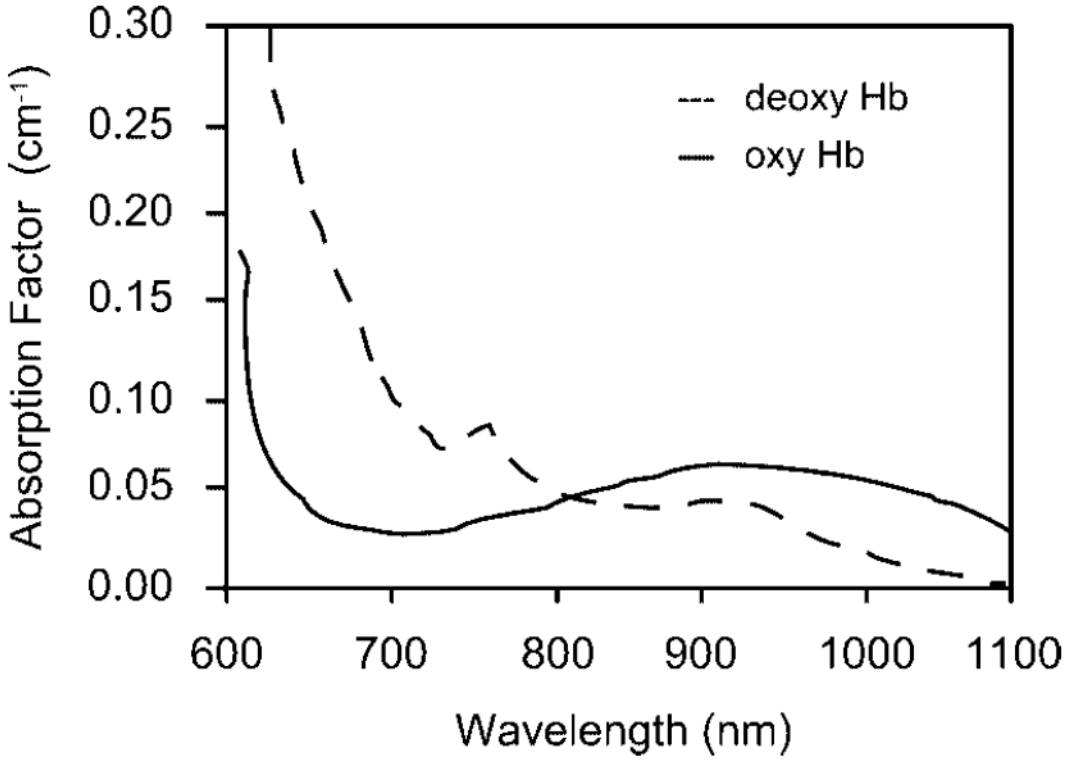

Reproduced from (179)

3.7.2. Tissue oxygen saturation

Tissue oxygenation can be described as the ratio of oxy- and deoxyhaemoglobin within its microvessels. This can be measured by applying a probe to the body surface over the tissue of interest, which emits light of different specific wavelengths. Emitted light of each wavelength will be absorbed to a different degree according to the relative concentrations of oxy- and deoxyhaemoglobin in the microvessels in its path. The remaining light is reflected back to a receiving probe, which detects light spectroscopically, and converts it to an electrical signal (mV) (Figure 22). Using the modified Beer-Lambert law, the signal is used to calculate the average ratio of oxygenated to total haemoglobin (%) in the arterioles, capillaries and venules of the tissue under its light path. This value is known as the tissue oxygen saturation (StO_2). Absolute concentrations cannot be calculated unless the path length of the light through the tissue is known. The absorption spectra of the three main chromophores present in human tissue overlap, such that their relative contribution to the overall NIRS signal are indistinguishable. A small proportion of the NIRS signal from human muscle is derived from myoglobin (10%) and cytochrome c oxidase (5%) (180).

Figure 22. Schematic to explain how NIRS estimates tissue oxygen saturation

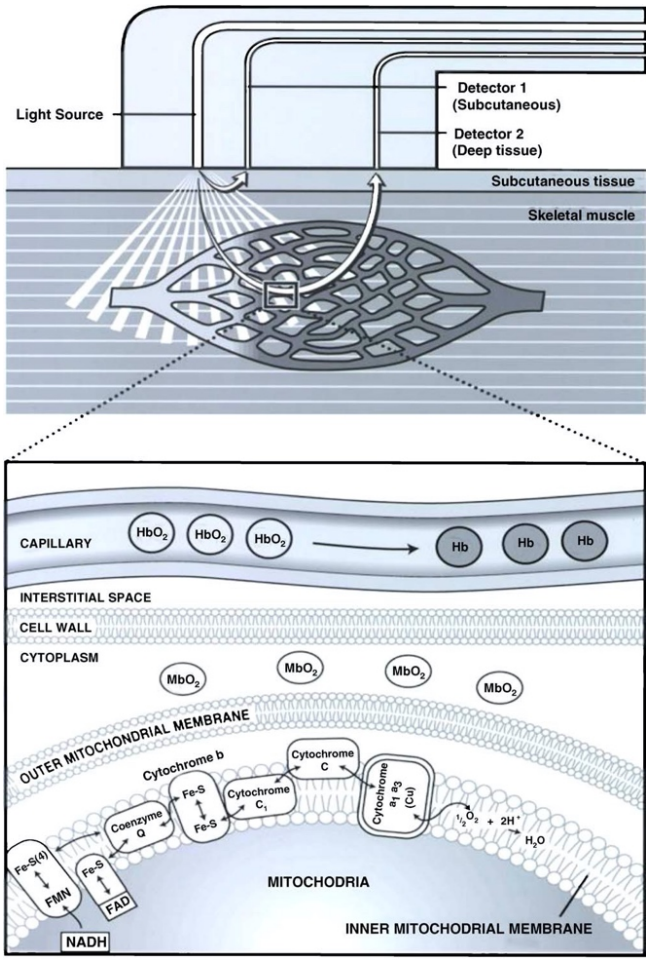

Figure reproduced from (181)

3.7.3. Clinical significance of tissue oxygen saturation

Tissue oxygen saturation (StO_2) measures the oxygen content in vessels less than 1 mm in diameter (arterioles, capillaries and venules), rather than in the systemic circulation. Light passing into vessels greater than this diameter will be completely absorbed and so make a negligible contribution to the NIRS signal (182). Studies have demonstrated that StO_2 may be a better indicator of compromised tissue blood flow than traditional indicators of global blood flow. Diminished StO_2 has been demonstrated in patients with organ dysfunction, compared to healthy controls (183). In patients with sepsis, those with shock had lower StO_2 levels than those without (184). Lower StO_2 levels have been associated with the development of multiple organ dysfunction, from different primary insults, including trauma (185), sepsis (184), hypotension and systemic inflammatory response syndrome(186), and surgery(187). In a study of critically ill patients admitted to ICU with elevated lactate levels, patients with persistently low thenar StO_2, despite resuscitation, exhibited greater degree of organ dysfunction as estimated by the SOFA score, compared to those with normal StO_2 (defined as ≥70%)(188). In patients with septic shock, StO_2 values following haemodynamic resuscitation were significantly lower in non survivors than survivors, despite there being no difference in their mean arterial pressure and central venous oxygen saturation, and there was no correlation between StO_2 and SpO_2 (189). A 2014 meta-analysis concluded that septic patients have lower StO_2 than healthy controls, whilst survivors of sepsis had higher StO_2 than non survivors (183).

3.7.4. Tissue haemoglobin index

The spectrometer also measures the overall intensity of the haemoglobin signal, known as the tissue haemoglobin index (THI), from the tissue underlying its optical sensor. The wavelength at which absorption is equal for the two compounds (the isobestic point, seen at

800 nm) can be used to calculate the haemoglobin concentration. The NIRS method for measuring THI assumes a constant but unknown path length, such that the tissue volume generating the signal is unknown. THI therefore represents the amount of haemoglobin within an unknown volume of tissue, hence it has no unit, and it is not known whether or not it can represent tissue haemoglobin concentration. The THI signal includes an unknown contribution from myoglobin, such that it may be less sensitive to total blood haemoglohin concentration, and tissue haemoglobin concentration. It has been shown that steady-state THI values do not reliably indicate blood haemoglobin concentration, and the contribution of myoglobin to the THI and StO_2 depends on the magnitude of the THI. At a THI of 4, almost all the THI and StO_2 signal from the thenar eminence is from myoglobin; while at a normal THI (>10) the StO_2 signal is mainly from tissue haemoglobin (190).

3.7.5. Microcirculatory assessment using a vascular occlusion test

Static values of StO_2 may vary widely but by measuring changes in StO_2 in response to a transient period of arteriovenous occlusion to the tissue, a number of values may be calculated which provide indirect information about oxygen consumption by the tissue, and the function of its microcirculation (147). The vascular occlusion test (VOT) consists of a short period of skeletal muscle ischaemia induced by an occlusive cuff proximal to the site of the NIRS probe. StO_2 is measured continuously using NIRS, and the measurements are plotted to produce an StO_2-time curve, such as the one in Figure 23. From this graph, the following functional indices can be estimated:

(1) Oxygen consumption rate of the tissue (StO_2 downslope)

(2) Microvascular reactivity or reperfusion rate (StO_2 upslope)

(3) Vascular reserve (hyperaemia area)

Figure 23. A tissue oxygenation-time curve

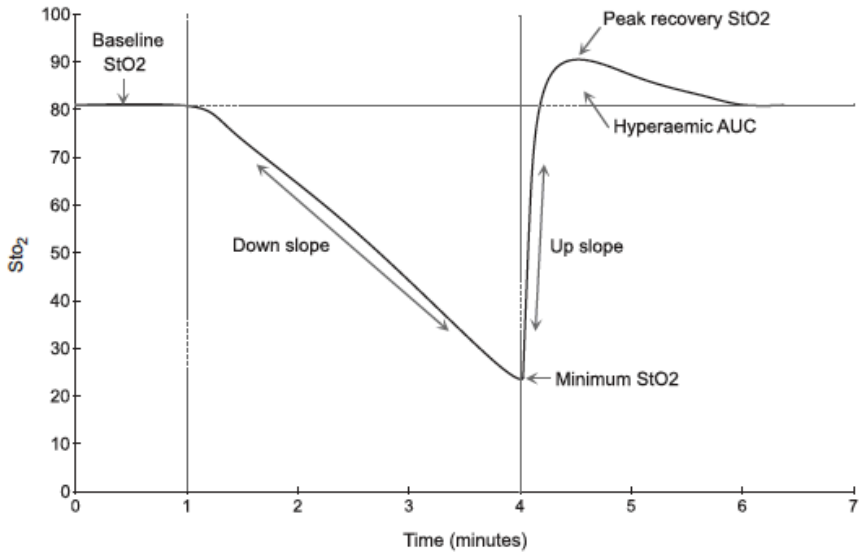

Curve measured using near-infrared spectroscopy before, during and after a 3 minute period of arteriovenous occlusion to the tissue. StO2: tissue haemoglobin saturation (%).

3.7.6. Tissue oxygen consumption rate: StO_2 downslope

Cuff inflation and loss of arterial inflow results in a steady decline in StO_2, as the tissue consumes O_2. The gradient of this decrease (StO_2 downslope) therefore represents the rate of decrease in saturation of haemoglobin per unit time (%/min) and can be taken to reflect the oxygen consumption rate of the underlying tissue. This has been evaluated in healthy subjects and septic patients with good reproducibility (177, 191). Lower StO_2 downslopes have been reported in patients with sepsis, and in patients with haemodynamic shock (184) and have been shown to correlate with the severity of critical illness (177). The StO_2 downslope does not directly measure oxygen consumption, as the amount of haemoglobin in the light path is not known, and the values may be affected by haemoglobin concentration.

3.7.7. Microvascular reactivity: StO_2 upslope

Following release of the cuff, there is rapid reperfusion of the tissue and deoxygenated haemoglobin is washed out by oxygenated haemoglobin. In the first few seconds following cuff release, this rapid increase in haemoglobin saturation (StO_2 upslope) is thought to depend primarily on the reperfusion rate of the tissue and endothelial-dependent vasodilation, together termed “microvascular reactivity”. StO_2 upslope has been shown to be markedly lower in critically ill patients compared to healthy volunteers (192). It has also been shown to decrease with increased severity of sepsis and chronic heart failure, implying a common impairment of endothelial function (193, 194). In patients with sepsis, StO_2 upslope was lower in patients with shock, compared to those without, and lower StO_2 upslope was associated with greater degree of organ impairment as measured by the SOFA score (184).

3.7.8. Vascular reserve: Hyperaemia recovery area

Following release of the occlusion, StO_2 may increase above the baseline value, followed by a slow recovery to baseline. Tissue hypoxia and lack of nutrient supply during the ischaemic phase results in the release of vasoactive mediators, which produces this reactive hyperaemia. The degree of the reactive hyperaemia is calculated as the area under the curve above the baseline value of StO_2, and has been used as an estimate of the ability of the microcirculation to respond to the ischaemic stimulus (vascular reserve) (193). After release of the occlusion, StO_2 may rapidly increase to a value of 100% in healthy subjects. The ceiling effect means StO_2 remains stable for a couple of seconds, and as recruitment of the microcirculation is reversed, it slowly decreases to baseline values. In these cases, calculation of area under the curve underestimates the reactive hyperaemia. In septic patients, reactive hyperaemia may be completely blunted. Differences in reactive hyperaemia in different patient groups have not yet been studied.

3.7.9. NIRS-VOT protocol

Patients rested for a minimum of 10 minutes in a supine position with their head elevated to approximately 30 degrees above the horizontal and their hand resting at the level of the heart, to prevent the influence of gravity on blood flow. A manual blood pressure cuff was placed around the upper arm. StO_2 measurements were made using a tissue spectrometer (InSpectra Model 325, Hutchinson Technology, MN, USA), with a probe containing an optode with 15 mm spacing, that emitted light at 680 nm, 720 nm and 760 nm respectively, and recorded StO_2 every 3 seconds. The probe was placed over thenar eminence and protected from interference from ambient light via a black adhesive seal. Care was taken to ensure that the probe did not compress the underlying microvasculature. Awake subjects were advised not to move their arm during the measurements, to prevent the effects of movement artefact and

muscle contraction from interfering with resting measurements. StO_2 was measured for 3 minutes to achieve a stable baseline reading. The blood pressure cuff was rapidly inflated to 250 mmHg (well above systolic pressure) for 3 minutes and then rapidly deflated. StO_2 measurements continued for 5 minutes after cuff deflation. The times of cuff inflation and deflation were recorded.

StO_2 measurements during the protocol were automatically uploaded to the device and analysed using automated InSpectra StO2 Researcher's Analysis Software version 4.01 (Hutchinson Technology), which plotted the StO_2-time graph, and determined the values for baseline, minimum, peak and recovery StO_2 (%). The functional variables were determined using algorithms in the software. The first-degree slope of StO_2 decrease with respect to time (StO_2 downslope, %/min) was calculated using linear regression analysis, using the slope of lease squares error linear equation. Only the first part of the curve, where the decrease can be considered linear, was used in the calculation. StO_2 downslope was calculated from the point at which StO_2 was 0.98 times the baseline value to the point 1 minute later. StO_2 upslope was calculated by extrapolating the slope following the release of the cuff. It was calculated from the point at which the recovering StO_2 first exceeded 1.05 times the minimum value for StO_2 to the point where it reached 0.85 times the baseline value. If the squared Pearson's correlation coefficient of the best fit linear equation was 0.94 or less, the value was excluded from the final analysis. Overshoot StO_2 (%) was calculated as the peak StO_2 minus the baseline StO_2. Ischaemic area was taken as the integrated area, below the baseline average, for the time interval between cuff inflation and deflation (or the minimum value if the minimum occurred after cuff deflation). The reactive hyperaemia area was calculated as the area under the curve above baseline values.

Precision

The reproducibility of NIRS-VOT variables has been demonstrated previously; with no significant difference between trials on the same subject repeated 4-6 times (195). Mean values for the coefficient of variation for the derived variables varied between 6-30%.

4. Chapter 4. Skeletal muscle bioenergetic phenotype in critical illness

4.1. Introduction and literature review

Cellular bioenergetic failure is presumed to play a role in organ dysfunction and death from critical illness (18), but neither the precise nature of the impairment, nor the mechanism leading to it, has been defined. As outlined in Chapter 1, bioenergetic capacity depends on multiple interrelated and dynamic elements, many of which may be subject to modification during critical illness. Energy failure may result from a critical limitation of oxygen and substrate provision to the cell, due to impairments in systemic oxygen transport (196) and abnormal microcirculatory blood flow (38). However, bioenergetic pathways may also be subject to modification by exposure to ROS, inflammatory and endocrine mediators or activation of the HIF pathway. Potential modifications to bioenergetic function include: alterations to the activity of metabolic enzymes or respiratory complexes, the coupling efficiency of oxidative phosphorylation, or the balance between mitochondrial degradation (autophagy) and generation (biogenesis) (122). As discussed in Chapter 1, use of steady-state concentrations of any single metabolite in isolation fails to characterise the true complexity of bioenergetic capacity, which depends on the interplay between the mitochondrial oxidative phosphorylation machinery, oxygen and substrate supply and intermediary metabolism (30). Current understanding of what happens to each of these components in human critical illness is reviewed below.

Metabolic pathways in critical illness

Critical illness is associated with a number of metabolic features, which distinguish it from health. There is a generalised catabolic response, which mobilises substrates from

endogenous stores (197). Lipolysis occurs in adipose tissue, to release free fatty acids (FFA) and glycerol into plasma (198, 199). In muscle, proteolysis releases amino acids, which can be recycled into glucose (mainly alanine and glutamine) or degraded into urea. Critically ill patients demonstrate a preference for glucose as a substrate and the liver produces large amounts of glucose, through both glycogenesis and gluconeogenesis (199). However, acute stress is also associated with insulin resistance, particularly in muscle, resulting in hyperglycaemia. The released glucose will be used by non-insulin-dependent organs (liver and brain). Metabolic pathways in different tissues are related, with the glycerol released from lipolysis used in the liver to produce glucose. In hypoxic tissues, lactate is produced from the anaerobic metabolism of glucose, and transported to the liver to regenerate glucose (the Cori cycle). Lactate is also formed under aerobic conditions, and interchanged between muscle cells, and high blood lactate levels down-regulate the use of glucose and FFA (200). There is evidence for reduced use of released FFA as a substrate for respiration, with decreased intramuscular concentrations of mitochondrial FAO enzymes (87) and triglyceride concentrations during the first week of critical illness (87).

Skeletal muscle mitochondrial structure and function in critical illness

Skeletal muscle is a relevant tissue in which to map out intracellular bioenergetic pathways in critically ill patients, as it represents a solid-end organ, subject to the impairments in tissue perfusion or oxygen delivery during critical illness, whilst being accessible without causing undue harm. Although skeletal muscle dysfunction is not often considered as part of the syndrome of multiple organ failure, its structure and function is modified by critical illness, with rapid onset muscle wasting reported in 50-100% of patients with multiple organ failure (201). Muscle wasting occurs at a rate of 2% per day, and to a greater extent in patients with more failing organs (202) and in non survivors compared to survivors (90). Although, at first

glance, skeletal muscle function may appear to be less critical for patient survival, than other tissues such as brain, heart or liver, the muscle weakness acquired during critical illness takes much longer to resolve than the impairments of respiratory, renal and cardiovascular systems, persisting for up to a year after hospitalisation in survivors (203), and is a major contributor to increased morbidity and mortality (204).

The concentration and activity of respiratory complexes involved in electron transport have been investigated in frozen muscle samples, but yield mixed results depending on the study and the normalisation of concentration or activity to tissue or mitochondrial content. Lower complex I activity and higher complex IV activity were demonstrated in non survivors of sepsis compared to healthy controls undergoing elective surgery, when these activities were expressed per citrate synthase activity (a putative marker of mitochondrial density) (20). In a subsequent study of septic patients with organ failure, non-survivors displayed lower concentrations of complex I and complex IV subunits, and a trend toward lower complex I activity than healthy controls (21). Another study comparing 10 patients with multiple organ failure secondary to sepsis and 10 healthy controls undergoing elective surgery, found lower complex I activity (when expressed per wet weight) in intercostal muscle, as well as lower citrate synthase activity, but reported no difference in complex IV activity(205). Also, when complex activity was expressed per citrate synthase activity, there was no difference between the groups, suggesting the decreased activity was due to a decrease in overall mitochondrial density, rather than a post-translational modification. When a different muscle (*vastus lateralis)* was examined in the same patients, citrate synthase and complex I activity (expressed per wet weight) did not differ between the groups, but complex IV activity was lower in patients with multiple organ failure than in controls. A heterogenous group of intensive care patients requiring mechanical ventilation for > 2 weeks were shown to have

lower concentrations of complexes II and IV in *vastus lateralis*, but when values were expressed relative to citrate synthase activity, there was no difference in complex I or IV, whilst complexes II and III were higher in the critically ill patients (131). In this cohort, measurement of muscle homogenate oxygen consumption rates (using high resolution respirometry) also demonstrated that the capacity for oxygen consumption driven by oxidative phosphorylation was lower than in healthy controls undergoing elective surgery. However, when this capacity was expressed relative to citrate synthase activity, there was no difference between the groups (131).

Skeletal muscle taken from 23 intensive care inpatients, with different primary diagnoses, demonstrated decreasing mitochondrial DNA copy numbers from day 1 to 7 of ICU admission(87). Greater mitochondrial dimensions have been measured in critically ill patients compared to the controls, with more swelling noted in the patients who died (estimated through measurements of mitochondrial outer membrane surface density and mitochondrial surface/volume ratio) (21). The same study demonstrated greater mRNA levels of a key mitochondrial biogenesis activator, PGC-1α, in survivors, compared to the controls, and markedly lower PGC-1α protein levels in the non survivors, compared to the controls. Exposure to endotoxin and exercise have been shown to activate muscle PGC-1α by protein phosphorylation (123, 206).

Cellular redox status in critical illness

Despite normal systemic oxygenation indices (PaO_2 and SpO_2), a study of skeletal muscle samples from 33 critically ill patients showed an increase in intramuscular HIF-1α protein concentration from day 1 to 7 of ICU admission (87). Greater activity of the antioxidant enzyme, superoxide dismutase, has been demonstrated in isolated mitochondria from

intercostal and *vastus lateralis* muscle in critically ill patients compared to healthy patients undergoing elective surgery - but no difference in superoxide dismutase activity in muscle homogenate as a whole (205). Survivors of critical illness have demonstrated greater intramuscular levels of mitochondrial superoxide dismutase proteins, compared to controls (21). In these patients, mitochondrial superoxide dismutase levels correlated with peroxisome proliferator-activated receptor gamma coactivator 1-alpha (PGC-1α), which also acts as co activator of gene expression for the mitochondrial oxidative stress response. Intramuscular concentrations of reduced glutathione were lower in critically ill patients compared to healthy controls suggesting the redox status of the cell was tipped towards increased oxidation, or reduced capacity to defend against ROS (207).

Mitochondrial function in other tissues in critical illness

In rapid postmortem studies of renal and cardiac tissue in 44 patients following death from sepsis, electron microscopy showed mitochondrial swelling, which were not observed in controls (208). In septic patients, platelet maximum oxygen consumption rate has been shown to correlate with the degree of organ failure and was higher in non survivors compared to survivors (209, 210). Several studies have demonstrated that peripheral blood mononuclear cells (PBMCs) from septic patients have greater oxygen consumption rates compared to controls (211, 212), along with greater markers of mitochondrial content (including citrate synthase activity, mitochondrial DNA and cytochrome c). Others have demonstrated lower oxygen consumption in septic PBMCs compared to controls (89, 213), despite unaltered mitochondrial content. In terms of functional relevance, blood cells are directly exposed to systemic cytokines and any other agents in the serum, and thus may be able to reflect "whole body" function, in response to inflammation and pharmacological agents. However, they will not be exposed to the same degree of hypoxia as the tissues. The

metabolic function of white blood cells themselves may be of prognostic value in critically ill patients, as they will reflect the degree of activation (or suppression) of the immune system.

4.2. Summary and study aims

Little is understood about how human cells produce energy during critical illness, and whether there are important differences in mitochondrial oxidative phosphorylation, intermediary metabolism and redox status which may be relevant for survival. Thus far, small studies in critically ill patients have focused on individual aspects of these interrelated processes and yielded mixed results. This study aimed to address a gap in the literature, by describing a comprehensive phenotype of skeletal muscle bioenergetic capacity in patients with multiple organ failure, by combining direct measurements of mitochondrial respiration with simultaneous targeted metabolomic analysis of related pathways, including intermediary metabolism and redox status. The primary aim was to determine if any aspects of this phenotype differed from that seen in health. The secondary aim was to determine if organ dysfunction or death from critical illness were related to any aspect of this cellular bioenergetic profile.

4.3. Hypothesis

It was hypothesised that critically ill patients would demonstrate a skeletal muscle bioenergetic and metabolic phenotype that was distinct from that in reference subjects. In particular, it was anticipated that direct measures of mitochondrial respiration in critically ill patients would demonstrate reduced capacity for oxidative phosphorylation compared to controls, in line with the decreased ATP concentrations found in previous studies. It was also hypothesised that non-survivors would have a greater degree of bioenergetic impairment compared to survivors, in line with the theory that death results from bioenergetic failure.

4.4. Objectives

- Carry out an observational case-control study, to compare the cellular bioenergetic profile in a group of critically ill patients with that of a reference group. Phenotype characterisation was based on direct measurements of mitochondrial respiration combined with targeted metabolomic analysis of related pathways, including intermediate metabolism and redox status.
- Carry out a prospective cohort study of critically ill patients, in order to compare bioenergetic profiles in survivors and non survivors, and to determine if any relationship existed between cell bioenergetic phenotype and clinical indicators of organ dysfunction.

4.5. Materials and Methods

4.5.1. Study design

The study was part of the TIMELORD study, the conduct of which is outlined in detail in Chapter 2. This component of the study encompassed two elements. The first was a case-control study comparing skeletal muscle bioenergetic and metabolic profile between a group of critically ill patients and a reference group undergoing elective orthopaedic surgery. The second element was a prospective cohort study comparing the skeletal muscle bioenergetic and metabolic profile in survivors and non survivors of critical illness and investigating potential associations with clinical markers of organ dysfunction. Study design, ethical approval, screening, consent and enrolment were described in full in Chapter 2.

4.5.2. Subjects

Subject selection and enrolment are outlined in section 2.4.2. Critically ill patients (cases) were patients with acute, severe physiological impairment from any primary cause, requiring at least two forms of organ support, and admitted to the ICU within the previous 48 hours. Reference subjects (controls), were age and sex-matched patients undergoing elective hip replacement under general anaesthesia.

4.5.3. Study specific measures

Following enrolment, skeletal muscle samples from *vastus lateralis* were taken from all participants and subsequently analysed to quantify multiple aspects of cellular bioenergetics, metabolic pathways and redox status. Biopsies were performed as described in section 0. For the critically ill patients muscle biopsies were performed within 48 hours of admission to the ICU, and again at day 5-7. All biopsies were performed by the same operator (the author). For the reference group (controls), vastus lateralis muscle was extracted by the surgeon (Mr Nicholas Garlick), immediately following planned exposure of the muscle, during the early stages of the operation, and prior to insertion and cementing of the joint prosthesis. The preparation and analysis of the skeletal muscle samples to characterise bioenergetic phenotype are outlined in detail in Chapter 3. The methodology for high resolution respirometry is outlined in section 3.2; characterisation of metabolic pathways using enzyme assays in section 3.3; and targeted metabolomic and redox analysis using ultra-high performance liquid chromatography is described in section 3.4.

4.5.4. Clinical data collection

Collection of clinical data from the two cohorts is outlined in section 2.4.5.

4.5.5. Data analysis

Data analysis was carried out as outlined in sections 2.4.6 and 2.5.7.

4.6. Results

4.6.1. Subject characteristics

The subjects are described in Chapter 2, section 2.5.8. The presenting diagnoses of the critically ill cohort are outlined in Table 4, the demographic and baseline clinical characteristics of the critically ill and reference cohorts are compared in Table 3 and the clinical characteristics of the critically ill patients at 48 h and day 5-7 in Table 5. Baseline characteristics of survivors and non survivors are compared in Table 6.

4.6.2. Comparison between critically ill and reference patient cohorts

Mass-specific respiration rates

The mass-specific respiration rates from the reference cohorts and critically ill patients at < 48 h and day 5-7 are summarised in Table 19. The criteria for quality control in respirometry were not met for three of the samples from the reference group, therefore only respirometry data from 9 subjects are included in the analysis. At both timepoints, the critically ill cohort demonstrated similar maximum respiratory capacities ($OXPHOS_{MAX}$ per mass and ETS_{MAX} per mass) as the reference cohort. Mass-corrected $LEAK_{FAO}$ and $OXPHOS_{FAO}$ were significantly lower in critically ill patients at < 48 hours compared to the controls ($p = 0.011$ and 0.0017 respectively). In critically ill cohort, ETS_{MAX} per mass increased from 48 hours to day 5-7 of ICU admission ($p = 0.0049$), which appeared to be due to an increase in complex I respiratory capacity during this time period ($p=0.0068$) rather than complex II ($p = 0.13$) (Table 19).

Table 19. Mass-specific respiration rates in the critically ill and reference cohorts

J_{O2} per mass (pmol/s/mg)	Reference group	Critically ill patients < 48 h	Critically ill patients day 5-7
$LEAK_{FAO}$	5.49 (4.82-6.75; 4.16-7.44)	4.55 (3.17-5.51;2.42-6.61) *	4.54 (3.62-6.02; 2.76 – 7.32)
$OXPHOS_{FAO}$	14.7 (10.5-17.1; 8.95-27.2)	9.96 (7.16-10.8; 5.15-13.2) **	9.25 (7.20-13.4; 6.54-20.5) *
$OXPHOS_{CI}$	26.2 (19.6-31.3; 14.6-42.2)	20.5 (17.3-23.5; 14.7-34.0)	26.8 (22.0-30.8; 19.0-40.7) $^{\#\#}$
$OXPHOS_{MAX}$	44.6 (38.4-59.4; 32.1-80.7)	44.8 (38.0-53.2; 34.0-63.4)	47.5 (45.9-58.2; 37.4-72.2)
ETS_{MAX}	53.0 (45.8-71.8; 37.1-98.1)	55.59 (48.0-66.6; 42.1-76.1)	62.6 (57.5-71.5; 47.9-84.9) $^{\#\#}$
ETS_{CII}	24.3 (21.0-32.9; 18.6-42.6)	24.5 (22.5-27.8; 18.3-41.1)	25.5 (22.2-32.3; 19.4-38.9)

Median (IQR; range) of respiratory capacities in reference group (n=9); critically ill patients at < 48 h (n=21) and day 5-7 (n=12). Respiratory capacities generated by sequential addition of substrates, uncouplers and inhibitors according to previously described SUIT protocol. $LEAK_{FAO}$: capacity for respiration supported by proton leak, in the presence of malate and octanoyl carnitine and absence of ADP; $OXPHOS_{FAO}$: capacity for oxidative phosphorylation supported by FAO, following addition of saturating ADP; $OXPHOS_{CI}$: capacity for oxidative phosphorylation supported by complex I; following addition of saturating pyruvate and glutamate; $OXPHOS_{MAX}$: maximum capacity for oxidative phosphorylation supported by complex I and complex II, following addition of succinate; ETS_{MAX}: maximum capacity of the electron transport system uncoupled from oxidative phosphorylation, following titration of uncoupler; ETS_{CII}; capacity of uncoupled electron transport system supported by complex II alone, following inhibition of complex I by rotenone. Median (IQR; range); * $p < 0.05$, ** $p < 0.01$ vs reference group; $^{\#}p < 0.05$, $^{\#\#}p < 0.01$ vs critically ill patients within 48 hours.

Oxphos coupling efficiency

Oxphos coupling efficiency was greater in critically ill patients at both timepoints compared to the reference group (Figure 24, p = 0.045 and 0.034 respectively), indicating greater extent of coupling of electron transport to ADP phosphorylation (coupling efficiency = 1 for a fully coupled system), and consistent with the reduced capacity for proton leak $LEAK_{FAO}$ per mass (Table 19). This suggests that the lower $LEAK_{FAO}$ in critically ill patients is a consequence of reduced capacity for leak respiration and not just reduced capacity for FAO-supported respiration.

Figure 24. OXPHOS coupling efficiency in critically ill and reference cohorts

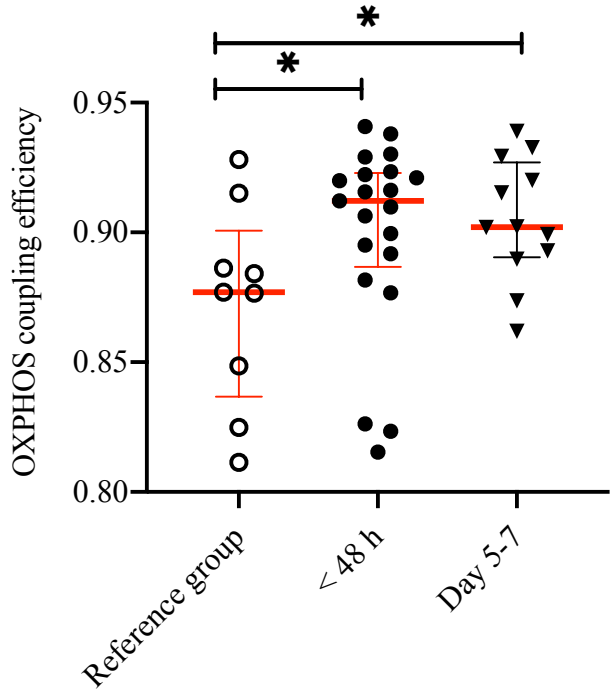

OXPHOS coupling efficiency (ratio) of skeletal muscle in reference group (n=9), critically ill patients at <48 h (n=21) and at day 5-7 (n=12). *p < 0.05. Error bars indicate median and interquartile range.

Flux control ratios

Flux control ratios were calculated to estimate the proportional contribution of various components of the mitochondrial system to total respiratory capacity, and the results are displayed in Figure 25. In this thesis, J_{O2} per mass measured in each respiratory state was divided by the maximum uncoupled respiratory capacity (ETS_{MAX} per mass), with ETS_{MAX} taken to represent a functional marker of mitochondrial content. As previously shown, ETS_{MAX} did not differ significantly between the three groups. Compared to the reference group, the relative capacity for leak respiration ($LEAK_{FAO}/ETS_{MAX}$) was lower in critically ill patients at both timepoints (p=0.024 and 0.034 respectively), as was the relative capacity for FAO-limited oxidative phosphorylation ($OXPHOS_{FAO}/ETS_{MAX}$) (p <0.0001 and 0.0005). These findings were consistent with the mass-specific values. In critically ill patients, the lower proportional contribution of maximum oxidative phosphorylation to ETS_{MAX} ($OXPHOS_{MAX}/ETS_{MAX}$), thought to represent the extent to which ATP synthase limits electron flux through the electron transport system, also points towards increased efficiency of the system, with less limitation of ATP synthase in the critically ill patients. Relative capacity for complex I-limited oxidative phosphorylation ($OXPHOS_{CI}/ETS_{MAX}$) was lower in critically ill patients at <48 hours compared to the control group (p = 0.0093), but no difference was observed between groups in terms of the relative capacity of Complex II ($OXPHOS_{CII}/ETS_{MAX}$).

Figure 25. Flux control ratios in the critically ill and reference cohorts

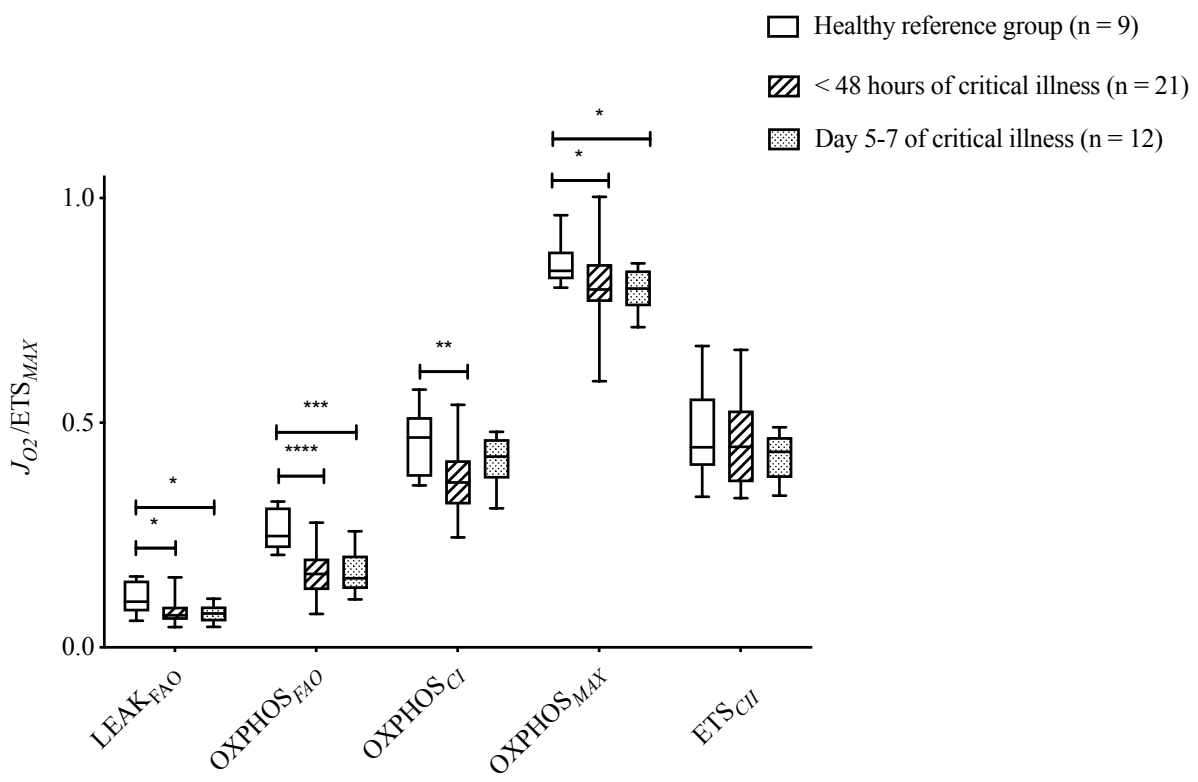

Box and whisker plot of individual respiratory capacities expressed relative to the maximum capacity of the uncoupled electron transport system (ETS$_{MAX}$) in reference group (n=9), critically ill patients at <48h (n=21) and day 5-7 (n=12). * $p < 0.05$, ** $p<0.01$, ***$p < 0.001$, ****$p<0.0001$ compared to reference group.

Respiratory capacities corrected to citrate synthase activity

Mass-specific respiratory capacities were also expressed relative to mass-specific citrate synthase activity (a putative marker of mitochondrial density). Mass-specific citrate synthase activity was markedly lower in the critically ill cohort, both at 48 hours ($p = 0.031$) and day 5-7 ($p=0.0028$) compared to the reference group (Figure 26). When expressed relative to citrate synthase activity, $OXPHOS_{MAX}$ and ETS_{MAX} were greater in critically ill patients at day 5-7 compared to controls ($p= 0.003$ and <0.001 respectively; Figure 27). At this later timepoint, critically ill patients also had greater citrate-synthase specific $LEAK_{FAO}$ ($p=0.031$), $OXPHOS_{CI}$ ($p=0.004$) and ETS_{CII} ($p = 0.002$) compared to the reference group.

Figure 26. Citrate synthase activity in critically ill and reference cohorts

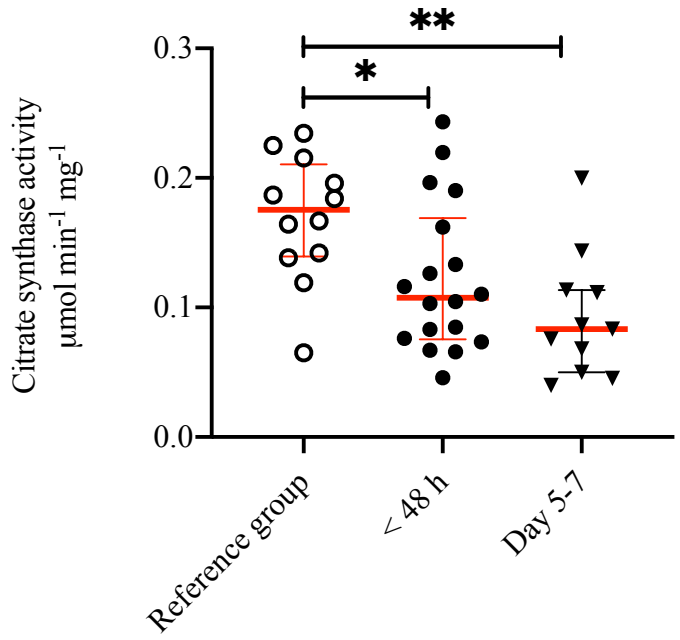

Mass-specific citrate synthase activity in skeletal muscle in reference group (n=9), critically ill patients at <48 h (n=21) and at day 5-7 (n=12). *p < 0.05, ** p<0.01 *vs* reference group. Error bars indicate median and interquartile range.

Figure 27. Citrate-synthase corrected respiratory capacities in critically ill and reference cohorts

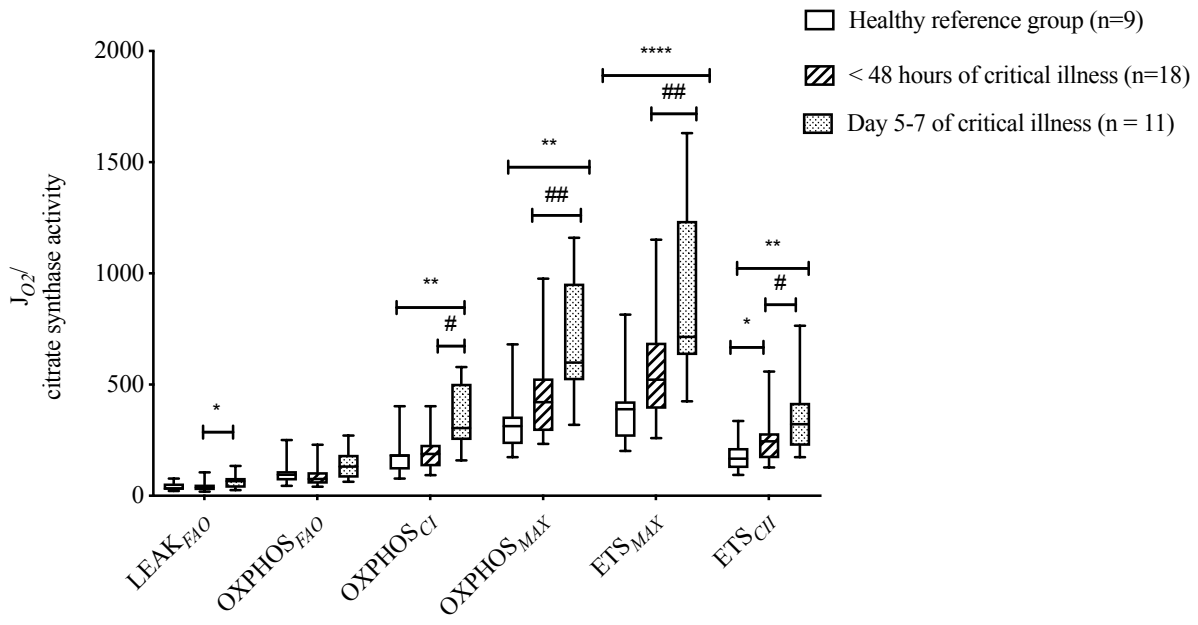

Box and whisker plot of mass-specific respiratory capacities expressed relative to mass-specific citrate synthase activity (a putative marker of mitochondrial volume density), in the reference group (n=9), critically ill patients at <48h (n=21) and day 5-7 (n=12). * $p < 0.05$, ** $p<0.01$, ***$p < 0.001$, ****$p<0.0001$ compared to reference group. # $p <0.05$, ## $p<0.01$ compared to first timepoint (<48 hours) of critical illness.

HADH activity

The mass-specific activity of the FAO enzyme, 3-hydroxyacyl dehydrogenase (HADH) was lower in critically ill patients at < 48 hours (p=0.035) and Day 5-7 (0.0083) compared to the reference group (Figure 28).

Figure 28. HADH activity in critically ill and reference cohorts

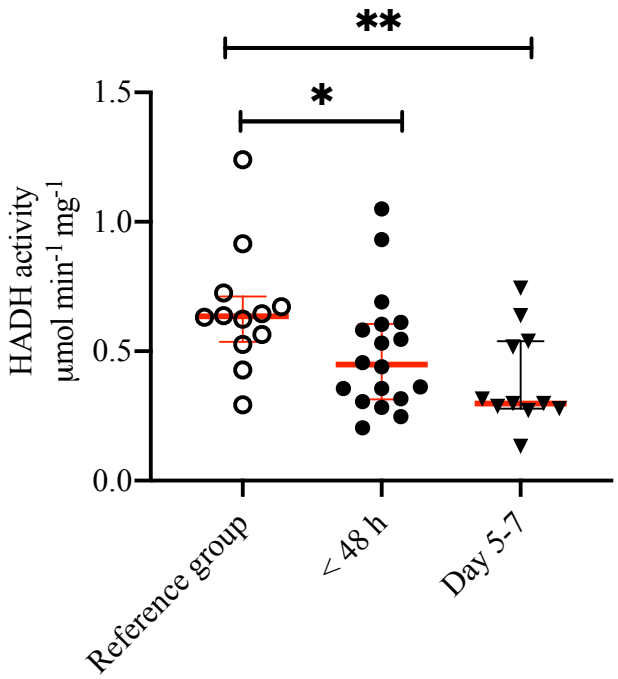

Specific activity of HADH enzyme (corrected to protein concentration) in skeletal muscle in reference group (n=12), critically ill patients at <48 h (n=21) and at day 5-7 (n=12). *p < 0.05, ** p<0.01 *vs* reference group. Error bars indicate median and interquartile range.

Energetics

Levels of phosphate-containing compounds in the critically ill and reference cohorts are demonstrated in Figure 29. Compared to the reference cohort, at 48 h the critically ill patients had higher relative levels of ATP (p 0.0047) and ADP (p=0.048), and higher levels of ATP (p =0.045) and GDP at day 5-7 (p= 0.0036). Levels of the energy storage molecule, PCr, along with AMP, GTP, NADP and NAD did not differ in critically ill patients compared to the reference group. Energetic ratios (including [ATP]/[ADP]; [GTP]/GTP] and [PCr]/[ATP] did not differ between the groups, nor did adenylate energy charge (Figure 30).

Figure 29. Intramuscular levels of phosphate-containing compounds in critically ill and reference cohorts

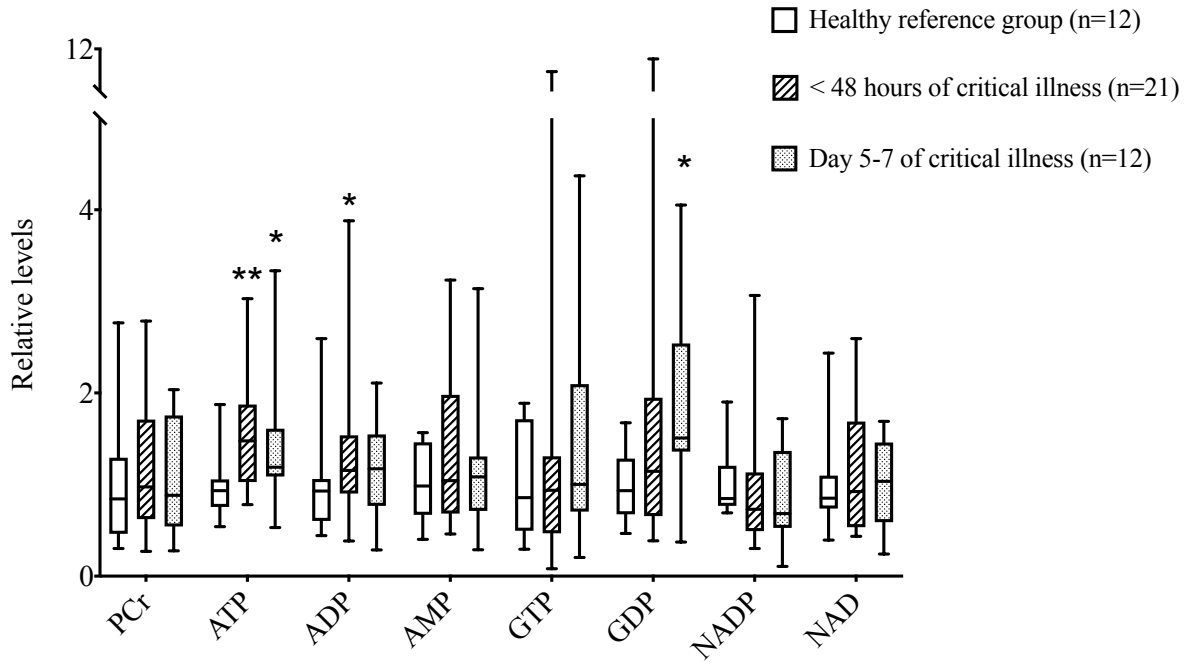

Box and whisker plot of phosphate-containing compounds in skeletal muscle, expressed relative to the mean value in the reference group, in the reference group (n=12), critically ill patients at <48h (n=21) and day 5-7 (n=12). * $p < 0.05$, ** $p<0.01$, vs reference group.

Figure 30. Skeletal muscle energetic ratios in critically ill and reference cohorts

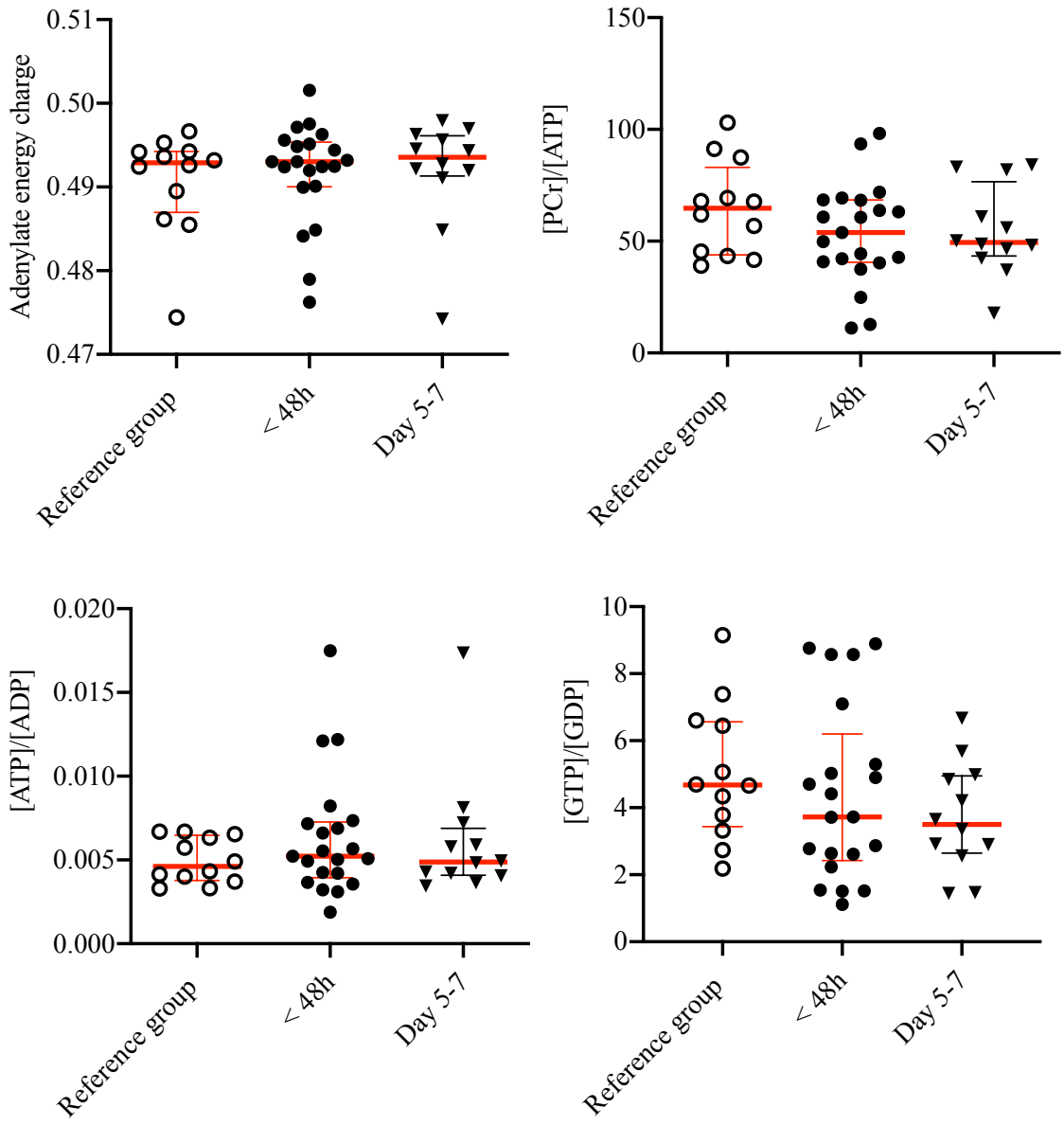

Energetic ratios in skeletal muscle in reference group (n=12), critically ill patients at <48 h (n=21) and at day 5-7 (n=12). Error bars indicate median and interquartile range.

Redox status

Ratios of known redox couples were quantified to give an indication of skeletal muscle redox status. The ratio of reduced methionine to its oxidised product, methionine sulphoxide ([Met]/[MetSO]) was greater in critically ill patients at Day 5-7 (median 3.38, IQR 2.63-4.3) compared to the reference group (median 2.44, IQR 1.84-2.85, p=0.028), indicating a more reduced state within the cell (Figure 31). However, the relative levels of both methionine and methionine sulphoxide were also greater in critically ill patients at both timepoints compared to the reference group ($p < 0.001$ for all) (Figure 31). Together, these findings imply that critically ill patients undergo an increase in both oxidative and reductive capacity, and that the increased reductive capacity in skeletal muscle more than compensates for the increased oxidation in critical illness. The ratio of reduced glutathione to oxidised glutathione disulphide ([GSH]/[GSSG]) was also greater in critically ill patients, at both < 48 h and day 5-7 ($p = 0.013$ and 0.001 respectively, Figure 32), but in this case the difference appeared to be driven by increasing reductive capacity in critically ill patients, with markedly greater GSH in critically ill patients compared to the reference group ($p = 0.027$ at < 48 h and 0.0014 at day 5-7), and no difference in GSSG between groups.

Figure 31. Skeletal muscle methionine redox status in critically ill and reference cohorts

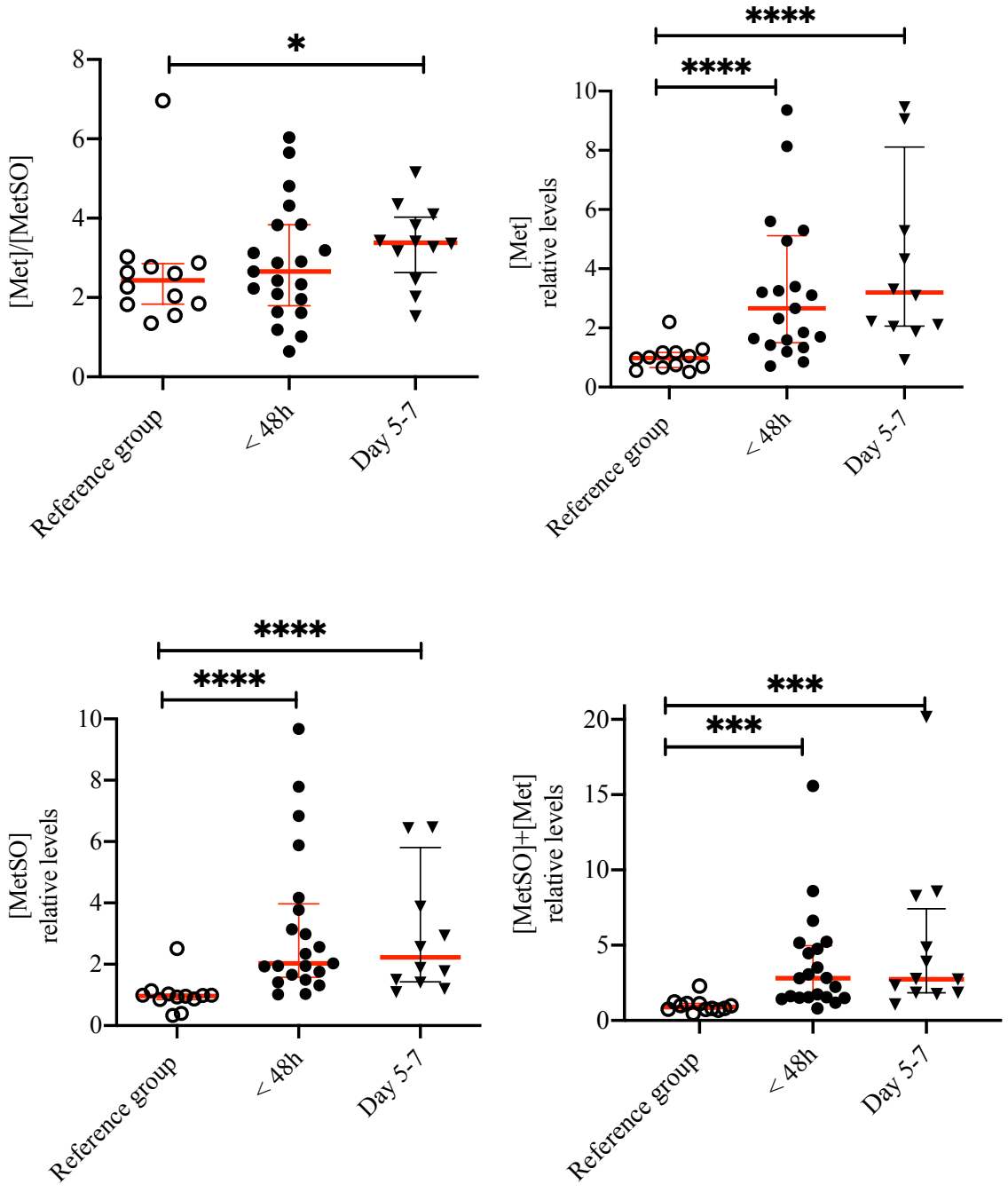

Ratios of reduced methionine (Met) and oxidised methionine sulphoxide (MetSO) and their relative levels in the reference group (n=12), critically ill patients at <48 h (n=21) and at day 5-7 (n=12). Error bars indicate median and interquartile range. *p < 0.05, **p<0.01, ***p < 0.001, ****p<0.0001 *vs* reference group.

Figure 32. Skeletal muscle glutathione redox status in critically ill and reference cohorts

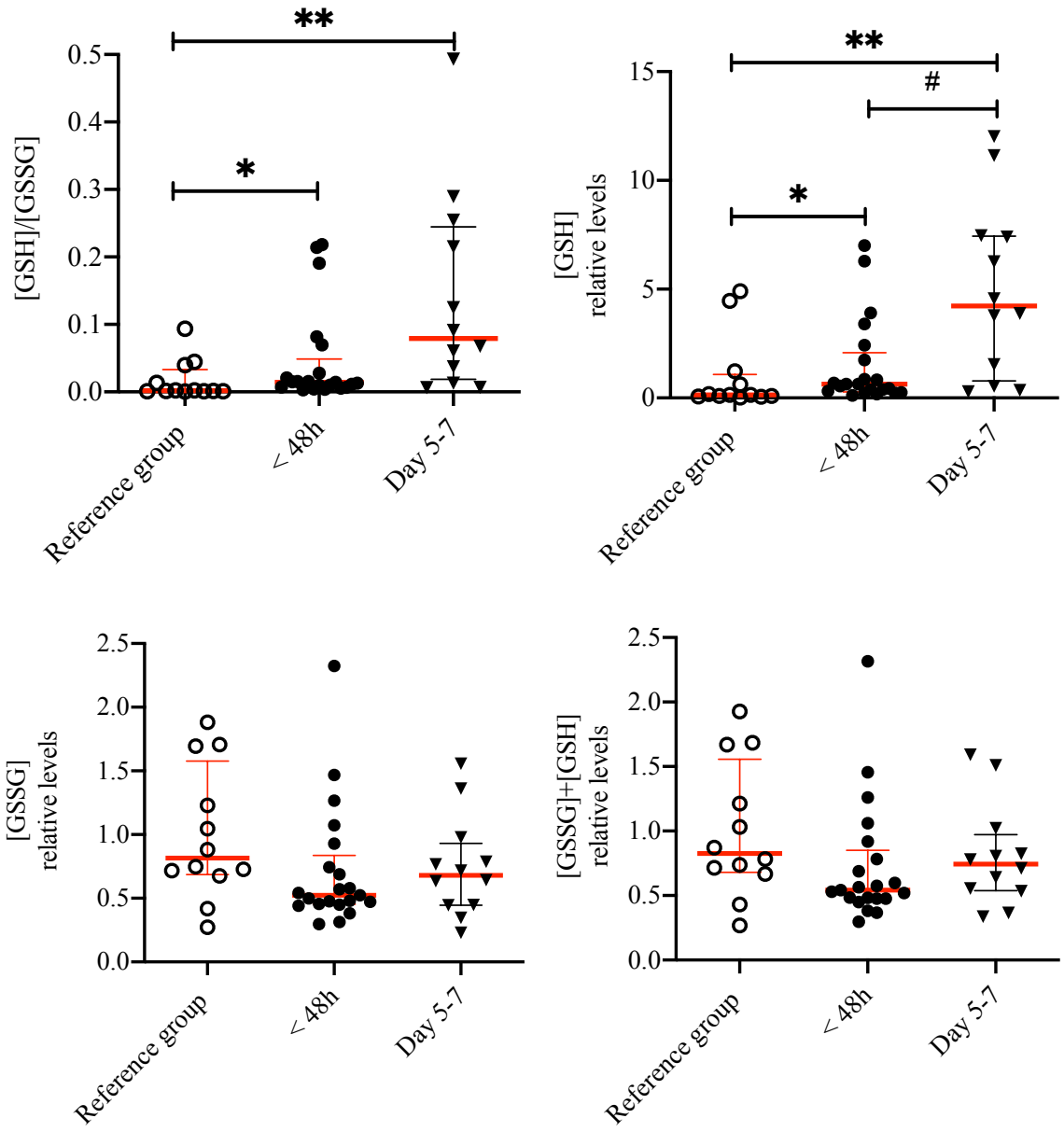

Ratios of reduced glutathione (GSH) and oxidised glutathione (GSSG) and their relative levels in the reference group (n=12), critically ill patients at <48 h (n=21) and at day 5-7 (n=12). Error bars indicate median and interquartile range. *p < 0.05, **p<0.01, ***p < 0.001, *vs* reference group. # p <0.05 compared to first timepoint (<48 hours) of critical illness.

Intermediary metabolism

Total glycolytic intermediates were greater in critically ill patients at < 48 h (median 2.09, IQR 0.9-2.74) compared to the reference group (median 0.72, IQR 0.4-1.14, p = 0.011; Figure 33). This difference was driven by intermediates later in the glycolytic pathway, with markedly higher levels of 2-3 phosphoglycerate (p = 0.0001)), phosphoenolpyruvate (p = 0.02) and pyruvate (p = 0.02) in the critically ill patients, and no difference between the groups in terms of the earlier intermediates, such as glucose-6-phosphate, fructose-6-phosphate or fructose bisphosphate (
Figure 34).

Critically ill patients had lower levels of the TCA intermediates immediately downstream of citrate synthase (Figure 35). Citrate was lower in critically ill patients (at < 48 h, median 0.43, IQR 0.28-0.93) compared to the reference group (median 0.80, IQR 0.58-1.44, p = 0.04)). Isocitrate was also lower in critically ill patients (median 0.44, IQR 0.33-0.85) compared to the reference group (median 0.87, IQR 0.50-1.30, p = 0.006). In contrast, in the latter part of the cycle, α-ketoglutarate, malate and oxaloacetate were all higher in the critically ill patients compared to the reference group (p = 0.0047, 0.022 and 0.007 respectively). This suggests a bottleneck at citrate synthase, which may be explained by the lower citrate synthase activity in critically ill patients, previously shown in Figure 26. It also suggests an alternative pathway for replenishing the latter half of the TCA cycle beyond isocitrate.

Asparagine, and the branched chain amino acids (BCAA), leucine, isoleucine and valine, were all markedly higher in critically ill patients than the reference group, whilst glutamate, glutamine and ornithine were all lower in critically ill patients (Figure 36).

Figure 33. Skeletal muscle total glycolytic metabolites in critically ill and reference cohorts

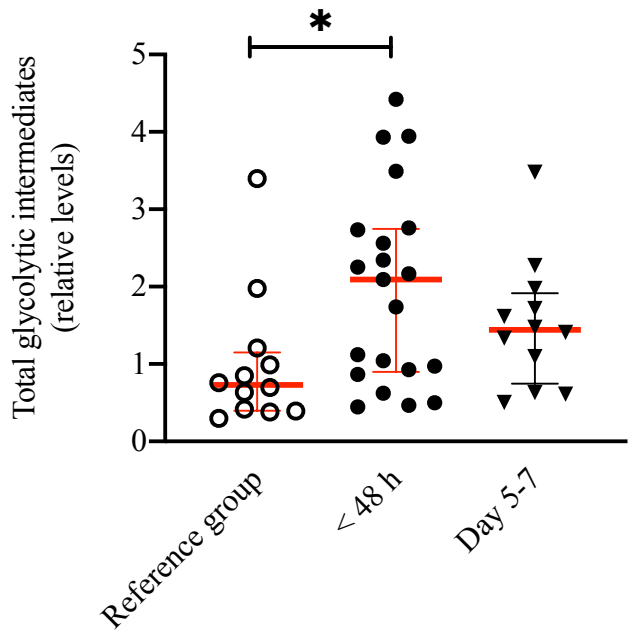

Combined levels of total glycolytic metabolites, expressed relative to the average of the reference group, in the reference group (n=12), critically ill patients at <48 h (n=21) and at day 5-7 (n=12). Error bars indicate median and interquartile range. *p < 0.05 v*s* reference group

Figure 34. Skeletal muscle glycolytic intermediates in critically ill and reference cohorts

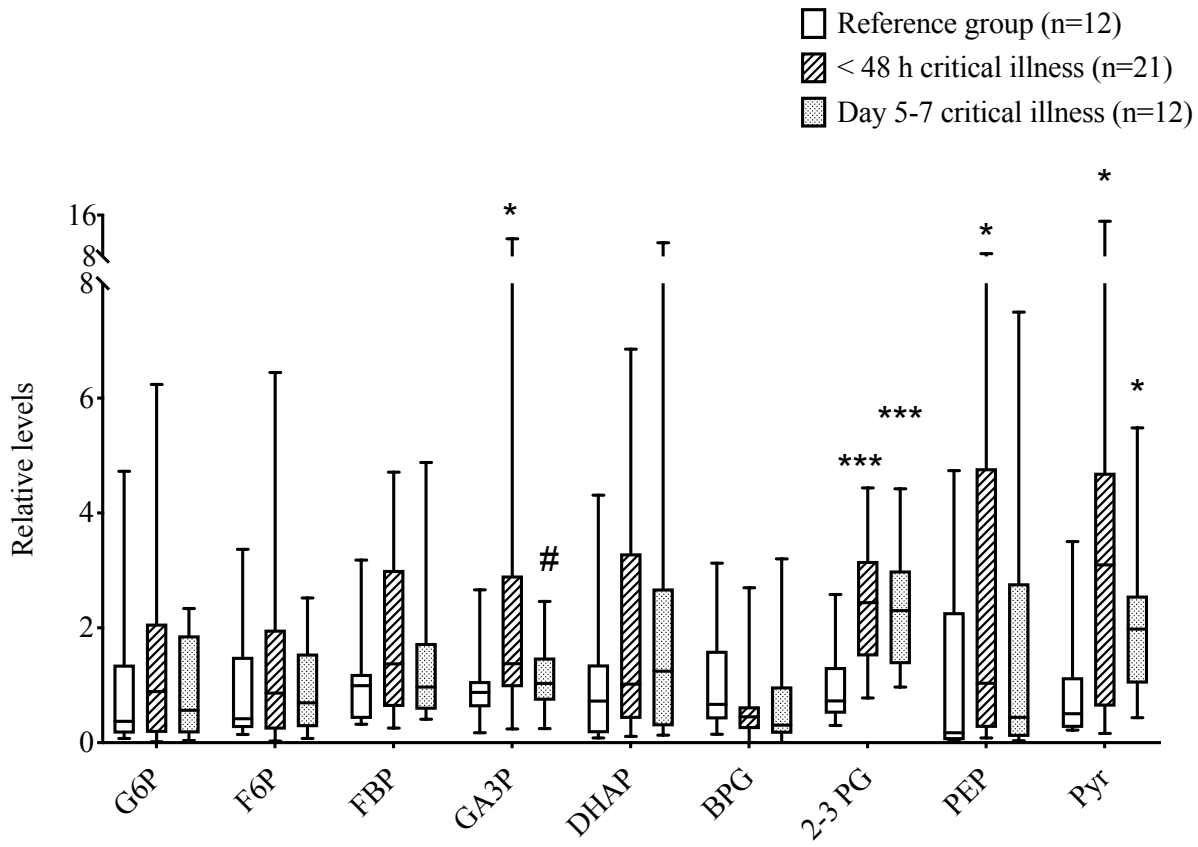

Box and whisker plot of skeletal muscle levels of glycolytic metabolites, expressed relative to the average of the reference group, in the reference group (n=12), critically ill patients at <48 h (n=21) and at day 5-7 (n=12). G6P: glucose-6-phosphate; F6P: fructose-6-phosphate; FBP: fructose bisphosphate; GA3P: glyceraldehyde-3-phosphate; DHAP: dihydroxyacetone phosphate; BPG: bisphosophoglycerate; 2-3 PG: 2-3 phosphoglycerate; PEP: phosphoenolpyruvate; Pyr: pyruvate. $p < 0.05$, ** $p<0.01$, ***$p < 0.001$ vs reference group. # $p <0.05$ compared to first timepoint (<48 hours) of critical illness.

Figure 35. Skeletal muscle TCA intermediates in critically ill and reference cohorts

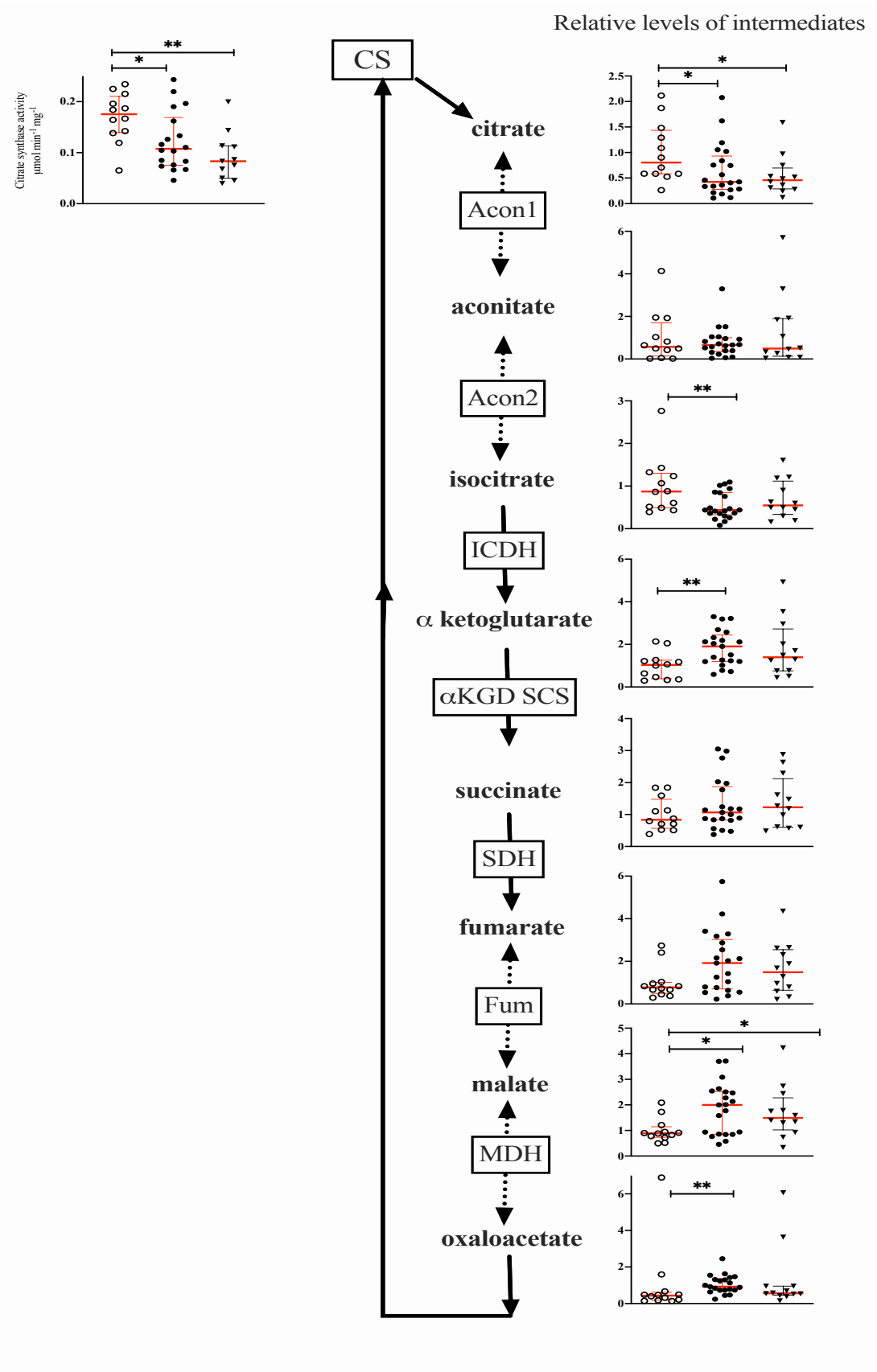

Levels quantified by mass spectroscopy and expressed relative to the average of the reference group. $p < 0.05$, ** $p<0.01$, ***$p < 0.001$ vs reference group. # $p <0.05$, ## $p<0.01$, ### $p <0.001$ compared to first timepoint (<48 hours) of critical illness. Error bars show median and interquartile range. Reference patients (n=12, unfilled circles), critically ill patients at < 48 hours of admission (n=18, filled circles) and at Day 5-7 of ICU admission (n=11, filled triangles). Levels are expressed relative to the average of the reference group**.**

Figure 36. Skeletal muscle amino acids in critically ill and reference cohorts

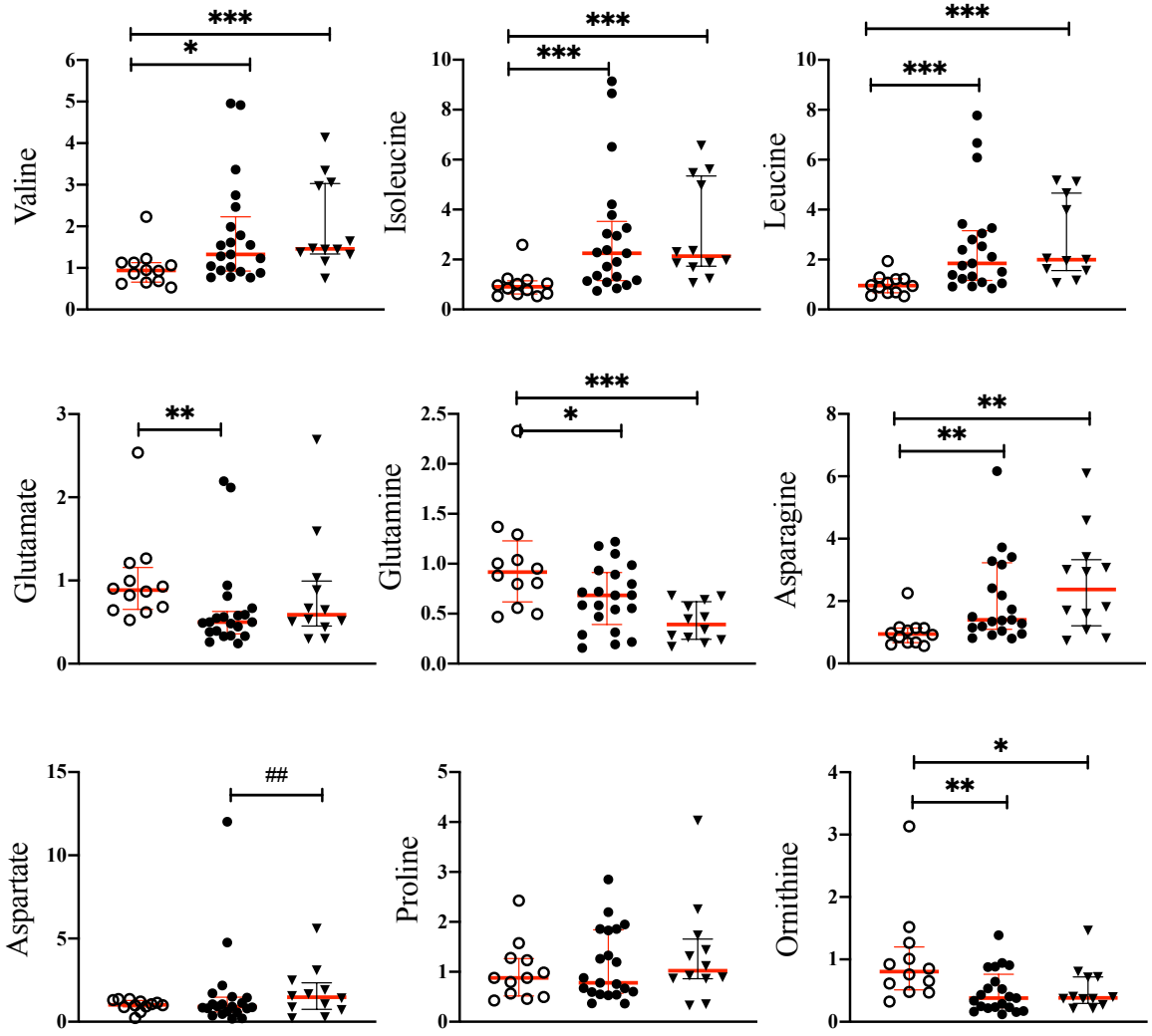

Levels are expressed relative to the average of the reference group. p < 0.05, ** p<0.01, ***p < 0.001 *vs* reference group. # p <0.05, ## p<0.01, ### p <0.001 compared to first timepoint (<48 hours) of critical illness. Reference patients (n=12, unfilled circles), critically ill patients at < 48 hours of admission (n=18, filled circles) and at Day 5-7 of ICU admission (n=11, filled triangles). Error bars show median and interquartile range.

Carnitine-based metabolites

The sum of total carnitines (total acyl carnitines plus free carnitine) was similar in the critically ill and reference cohorts (Figure 37). Short chain acyl carnitines (2-6 carbons) did not differ between critically ill patients and the reference group, but medium chain (7-12 carbons) and long chain (>12 carbons) were markedly greater at < 48 h of critical illness compared to the reference group (p =0.016 and <0.0001). This difference persisted at day 5-7 (p = 0.04 and 0.004 respectively, Figure 38). Free carnitine was also greater in critically ill patients at < 48 h (p = 0.002). A heat map showing levels of the individual carnitines (expressed relative to the average of the reference cohort) measured in the critically ill cohort at both timepoints, is shown in Figure 39. The greatest increases were seen in carbon chain lengths 5 and 20.

Figure 37. Skeletal muscle total carnitines in critically ill and reference cohorts

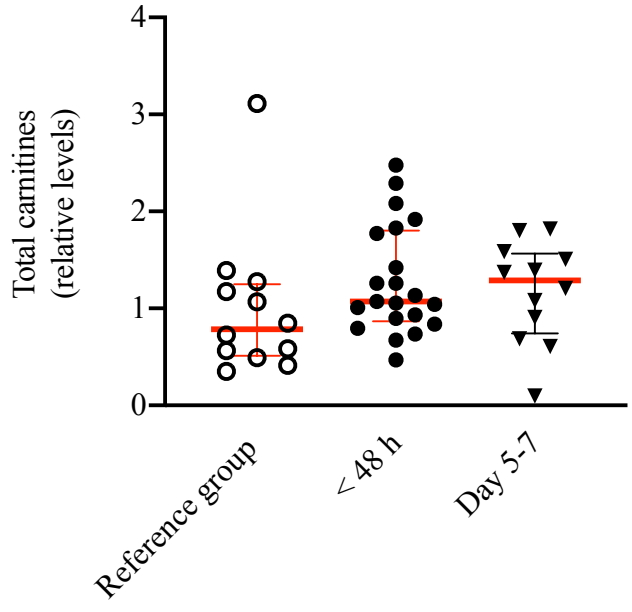

Total carnitine levels are expressed relative to the average of the reference group. * p < 0.05 *vs* reference group. Error bars show median and interquartile range.

Figure 38. Skeletal muscle carnitine groups in critically ill and reference cohorts

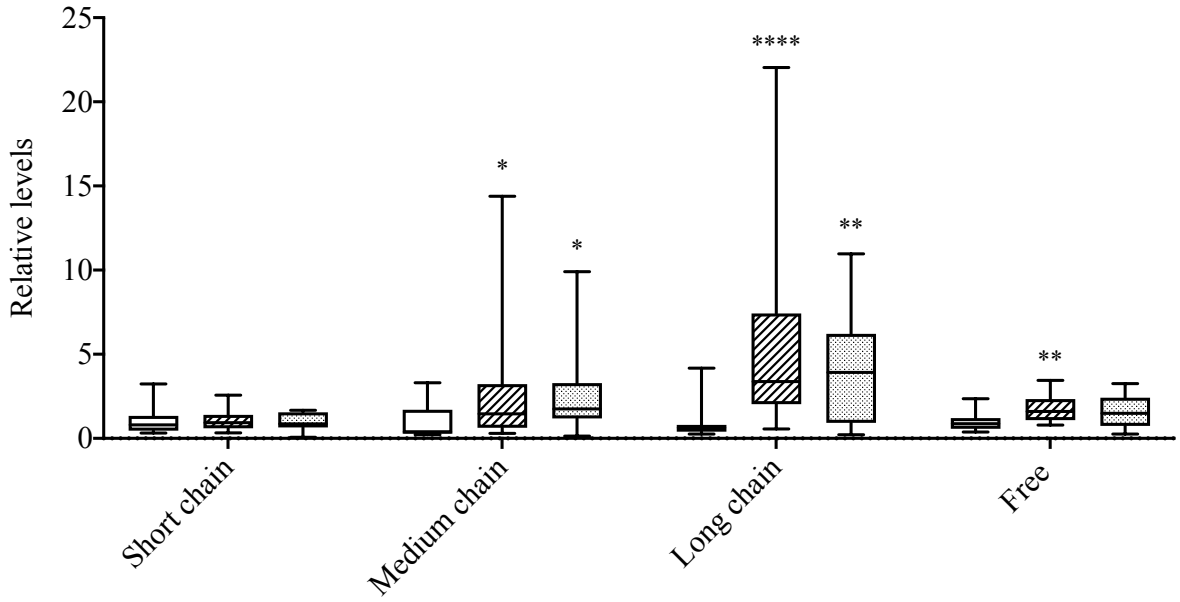

Relative levels of short (2-6 carbons), medium (7-12 carbons) and long chain (>13 carbons), and free carnitine. Levels are expressed relative to the average of the reference group. $p < 0.05$, ** $p<0.01$, ***$p < 0.001$ vs reference group. # $p <0.05$, ## $p<0.01$, ### $p <0.001$ compared to first timepoint (<48 hours) of critical illness. Reference patients (n=12, unfilled box), critically ill patients at < 48 hours of admission (n=18, diagonal stripes) and at Day 5-7 of ICU admission (n=11, grey dots). Error bars show median and interquartile range.

Figure 39. Heat map of skeletal muscle levels of individual acyl carnitines in critically ill and reference cohorts

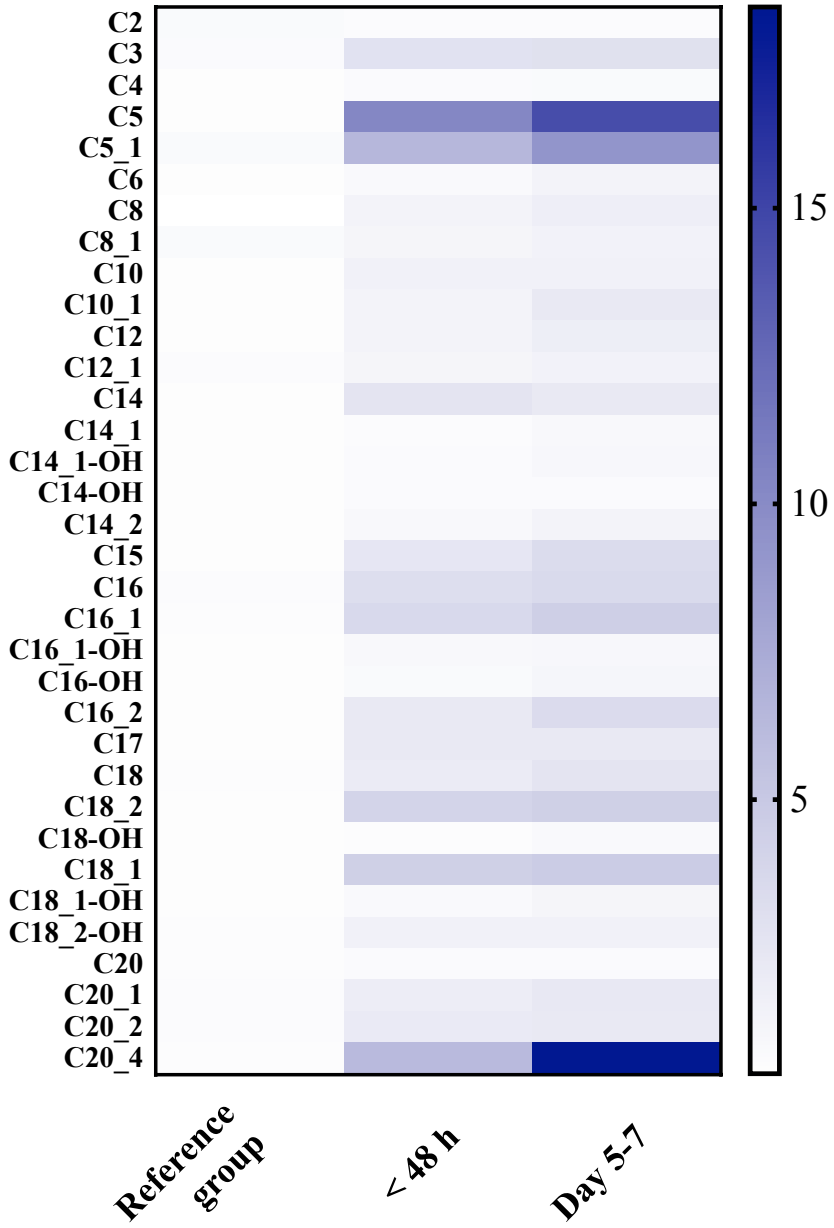

C: carbon chain length. Levels expressed relative to the average of the reference group. Colour intensity represents degree of increase above the average of the reference group (0-20 fold).

4.6.3. Survival phenotype in skeletal muscle of critically ill patients

Of the 21 critically ill patients tested at < 48 hours, 12 died prior to hospital discharge. Non survivors were older and sicker on admission, according to APACHE II and SOFA scores (Table 6).

Skeletal muscle respiratory function

Mass-specific and relative respiratory capacities in survivors and non survivors at < 48 h and day 5-7 are summarised in Table 20. There was no difference between survivors and non survivors in terms of any mass-corrected respiratory capacities at < 48 h or Day 5-7. Survivors had lower relative capacity for complex-I supported respiration ($OXPHOS_{CI}/ETS_{MAX}$, median 0.32, IQR 0.31-0.35) compared to non survivors (median 0.41, IQR 0.37-0.45, p = 0.01). The ratio of $OXPHOS_{MAX}/ETS_{MAX}$ was also lower in survivors (median 0.78, IQR 0.75-0.80) compared to non survivors (median 0.83, IQR 0.79-0.89, p = 0.04). There was a trend towards lower proportional capacity for FAO-supported respiration ($OXPHOS_{FAO}$ / ETS_{MAX}) in survivors (median 0.13, IQR 0.12-0.18) compared to non survivors (median 0.19, IQR 0.14-0.23, p = 0.06). There was no difference between survivors and non survivors in any of the ETS_{MAX}-corrected values at Day 5-7. There was no difference between survivors and non survivors in terms of their OXPHOS coupling efficiency at < 48 h (p = 0.28) or Day 5-7 (p =0.93).

Table 20. Skeletal muscle respiratory capacities in survivors and non survivors at < 48 h and day 5-7

Skeletal muscle analytes	Critically ill patients at < 48 h		Critically ill patients at day 5-7	
	Survivors (n=9)	Non survivors (n=12)	Survivors (n=4)	Non survivors (n=8)
Mass-specific respiratory capacity (pmol/s/mg)				
$LEAK_{FAO}$	4.48 (2.82-5.08; 2.42-5.81)	4.57 (3.29-5.96; 2.64-6.61)	5.02 (3.79-6.88; 3.66-7.23)	4.34 (3.31-5.98; 2.76-7.32)
$OXPHOS_{FAO}$	9.28 (6.31-11.3; 5.74-13.2)	9.98 (7.73-10.9; 5.15-12.0)	11.3 (9.17-14.5; 9.09-15.0)	7.95 (7.07-13.2; 6.54-20.5)
$OXPHOS_{CI}$	20.4 (16.2-23.2; 14.7-34.0)	20.6 (17.6-24.8; 16.7-28.7)	29.2 (24.0-38.3; 22.9-40.7)	24.6 (20.5-29.7; 19.0-35.9)
$OXPHOS_{MAX}$	47.7 (38.3-54.6; 37.7-58.7)	40.7 (37.8-52.9; 34.0-63.4)	53.7 (46.3-59.1; 45.8-72.2)	47.1 (45.2-54.0; 37.4-66.8)
ETS_{MAX}	63.1 (49.7-73.1; 47.2-76.1)	51.8 (44.3-63.1; 42.2-69.2)	67.0 (62.1-81.7; 62.1-84.9)	62.3 (55.3-69.0; 47.9-79.6)
ETS_{CII}	25.8 (22.0-28.7; 20.6-39.2)	24.1 (22.6-25.9; 18.3-41.1)	27.4 (22.0-36.1; 21.0-38.2)	25.4 (22.2-32.3; 19.4-38.9)
Relative respiratory capacities (relative to ETS)				
$LEAK_{FAO}$	0.0630 (0.0515-0.0.0794; 0.0465-0.0971)	0.0747 (0.0675-0.126; 0.0453-0.0156)	0.0756 (0.0616-0.0857; 0.0589-0.0871)	0.0761 (0.0511-0.103; 0.0457-0.108)
$OXPHOS_{FAO}$	0.132 (0.122-0.176; 0.114-0.192)	0.185 (0.139-0.231; 0.0746-0.277)	0.154 (0.147-0.195; 0.146-0.208)	0.148 (0.115-0.212; 0.107-0.259)
$OXPHOS_{CI}$	0.321 (0.312-0.357; 0.285-0.448)	0.408 (0.367-0.445; 0.245-0.540)*	0.436 (0.385-0.480; 0.369-0.480)	0.410 (0.375-0.464; 0.309-0.475)
ETS_{CII}	0.432 (0.367-0.486; 0.339-0.549)	0.466 (0.367-0.573; 0.332-0.662)	0.408 (0.354-0.446; 0.338-0.457)	0.463 (0.377-0.475; 0.352-0.490)
OXPHOS coupling efficiency	0.920 (0.891-0.943; 0.877-0.941)	0.911 (0.843-0.921; 0.815-0.929)	0.902 (0.900-0.916; 0.900-0.920)	0.904 (0.878-0.932; 0.862-0.939)

Median (IQR; range) of skeletal muscle respirometry variables < 48 h in survivors (n=9) and non survivors (n=12) and at day 5-7 in survivors (n=4) and non survivors (n=8). Mass specific respiratory capacities (pmol/s/mg) generated by sequential addition of substrates, uncouplers and inhibitors according to previously described SUIT protocol. $LEAK_{FAO}$: capacity for respiration supported by proton leak, in the presence of malate and octanoyl carnitine and absence of ADP; $OXPHOS_{FAO}$: capacity for oxidative phosphorylation supported by FAO, following addition of saturating ADP; $OXPHOS_{CI}$: capacity for oxidative phosphorylation supported by complex I; following addition of saturating pyruvate and glutamate; $OXPHOS_{MAX}$: maximum capacity for oxidative phosphorylation supported by complex I and complex II, following addition of succinate; ETS_{MAX}: maximum capacity of the electron transport system uncoupled from oxidative phosphorylation, following titration of uncoupler; ETS_{CII}; capacity of uncoupled electron transport system supported by complex II alone, following inhibition of complex I by rotenone. Relative respiratory capacities expressed relative to ETS_{MAX}. OXPHOS coupling efficiency calculated as $OXPHOS_{MAX}$-$LEAK_{FAO}$/$OXPHOS_{MAX}$. * p <0.05 (vs the survivor group at the same timepoint).

The direction of change in respiratory variables

Relative capacity for FAO-supported respiration ($OXPHOS_{FAO}/ETS_{MAX}$) increased in all survivors by Day 5-7 but decreased in all non survivors (Figure 40). There was a significant difference in the percentage change in $OXPHOS_{FAO}/ETS_{MAX}$ between the groups, with the median % change 11.7 (IQR 11-28) in survivors; compared to -8.5 (IQR -32 to -6) in non survivors ($p = 0.008$). Similarly, relative capacity for complex I-supported respiration ($OXPHOS_{CI}/ETS_{MAX}$) increased in all survivors but did not change in non survivors (Figure 41). There was a significant difference in the percentage change in $OXPHOS_{CI}/ETS_{MAX}$ between the groups, with the median % change +23.6 (IQR 10-35) in survivors and -1.8 (IQR -9.5-10.3) in non survivors; $p = 0.016$ (Figure 41)

Figure 40. Change in relative capacity for FAO-supported respiration from <48 h to day 5-7 in survivors and non survivors

A

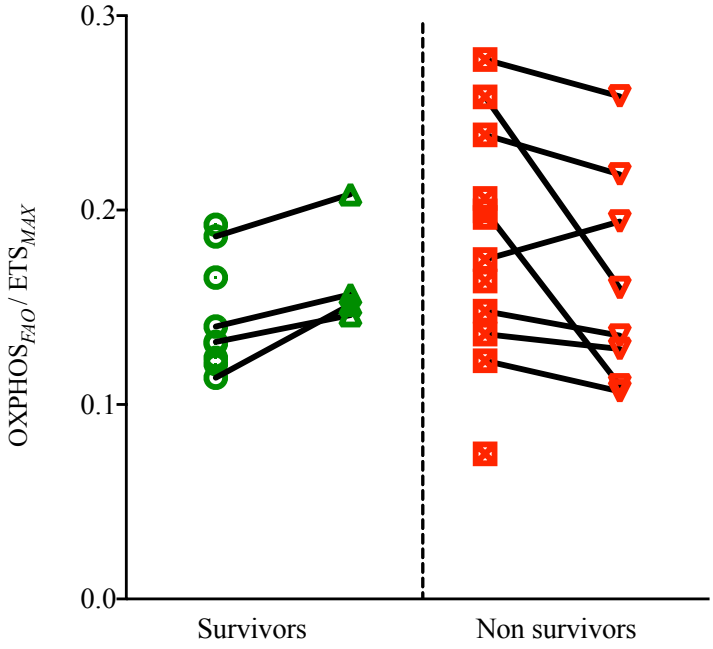

B

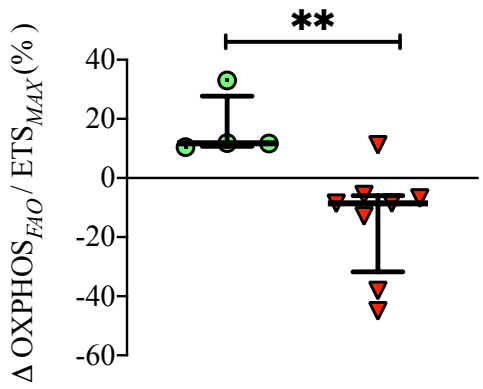

Relative capacity for FAO-supported respiration. (A) Survivors at < 48 h (green circles, n=9) and at day 5-7 (green triangles, n=4). Non survivors at < 48 h (red squares, n=12) and at day 5-7 (red triangles, n=8). Paired values from the same subjects connected by black line. (B) % change within subjects from <48 h to day 5-7; with survivors shown in green (n=4 at both timepoints) and non survivors in red (n=8 at both timepoints). Error bars indicated media and IQR. * $p < 0.05$, ** $p<0.01$ *vs* survivors.

Figure 41. Change in relative capacity for complex 1-supported respiration

A

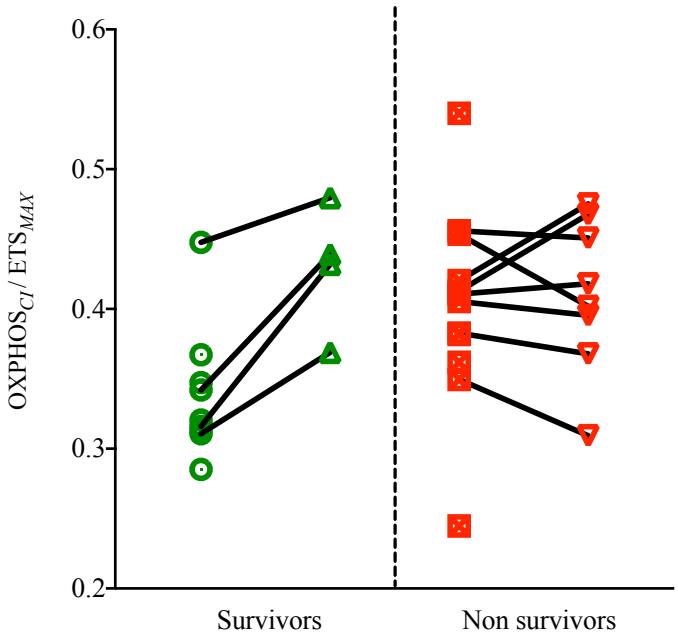

B

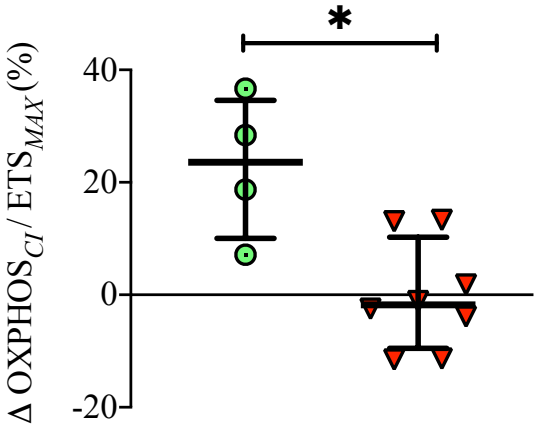

Relative capacity for complex I-supported respiration. (A) Survivors at < 48 h (green circles, n=9) and at day 5-7 (green triangles, n=4). Non survivors at < 48 h (red squares, n=12) and at day 5-7 (red triangles, n=8). Paired values from the same subjects connected by black line. (B) % change within subjects from <48 h to day 5-7; with survivors shown in green (n=4 at both timepoints) and non survivors in red (n=8 at both timepoints). Error bars indicates media and IQR. * $p < 0.05$ *vs* survivors.

Enzyme activities

There was no difference in citrate synthase activity between survivors and non survivors at < 48 h (p =0.20) or Day 5-7 (p = 0.11). There was no difference in HADH activity at < 48 h, but by day 5-7, non survivors had lower HADH activity (median 0.29, IQR 0.27-0.31) compared to survivors (median 0.58, IQR 0.35-0.72, p = 0.049).

Table 21. Skeletal muscle enzyme activities in survivors and non survivors at < 48 h and day 5-7.

Enzyme activities (µmol/min/mg)	**Critically ill patients at < 48 h**		**Critically ill patients at day 5-7**	
	Survivors (n=9)	Non survivors (n=12)	Survivors (n=4)	Non survivors (n=8)
Citrate synthase	0.130 (0.0912-0.183; 0.0735-0.196)	0.0931 (0.0667; 0.142; 0.0459-0.243)	0.129 (0.066-0.186; 0.0501-0.200)	0.0756 (0.0454-0.0866; 0.0398-0.111)
HADH	0.575 (0.319-0.672; 0.283-1.05)	0.399 (0.299-0.544; 0.205-0.931)	0.577 (0.353-0.718; 0.298-0.7444)	0.287 (0.271-0.315; 0.133-0.538)*

Median (IQR; range) of skeletal muscle enzyme activities < 48 h in survivors (n=9) and non survivors (n=12) and at day 5-7 in survivors (n=4) and non survivors (n=8). * p <0.05 (vs the survivor group at the same timepoint).

Energetics

There was no difference between survivors and non survivors in terms of relative levels of phosphocreatine (PCr) and adenosine or guanosine phosphates (Table 22). Survivors and non survivors did not differ at either timepoint in terms of their ratios of [ATP]/[ADP], [PCr]/[ATP] or adenylate energy charge.

Table 22. Skeletal muscle energetic metabolites at < 48 h and day 5-7 in survivors and non survivors.

Energetic metabolites (levels expressed relative to control)	**Critically ill patients at < 48 h**		**Critically ill patients at day 5-7**	
	Survivors (n=9)	Non survivors (n=12)	Survivors (n=4)	Non survivors (n=8)
PCr	0.795 (0.474-1.73; 0.302-2.79)	1.14 (0.713-1.84; 0.271-2.30)	0.797 (0.575-1.28; 0.510-1.43)	1.11 (0.507-1.99; 0.277-2.04)
ATP	1.08 (0.843-1.85; 0.781-2.71)	1.54 (1.12-2.24;1.02-3.03)	1.17 (0.822-1.19; 0.710-1.120)	1.29 (1.09-2.17; 0.530-3.34)
ADP	1.30 (1.10-1.58; 0.707-2.43)	1.09 (0.727-1.54; 0.383-3.88)	1.17 (0.845-1.49; 0.771-1.56)	1.18 (0.639-1.73; 0.286-2.11)
AMP	1.63 (0.80-2.64; 0.46-3.23)	0.87 (0.66-1.61; 0.53-2.13)	0.87 (0.59-1.19; 0.56-1.23)	1.20 (0.81-1.55; 0.29-3.14)
GTP	0.98 (0.69-1.74; 0.58-2.12)	1.86 (1.13-3.02; 1.05-3.24)	0.72 (0.29-1.07; 0.08-9.87)	0.78 (0.57-1.07; 0.20-4.37)
GDP	1.52 (1.03-2.40; 0.66-3.20)	0.76 (0.56-1.71; 0.39-11.07)	2.00 (1.50-2.54; 1.49-2.56)	1.44 (1.16-2.86; 0.37-4.05)
NADP	0.67 (0.55-1.13; 0.40-1.62)	0.93 (0.68-1.53; 0.61-1.72)	0.76 (0.47-1.12; 0.30-3.07)	0.67 (0.43-1.30; 0.11-1.60)
NAD	0.82 (0.53-1.67; 0.44-2.59)	0.99 (0.57-1.72; 0.45-1.91)	0.79 (0.53-1.24; 0.53-1.30)	1.08 (0.77-1.52; 0.24; 1.69)
Energetic ratios				
[ATP]/[ADP]	199 (186-295; 145-322)	236 (210-277; 202-290)	146 (92.3-229; 57.2-530)	171 (127-237; 57.6-274)
[PCr]/[ATP]	60.6 (39.9-66.3; 12.8-72.0)	47.1 (40.4-68.5; 11.2-98.2)	49.4 (47.1-75.0; 46.5-83.2)	52.1 (38.4-76.7; 17.8-84.1)
Adenylate energy charge	0.493 (0.482-0.496; 0.476-0.498)	0.493 (0.493-0.495; 0.490-0.502)	0.495 (0.493-0.495; 0.492-0.496)	0.493 (0.486-0.497; 0.474-0.498)

Median (IQR; range) of skeletal muscle phosphate-containing compounds and energetic ratios at < 48 h in survivors (n=9) and non survivors (n=12) and at day 5-7 in survivors (n=4) and non survivors (n=8). * $p < 0.05$ (vs the survivor group at the same timepoint).

Intermediary metabolism

There was no difference between survivors and non survivors, at either timepoint, in levels of total glycolytic intermediates or any of the individual intermediates in the glycolytic pathway (Table 23). There was no difference between survivors and non survivors, at either timepoint, in levels of TCA intermediates (Table 24) or amino acids (Table 25). The sum of total carnitines (total acyl carnitines plus free carnitine) did not differ between survivors and non survivors at either timepoint and there was no difference between survivors and non survivors, at either timepoint, in short (2-6 carbons), medium (7-12 carbons), long (> 13 carbons) chain lengths, or in free carnitine (Table 26).

Table 23. Skeletal muscle glycolytic metabolites in survivors and non survivors at < 48 h and day 5-7

Glycolytic metabolites (levels expressed relative to average in reference group)	Critically ill patients at < 48 h		Critically ill patients at day 5-7	
	Survivors (n=9)	Non survivors (n=12)	Survivors (n=4)	Non survivors (n=8)
Total glycolytic intermediates	2.09 (0.74-3.34; 0.47-3.95)	2.00 (0.99-2.71; 0.45-3.95)	1.47 (1.16-1.89; 1.10-1.98)	1.44 (0.62-2.14; 0.51-3.48)
Glucose-6-phosphate	1.10 (0.26-4.31; 0.02-6.24)	0.71 (0.16-1.53; 0.09-5.43)	0.73 (0.17-1.90; 0.13-2.15)	0.56 (0.11-1.87; 0.04-2.33)
Fructose-6-phosphate	1.19 (0.29-3.40; 0.03-6.45)	0.73 (0.22-1.48; 0.12-4.96)	0.65 (0.35-1.65; 0.35-1.89)	0.70 (0.12-1.55; 0.07-2.52)
Fructose bisphosphate	1.33 (0.54-3.54; 0.28-3.85)	1.71 (0.70-2.63; 0.25-4.71)	1.47 (1.21-1.74; 1.12-1.82)	0.61 (0.62-4.88; 0.41-4.88)
Glyceraldehyde-3-phosphate	1.25 (0.96-1.79; 0.24-5.79)	1.68 (0.97-3.44; 0.29-11.42)	1.07 (0.77-1.16; 0.69-1.18)	1.01 (0.57-2.20; 0.24-2.46)
Dihydroxyaceteone phosphate	1.02 (0.36-3.30; 0.23-5.32)	1.30 (0.44-4.06; 0.11-6.85)	1.60 (1.32-3.29; 1.25-3.83)	0.31 (0.22-2.58; 0.13-10.65)
Bisphosphoglycerate	0.51 (0.40-0.82; 0.25-1.38)	0.38 (0.21-0.61; 0.16-2.70)	0.73 (0.22-2.66; 0.15-3.20)	0.42 (0.18-1.16; 0.17-2.18)
2-3 phosphoglycerate	2.31 (1.38-3.35; 0.79-3.98)	2.62 (1.50-3.24; 0.78-4.44)	2.37 (2.04-2.64; 2.02-2.65)	2.04 (1.23-4.03; 0.97-4.43)
Phosphoenolpyruvate	0.44 (0.26-4.78; 0.24-5.51)	1.25 (0.24-5.25; 0.08-8.57)	0.19 (0.10-2.46; 0.09-3.18)	0.89 (0.18-3.22; 0.04-7.50)
Pyruvate	3.67 (1.35-6.14; 0.61-14.81)	1.53 (0.39-3.23; 0.16-9.57)	1.60 (1.05-2.45; 1.01-2.60)	2.10 (0.80-3.98; 0.43-5.48)

Median (IQR; range) of skeletal muscle glycolytic metabolites at < 48 h in survivors (n=9) and non survivors (n=12) and at day 5-7 in survivors (n=4) and non survivors (n=8). * $p < 0.05$ (vs the survivor group at the same timepoint).

Table 24. Skeletal muscle TCA metabolites in survivors and non survivors at < 48 h and day 5-7

Tricarboxylic acid cycle metabolites (levels expressed relative to average in reference group)	Critically ill patients at < 48 h		Critically ill patients at day 5-7	
	Survivors (n=9)	Non survivors (n=12)	Survivors (n=4)	Non survivors (n=8)
Total TCA metabolites	0.86 (0.57-1.27; 0.53-1.81)	0.88 (0.57-1.29; 0.32-2.30)	0.72 (0.65-0.87; 0.62-0.91)	0.63 (0.47-1.74; 0.45-2.25)
Citrate	0.36 (0.24-0.59; 0.19-1.62)	0.66 (0.30-1.05; 0.11-2.08)	0.40 (0.32-0.50; 0.31-0.52)	0.51 (0.24-0.92; 0.12-1.59)
Aconitate	0.63 (0.31-1.04; 0.06-1.52)	0.67 (0.33-0.93; 0.03-3.29)	0.67 (0.10-1.70; 0.04-1.92)	0.49 (0.15-2.93; 0.08-5.71)
Isocitrate	0.36 (0.24-0.70; 0.17-1.10)	0.46 (0.38-0.85; 0.08-1.05)	0.61 (0.49-0.83; 0.46-0.90)	0.50 (0.22-1.21; 0.16-1.61)
ketoglutarate	1.27 (0.96-2.50; 0.59-3.22)	2.08 (1.27-2.48; 0.78-3.30)	1.01 (0.57-1.43; 0.51-1.49)	1.87 (0.89-3.40; 0.44-4.93)
Succinate	1.14 (0.70-1.51; 0.37-2.99)	0.94 (0.83-2.01; 0.47-3.05)	080 (0.60-1.14; 0.60-1.19)	1.55 (0.75-2.44; 0.48-2.88)
Fumarate	2.87 (0.70-3.82; 0.55-5.75)	1.34 (0.60-2.15; 0.22-3.18)	1.80 (0.92-2.57; 0.80-2.65)	1.33 (0.40-2.44; 0.21-4.36)
Malate	2.47 (0.89-2.82; 0.84; 3.72)	1.88 (0.79-2.24; 0.46-3.70)	1.67 (1.45-1.78; 1.40-1.78)	1.32 (0.78-2.66; 0.34-4.23)
Oxaloacetate	0.93 (0.60-1.37; 0.24-1.47)	0.94 (0.74-1.48; 0.45-2.45)	0.51 (0.23-0.67; 0.16-0.70)	0.75 (0.52-2.97; 0.38-6.07)

Median (IQR; range) of skeletal muscle TCA metabolites at < 48 h in survivors (n=9) and non survivors (n=12) and at day 5-7 in survivors (n=4) and non survivors (n=8). * $p < 0.05$ (vs the survivor group at the same timepoint).

Table 25. Skeletal muscle aminos acids at < 48 h and day 5-7 in survivors and non survivors

Amino acids (levels expressed relative to average in reference group)	Critically ill patients at < 48 h		Critically ill patients at day 5-7	
	Survivors (n=9)	Non survivors (n=12)	Survivors (n=4)	Non survivors (n=8)
Leucine	1.84 (1.36-2.91; 1.09-6.67)	2.02 (0.96-3.21; 0.85-7.77)	1.78 (1.28-1.98; 1.17-2.00)	3.99 (1.56-5.12; 1.06-5.17)
Isoleucine	2.25 (1.53-3.15; 1.18-8.66)	2.00 (1.22-2.34; 1.07-2.35)	1.85 (1.00-4.10; 0.74-9.14)	3.47 (1.86-5.58; 1.23-6.56)
Valine	1.33 (1.14-2.15; 0.91-4.92)	1.32 (0.81-2.35; 0.77-4.95)	1.38 (1.20-1.59; 1.16-1.64)	2.22 (1.39-3.27; 0.75-4.13)
Asparagine	1.35 (1.03-1.96; 0.80-3.28)	1.96 (1.10-3.64; 0.81-18.12)	1.44 (0.88-2.75; 0.82-3.07)	2.97 (1.63-4.29; 0.73; 6.09)
Aspartate	0.85 (0.41-1.09; 0.18-1.50)	0.99 (0.62-2.06; 0.36-12.02)	0.58 (0.23-2.09; 0.22-2.49)	1.60 (1.14-2.79; 0.71-5.60)
Glutamate	0.56 (0.42-0.70; 0.34-2.18)	0.49 (0.33-0.64; 0.24-2.20)	0.59 (0.46-0.94; 0.44-1.03)	0.59 (0.35-1.41; 0.30-2.69)
Proline	0.78 (0.54-1.58; 0.37-1.86)	0.93 (0.60-1.93; 0.37-2.85)	1.02 (0.88-1.36; 0.86-1.44)	1.10 (0.48-2.12; 0.33-4.03)
Glutamine	0.56 (0.24-0.76; 0.16-0.89)	0.70 (0.50-1.07; 0.22-1.22)	0.46 (0.24-0.62; 0.17-0.68)	0.31 (0.24-0.62; 0.21-0.68)
Ornithine	0.40 (0.25-0.70; 0.16-0.94)	0.37 (0.22-0.82; 0.12-1.39)	0.56 (0.38-0.78; 0.37-0.80)	0.37 (0.23-0.64; 0.21-1.46)

Median (IQR; range) of skeletal muscle amino acids at < 48 h in survivors (n=9) and non survivors (n=12) and at day 5-7 in survivors (n=4) and non survivors (n=8). * p <0.05 (vs the survivor group at the same timepoint).

Table 26. Skeletal muscle carnitines at < 48 h and day 5-7 in survivors and non survivors

Carnitines (levels expressed relative to average in reference group)	Critically ill patients at < 48 h		Critically ill patients at day 5-7	
	Survivors (n=9)	Non survivors (n=12)	Survivors (n=4)	Non survivors (n=8)
Total	1.05 (0.79-1.67; 0.67-2.29)	1.16 (0.91-1.82; 0.47-2.48)	1.14 (0.95-1.67; 0.91-1.82)	1.38 (0.63-1.57; 0.10-1.80)
Short chain (C2-6)	0.90 (0.58-1.16; 0.40-1.43)	1.00 (0.59-1.62; 0.32-2.57)	0.83 (0.75-1.64; 0.73-0.91)	0.94 (0.47-1.56; 0.07-1.67)
Medium chain (C7-12)	2.52 (1.03-11.5; 0.55-14.4)	1.35 (0.56-2.13; 0.30-5.10)	5.42 (1.24-9.59; 0.92-9.90)	1.60 (1.18-2.11; 0.14-3.65)
Long chain (> C12)	6.09 (2.33-9.40; 1.84-22.04)	2.71 (1.77-4.46; 0.56-12.11)	5.84 (2.01-9.87; 0.98-10.97)	3.53 (0.72-7.18; 0.22-7.18)
Free	1.23 (0.88-2.05; 0.80-3.29)	1.71 (1.19-2.56; 1.07; 3.45)	1.18 (0.74-1.63; 0.73-1.64)	1.74 (0.74-2.91; 0.25-3.26)

Median (IQR; range) of skeletal muscle carnitines at < 48 h in survivors (n=9) and non survivors (n=12) and at day 5-7 in survivors (n=4) and non survivors (n=8). * p <0.05 (vs the survivor group at the same timepoint).

Redox status

Survivors and non survivors did not differ in terms of their ratios of reduced and oxidised methionine or glutathione at either timepoint (Table 27).

Table 27. Skeletal muscle redox profile at < 48 h and day 5-7 in survivors and non survivors

Redox couples (levels expressed relative to average in reference group)	**Critically ill patients at < 48 h**		**Critically ill patients at day 5-7**	
	Survivors (n=9)	Non survivors (n=12)	Survivors (n=4)	Non survivors (n=8)
[Met]	3.11 (1.78-4.43; 1.34-8.13)	2.15 (1.25-5.21; 0.72-18.93)	2.66 (2.09-3.25; 2.05-3.30)	4.80 (1.93-9.36; 0.92-22.21)
[MetSO]	1.95 (1.63-3.06; 1.03-4.17)	2.45 (1.48-6.60; 1.02-9.68)	1.69 (1.19-2.39; 1.09; 2.56)	3.41 (1.50-6.46; 1.20-15.41)
[Met]/[MetSO]	3.13 (254-4.08; 1.62-6.03)	2.16 (1.30-3.12; 0.64-5.65)	3.13 (2.54-4.08; 1.62-6.03)	2.16 (1.30-3.12; 0.64-5.65)
[GSH]	0.86 (0.41-2.91; 0.12-7.01)	2.21 (0.40-5.67; 0.35-6.26)	0.41 (0.27-0.80; 0.23-6.29)	5.98 (2.10-10.22; 0.29-12.02)
[GSSG]	0.40 (0.48-0.72; 0.46-2.33)	0.52 (0.40-1.04; 0.30-1.47)	0.71 (0.50-0.93; 0.45-0.97)	0.68 (0.37-1.21; 0.23-1.56)
[GSH]/[GSSG]	0.02 (0.0085-0.076; 0.0032-0.21)	0.011 (0.0069-0.016; 0.0038-0.22)	0.037 (0.0083-0.18; 0.0069-0.21)	0.11 (0.045-0.28; 0.0062-0.49)

Median (IQR; range) of skeletal redox couples; reduced methionine [Met] and oxidised methionine sulfoxide [MetSO] and reduced glutathione [GSH] and glutathione disulphide [GSSG] at < 48 h in survivors (n=9) and non survivors (n=12) and at day 5-7 in survivors (n=4) and non survivors (n=8). * $p < 0.05$ (vs the survivor group at the same timepoint).

4.6.4. Relationships between organ failure and skeletal muscle bioenergetic-redox phenotype

To investigate the potential relationship between bioenergetic function and organ failure in the critically ill cohort, correlation between the degree of organ failure on admission (as defined by the APACHE II score) and respirometry variables measured at < 48h (n=21) was assessed. To investigate the relationship at a multiple timepoints, correlation between the degree of organ failure (defined by the SOFA score) measured at the same times as the respirometry variables at < 48 h and day 5-7 (n=33) was also assessed. In the critically ill cohort, there was positive correlation between the degree of organ failure, as estimated from the APACHE II score, and the relative capacity for leak respiration ($LEAK_{FAO}/ETS_{MAX}$); Spearman's r = 0.53, p =0.013 (Figure 42). There was also positive correlation between APACHE II score and relative capacity for FAO-supported respiration ($OXPHOS_{FAO}/ETS_{MAX}$), Spearman's r = 0.51, p = 0.019 (Figure 43). There was no association between any skeletal muscle respiratory capacities and arterial oxygen content (CaO_2), vasopressor requirement or mean arterial pressure. Muscle concentrations of MetSO and Met, both higher in critical illness compared to the reference group, were moderately correlated with degree of organ dysfunction, as measured by the SOFA score (r = 0.6, p = 0.0002 for MetSO, r=0.53, p =0.0014 for Met), as shown in Figure 44. There were no associations between any of the redox ratios and respiratory capacity, including relative capacity for complex-I supported respiration. There was no association between nutritional intake (in terms of absolute calories, or amount of fat, protein and carbohydrate) and any of the skeletal muscle respiration variables or enzyme activities.

Figure 42. Correlation between organ failure and skeletal muscle capacity for leak respiration

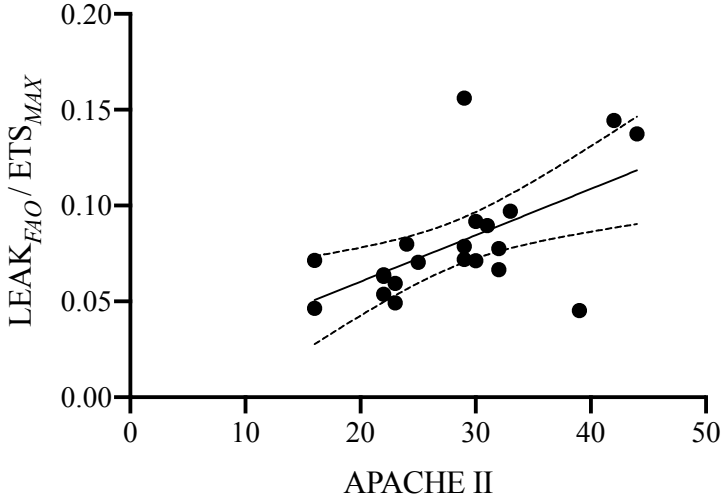

APACHE II score calculated on admission and relative capacity for leak respiration ($LEAK_{FAO}/ETS_{MAX}$) within 48 h of admission to ICU (n=21)

Figure 43. Correlation between organ failure and skeletal muscle capacity for FAO-supported respiration

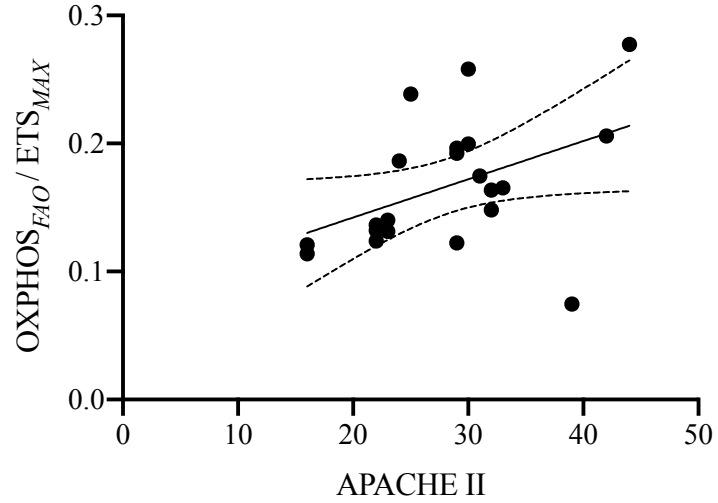

APACHE II score calculated on admission and relative capacity for FAO-supported respiration ($OXPHOS_{FAO}/ETS_{MAX}$) within 48 h of admission to ICU (n=21)

Figure 44. Relationship between organ failure and reduced and oxidised forms of methionine

A

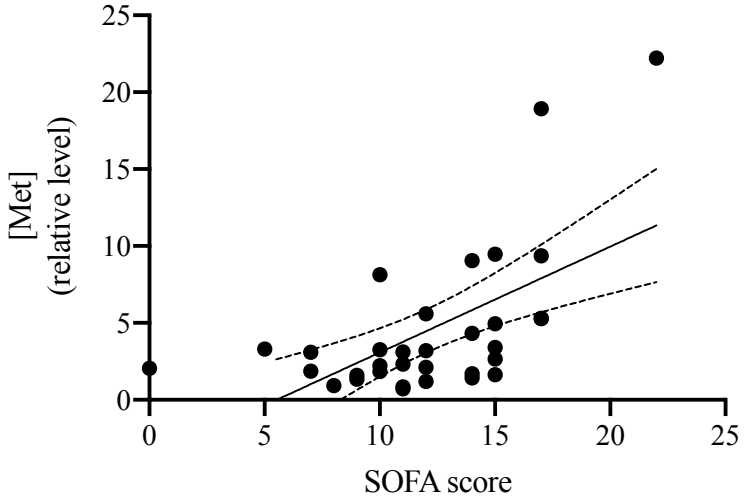

B

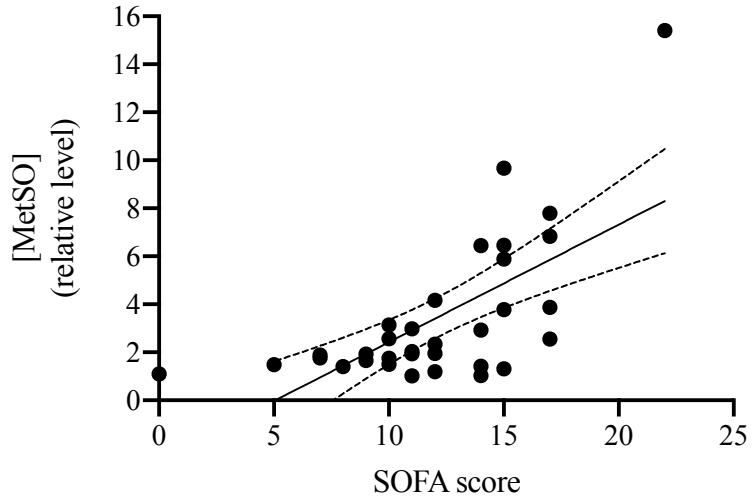

SOFA score and relative levels of reduced and oxidised methionine [Met] and [MetSO] calculated in critically ill patients at < 48 h and day 5-7 (n=33)

4.7. Discussion

4.7.1. Summary of key findings

The skeletal muscle phenotype in critical illness

The critical illness skeletal muscle phenotype is summarised in Table 28 and Figure 45. In critical illness, theoretical bioenergetic capacity was preserved in skeletal muscle, in terms of both maximum capacity for oxidative phosphorylation ($OXPHOS_{MAX}$) and the uncoupled electron transport system (ETS_{MAX}). These functional indices in intact mitochondria were consistent with preserved skeletal muscle energetics in critical illness. However, there were specific modifications to the skeletal muscle phenotype within the first 48 h of ICU admission compared to health, including greater coupling efficiency and lower capacity for complex I and FAO-supported respiration. These functional mitochondrial modifications were accompanied by diminished FAO enzyme activity and accumulation of medium and long chain carnitines. Citrate synthase activity was reduced in critical illness, and lower levels of early TCA intermediates in conjunction with increased levels of glycolytic intermediates suggested a switch away from oxidative metabolism towards anaerobic glycolysis. There were markedly higher levels of all BCAAs, as well as asparagine and aspartate, but lower concentrations of ornithine, glutamate and glutamine. In terms of redox status, skeletal muscle was more reduced in critical illness, according to ratios of [Met]/[MetSO] and [GSH]/[GSSG], though both the oxidised and reduced components of methionine were markedly greater in the critically ill patients.

Table 28. Summary of differences between the skeletal muscle phenotype in critically ill patients and reference patients

Skeletal muscle profile	Critically ill phenotype	Evidence*
Bioenergetic capacity	⇔	No difference in $OXPHOS_{MAX}$/mg; ETS_{MAX}/mg; [ATP]/[ADP]; [ATP]/[PCr]; adenylate energy charge
Bioenergetic efficiency	⇑	Higher Oxphos coupling efficiency Lower relative leak-supported respiration Lower relative FAO-supported respiration
Complex I capacity	⇓	Lower relative complex I supported respiration Lower early TCA cycle intermediates
Glycolysis	⇑	Higher total glycolytic intermediates Lower early TCA cycle intermediates
TCA cycle	Mixed	Lower early TCA cycle intermediates and citrate synthase activity Higher later TCA cycle intermediates
FAO	⇓	Lower relative $OXPHOS_{FAO}$ and HADH activity Higher medium and long chain carnitines
Amino acid oxidation	Mixed	Higher BCAA (leucine, isoleucine, valine) Lower glutamate/glutamine
Antioxidant/ oxidant status	⇑	Higher [Met]/[MetSO] and [GSH]/[GSSG] Higher [Met] and [MetSO]

* statistically significant differences *vs* reference cohort undergoing elective surgery

Figure 45. Schematic of the skeletal muscle phenotype in critical illness

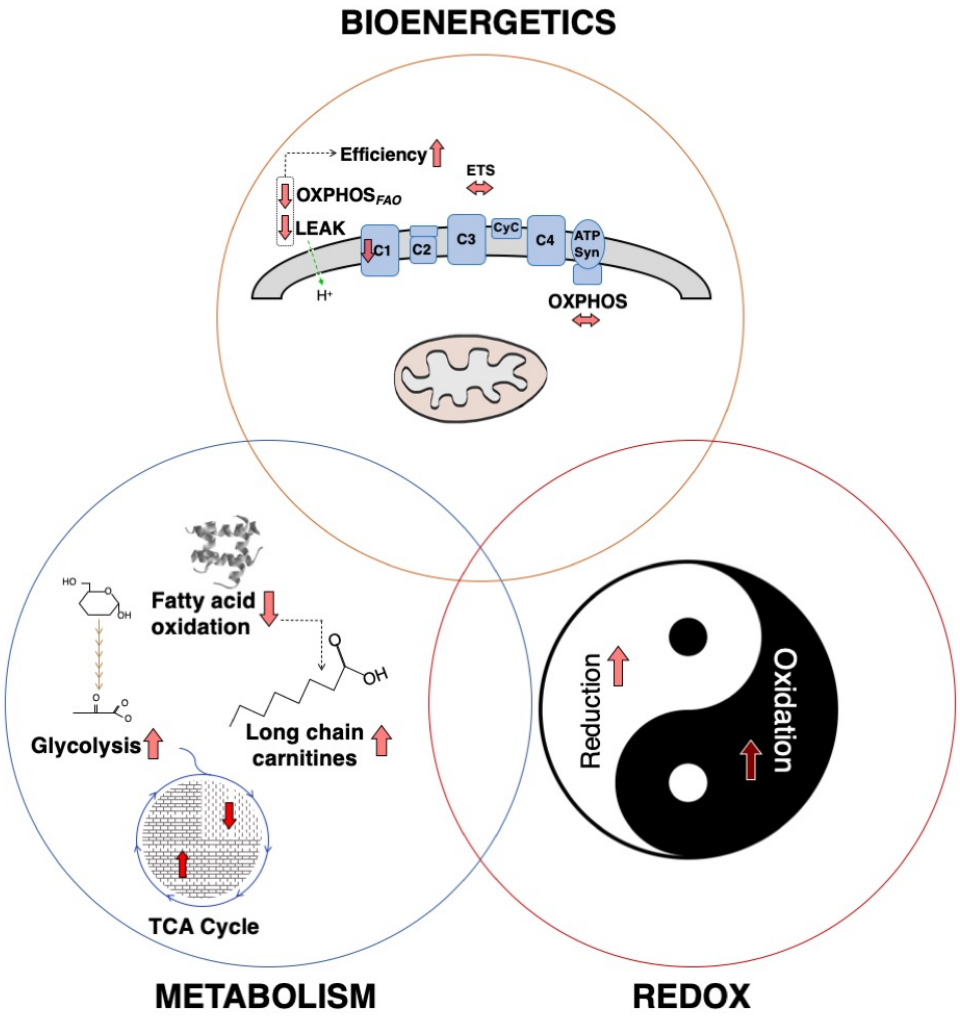

The skeletal muscle phenotype in survivors of critical illness

The skeletal muscle survival phenotype is summarised in Table 29. Survivors of critical illness demonstrated lower capacity for complex I-supported respiration, and a trend towards lower capacity for FAO-supported respiration, compared to non survivors. The percentage change in these variables, from 48 h to day 5-7, was significantly different in survivors and non survivors. Capacity for complex I-supported respiration increased in survivors but did not change in non survivors. Capacity for FAO-supported respiration increased in survivors but decreased in non survivors. Activity of the FAO enzyme, HADH, was also lower in non survivors than survivors by day 5-7. There was no difference in theoretical maximum respiratory capacity between survivors and non survivors, either in terms of $OXPHOS_{MAX}$ or ETS_{MAX} in intact mitochondria or energetic ratios. Relative capacity for leak- and FAO-supported respiration was greater in patients with greater initial severity of organ failure, as indicated by the APACHE II score. There was a moderate association between both oxidised and reduced forms of methionine and the SOFA score.

Table 29. Summary of differences in skeletal muscle phenotype between survivors and non survivors

Skeletal muscle bioenergetic profile	Survivor phenotype
Relative capacity for complex I-supported respiration	Lower at 48 h* (Increases by day 5-7)
Relative capacity for FAO- supported respiration	Lower at 48 h (Increases by day 5-7)
FAO enzyme activity	Higher at day 5-7*

*indicates statistically significant differences *vs* non survivor cohort

4.7.2. Interpretation and significance

Overall skeletal muscle bioenergetic capacity is preserved in critical illness

Direct measurements of mitochondrial respiration in permeabilised skeletal muscle challenge the prevailing assumption that cellular bioenergetic collapse underlies multiple organ failure. The preserved energetic capacity and reserve was internally consistent, with intramuscular energetic ratios in critically ill patients maintained at the same level as the reference group. Although some previous studies have demonstrated lower intramuscular ATP concentrations in patients with critical illness compared to healthy controls (87, 205), others have shown elevated ATP concentrations in critically ill survivors compared to controls (20). Inconsistencies in the literature may arise from the fact that ATP may be rapidly metabolised (to ADP, AMP or adenosine) during the process of extraction, prior to freezing and quantification. Use of tissue concentration of ATP, or any metabolite, to reflect function is hindered by the fact that the concentration will reflect both its rate of production and consumption, both of which are highly regulated. This was the first study to undertake direct measures of intact mitochondria in skeletal muscle in patients with acute critical illness. One previous study used high resolution respirometry to analyse muscle fibres from critically ill patients following > 2 weeks ICU admission (131). Those patients, characterised by protracted muscle weakness rather than the acute physiological derangement and multiple organ failure under investigation in the current study, exhibited diminished maximum oxidative phosphorylation capacity compared to health. Direct measures of intact mitochondrial respiration in other cell types have reported inconsistent results in critically ill patients. Increased capacity of the electron transport system was reported in studies of platelets taken from patients within 48 h of developing severe sepsis or septic shock (210). One study of PBMCs in patients during the first week of ICU admission demonstrated elevated respiratory capacities compared to controls (211), whilst another showed decreased

oxidative phosphorylation capacity in critically ill patients compared to controls (213). PBMCs extracted from critically ill patients displayed a blunted response to ADP stimulation (212). The differences between these findings and those of the current study may be explained by the fact that the respiratory capacity of circulating platelets and blood cells within the systemic compartment may be directly subject to systemic mediators and higher PO_2 than the cells of end-organs such as the skeletal muscle fibres in this study (214). It has previously been shown that bioenergetic alterations observed in critical illness can be induced in control cells by incubating them in plasma from the critically ill patients (212), and that the changes in critically ill cells can be abolished by suspending them in buffer instead of their own plasma (210). Different bioenergetic modifications may be expected in white blood cells and platelets in the central compartment, reflecting respective activation of immune and coagulation systems, than in skeletal muscle, which is generally inactive during multiple organ failure.

Reduced oxygen dependence of energy production in critically ill patients

Two alterations to the mitochondrial oxidative phosphorylation machinery have the effect of augmenting bioenergetic efficiency with respect to oxygen consumption. These modifications may thus have contributed to preservation of muscle energetics despite the diminished capacity of complex I observed in critical illness. Greater coupling efficiency in critical illness represents a relative reduction in mitochondrial proton leak relative to oxidative phosphorylation. Reduced proton leak means a greater proportion of the substrate and oxygen consumption which drive mitochondrial electron transport will be channelled towards ATP production (30). The means by which this "tuning down" of leak respiration was not determined in this work. Cells can modulate the permeability of their mitochondrial inner membrane to protons, through altered expression of UCPs (32), but these were not

quantified here. Long-chain fatty acids have been known to promote mitochondrial uncoupling, as they act as natural protonophores in the mitochondrial inner membrane (215), but intramuscular long-chain carnitines were shown to be higher in critically ill patients in the current study.

Bioenergetic efficiency also theoretically increased via a reduction in metabolic flexibility. The demonstration of a substrate switch away from FAO was internally consistent within the study, with lower capacity for respiration supported by FAO accompanied by decreased activity of the FAO enzyme, HADH, and an accumulation of medium and long chain carnitines within muscle. Respiration supported by FAO produces fewer ATP molecules per mole of oxygen consumed, compared with carbohydrate oxidation (59). From their respective stoichiometry, it is estimated that the oxidation of fat, which is highly reduced, requires 11-12% more oxygen to produce the same amount of ATP as the oxidation of glucose (60).

Elevated levels of glycolytic intermediates, particularly pyruvate, occurred in parallel with reduced levels of early (6-carbon) TCA cycle intermediates, and reduced citrate synthase activity. This was suggestive of upregulation of glycolysis and shunting of pyruvate away from the TCA cycle (and oxidative phosphorylation) towards lactate production instead, to regenerate the NAD^+ required to permit glycolysis to continue (26, 27). To maintain ATP production under oxygen limited conditions, muscle lactate must be transported to the liver and converted back into pyruvate and then glucose to drive further glycolysis in muscle (Cori cycle)(27). This may have contributed to the preserved muscle energetic ratios observed in the patients with organ failure, but ultimately the process is unsustainable, as it yields 2 ATP in muscle at the cost of 6 ATP in the liver (216).

Skeletal muscle modifications in acute organ failure mirror aspects of hypoxia adaptation

The co-existence of the skeletal muscle bioenergetic and metabolic modifications in patients with organ failure described in this study suggests a potential role for HIF-1, which in cell models has been shown to mediate a series of similar responses to promote survival under hypoxic conditions. The bioenergetic-metabolic phenotype induced by HIF in such models includes: increased efficiency of oxidative phosphorylation (56) through downregulation of UCPs(62); reduced FAO (217), increased transcription of glycolytic enzymes and lactate dehydrogenase, which promotes the conversion of pyruvate to lactate; and pyruvate dehydrogenase kinase 1, which shunts pyruvate away from mitochondria(26, 57). Similar responses have been demonstrated in human skeletal muscle during acclimatisation to hypobaric hypoxia at high altitude, including increased coupling efficiency, reduced FAO and increased glycolytic flux (68). Furthermore, native Himalayan Sherpas have greater coupling efficiency and diminished capacity for FAO-supported respiration than lowlanders at high altitude, and these changes have been proposed to underpin the augmented cellular energetics and superior performance of Sherpas compared to lowlanders in the hypobaric hypoxia of high altitude (68). The implication of these similarities is that the modifications to skeletal muscle phenotype described in this study may represent a beneficial adaptation to cellular hypoxia: an attempt to "acclimatise" to critical illness. Intracellular levels of HIF-1α increase in response to reduced oxygen availability and activate the transcription of genes involved in the adaptive response to hypoxia described above (52). Although none of the patients with organ failure were hypoxaemic, as judged by PaO_2, SpO_2 or CaO_2, the skeletal muscle tissue PO_2 was not measured. In multiple organ failure, cellular oxygen supply may be limited, even when cardiac output and convective oxygen transport are resuscitated, due to microcirculatory disturbance (218). Elevated skeletal muscle concentrations of HIF-1α have

been reported in similar cohort of critically ill patients with normal arterial oxygenation indices (87). One of the downstream targets of HIF is another transcription factor, peroxisome proliferator-activated receptor-alpha (PPARα), which regulates the expression of enzymes involved in FAO, uncoupling proteins and inflammatory mediators (61). Through suppression of this pathway, HIF-1α mediates a substrate switch away from FAO, and thus improves the efficiency of respiration. This pattern of substrate reprogramming reflects that seen in the hypoxic fetus (76) and is inducible in adult cardiac muscle in response to cellular oxygen limitation (60). HIF expression and activity was not quantified in this study, but the skeletal muscle phenotype demonstrated in the critically ill cohort calls for further investigation of its potential role in adaptive modifications to oxygen limitation.

Evidence for alternative metabolic pathways to replenish the TCA cycle

In organ failure, elevation in the latter (5- and 4-carbon) metabolites of the TCA cycle, despite the depletion in the early intermediates suggests the existence of an alternative pathway for replenishing the cycle, via α-ketoglutarate. This same pattern has been observed in lowlanders ascending to high altitude (68). Alternative pathways to maintain TCA cycle turnover under hypoxic conditions have been demonstrated in human cell lines, including via glutamine-derived alpha-ketoglutarate (219, 220). Glutamine, and its precursor, glutamate, were indeed lower in early organ failure, consistent with a diversion of amino acids to replenish the TCA cycle. Glutamine is also an important energy substrate for rapidly dividing cells (such as immune cells, or cells of the GI tract)(220) and required for glutathione biosynthesis, so glutamine and its precursors may be rapidly depleted in times of stress. Their depletion may be part of the mechanism of rapid muscle wasting in critical illness (90), as they play an important role in inhibiting protein degradation and stimulating protein synthesis (220).

Resilience associated with dynamic modification to Complex I and FAO-supported respiration

Two critical illness modifications were more marked in eventual survivors. Within the first 48 h of critical illness, eventual survivors demonstrated lower $OXPHOS_{CI}$ and lower $OXPHOS_{FAO}$ (*trend*) compared to non survivors. This argues against a generalised bioenergetic malfunction and instead implies an active regulation of the oxidative phosphorylation machinery in response to stress, conveying resilience. These two respiratory indices also evolved in different directions in survivors and non survivors. In survivors, these specific capacities increased towards reference group values by day 5-7; whilst in non survivors, they did not recover ($OXPHOS_{CI}$) or declined further ($OXPHOS_{FAO}$). The divergence between survivors and non-survivors in the dynamics of these alterations reveals the importance of the timing of engagement and release of this "brake" for patient outcome, with brisker onset and swifter resolution being associated with survival. Further support for this concept was provided by finding that by day 5-7, non survivors had lower FAO enzyme activity compared to survivors, emphasising that persistent impairment in FAO was a hallmark of poor outcome.

Lipid overload is a corollary of metabolic remodelling in critical illness

A picture of skeletal muscle carnitine backlog accompanied the diminished mitochondrial capacity for FAO respiration and inhibition of HADH activity. The same consequences have been described in lowlanders acclimatising to hypobaric hypoxia (68). Ectopic (non-adipose) lipid deposition has been associated with the development of metabolic dysfunction and cell toxicity (73). In cardiac muscle, accumulation of triacylglyerol (TAG) and ceramide, which occurs in obesity and diabetes, has been shown to cause apoptosis, fibrosis, and cardiac

contractile dysfunction (221). There is evidence that accumulation of lipid within skeletal muscle, attributed to mitochondrial insufficiency, underlies the development of skeletal muscle insulin resistance (222, 223). Multiple organ failure is a lipolytic state, associated with increased mobilisation of FFA and glycerol from adipose tissue, into the plasma, with the rise in circulating free fatty acids observed in patients suffering from trauma, burns and sepsis (224), which persists even when exogenous lipid or carbohydrate is administered (198, 199). In this study, we also demonstrate that, in addition to increased lipolysis, elevation of plasma lipids may be compounded by reduced mitochondrial capacity to oxidise fatty acids, such that the muscle cannot keep pace with the supply. This view fits with the findings of a recent study of skeletal muscle metabolism in patients in the early phase of critical illness, from heterogenous causes, which demonstrated decreased concentrations of a several mitochondrial enzymes involved in FAO and accumulation of intramuscular triglycerides, in conjunction with hypoxic and inflammatory signalling (increased intramuscular concentrations of HIF-1α and inflammatory cytokines, such as IL-10) (87). It is possible that the consequence of a potential bioenergetic adaptation (improved oxygen efficiency) may be the accumulation of toxic lipid metabolites. Exposure to exogenous lipid has been shown to increase the inflammatory response in critically ill patients (225). In a canine model of acute ischaemic left ventricular failure, infusion of plasma free fatty acids increased oxygen requirement and worsened left ventricular function (226). Reduced skeletal muscle FAO in organ failure was accompanied by accumulation of muscle BCAAs (leucine, isoleucine and valine). Unlike other amino acids, BCAAs are primarily metabolised in muscle, hence this finding may imply reduced muscle consumption. HADH is also involved in BCAA oxidation, and its reduced activity may contribute to impaired BCAA oxidation, which has also been associated with the development of insulin resistance (227–229).

Novel interpretation of diminished complex I capacity and redox modifications in acute organ failure

Diminished $OXPHOS_{CI}$ in critical illness was consistent with the reduced expression and activity of complex I previously reported in frozen muscle samples from critically ill patients (21, 205). Previously, lower complex I activity was associated with greater severity of shock in critically ill patients with sepsis (20). Here we demonstrate for the first time that these protein changes have functional relevance and translate into altered respiratory capacity in intact mitochondria. Instead of reflecting mitochondrial dysfunction in organ failure, early downregulation of complex I may be protective. Downregulation of complex I in skeletal muscle of lowlanders acclimatising to hypobaric hypoxia has been proposed as an adaptive response to protect the cell against ROS production (69). Complex I is a major site of generation of reactive oxygen species (ROS), particularly superoxide (230). Addition of complex I substrates, such as glutamate and malate, augment NADH levels and stimulate hydrogen peroxide activity 10-fold in isolated brain mitochondria (231). Reducing complex I respiratory capacity could potentially decrease ROS production via this route, at the cost of reduced electron transport. Under low oxygen conditions, inhibition of complex I activity through induction of the HIF1 target, mitochondrial NDUFA4L2, attenuates mitochondrial oxygen consumption and limits production of intracellular ROS (232). The downregulation of complex I capacity in early critical illness may thus confer benefit through reduced exposure to complex I-generated superoxide. Complex I inhibition also appears to inhibit mitochondrial permeability transition pore-induced cell death (233). In human placental tissue, the mechanism underlying hypoxic downregulation of complex I has been shown to involve the HIF-responsive microRNA-210, which represses iron-sulphur protein assembly of complex I (234). Hypoxia-associated deactivation of complex I in endothelial cells produces a superoxide burst, which may play a role in cellular adaptation to acute hypoxia

(235, 236). Thus, complex I inhibition in early critical illness may represent a key component of mitochondrial reprogramming in hypoxia adaptation.

Enhanced skeletal muscle reductive capacity in critical illness

Organ failure and risk of death have previously been associated with increased by-products of oxidative stress in various compartments (237, 238) and correspondingly, we found higher intramuscular levels of the oxidised component of the methionine redox couple, methionine sulphoxide, in patients with organ failure compared to the reference group. However, increased oxidation was accompanied by an even greater increase in the reduced form. At first glance, this observation appears counterintuitive. Both reduced and oxidised forms of methionine were moderately correlated with the degree of organ dysfunction. Instead of a simple shift toward uncompensated oxidative stress in organ failure, suggested by previous single biomarker approaches, these findings suggest an enhanced redox drive within skeletal muscle, with active upregulation of cellular antioxidant capacity in the face of an increased oxidative burden.

4.7.3. Strengths and limitations of the study

The strengths and limitations related to subject selection for the critically ill and reference cohorts were discussed previously in Chapter 2 (section 2.5.9). Strengths and limitations specific to the techniques used in this study are discussed below.

4.7.4. Strengths

The primary strength of this study is that humans were studied rather than animal models or cell lines. In addition, a cohort of patients reflecting the true complexity of critical illness was studied, which allowed the investigation of the effect of this real-world stress at the cell

level. To date, this study represents the largest data set of direct measurements of skeletal muscle respiration in patients with acute multiple organ failure. The use of respirometry to quantify relevant end points of integrated mitochondrial capacity, and integration of these with contemporaneous quantification of related metabolites and enzyme activities, allowed a broad and detailed cellular bioenergetic phenotype to be characterised. The use of multiple modalities provided internal support for important findings and suggested an overall signature consistent with hypoxic adaptation. Critical illness is a dynamic condition and only by repeating analysis at multiple timepoints did the relevance of the dynamics of cellular modifications emerge.

The methods used in this chapter (respirometry, spectrophotometric assays of enzyme activity, and metabolite identification by ultra-high performance liquid chromatography mass spectrometry) all represent gold-standard techniques, which have undergone validation in human subjects, and have been widely reported in the literature. Muscle sample collection, preparation and storage were carried out according to a strict protocol, to minimise any experimental variation. For the critically ill patients, all *vastus lateralis* biopsies were performed by the same operator on ICU (the author); and for the control group, all vastus lateralis biopsies were performed by the same surgeon (Mr Nicholas Garlick) according to the same protocol, at the same phase of the same operation. Respirometry analysis was undertaken on site without delay (< 15 minutes from extraction of tissue to onset of permeabilisation), and all assays performed by the same operator under identical laboratory conditions. Tissue for later analysis was rapidly snap-frozen (within 10 seconds of extraction) to allow confidence in the characterisation of enzyme activity and metabolic intermediates. This consistency minimised any differences in sample processing time and processing technique, as samples from participants in both groups were handled by the same

operator, and processed onsite, in the same laboratory. However, the fact that the muscle was exposed briefly prior to the biopsy in the reference cohort could represent an important systematic difference between the sample extraction in the two groups.

4.7.5. Limitations

Study design

A key limitation of the study was the heterogeneity of the critically ill cohort, which is discussed in depth in Chapter 2 (section 2.4.8). It is not possible to determine which individual aspects of the critical illness syndrome (impaired substrate supply, effects of hypoxia, inflammatory mediators, drugs, immobility or nutrition) are responsible for the cell modifications observed in this work. However, the primary aim of the study was to determine the effect of critical illness (a complex stress, generated by multiple interacting stressors) on fundamental cell functions. The consistent differences noted between critically ill patients and the reference group represent the combined effect of the multiple diverse stresses, resulting in the syndrome of critical illness and multiple organ failure. It is the effect of this complex stress, in the cells of human patients, that was the subject of this study, rather than individual aspects (such as hypoxia, inflammation, immobility or drug effects) in isolation. In similarly heterogenous cohorts of critically ill patients, specific patterns of acute muscle wasting muscle, function and molecular biology, have been demonstrated, despite the variation in the presenting disease (90, 239). The fact that clear differences in complex I capacity were observed between survivors and non survivors supports the universal nature of this response in a mixed ICU population.

Another important limitation of the study design was the reference group, which was comprised of patients exposed to general anaesthesia and surgical stress, both of which may

also influence the cell functions under investigation. Previous work has demonstrated the inhibitory effects of general anaesthesia on mitochondrial oxidation of glutamate and succinate in skeletal muscle, in comparison to local anaesthesia during an orthopaedic procedure (240). The reference patients were not receiving ongoing nutrition at the time of the biopsy and had been fasting for at least 6 hours prior to the muscle biopsy (as dictated by hospital policy). This was in contrast to the critically ill patients, most of whom received ongoing enteral or parenteral feeding at the time of the biopsy (over half at < 48 hours and all patients at days 5-7). Prolonged fasting (60 hours) ultimately results in increased whole body fat oxidation, with elevated plasma FFA and increased lipid concentrations in skeletal muscle with decreased insulin sensitivity. In permeabilised skeletal muscle mitochondria, capacity for oxidative phosphorylation and uncoupled electron transport system are reduced after a prolonged fast (241). Ongoing nutritional intake, and accompanying hormonal changes, will affect the cellular metabolic profile and mitochondrial function, and is an important limitation of the study. There was a greater proportion of females in the reference group, but none of the variables were found to differ significantly between males and females.

Causality cannot be inferred from the difference in complex I capacity observed between survivors and non survivors. At baseline, survivors were younger (15 years on average), and had less severe organ failure at presentation, as judged by the APACHE II and SOFA scores. It is not possible to ascertain whether the diminished complex I capacity is a protective response in survivors, or whether it results from another confounding factor which may enhance survival, such as youth or less severe disease burden. However, the results may provide information about the mechanism by which younger patients are more resilient during critical illness, such as better ability to retain metabolic flexibility.

Multiple comparisons

The aim of this exploratory study was to describe a complex phenotype in critically ill patients, including potential differences from health in terms of multiple aspects of bioenergetic, metabolic and redox function; which cannot be described using a single variable. The problem with performing multiple comparisons using a given data set is the potential inflation of type I error rate (the false positive rate, or the probability of detecting a difference between the groups when it does not exist). One approach to dealing with this problem is to adjust for multiplicity, using techniques such as the Bonferonni method, which apply a more stringent criterion to determine statistical significance (by reducing alpha, or the probability of detecting x,) than the conventional 0.05. However, this also increases the likelihood of a type II error (242). In an exploratory pilot study, the detection of subtle differences was prioritised, and minimising the risk of missing true differences was priorised at the expense of increasing type I error. However, according to their inventor, Ronald Fisher, p values should be interpreted as "graded measures of the strength of evidence against the null hypothesis" (243). The threshold for acceptable type I error is arbitrarily set at 5% ($p < 0.05$), with an inevitable trade off between sensitivity and specificity. When the aim of the study is to discover potential differences, it can be argued that it is more important to allow the detection of false signals, rather than missing genuine signal.

Ex vivo respirometry studies

Ex vivo studies of theoretical mitochondrial respiratory capacities given saturating concentrations of substrate and oxygen do not represent physiological conditions. However, it could be argued that capacity is biologically relevant, because although biological systems do not always operate at capacity, they may operate at a percentage of it. Biology is conservative and capacity is likely to reflect the minimum required to promote survival.

Large scale studies have demonstrated parallels between in vivo oxidative capacity and muscle strength (244). In the current study, the metabolomic and enzyme activity analysis supported the respirometry findings. Respirometry as a means of quantifying mitochondrial respiration does not account for extramitochondrial oxygen consumption, however, this represents an almost negligible component, and substrates for these enzymes were not provided in the protocol. The respiratory capacities were not normalised to mitochondrial content, but rather to tissue mass and then a functional indicator of mitochondrial density (ETS_{MAX}). Citrate synthase was used as a putative marker of mitochondrial density, but it is an imperfect marker, as it has been shown to fall when other markers of mitochondrial activity do not, and normalising to it can be misleading and falsely suggest an intrinsic increase in mitochondrial respiratory capacity (245).

Precision

In this work, evaluation of the operator-specific precision of the various methods used (respirometry, targeted metabolomic analysis, enzyme activity) was not undertaken, due to time and resource restraints. It is therefore not possible to demonstrate the intra-assay reproducibility due to individual operator factors, which may have contributed to the large variation seen in some of the measured variables (in particular, the metabolomic assessment of energetic and redox metabolites in skeletal muscle). However, the data set provides information about the degree of variation in the reference group, and despite the expected variation in the extremely heterogenous critically ill cohort, it was still possible to detect significant differences between the groups.

Generalisability to other tissues

It is not known whether the modifications observed in skeletal muscle in critically ill patients are generalisable to other tissues, such as kidney, heart, liver and brain, the function of which are thought to have greater acute relevance to human survival. In a study of whole-body oxygen consumption in critically ill patients, patients with sepsis demonstrated elevated oxygen consumption compared to normal basal metabolism, but those with organ impairment had markedly lower oxygen consumption than patients with uncomplicated sepsis (88). The skeletal muscle modifications described in the current study may not therefore reflect changes in all other organs, or the net effect on whole-body oxygen consumption. Although often disregarded as a target of intensive care interventions, skeletal muscle represents an organ whose function is impaired in the syndrome of multiple organ failure. Skeletal muscle weakness and wasting is rapid and severe during acute critical illness and its extent is related to degree of organ failure (90). Muscle dysfunction is associated with failure to wean from mechanical ventilation, increased length of stay in the ICU and hospital, and increased risk of death (246–248).

4.7.6. Unanswered questions and future work

This chapter identified a comprehensive skeletal muscle phenotype with many similarities to the universal cellular response to hypoxia. However, further work is required to confirm whether or not the skeletal muscle modifications observed in critical illness are actually associated with tissue hypoxia and to determine how they are triggered. In particular, the modifications observed in this chapter call for further exploration of the potential role of the HIF pathway, and the expression and activity of one the HIF downstream targets, PPARα, which regulates the expression of UCPs, as well acting as a master regulator of fat metabolism. Genetic variation in HIF subunits and targets downstream of HIF, including PPAR, have been linked to human hypoxia adaptation in high altitude populations (68, 249).

Mapping out the potential relationship between genotype, biological phenotype and clinical outcomes could inform the prediction of which patients are at greatest risk from multiple organ failure and enable the development of personalised approaches to support the expression of a survival phenotype. Developing life support will require greater understanding of how these cellular modifications relate to less invasive measures of systemic physiology, microcirculatory function or plasma biomarkers. In subsequent chapters of this thesis, attempts were made to determine whether or not these skeletal muscle modifications were associated with systemic measures of redox status in plasma (Chapter 5), or skeletal muscle microcirculatory function (Chapter 6).

4.8. Conclusions

Acute organ failure is associated with rapid, specific and co-ordinated alterations to respiratory capacity, intermediary metabolism and redox status in skeletal muscle. Despite the heterogeneity of the patients with organ failure, in terms of age, underlying pathology, co-morbidity, pharmacological treatment and nutritional intake, there was a coherent profile of modifications, which shared many features previously described in models of cellular adaptation to hypoxia. Specific aspects of the organ failure phenotype appeared to confer resilience, with greater initial divergence from normal associated with survival. The temporal nature of the modifications was crucial, with early deviation but quicker resolution evident in survivors, while persistence or progression over several days was associated with death. The interpretation of the bioenergetic changes is at variance with previous work in this field. Regulation of complex systems involved in bioenergetic capacity and redox architecture can neither be understood nor adequately captured by measuring shifts in steady-state concentration of a single biomarker or cross-sectional assessment of multiple markers at a single timepoint. By combining functional analyses of intact mitochondria with

metabolomic analyses a coherent picture emerges, which attests to altered mitochondrial substrate utilisation and reduced metabolic flexibility associated with incomplete lipid metabolism in response to stress.

5. Chapter 5. The plasma reactive species interactome in critical illness

5.1. Introduction

Survival is contingent on the ability of cells to accommodate variations in metabolic need and environmental conditions. During multiple organ failure, in which cells of different tissues are struggling to function outside normal limits, stress signalling plays a crucial role in securing survival. Chapter 4 described a signature of skeletal muscle bioenergetic modifications in critical illness, several of which were associated with survival. It is not known how these cellular accommodations to challenges are co-ordinated, either within cells or across tissues, let alone in humans under conditions of life-threatening stress. In Chapter 1, the concept of the reactive species interactome was described: a complex network of reduction-oxidation (redox) reactions, which spans cells and different body compartments, integrating stress signalling and functional changes relevant to survival (93). A key role of redox survival signalling is thought to be the control of bioenergetic function. Bioenergetic function and redox status are interlinked, as mitochondria are major sources of reactive oxygen species (ROS) and reactive nitrogen species (RNS), as well as important targets of their actions (102). Through oxidation, nitrosylation and nitration, ROS and RNS are involved in cell signalling, but if the regulatory system of antioxidants is overwhelmed, uncontrolled reactions cause indiscriminate damage cell components, such as proteins, lipids and DNA (known as oxidative and nitrosative stress) (250). The reactive species interactome may be relevant to survival from critical illness, by virtue of both its role as a potential stress signalling network, and its potential contribution to organ dysfunction through oxidative modification of functional cell components. To improve understanding of what determines survival in human multiple organ failure, it is necessary to investigate the role of the reactive

species interactome in human critical illness, and to determine how it relates to systemic physiology, cellular bioenergetics, organ dysfunction and survival.

The relevance of oxidative stress in critical illness

Critically ill patients with sepsis have been shown to have increased plasma levels of lipid peroxides and decreased concentrations of antioxidants compared to healthy volunteers (132, 251). Oxidative stress has also been implicated in the pathophysiology of SIRS, with patients meeting the criteria for this syndrome exhibiting increased plasma lipid peroxidation and reduced antioxidant capacity compared to controls (237). Another critical illness syndrome, acute respiratory distress syndrome (ARDS) is associated with increased markers of oxidative stress and decreased levels of antioxidants in alveolar fluid (252, 253) and exhaled breath (254, 255). Increased oxidative stress and decreased antioxidant capacity has been associated with mortality from sepsis (238, 256). Markers indicative of increased NO production in sepsis have been associated with poor outcome (257), but while NO readouts are typically elevated in bronchial secretions and exhaled breath in inflammatory lung disease, elevated urinary NO metabolites have been shown to be associated with favourable outcome (258). The latter is compatible with the concept that upregulation of NO at the whole-body level is protective. These data have led to the concept that increased production of ROS and RNS, and exhaustion of regulatory antioxidant reserve, are important components of the pathways leading to cell dysfunction and damage, multiple organ failure and death.

Oxidative stress has been investigated as a therapeutic target in critically ill patients for decades. Strategies have included administration of exogenous and untargeted antioxidants, such as N-acetylcysteine, which can replenish glutathione levels and scavenge ROS, or restoration of endogenous antioxidants, such as vitamin C, E or selenium. The results have been inconsistent and no clear benefit was demonstrated in either ARDS (259) or sepsis

(260). In the largest clinical trial targeting oxidative stress (a blinded, randomised 2 x 2 factorial trial, n=1223) , antioxidant supplementation for patients with multiple organ failure had no effect on 28-day mortality, and there was a trend towards increased mortality with glutamine (32 v 27%, p=0.05) (261). Antioxidant therapy has also failed in other conditions associated with oxidative stress, such as diabetes, cancer, inflammation and neurodegeneration (262). Many reasons have been suggested for the lack of clinical efficacy from antioxidants: the wrong agent, the wrong dose, wrong timing, failure of the agent to reach the intended target (263). Investigations are ongoing regarding the potential benefit of targeting of antioxidants to the mitochondria as both a key source of ROS and susceptible victim to the effects of unbuffered oxidation (264). Antioxidants can be delivered to the mitochondria using a range of strategies, including conjugation with a lipophilic cation (triphenylphosphonium) which accumulate within the mitochondrial matrix, due to the negative potential across its membrane (265). Antioxidant peptides with specific amino acid sequences ensuring positive charge at physiological pH enable their penetration into cells and mitochondria. It is proposed that such strategies may provide better protection against oxidative injury than untargeted antioxidants (265). For example, the antioxidant α-tocopherol inhibits LPS signalling cascades in neutrophils in cell models and macrophages in a murine model (266, 267); and when targeted to mitochondria in a rat model of sepsis, have been shown to reduce levels of circulating inflammatory mediators (268). By altering the redox state in a non-specific manner, they may have a multitude of off-target effects including alterations in redox signalling, the complexity of which is still not well understood. For example, administration of antioxidants during exercise impairs oxidative signalling and prevents the expression of beneficial adaptative responses (269). In critical illness, specific redox changes may be vital for processes such as the immune response, as well as co-ordinating modification of cell bioenergetics and metabolism in response to changing

demand. Under these conditions, non-specific administration of antioxidants, by virtue of their potential to interfere with physiological redox signalling, may result in more damage than a transient overproduction of ROS. Like other clinical interventions, it is likely that any potential benefit from antioxidants would depend on administration of the correct dose: and it may be possible that either too much or too little may be detrimental. U-shaped survival curves have been proposed for intra-operative fluid therapy (270)and inspired oxygen supplementation in critical illness (271) and during surgery (272). Different tissues express different antioxidant responses (273); and tissue specificity may also be relevant to the efficacy of exogenously administered antioxidants.

5.1.1. Barriers to characterising the reactive species interactome in critical illness

Distinguishing between 'redox signalling' and 'redox stress' is challenging, as both may be expected to increase with the degree of physiological derangement. It is difficult to distinguish potentially beneficial redox changes necessary for survival, from excessive and non-specific reductive or oxidative stress which result in organ dysfunction and death. ROS and RNS are too short-lived to measure directly, and common approaches to characterise redox status include quantification of longer-lived products of oxidation and nitrosation reactions, such as lipid peroxides and nitrosylated proteins, or measuring levels of known antioxidants, such as reduced glutathione. There is no consensus on which species to measure to gauge the functional status of the reactive species interactome and its key regulatory nodes. Redox molecules are constantly interacting with each other, and the molecules themselves are not necessarily stable, only existing for a short period of time in their reduced or oxidised form. Due to the short half-life of many of these reactive species, only the more stable products of these redox reactions, such as byproducts of macromolecule

oxidation, can be measured. Redox alterations in one compartment (mitochondria; cytoplasm, extracellular fluid, circulating plasma, arterial and venous circulatory systems or remote organs) will influence the redox state in others (96). This complex, dynamic, multilevel system presents a challenge to investigation. Currently, discriminating between redox-mediated stress signalling versus oxidative injury in critical illness is constrained by the paucity of high quality, high resolution data across multiple levels of regulation, from organelle to whole-body. The traditional biomarker approach of quantifying specific oxidised macromolecules within a specific compartment in isolation, lacks specificity in characterising redox state in human disease (274). Combining measures of different by-products of oxidation and nitrosation may offer a more comprehensive picture of the different aspects of redox changes and their downstream effects. Assessment of the tissue or plasma capacity to react with a known reductant (or oxidant) may also allow assessment of the overall redox state of that compartment. To gain better insight into the function of redox changes in critical illness, it will be necessary to characterise the reactive species interactome, using an integrative approach which includes a combination of measures, of different redox molecules, from multiple compartments (subcellular, cellular, tissue/organ and whole body). Both temporal and spatial considerations are likely to be important, but little is known about how to distinguish global from systemic redox changes. In this chapter, a complementary, multi-level approach to assessing the reactive species interactome was based on the following literature review of redox-sensitive components, and their potential relevance in critical illness.

5.2. Literature review: methods for characterising the reactive species interactome

5.2.1. Plasma lipid peroxides as a measure of oxidative cell damage

Quantification of plasma lipid peroxides was selected as a measure of the deleterious effects of oxidation on cell membrane constituents. Lipid peroxidation occurs when unsaturated fatty acids, either in their free form or within intact phospholipids or triglycerides, react with ROS. The lipid peroxides themselves are often unstable and decompose into reactive aldehydes such as malondialdehyde (MDA) and 4-hydroxylnonenal (4-HNE). These secondary byproducts of lipid peroxidation are generally accepted markers of oxidative stress, with elevated levels demonstrated on exposure to a wide range of stressors, from acute hyperoxia (275) to chronic disorders involving diverse tissues (276–278) to the normal aging process (279). Lipid peroxidation is a well-defined mechanism of cellular damage; altering the permeability of plasma or mitochondrial membranes and affecting the critical functions of embedded receptors and enzymes (280). When cells are damaged by lipid peroxidation, aldehydes are released into the blood, such that their levels within the circulating compartment may represent a marker of oxidative damage. Lipid peroxides are not simply inactive bystanders, representing historical oxidative events; they have been found to activate signalling cascades involved in regulating bioenergetic function and antioxidant production. As discussed in Chapter 1, the key cellular antioxidant response is controlled by the Keap1-NFE2L2 pathway. The co-ordinated expression of large number of antioxidant proteins, including NADPH quinone oxidoreductase; haem oxygenase I, glutamate-cysteine ligase and glutathione S transferase, occurs through the binding of the transcription factor, NFE2L2, to the antioxidant response elements (ARE) in regulatory regions of these target genes. NFE2L2 is normally targeted for degradation by the ubiquitin proteasome pathway, through binding by Keap1. However, lipid peroxides interact with thiol residues in Keap1, altering

their redox status and thus disrupt the interaction of Keap1 with NFE2L2, allowing it to escape degradation and translocate to the nucleus to trigger this cellular antioxidant response(281).

Circulating malonyldialdehyde (MDA)

A positive relationship between circulating levels of MDA and severity of organ dysfunction has been demonstrated in critically ill patients with sepsis (282). The same study demonstrated a potential relationship between serum MDA and metabolic phenotype, with positive correlation between MDA and the degree of anaerobic respiration (as judged by serum lactate concentrations). Serum MDA levels > 4.11 nmol/ml could predict 30-day mortality from severe sepsis, albeit with moderate specificity and poor sensitivity. The dynamics of serum MDA concentration also differed between survivors and non-survivors. In survivors, serum MDA returned to healthy control levels by day 4 of critical illness, but remained elevated in non-survivors. Another study of patients with SIRS demonstrated greater plasma concentration of lipid peroxides in those patients with multiple organ failure compared to those without (283).

F2-isoprostanes

An alternative class of stable lipid peroxidation products is the F2-isoprostanes. These are formed from the non-enzymatic, free-radical catalysed peroxidation of arachidonic acid (284). In contrast to MDA, their plasma levels are not affected by lipid levels in the diet, and thus perhaps more closely represent endogenous oxidant production. Formation of F2-isoprostanes have been shown to increase dramatically *in vivo* in animal models of oxidant injury. F2-isoprostanes also have specific biological activity, including vasoconstriction (285) and activation of thromboxane and prostanoid receptors (286). In a study of 50

critically ill patients with severe sepsis, plasma levels of F2-isoprostanes (measured using mass spectroscopy) at day 2 of ICU admission were higher in patients who developed renal failure and hepatic failure compared to those who did not. Within this cohort, patients with isoprostane levels above the 25th centile had higher mortality compared with patients below the 25th centile (42% compared to 8%)(287). However, circulatory failure and acute lung injury were not associated with elevated levels of isoprostanes. A specific compound in the F2 isoprostane class, 8-isoprostane (8-iso-$PGF_{2\alpha}$) has been proposed as the most useful, specific marker of oxidative damage, with small increases observed in hypertension, metabolic syndrome, asthma, and tobacco smoking, and large increases in chronic renal insufficiency, obstructive sleep apnoea, cystic fibrosis and pre-eclampsia (274). It is now thought that 8-iso-$PGF_{2\alpha}$ can be formed by prostaglandin endoperoxidase synthase enzymes during inflammation (288). 8-iso-$PGF_{2\alpha}$ has also been shown to increase in the alveolar fluid of patients with interstitial lung diseases and in breath condensate of patients with asthma (289). It is not clear whether lipid peroxidation results from or contributes to the organ dysfunction observed in critical illness.

5.2.2. Plasma antioxidant capacity

The reactive species interactome comprises reductants as well as oxidants (290). Circulating plasma contains multiple reducing compounds. The antioxidant present at the highest concentration in plasma is the high molecular weight protein, albumin (527-783 μM), followed by low molecular weight antioxidants such as (in order of concentration): urate (160-450 μM), ascorbate (Vitamin C, 30-150 μM), α and γ-tocopherol (Vitamins A and E, 15-40 μM), reduced low-molecular weight thiols (12-20 μM), and bilirubin (5-20 μM). Other plasma antioxidants present at sub-micromolar concentrations include lycopene, β-carotene, ubiquinol 10, as well as high molecular weight glutathione peroxidase,

selenoprotein P, thioredoxin, thioredoxin reductase and glutaredoxin (291). Their concentrations have been shown to increase in response to acute oxidative stress, suggesting a feedback mechanism to protect against uncontrolled oxidation. Plasma concentrations of specific antioxidants (Vitamin A and E) are lower in septic shock patients compared to healthy controls and there is negative correlation between antioxidant concentration and markers of lipid peroxidation in these patients (251). This fits with the theory that increased levels of oxidants, and decreased ability to buffer them, results in tissue damage and dysfunction in critical illness.

An alternative approach to measuring individual levels of known antioxidants is to assess the total antioxidant capacity of plasma, to provide an integrated index of redox status, reflecting the combined ability of all the reducing entities within plasma to buffer against oxidation (292). A number of different analytical techniques are in use to assess this property, including the reduction of the oxidised form of a metal such as Cu^{2+} or Fe^{3+} followed by quantification of the amount of reduced metal (i.e. Cu^{+} and Fe^{2+}) or radical trapping, but a detailed discussion of these different approaches is beyond the scope of the present chapter. In a study of 68 consecutive patients admitted to ICU, venous plasma was sampled within 24 hours of admission, and patients meeting the criteria for SIRS had lower plasma total antioxidant capacity compared to patients who did not (237). In a study of 73 patients admitted consecutively to ICU, the ratio of plasma total antioxidant capacity to lipid peroxidases was negatively correlated with APACHE III score ($p < 0.001$) (293). However, serum total antioxidant capacity (measured by total peroxyl trapping method) was actually found to be greater in patients with septic shock, compared to healthy patients following general anaesthesia for elective surgery, driven by bilirubin and urate (294). (The same study found lower antioxidant capacity in patients with sepsis, without shock, compared to the

healthy controls.) The suggestion that antioxidant capacity increases along with disease severity was corroborated by the finding that plasma taken from non-survivors of SIRS had greater endogenous peroxyl-radical scavenging ability compared to the survivors (295). Similarly, non survivors from unspecified ICU admission had greater total serum antioxidant capacity compared to survivors along with greater urate levels, both of which were positively correlated with APACHE II scores (290). A third study of patients with severe sepsis (n=73) demonstrated significant correlation of total antioxidant capacity (and urate) with APACHE II score, and greater levels in non-survivors (256). A study of septic and septic shock patients and healthy volunteers demonstrated no differences in total antioxidant capacity at the onset of illness, regardless of the severity, but a decline in time for the septic and septic shock patients. Total antioxidant capacity correlated with urate, albumin and bilirubin, but not with antioxidant vitamins (296).

5.2.3. Plasma free thiols as functional targets of redox reactions

Protein thiols represent an important system involved in sensing and transducing redox signals (297, 298). Thiols (reduced sulfhydryl groups, R-SH) are found in cysteine and derived molecules of low to high molecular weight, such as glutathione and albumin respectively (291). Non-thiol protein constituents including methionine, tryptophan, tyrosine and histidine moieties also have antioxidant properties, but their functional significance is less well understood. Thiols readily undergo oxidation to disulphide, reacting by donating one or two electrons, and are susceptible to reversible and irreversible modification. Within proteins, the thiol/disulphide couple functions as a redox switch, capable of altering the structural, catalytic and regulatory function of the protein, in response to oxidation, nitrosation (donation of NO^+ ions), thiolation and sulfidation of the -SH group. Biological targets that carry cysteine redox switches include protein kinases, phosphatases, ion channels,

transporters and enzymes (e.g. involved in intermediary metabolism). This mechanism allows redox changes to transduce short-term functional adjustments in response to variation in demand. Longer-term adjustments are mediated by interaction with redox sensitive transcription factors, such as HIF (96). Cysteine modifications are also coupled to regulatory feedback, stimulating reductases, denitrosylases and desulphurases (thioredoxin, glutaredoxin, periredoxin enzymes) to maintain thiol modifications at a low level.

Thiols exist in both the intracellular and extracellular compartments. Within cells, thiols are present at millimolar concentrations and highly reduced, with protein thiols more abundant than glutathione, representing 70% of the total pool of reduced thiols (299). Important intracellular thiol networks include glutathione, glutaredoxin and glutathione reductase, and thioredoxin and thioredoxin reductase. Intracellular thiols are kept reduced by the action of NADPH. In contrast, in the extracellular compartment, such as blood plasma, the concentrations of thiols are relatively low, and thiols are more oxidised. The concentration of total reduced thiols in plasma is in the range of 0.4-0.6 mM. The most abundant plasma thiol is the single free cysteine group of serum albumin (Cys-34), and it is reduced by 75% (291). It is considered as a vital target for oxidants, because of its reactivity with a wide variety of species and its relatively high concentration. Low-molecular weight reduced thiols include cysteine, cysteinylglycine, glutathione, homocysteine and γ-glutamylcysteine, which together contribute only 12-20 μM. Glutathione makes up 6 μM and 55% of the total is reduced, while the others range from 1-9% reduced (291). The plasma concentrations of thiols and their oxidised derivatives are influenced by the rates of thiol-disulphide exchange ratios, the rates of thiol oxidation by reactive species, the rates of enzymatic degradation of glutathione, the rates of transport between the plasma compartments and cells (including erythrocytes and endothelial cells) and rates of production and release of albumin and glutathione from the

liver, rates of renal excretion and intracellular metabolism. Thus, multiple mechanisms contribute to and may influence the steady-state levels of different thiols in plasma.

Plasma concentrations of different thiols and oxidised derivatives are tightly regulated in health, and alterations are associated with cellular responses. Increased oxidation of plasma thiols to the disulphide form (often reflected as diminished plasma free thiols) has been associated with aging, smoking, obesity and alcohol abuse (300). Reduced levels of serum protein thiols have also been found in nine different active disease processes in humans (including cancer, cardiovascular disease, diabetes, inflammatory disease) compared to healthy controls (301). Plasma free thiol levels have also been inversely associated with the risk of death from chronic conditions. In a study of 1411 patients undergoing coronary angiography, plasma levels of cysteine and glutathione and their oxidised derivatives were measured. High levels of cysteine oxidation and low levels of reduced glutathione were associated with higher mortality (OR 1.63) (302). In a study of 101 patients with chronic heart failure, serum thiols adjusted for total serum protein were higher than average in patients with better renal function and lower pro-BNP levels, and these patients survived for longer (176). Free thiol groups, corrected for total protein, in serum from 695 patients following renal transplant, were inversely correlated with all-cause mortality and graft failure (303). However, in a study of 160 patients with hospital-acquired AKI, although serum protein thiol levels were markedly lower in patients with AKI than in 72 healthy subjects, 90-day mortality was higher in AKI patients with *high* serum protein thiols than those with low levels, and in multivariate analysis, serum protein thiol levels were independently associated with mortality after adjustment for age, sex, sepsis and the APACHE II score (304). Plasma free thiols and cysteine increased acutely following one week of hypobaric hypoxia at 4559 m (146). It was proposed that an increase in free thiol availability may have been activated

as an antioxidant buffer to increased ROS production. Thiol availability may alter the production of other reactive species, particularly NO, allowing signalling cross-talk in response to hypoxic stress.

Total free thiol status of plasma, appropriately normalised to protein content, as albumin represents the major protein in plasma/serum, contributes to the plasma antioxidant status of the body as they can avidly interact with ROS and other reactive species (305). Plasma free thiol status may also influence intracellular redox status. For example, oxidation of thiols in membrane proteins may trigger intracellular signalling, and transport of cysteine disulphide into cells, and subsequent reduction within the cell will lead to increased glutathione synthesis and excretion of surplus cysteine. The uptake of cysteine disulphide is closely related to the transport of glutamate.

5.2.4. Nitric oxide

NO signalling and metabolism

NO is another biological important reactive species, whose production and metabolism depends on redox status. NO is a ubiquitous signalling molecule: it regulates vascular tone and permeability, platelet and leukocyte adhesion, mitochondrial respiration and antioxidant production (306). It can also inhibit enzyme function, promote DNA damage and activate inflammatory processes. Perturbation of NO regulation is thought to be involved in sepsis, ARDS and multiple organ failure (307) but the nature of NO signalling is highly complex. NO levels are influenced by multiple factors, whilst its actions, which are mediated through diverse pathways, depend on its location, concentration, and its concentration relative to other reactive species. NO production can occur through enzymatic metabolism of L-arginine and oxygen by nitric oxide synthases (NOS), at a rate that is dependent on the concentration of

both substrates as well as NADPH and tetrahydrobiopterin as cofactors (the latter is highly sensitive to oxidation). NO metabolism involves oxidation to nitrate and nitrate, but it can also be generated by reversal of this pathway under conditions of low oxygen (where nitrate is first reduced to nitrite, and finally to NO) (308).

Downstream effects of NO

NO has direct effects on guanylyl cyclase, lipid radicals and metal complexes such as haemes and cytochromes. It also has indirect effects through nitration reactions to form nitrotyrosine/nitroguanosine, nitrosation reactions to form nitrosothiols and nitrosamines, and through combination with oxidative radicals, to form RNS, such as peroxynitrite ($ONOO^-$) (306) (Figure 46). NO stimulation of soluble guanylyl cyclase results in the formation of the second messenger, guanosine 3',5'-cyclic monophosphate (cGMP), which plays a key role in cell signalling pathways. Following this action, NO is converted to nitrite and nitrate by reaction with dissolved (nitrite) or haeme-bound oxygen (nitrate). NO (via RNS) can also react with protein cysteine residues (free thiols), to produce nitrosothiols (S-nitrosylation), modifying their structure and function (309). S-nitrosation is thought to occur by means of NO_2 production, followed by reaction with NO to generate N_2O_3, or via peroxynitrite ($ONOO^-$), NO-thiol interactions in the presence of electron acceptors, or direct transfer of an NO^+ equivalent from one nitrosated molecule to another (transnitrosation mechanism)(250). S-nitrosothiols play key roles in human health and disease (310). They participate in trans-nitrosation reations, modulate the function and activity of transcription factors, enzymes, membrane receptors, ion channels, and have been implicated in controlling oxygen delivery to tissues. S-nitrosylation of thiols in blood (such as albumin in plasma or haemoglobin in erythrocytes) may act as a buffer for excess NO. It may also allow NO to exert distant effects, transporting NO activity to different parts of the body (311). NO exerts different

actions according to its concentration, with lower levels associated with cGMP mediated processes, higher levels stimulating tissue repair and HIF-1α stabilisation, and higher still, resulting in nitrosative damage and cell death (312). The effects of NO also depend on its concentration relative to other interacting reactive species, such as ROS. For example, when NO levels exceed superoxide concentrations, NO tends to reduce oxidative stress from superoxide. When superoxide levels exceed NO levels, the amount of available NO decreases. When their concentrations are roughly equimolar, the highly reactive and toxic peroxynitrite is formed (313).

NO and bioenergetics

NO is thought to downregulate mitochondrial ATP production by reversibly inhibiting cytochrome *c* oxidase (complex IV), the terminal acceptor in the mitochondrial electron transport chain (314). This can be beneficial, in low doses, by opening K_{ATP} channels, but at very high levels of NO, uncoupling of oxidative phosphorylation and opening of the mitochondrial permeability transition pore, can cause cell death. Long-term exposure to NO may lead to persistent inhibition of complex I that is concomitant with a reduction in the intracellular concentration of reduced glutathione (315). This inhibition involved the S-nitrosylation of critical thiols in the enzyme complex, and was immediately reversible by replenishment of reduced glutathione, or exposure to high intensity light (triggering cleavage of the S-N bond of nitrosothiols, regenerating free thiol functionality). Decreasing the concentration of reduced glutathione accelerated the process of persistent inhibition.

Figure 46. Direct and indirect effects of nitric oxide

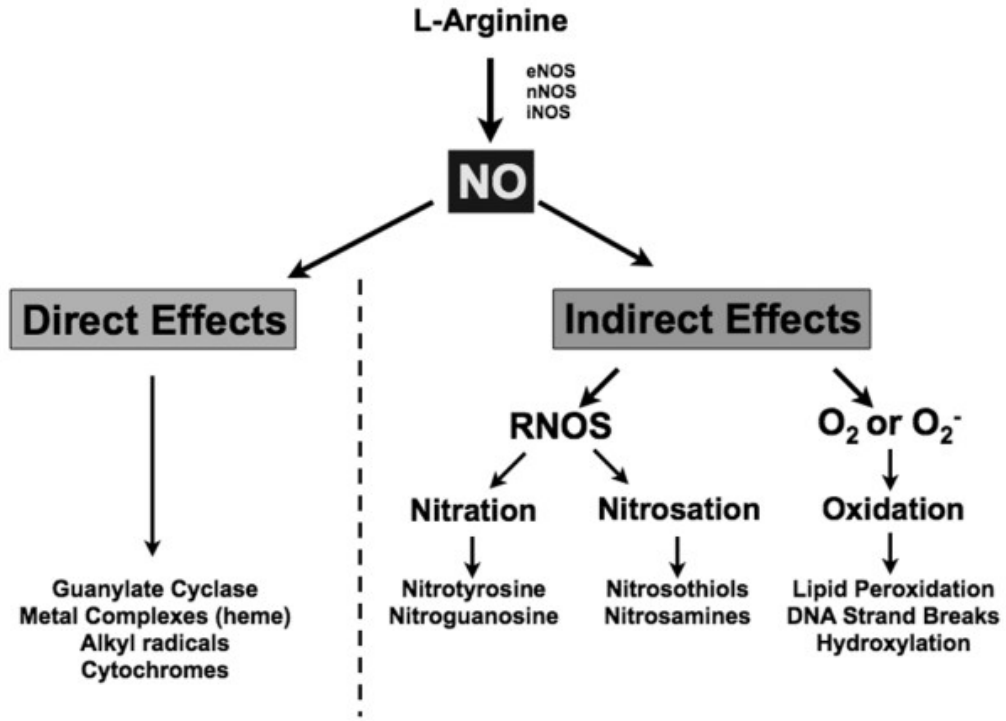

Adapted from (306).

Surrogate markers of NO synthesis and activity

Circulating nitrate, nitrate, cGMP and nitrosothiols have been used as markers of NO synthesis and activity. Within the circulation, nitrite is thought to act as the most important marker of NO bioactivity (316, 317). It is relatively stable and can be reduced to NO under acidaemic and ischaemic conditions (318), increasing blood flow in hypoxic conditions where NOS is compromised. In a study of patients admitted to ICU, nitrate and nitrite concentrations (following correction for renal failure) were higher in patients with septic shock, compared to those without (319). In a logistic regression, falling nitrite/nitrate concentrations were associated with survival 28 days later. Increased NO production via cytokine activation of inducible isoform of NOS has been implicated in microcirculatory failure and organ dysfunction in sepsis. NOS inhibition prevented vasodilatation and hypotension in animal models (320)

But administration of a non-specific NOS inhibitor did not improve mortality in a multicentre, randomised, double blind placebo-controlled trial of patients with septic shock, despite improvements in hypotension (321); in fact it increased mortality, leading to premature termination of the study. Similarly, NOS inhibition in 398 patients with cardiogenic shock did not improve mortality in a multicentre, randomised, double blind placebo-controlled trial (322). It has been argued that inhibition of NO production fails to provide clinical benefit because of its multiple roles. Mice with impaired NOS activity have impaired bacterial clearance and decreased survival in sepsis. Higher urinary NO metabolites were associated with lower mortality and more organ-failure free days in a trial 566 patients with acute lung injury (258). Together with the observation that nitrite/nitrate levels were markedly elevated in bronchial secretions in these patients, indicative of local pulmonary epithelial cell inflammation and iNOS upregulation, possibly contributing to lung damage,

increased NO production at the whole body (as mirrored by elevated urinary nitrite/nitrate excretion) may be protective.

5.2.5. Redox differences in arterial and venous compartments

The potential significance of arterio-venous concentration differences in multiple redox measures has not been explored in critical illness. Arterial and venous profiles of many metabolic markers, including those known to directly influence redox systems, such as glutamate, differ in peripheral muscle compartments (323). Tissue oxygen extraction alters during critical illness syndromes such as sepsis (324). Paired samples from arterial and venous compartments, may reveal information about potential differences between the two compartments, which could relate to net consumption or production of these species or their precursors upon passage through body organs, or variations in oxygenation or pH that exist between the two compartments. Indeed, the measurement of arterial-venous concentration differences in several constituents of the "reactive species interactome" have recently been suggested to provide a unique window into "redox metabolomics" and its regulation at the whole body level (146).

5.3. Summary

Redox processes are thought to play a critical role in sensing changes in metabolic demand and transducing appropriate responses to promote organism survival, but their complex role in human critical illness is not well understood. There is evidence for increased plasma lipid peroxidation in critical illness, in a manner that is associated with organ dysfunction and death. There are conflicting findings regarding antioxidant capacity, with some studies finding lower levels while others find greater levels in critical illness. The role of plasma reduced thiols, known to predict mortality in chronic illness, has not been investigated in

acute critical illness. Higher than normal levels of NO surrogates have been found in different critical illness states, such as sepsis, cardiogenic shock and ARDS, but non-specific inhibition does not improve outcome.

5.4. Aims

The primary aim of this study is to characterise the reactive species interactome during human life-threatening stress, using a complementary approach which encompasses multiple biologically relevant redox-sensitive markers, across different compartments, at multiple timepoints. The purpose was to investigate the potential relationship between plasma redox status and clinical outcome. The second aim was to investigate the potential relationships between plasma redox state and systemic oxygenation and inflammation. The third aim was to investigate the relationship between plasma redox changes and cellular bioenergetics, metabolism and redox state.

5.5. Hypothesis

I hypothesised that alterations to the reactive species interactome will be associated with the severity of critical illness, with higher markers of oxidative stress and depleted antioxidant capacity associated with organ failure and death. There will be a relationship between redox status across different body compartments: such as the central compartment (circulating plasma, including venous and arterial sub-compartments) and the peripheral compartment (cells within end-organs). Greater levels of oxidation in plasma will be associated with increased oxidative stress in tissue.

5.6. Objectives

- Conduct a literature review to select appropriate measures of plasma redox status to build a comprehensive picture of different aspects of the reactive species interactome, relevant to human critical illness.
- Quantify redox components in plasma sampled from critically ill patients at different timepoints in a precise and reliable manner.
- Compare the absolute concentrations and the temporal changes in concentration (i.e the trajectory) of those redox constituents in survivors and non-survivors of critical illness.
- Determine whether any of the measured plasma redox components were related to clinical measures of organ dysfunction, inflammation or systemic oxygenation.
- Determine if plasma redox changes were related to skeletal muscle bioenergetic and redox phenotype (described in Chapter 4).

5.7. Methods

5.7.1. Study design and subject selection

The study was part of the TIMELORD study, the conduct of which is outlined in detail in Chapter 2. This component of the study was a prospective longitudinal cohort study comparing the plasma redox profile during the first week of critical illness in survivors and non-survivors. Study design, ethical approval, screening, consent and enrolment were described in full in section 2.5.2.

5.7.2. Study specific measures

Following enrolment, all subjects underwent testing within 48 hours of admission to the ICU. Where possible, testing was repeated at day 3-4 and again at day 5-7. Venous and arterial

blood was extracted from indwelling catheters (previously placed as part of the routine clinical management for critically ill patients). The fluid and blood occupying the line (3-5 ml) was first aspirated and discarded, then 10 ml blood was aspirated using a 10 ml syringe and placed in an EDTA tube and transferred immediately, on ice, to the centrifuge. Plasma was separated from blood cells by centrifugation of whole blood at 2500 rpm for 15 minutes at 0°C. Plasma was transferred into cryovials in 1 ml aliquots and the red blood cell pellet was collected into a 1 ml cryovial. These aliquots were taken immediately, on ice, to be stored at -80°C until analysis.

5.7.3. Quantification of redox status

Analysis of blood samples was carried out at Southampton University, under the supervision of Professor Martin Feelisch and Dr Bernadette Fernandez, with assistance from Adam Todd and Laurie Lau. The methodology for quantification of the different analytes is described in Chapter 3 (section 3.5). Lipid peroxides were quantified to give an indication of the degree of oxidative damage, using the thiobarbituric acid reacting substances (TBARS) assay, as outlined in section 3.5.2. Isoprostanes (8-iso-prostaglandin F2α) were quantified to give an alternative, specific measure of arachidonic acid peroxidation, as described in section 3.5.5. Plasma total antioxidant capacity was quantified to provide an insight into redox balance, and potential adaptive responses in response to the stress of critical illness. This was measured using the ferric reducing ability of plasma (FRAP) assay, as described in section 3.5.1. Plasma total free thiols were quantified to provide an indication of the availability of this pool of redox-sensitive targets and potential antioxidants, as described in section 03.5.3. Concentration of plasma free thiols was also expressed relative to total plasma protein (in μM/g protein), with the latter quantified using the Coomassie assay (described in section 3.5.4). Production, metabolism and bioavailability of NO were assessed by quantification of

the oxidative decomposition products, nitrate (NO_2^-) and nitrite (NO_3^-), the second messenger cyclic 3',5'-guanosine monophosphate (cGMP) and protein nitrosation products in plasma (RXNO), as described in section 3.6. The procedure used for quantification of nitrite and nitrate was outlined in section 3.6.2; that for quantification of cyclic GMP in section 3.6.5. Total nitrosospecies (RXNO, the sum of nitrosothiols and nitrosoamines) were detected using gas-phase chemiluminescence, as described in section 3.6.4.

Sample processing

Ideally, all analytes would have been performed under the same conditions, on first thaw of the plasma samples. However, this would have required more trained personnel and laboratory equipment than was available. The priority was to undertake the analysis of a given analyte under the same conditions for all plasma samples (on the same day, in the same experimental run, and within the same freeze-thaw cycle). The analytes that previous work within the laboratory or from the literature had shown to be most sensitive to the freeze-thaw cycle (lipid peroxides, total free thiols, nitrite, nitrate and RXNO, were assessed immediately on the first thaw of the plasma aliquots. This required three investigators to perform these assays simultaneously (myself, Bernadette Fernandez and Adam Tod). Total antioxidant capacity, isoprostanes, cGMP and protein were assessed immediately following the second thaw of the plasma aliquots, after internal validation experiments carried out previously by members of the same laboratory using the protocols in this thesis demonstrated less compromise following a single freeze-thaw cycle (Feelisch laboratory, *unpublished data*). All determinations were carried out in triplicate, with repeated daily calibrations. For nitrite and nitrate analysis, reported values were corrected for background contaminant levels of nitrite and nitrate.

Precision

In this work, evaluation of the operator-specific precision of the plasma redox assays (using replicate number of n > 6) was not undertaken, due to time and resource restraints. Variation within normal populations, and sensitivity to detect changes under experimental conditions have been demonstrated using particular protocols by the same laboratory who supervised my experiments. It is therefore not possible to demonstrate the intra-assay reproducibility due to individual operator factors, which may have contributed to the large variation seen in some of the measured variables. Table 23 demonstrates the within run variation within the same plasma samples, using the maximum number of repeats possible with the sample available.

5.7.4. Clinical data collection

Collection of clinical data from the critically ill cohort at the three timepoints is outlined in section 2.5.6

5.7.5. Data analysis

Data analysis was carried out as outlined in section 2.5.7.

5.8. Results

5.8.1. Subject characteristics

The subjects are described in Chapter 2, section 2.5.8. The presenting diagnoses of the critically ill cohort are outlined in Table 3, the clinical characteristics of the cohort at the three timepoints are summarised in Table 5. Baseline characteristics of survivors and non survivors are compared in Table 6.

5.8.2. Assay reproducibility

For each sample, assessment of plasma lipid peroxidation, isoprostanes, total antioxidant capacity, total free thiols, protein and cGMP was performed in triplicate and the co-efficient of variation (CV) of the replicates was calculated as the standard deviation divided by the mean (x 100%). If the CV for a given set of replicates was > 15%, the assay was repeated, and if the CV for the subsequent run was lower, these values were used for the final analysis. The average and maximum values for the coefficients of variation for each assay are shown in Table 30.

Table 30. Coefficient of variation for triplicate assays

Plasma marker	Coefficient of variation (%)	
	Mean	Max
Lipid peroxidation (TBARS assay)	9.1	31
8-Isoprostanes PGF2a (Immunoassay)	13	56
Total antioxidant capacity (FRAP assay)	2.8	22
Total free thiols (DNTB assay)	2.2	13
Protein (Coomassie assay)	5.5	16
cGMP (Immunosassay)	6.8	28

5.8.3. Changes in venous redox profile during the first week of critical illness

Venous samples were successfully collected from 20 subjects at the first timepoint. One subject did not have central venous access at this timepoint. From this group, analysis was completed for 15 subjects at the second timepoint, and 14 subjects at the final timepoint. The median (IQR; range) concentrations of the venous plasma analytes at the three timepoints are shown in Table 31. Across all subjects, only venous plasma total antioxidant capacity altered significantly between timepoints of critical illness, undergoing an average decrease of 19% from the first to the second timepoint (p=0.0098).

Table 31. Venous plasma redox profile during the first week of critical illness

Venous plasma marker	< 48 h (n=20)	Day 3-4 (n=15)	Day 5-7 (n=14)	Friedman's p value
Lipid peroxides (μM)	2.69 (1.90-4.79; 1.03-6.34)	2.67 (1.35-3.73; 1.03-5.26)	2.24 (1.49-3.29; 0.95-6.81)	0.79
Isoprostanes (μM)	227 (193-311; 97-2860)	221 (182-310; 122-2252)	246 (189-331; 136-897)	0.93
Total antioxidant capacity (μM)	959 (716-1618; 620-2956)	776 (639 -1130; 474-3087)**	873 (791-1153; 456-2334)	0.013
Total free thiols (μM)	172 (141-236; 96-341)	177 (140-192; 96-368)	180 (153-213;100-262)	0.79
Total free thiols per protein (μM/g protein)	4.39 (3.75-5.74; 1.79-7.15)	4.54 (3.75-5.95; 2.43-5.95)	4.62 (3.67-6.48; 2.29-6.48)	0.92
Nitrite (μM)	0.18 (0.11-0.39; 0.07-0.71)	0.23 (0.14-0.38; 0.09-1.03)	0.23 (0.13-0.82; 0.06-1.30)	0.74
Nitrate (μM)	50.1 (28.3-107.6; 15.0-260.1)	47.4 (24.8-76.3; 17.0-90.5)	39.6 (25.6-58.6; 19.0-152.4)	0.5
cGMP (μM)	131.0 (98.5-162.5; 59.0-231.1)	153.2 (120.0-165.5; 62.6-225.4)	161.0 (113.7-182.8; 90.8-207.2)	0.063
Total nitrosospecies (μM)	80.7 (42.1-151.8; 12.1-442.6)	53.8 (22.5-97.0; 15.7-594)	42.8 (23.6-83.0; 16.5-470.7)	0.50

Median (IQR; range) of venous plasma redox variables at < 48h, day 3-4 and day 5-7 of critical illness. Change across subjects with measured variables at all 3 timepoints assessed using Friedman's test; adjusted p value for multiple comparisons using Dunn's test: * $p < 0.05$ vs 48 h timepoint.

5.8.4. Changes in arterial redox profile during the first week of critical illness

Arterial samples were successfully collected from 21 subjects at the first timepoint. From this group, analysis was completed for 16 subjects at the second timepoint, and 12 subjects at the final timepoint. At the second timepoint, one subject no longer had an arterial catheter in situ, and at the third timepoint, two subjects no longer had arterial lines, which meant that arterial samples could not be taken. The median (IQR; range) concentrations of the arterial plasma analytes at the three timepoints are shown in Table 32. Similar to the pattern seen in venous plasma, arterial plasma total antioxidant capacity decreased from the first to the second timepoint, by an average of 13 % ($p=0.043$). No other significant changes in arterial plasma analytes were detected between any of the timepoints.

Table 32. Arterial plasma redox profile during the first week of critical illness

Arterial plasma marker	< 48 h (n=21)	Day 3-4 (n=16)	Day 5-7 (n=12)	Friedman's p value
Lipid peroxides (μM)	2.24 (1.51-3.06; 1.03-7.56)	2.58 (1.35-2.98; 1.24-6.17)	2.86 (1.41-3.95; 1.21-6.84)	0.26
Isoprostanes (μM)	217 (188-408; 106-427)	211 (179-277; 151-461)	231 (205-286; 120-438)	0.92
Total antioxidant capacity (μM)	874 (722-1598; 592-2773)	764 (547-985; 488-985)*	818 (627-1142; 443-2358)	0.049
Total free thiols (μM)	174 (152-237; 88-315)	179 (136-197; 95-351)	174 (140-232; 104-268)	0.097
Total free thiols per protein (μM/g protein)	4.94 (4.08-5.84; 2.54-8.18)	4.40 (3.23-5.54; 2.85-9.29)	4.60 (3.42-6.42; 3.29-7.37)	0.36
Nitrite (μM)	0.26 (0.16-0.51; 0.08-0.83)	0.28 (0.20-0.45; 0.16-0.89)	0.32 (0.21-0.60; 0.13-1.32)	0.92
Nitrate (μM)	53.6 (32.7-105.1; 11.6-273.1)	46.0 (25.4-83.1; 17.4-94.0)	40.8 (23.1-53.7; 20.0-143)	0.34
cGMP (μM)	119.3 (94.6-146.9; 36.8-206.1)	143.8 (113.5-161.1; 73.4-213.2)	143.6 (134.1-164.4; 130.2-107.3)	0.34
Total nitrosospecies (μM)	69.8 (36.8-131.3; 15.9-366)	53.8 (34.4-91.8; 17.8-431)	51.8 (31.1-88.5; 19.6-363)	0.17

Median (IQR; range) of arterial plasma redox variables at < 48h, day 3-4 and day 5-7 of critical illness. Change across subjects with measured variables at all 3 timepoints assessed using Friedman's test; adjusted p value for multiple comparisons using Dunn's test: * $p < 0.05$ vs 48 h timepoint.

5.8.5. Arterio-venous differences in plasma markers

The medians (IQR) of the difference between paired arterial (A) and venous (V) plasma values (expressed relative to the arterial value) are shown in Figure 47. Absolute differences between paired samples are shown in Figure 48. Arterial nitrite was consistently higher than the paired venous value (median absolute A-V difference 0.071 μM, p = 0.001). However, downstream markers of NO activity, cGMP and total nitroso species, were consistently lower in the arterial compartment compared to venous (median absolute A-V difference for cGMP -7.68 μM, p =0.042, and for total nitroso species, -2.75 μM, p = 0.028). When the paired arterial and venous values were compared using the Wilcoxon matched-pairs signed rank test, total antioxidant capacity was marginally higher in the venous compartment (median absolute A-V difference - 16.8 μM, p = 0.03).

Figure 47. Arterio-venous differences in plasma redox measures

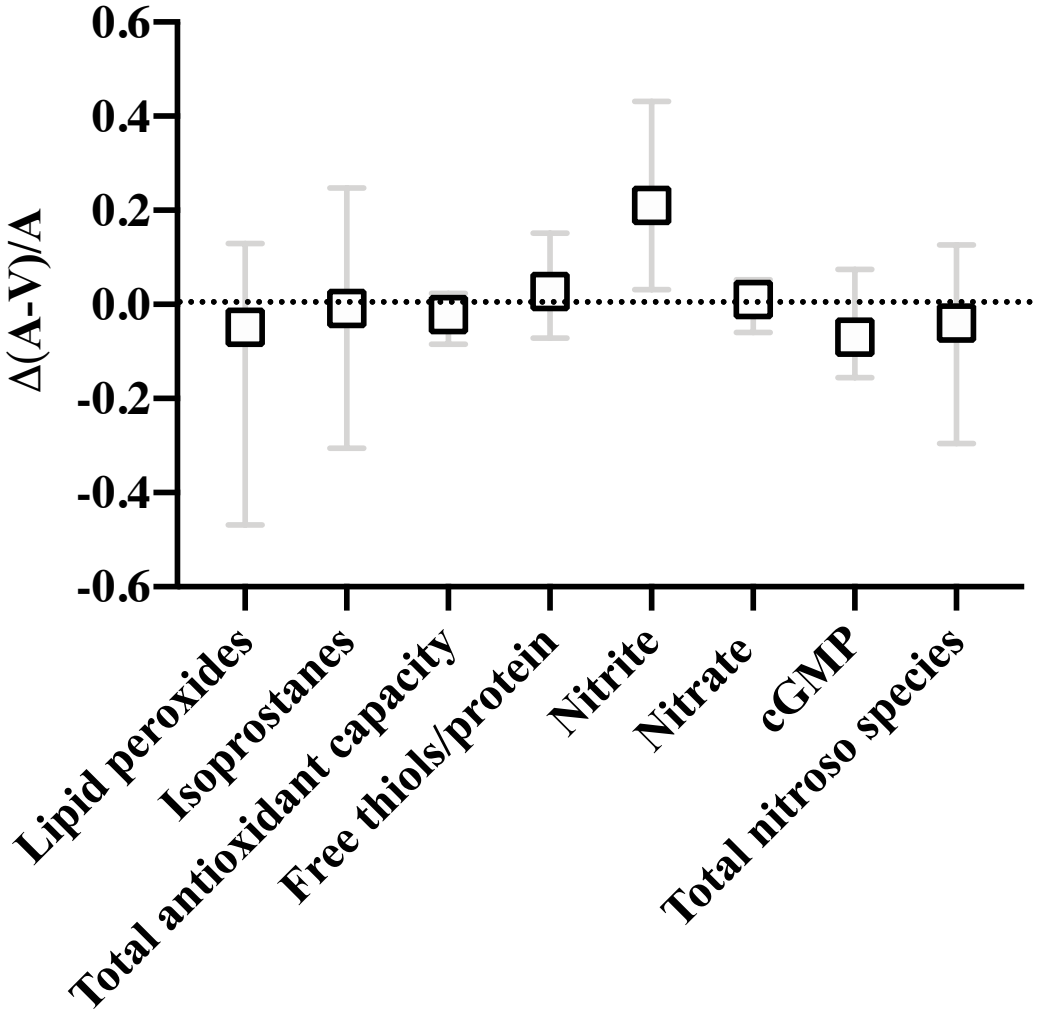

Median (IQR) of arterio-venous differences (relative to arterial value) in plasma redox measures, calculated as the arterial value (A) minus the paired venous value (V) divided by the arterial value (A).

Figure 48. Paired arterial and venous values for plasma redox markers

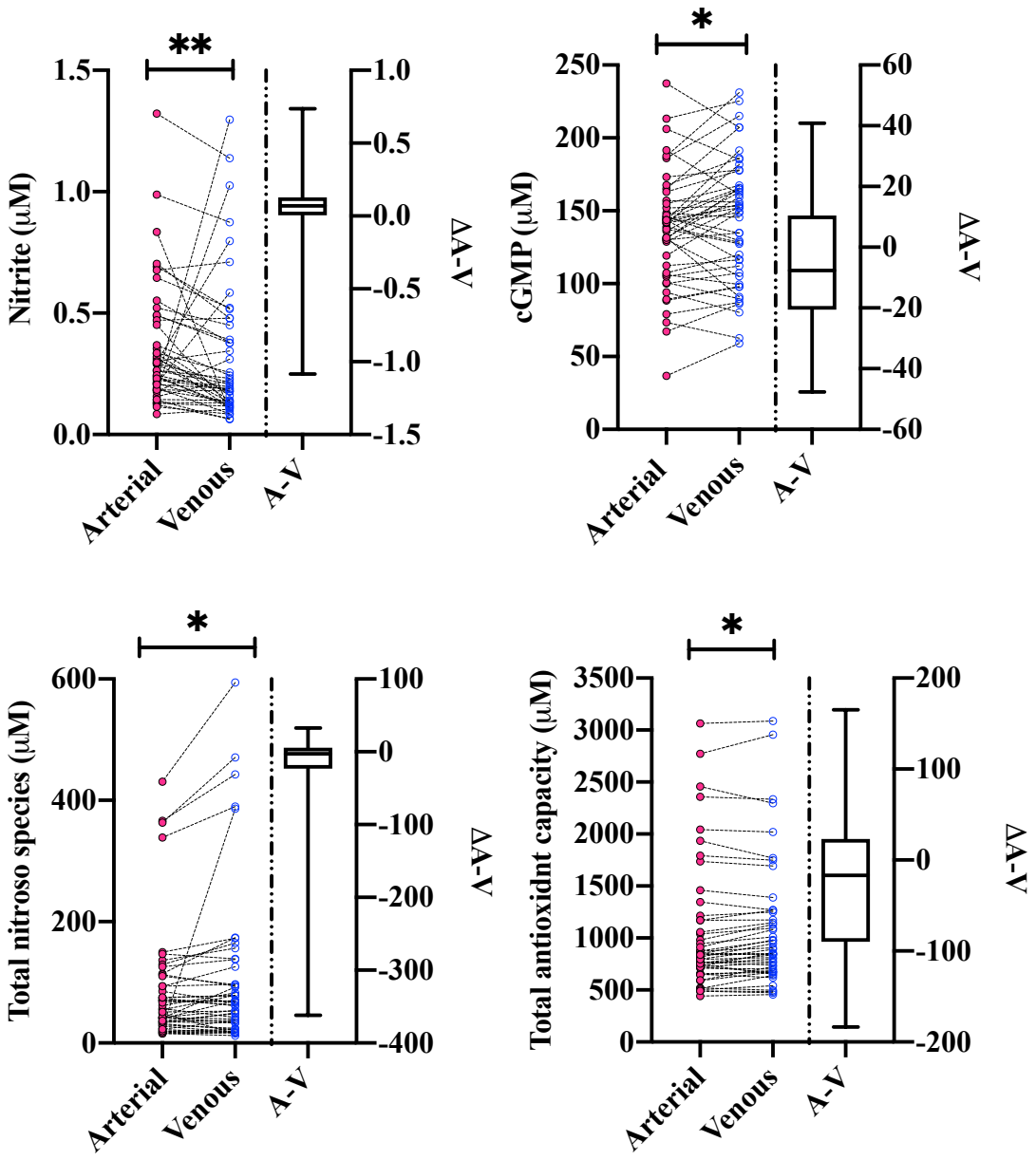

5.8.6. Venous redox profile in survivors and non survivors

Of the 20 patients in whom venous plasma was sampled at < 48 hours, 9 survived the episode of critical illness. Of the 15 patients still enrolled at the study at day 3-4, 7 survived; and of the 14 patients still enrolled at day 5-7, 6 survived. The median (IQR) of the redox measures in survivors and non survivors at the three different timepoints are summarised in Table 33. Venous plasma lipid peroxides were markedly higher in non survivors compared to survivors at all three timepoints; and this difference was statistically significant at day 3-4 and day 5-7 (p= 0.04 and 0.013 respectively). However, no difference in venous plasma isoprostanes was observed between survivors and non survivors at any timepoint. Venous total antioxidant capacity was significantly higher in non survivors at the first timepoint (p = 0.012), and total free thiols per total protein were higher in non survivors at day 3-4 (p = 0.014). Separation between survivors and non survivors is demonstrated in Figure 49. There was no difference between survivors and non-survivors at any timepoint in terms of venous nitrite, nitrate or cGMP, but total nitroso species were markedly lower in survivors at all timepoints, with a significant difference noted at < 48 hours (p = 0.016) (Figure 50).

Table 33. Venous redox profiles in survivors and non survivors

Venous plasma marker	Timepoint	Survivors	Non survivors	Mann Whitney p value
Lipid peroxides (μM)	< 48 hours	2.05 (1.57-3.55; 1.03-4.93)	3.74 (2.05-5.29; 1.89-6.34)	0.067
	Day 3-4	1.46 (1.15-2.44; 1.03-3.73)	3.23 (2.67-3.37; 1.08-5.26)*	0.04
	Day 5-7	1.62 (0.96-2.21; 0.95-2.87)	3.07 (2.19-4.60; 1.54-6.81)*	0.013
Isoprostanes (μM)	< 48 hours	218 (189-277; 152-1146)	228 (197-342; 97-2860)	0.503
	Day 3-4	221 (154-386; 143-2252)	222 (185-303; 123-452)	0.779
	Day 5-7	208 (169-464; 136-898)	268 (227-334; 148-344)	0.414
Total antioxidant capacity (μM)	< 48 hours	846 (685-938; 620-1094)	1389 (946-2020; 671-2956)*	0.012
	Day 3-4	739 (653-838; 474-1130)	939 (566-1640; 486-3087)	0.463
	Day 5-7	838 (488-917; 456-1010)	1018 (821-1245; 726-2334)	0.142
Free thiols (μM)	< 48 hours	169 (132-201; 118-237)	194 (156-269; 96-341)	0.152
	Day 3-4	156 (119-165; 96-215)	188 (179-323; 97-368)	0.054
	Day 5-7	171 (119-184; 100-192)	194 (165-252; 130-262)	0.108
Free thiols per protein (μM/g)	< 48 hours	4.34 (3.75-4.81; 1.79-5.64)	4.68 (3.74-5.96; 2.50-7.16)	0.37
	Day 3-4	3.78 (2.62-4.20; 2.43-4.81)	5.39 (4.55-7.94; 2.82-8.56)*	0.014
	Day 5-7	3.98 (3.23-5.83; 2.29-9.53)	5.33 (4.06-7.43; 3.12-8.27)	0.23
Nitrite (μM)	< 48 hours	0.18 (0.11-0.28; 0.07-0.52)	0.21 (0.11-0.45; 0.08-0.71)	0.503
	Day 3-4	0.14 (0.11-0.48; 0.09-1.03)	0.24 (0.19-0.37; 0.14-0.48)	0.336
	Day 5-7	0.15 (0.11-0.46; 0.06-0.52)	0.53 (0.19-1.07; 0.11-1.30)	0.108
Nitrate (μM)	< 48 hours	46.3 (26.1-129; 18.9-260)	52.5 (27.9-108; 15.0-255)	> 0.99
	Day 3-4	47.4 (25.3-76.3; 17.0-90.5)	50.6 (21.8-81.4; 18.7-87.6)	> 0.99
	Day 5-7	39.6 (24.8-58.6; 19.0-53.6)	39.1 (23.9-67.5; 21.9-152)	0.95
cGMP (μM)	< 48 hours	135 (103-172; 86-207)	127 (98.1-152; 59-231)	0.71
	Day 3-4	156 (128-163; 90-215)	151 (90.2-175; 63-225)	0.867
	Day 5-7	163 (103-183; 97-186)	158 (121-185; 91-207)	0.95
Total nitroso species (μM)	< 48 hours	49.6 (17.1-85.6; 12.1-156)	138 (69.1-174; 39.6-443)*	0.016
	Day 3-4	22.5 (17.1-165; 15.7-386)	63.8 (53.1-89.7; 33.8-594)	0.152
	Day 5-7	23.1 (18.8-59.4; 16.5-126)	73.7 (39.9-91.9; 33.5-471)	0.059

Median (IQR; range) of venous plasma redox analytes in survivors at < 48 h (n= 9); day 3-4 (n=7) and day 5-7 (n=6); and non survivors at < 48 h (n=11); day 3-4 (n=8) and day 5-7, n=8). Difference between survivors and non survivors at each time point using Mann Whitney (uncorrected); *$p < 0.05$.

Figure 49. Trajectory of changes in venous redox measures in survivors and non survivors

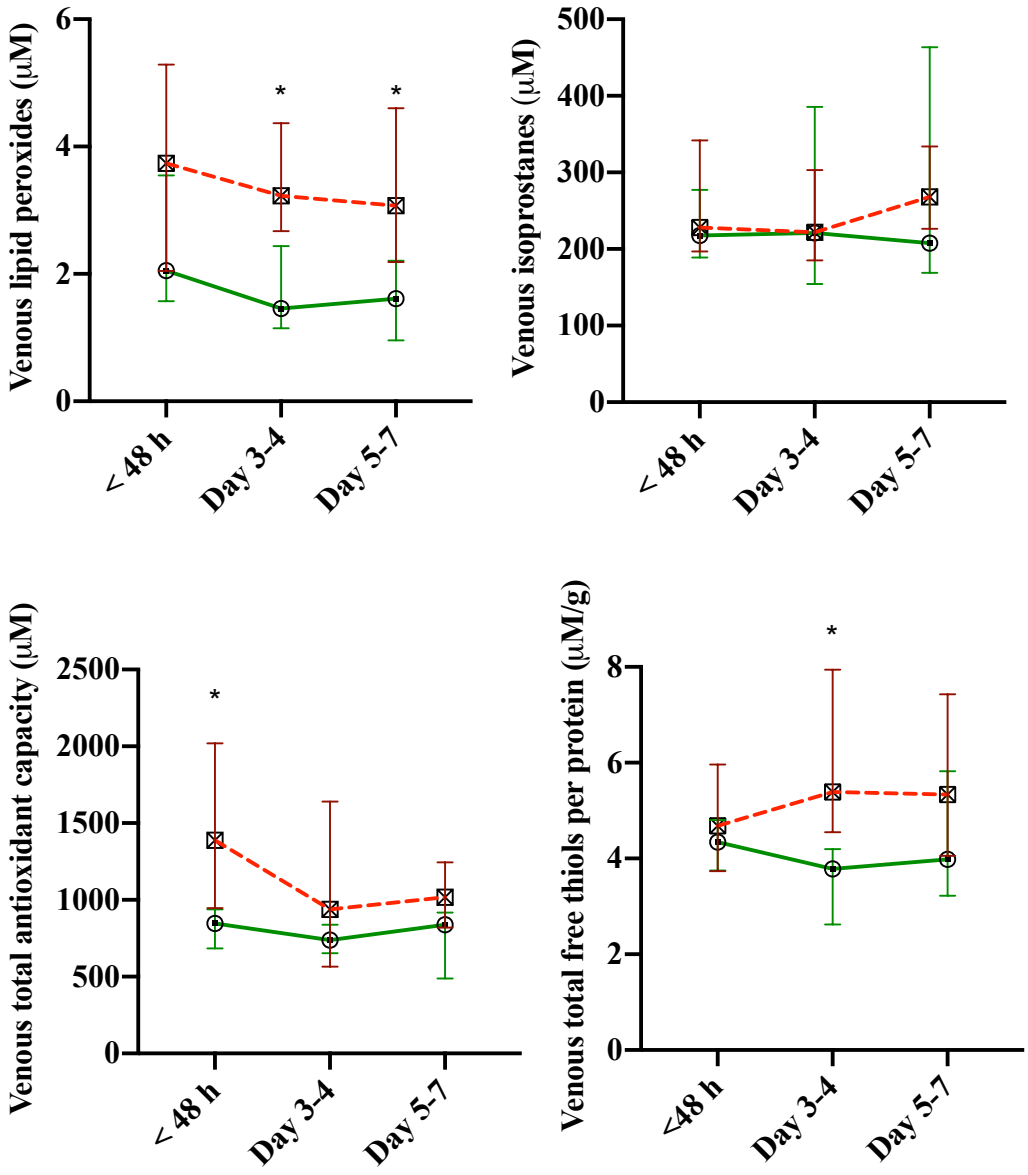

Median (IQR) of venous plasma redox analytes in survivors (circles joined by green lines) at < 48 h (n= 9); day 3-4 (n=7) and day 5-7 (n=6); and non survivors (squared joined by red lines) at < 48 h (n=11); day 3-4 (n=8) and day 5-7, n=8). Difference between survivors and non survivors at each time point using Mann Whitney (uncorrected); *p < 0.05.

Figure 50. Trajectory of changes in venous plasma measures of NO metabolism in survivors and non survivors

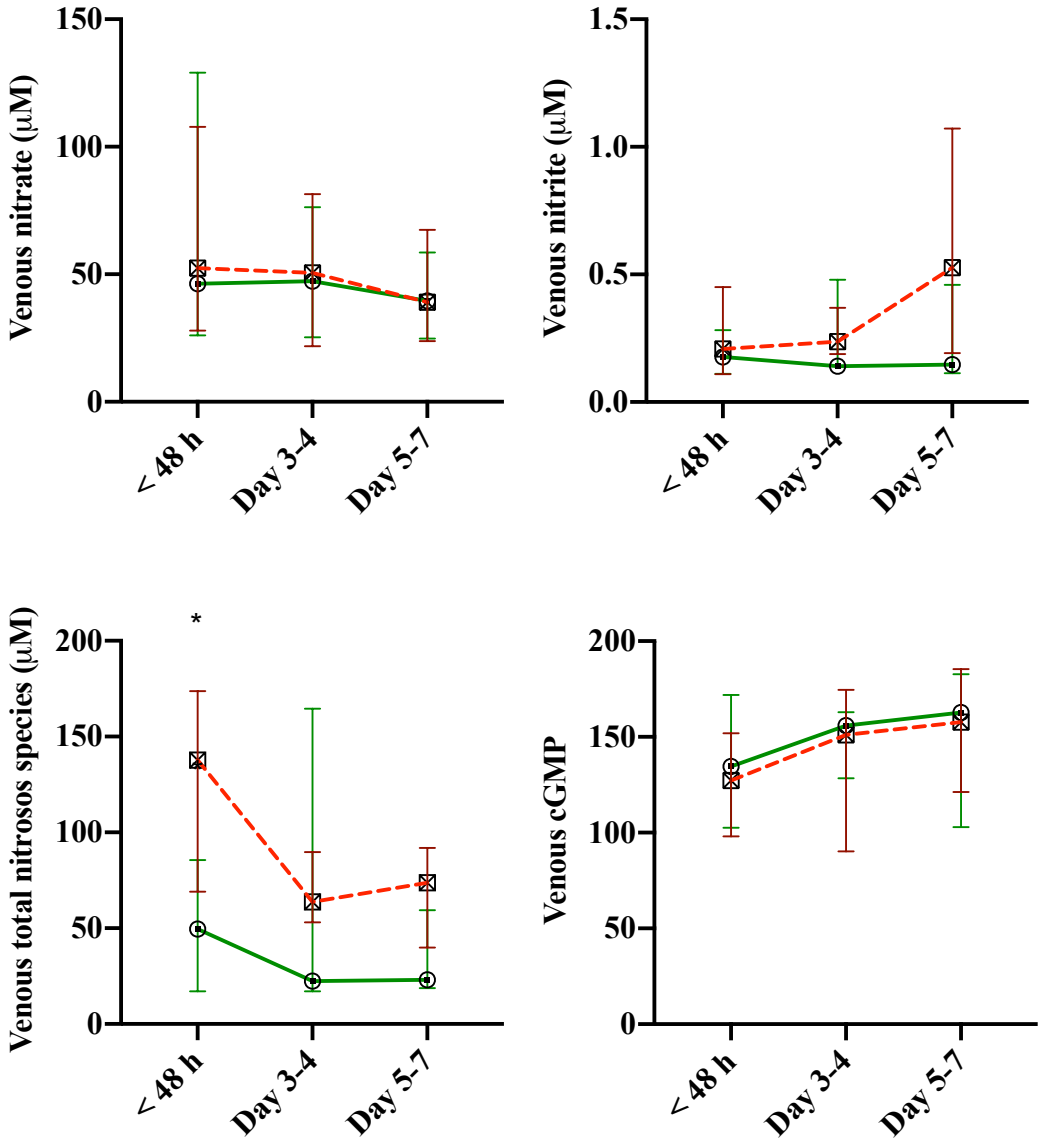

Median (IQR) of venous plasma nitric oxide analytes in survivors (circles joined by green lines) at < 48 h (n= 9); day 3-4 (n=7) and day 5-7 (n=6); and non survivors (squared joined by red lines) at < 48 h (n=11); day 3-4 (n=8) and day 5-7, n=8). Difference between survivors and non survivors at each time point using Mann Whitney (uncorrected); *p < 0.05.

5.8.7. Arterial redox profile in survivors and non survivors

Of the 21 patients in whom arterial plasma was sampled at < 48 hours, 9 went on to survive. Of the 16 patients still enrolled at the study at day 3-4, 7 survived. Of the 12 patients still enrolled at day 5-7, 4 survived. The median (IQR) of the arterial redox measures in survivors and non survivors at the three different timepoints are summarised in Table 34. The pattern of differences between survivors and non-survivors in arterial plasma closely resembled that seen previously in the venous plasma. Arterial measures of lipid peroxidation were again higher in non survivors at all timepoints (although this difference was significant at the first timepoint ($p = 0.018$) rather than the later two timepoints, as seen in venous plasma), and isoprostanes were not significantly different between the two groups (Figure 51). As observed in venous plasma, arterial total antioxidant capacity was higher in non survivors compared to survivors at < 48 hours ($p = 0.034$), as were total free thiols per protein at day 3-4 only ($p = 0.040$). Again, in a similar pattern to that seen in venous plasma, survivors and non-survivors did not differ in terms of nitrite, nitrate or cGMP, but non survivors had markedly higher levels of arterial total nitroso species than survivors ($p = 0.001$ at < 48 hours, $p=0.042$ at day 3-4), shown in Figure 52.

Table 34. Arterial plasma redox profile in survivors and non survivors

Arterial plasma marker	Timepoint	Survivors	Non survivors	p value
Lipid peroxides (µM)	< 48 hours	1.44 (1.30-2.61; 1.03-2.99)	2.74 (1.91-4.35; 1.57-7.56)*	0.018
	Day 3-4	1.53 (1.26-2.75; 1.25-2.78)	2.80 (2.14-3.80; 1.24-6.17)	0.071
	Day 5-7	1.47 (1.24-3.64; 1.21-4.32)	3.08 (2.02-3.95; 1.25-6.84)	0.283
Isoprostanes (µM)	< 48 hours	212 (184-408; 106-2923)	226 (200-395; 133-2637)	0.554
	Day 3-4	193 (158-193;151-2638)	247 (187-271; 176-394)	0.606
	Day 5-7	227 (162-273; 148-280)	231 (209-327;120-438)	0.57
Total antioxidant capacity (µM)	< 48 hours	842 (684-876; 650-1040)	1403 (826-1980; 592-2773)	0.034
	Day 3-4	761 (645-770; 488-980)	911 (509-1574; 492-3065)	0.408
	Day 5-7	624 (462-891; 443-946)	948 (797-1171; 593-2358)	0.073
Free thiols (µM)	< 48 hours	174 (147-205; 127-236)	182 (156-271; 88-315)	0.508
	Day 3-4	145 (128-175; 104-217)	192 (179-256; 95-351)	0.055
	Day 5-7	150 (111-183; 104-188)	192 (165-247; 117-268)	0.154
Free thiols per protein (µM/g)	< 48 hours	4.94 (4.37-5.32; 2.54-6.74)	4.96 (3.75-6.90; 2.84-8.18)	0.702
	Day 3-4	3.56 (3.09-4.06; 2.97-5.55)	5.07 (4.40-7.24; 2.85-9.29)*	0.0402
	Day 5-7	3.84 (3.29-6.28; 3.29-6.91)	5.26 (3.59-6.42; 3.40-9.29)	0.368
Nitrite (µM)	< 48 hours	0.23 (0.13-0.43; 0.08-0.69)	0.29 (0.19-0.51; 0.11-0.83)	0.464
	Day 3-4	0.24 (0.18-0.33; 0.16-0.70)	0.30 (0.26-0.48; 0.18-0.89)	0.114
	Day 5-7	0.25 (0.13-0.57; 0.13-0.65)	0.32 (0.22-0.85; 0.21-1.32)	0.461
Nitrate (µM)	< 48 hours	38.2 (26.6-128; 19.2-246)	54.7 (35.8-104; 11.6-273)	0.754
	Day 3-4	47.9 (27.5-71.4; 17.4-94.0)	44.1 (24.4-87.8; 19.5-88.5)	>0.99
	Day 5-7	41.6 (24.8-49.7; 20.0-51.5)	38.2 (23.1-74.8; 20.9-143)	0.808
cGMP (µM)	< 48 hours	129 (94.3-155; 67.2-173)	113 (93.1-147; 36.8-206)	0.962
	Day 3-4	139 (132-157; 101-186)	147 (101-163; 73.4-213)	0.873
	Day 5-7	143 (133-162; 130-167)	144 (134-182; 130-237)	0.808
Total nitroso species (µM)	< 48 hours	33 (17.4-48.1; 15.9-136)	120 (70-149; 41.7-366)*	<0.001
	Day 3-4	31.8 (22.2-56.6; 17.8-129)	74.2 (46.7-142; 42.1-431)*	0.042
	Day 5-7	32.8 (22.2-78.7; 19.6-93.0)	70.7 (35.2-101; 22.5-363)	0.283

Median (IQR; range) of arterial plasma redox analytes in survivors (circles joined by green lines) at < 48 h (n=9); day 3-4 (n=7) and day 5-7 (n=4); and non survivors (squared joined by red lines) at < 48 h (n=12); day 3-4 (n=9) and day 5-7, n=8). Difference between survivors and non survivors at each time point using Mann Whitney (uncorrected).

Figure 51. Trajectory of changes in concentration of arterial plasma redox components in survivors and non survivors

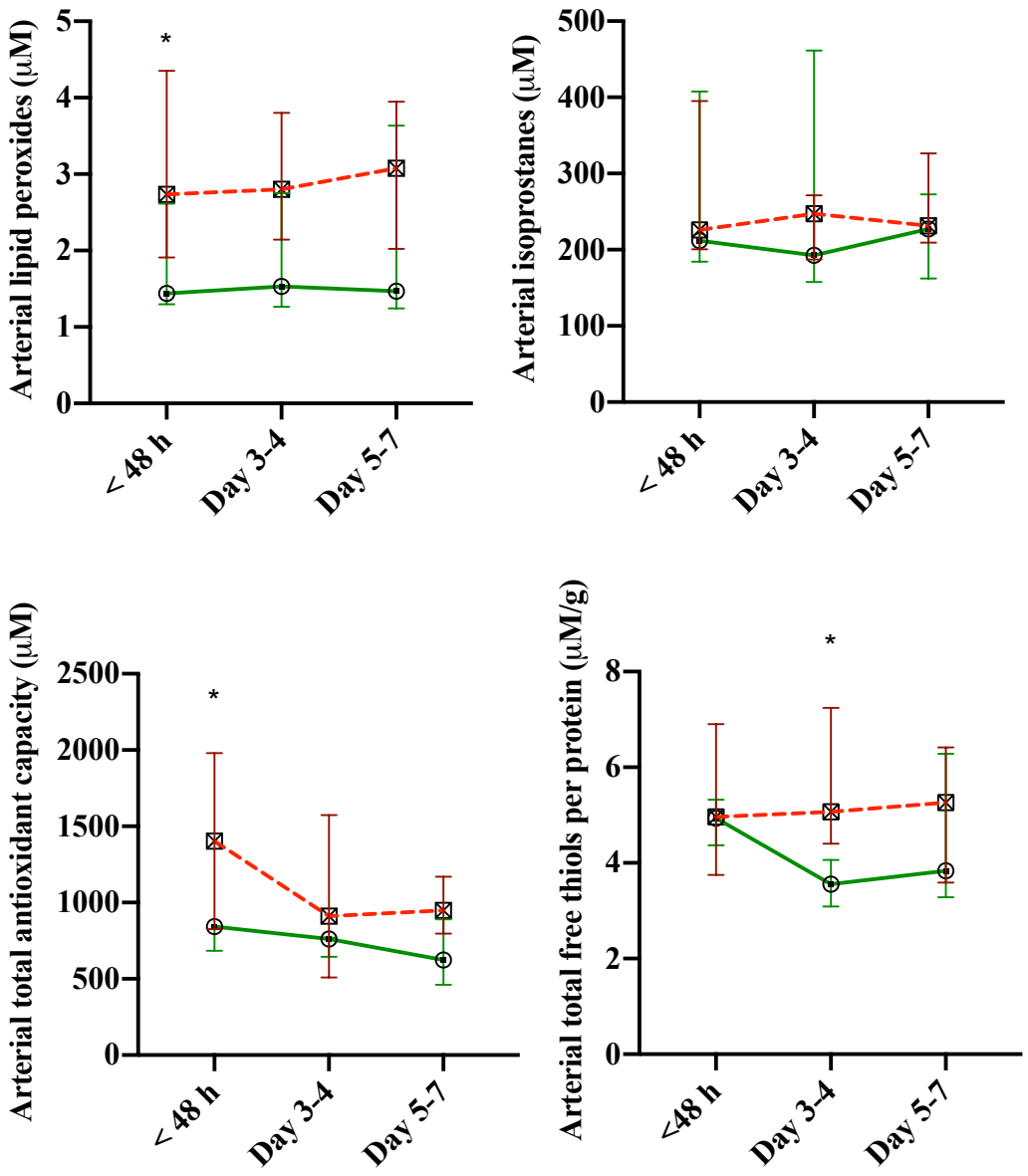

Median (IQR) of arterial plasma redox analytes in survivors (circles joined by green lines) at < 48 h (n=9); day 3-4 (n=7) and day 5-7 (n=4); and non survivors (squared joined by red lines) at < 48 h (n=12); day 3-4 (n=9) and day 5-7, n=8). Difference between survivors and non survivors at each time point using Mann Whitney (uncorrected).

Figure 52. Trajectory of changes of arterial plasma measures of NO metabolism in survivors and non survivors

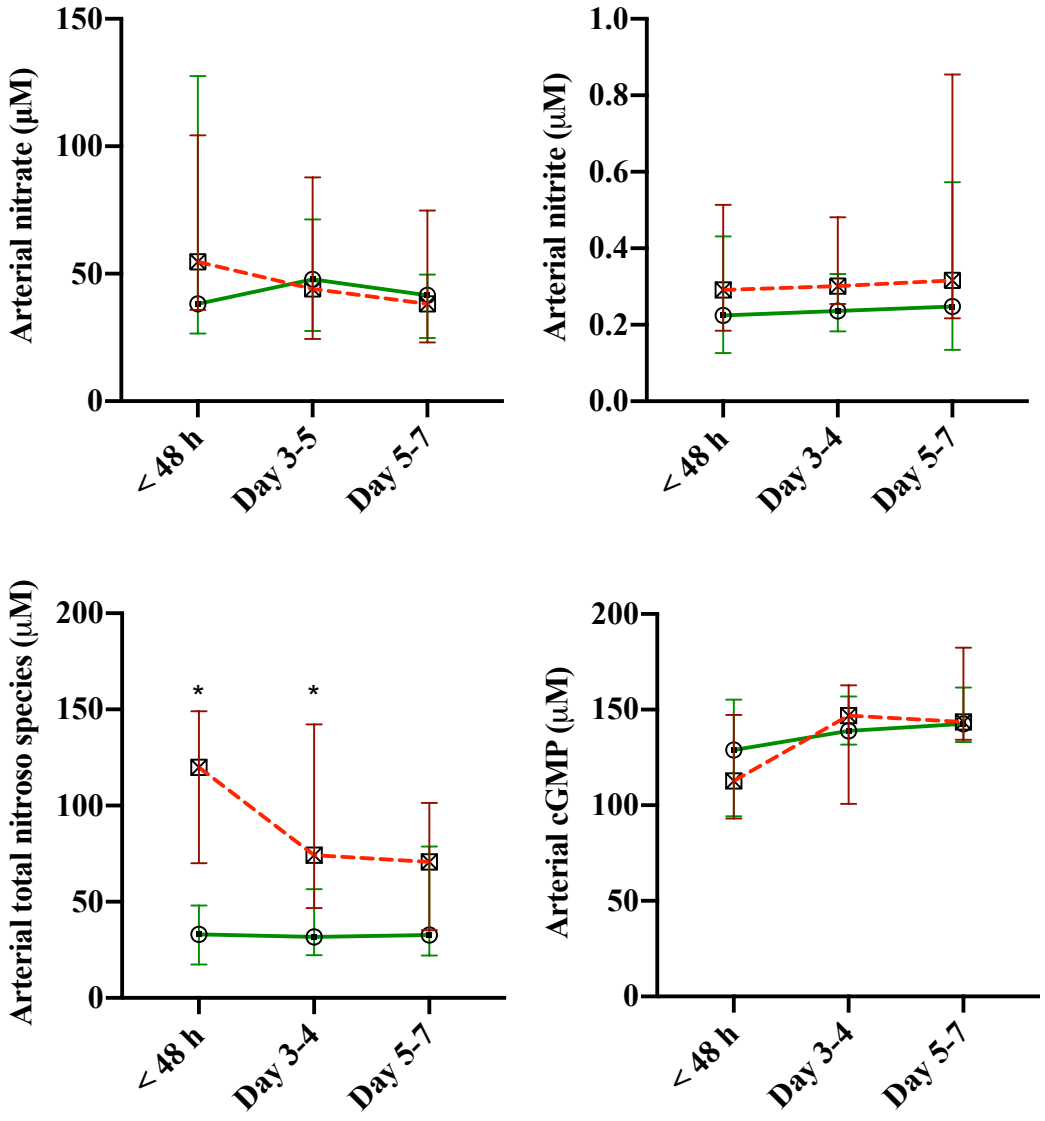

Median (IQR) of arterial nitric oxide analytes in survivors (circles joined by green lines) at < 48 h (n=9); day 3-4 (n=7) and day 5-7 (n=4); and non survivors (squared joined by red lines) at < 48 h (n=12); day 3-4 (n=9) and day 5-7, n=8). Difference between survivors and non survivors at each time point using Mann Whitney (uncorrected).

5.8.8. Assessing the utility of plasma redox measures as biomarkers

To assess the sensitivity and specificity of the plasma redox measures as biomarkers to predict non-survival, receiver operating characteristic (ROC) curves were plotted for lipid peroxides, total antioxidant capacity, total free thiols per protein and total nitroso species. For each ROC curve, the area under the curve (AUC) was calculated and the optimum cut-off was estimated using Youden's J statistic, calculated according to Equation 32. The optimum cut-off was determined as that corresponding to the maximum calculated Youden's index, which is considered to represent a valid discriminator if > 50%. These values are summarised for each relevant redox measure Table 35 and the ROC curves for arterial lipid peroxides, total antioxidant capacity and total nitroso species are compared in Figure 53. Arterial plasma nitroso species, above a cut off of 59 μM, predicted death from critical illness with a sensitivity of 76% and a specificity of 85%.

Equation 32. Calculation of Youden's J statistic

$$Youden'sJ\ statistic\ (\%) = Sensitivity(\%) + Specificity\ (\%) - 100\ \%$$

Figure 53. ROC curves for plasma redox measures

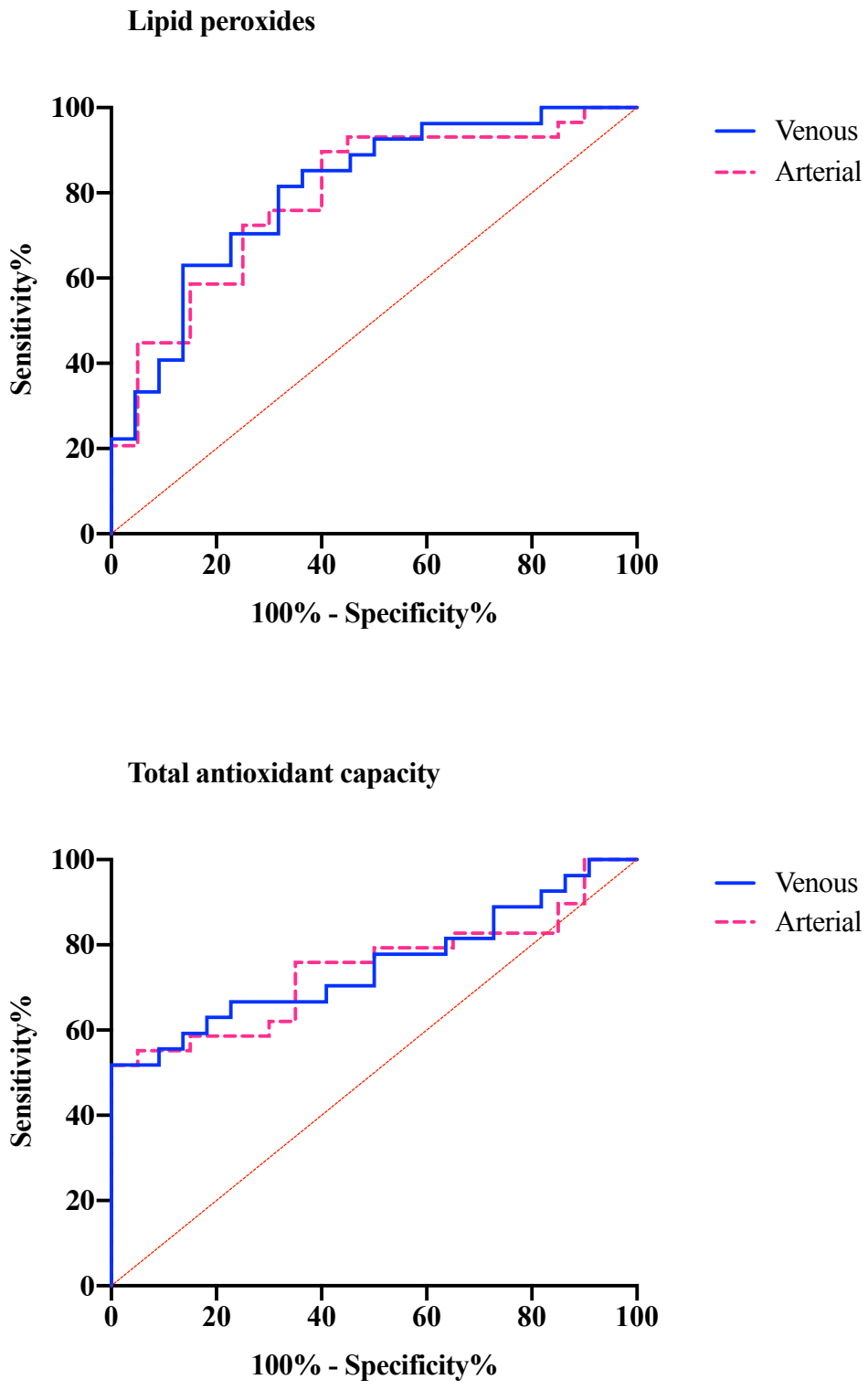

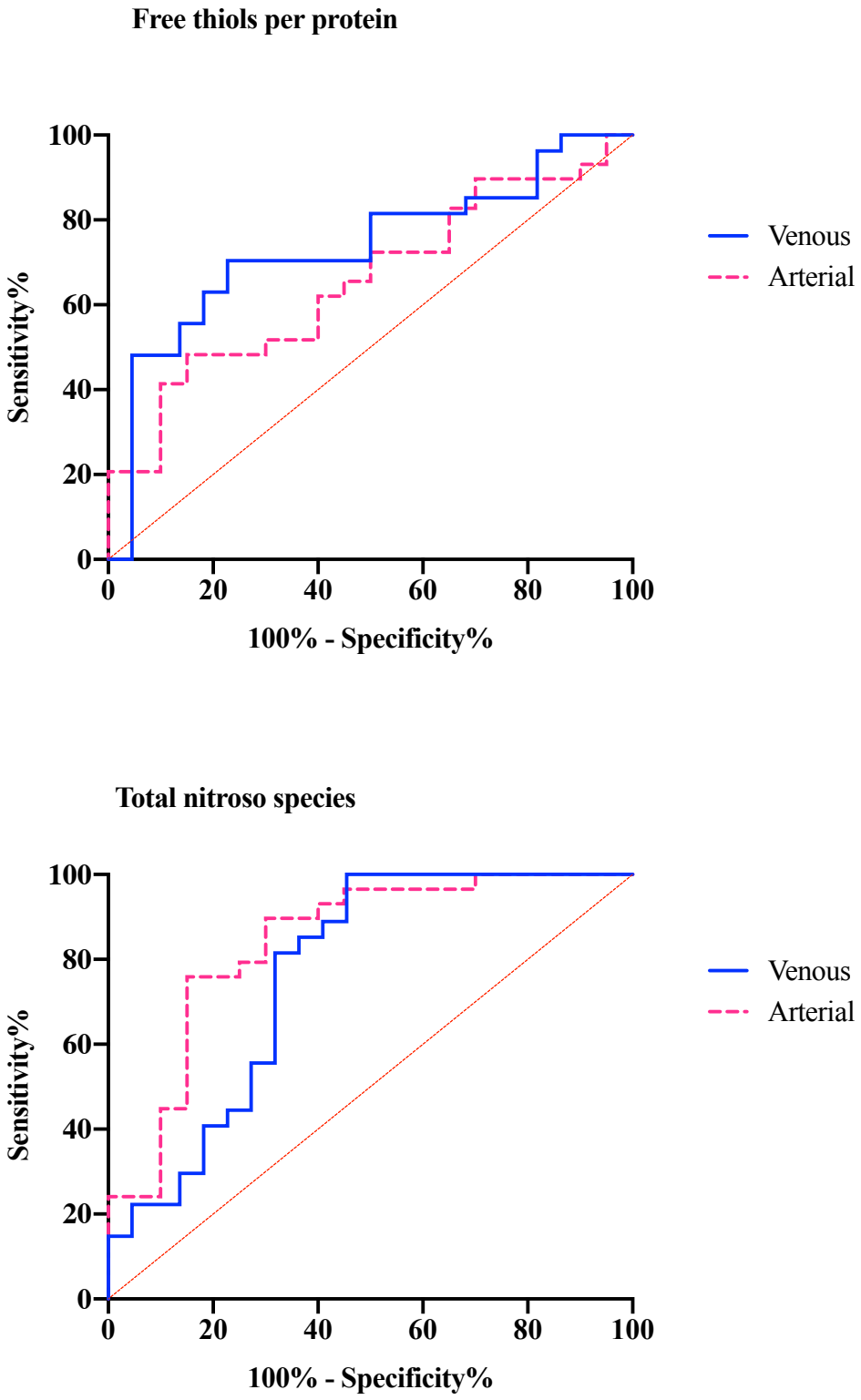

Solid blue line represents measures in venous plasma; dashed pink line represents measures in arterial plasma.

Table 35. Summary of area under the curve (AUC) data from plasma redox ROC curves

Putative plasma biomarker	Compartment	Area	95% CI	p value	Optimum cut off	Sensitivity	Specificity	Youden's J	LR
Lipid peroxides	Arterial	0.79	0.66 - 0.92	0.0006	> 1.647	89.66	60	49.7	2.241
	Venous	0.8	0.68 - 0.93	0.0003	> 2.898	62.96	86.36	49.32	4.62
Total antioxidant capacity	Arterial	0.74	0.61-0.88	0.0041	> 1048	51.72	100	51.7	
	Venous	0.75	0.61-0.89	0.0027	> 1138	51.85	100	51.9	
Free thiols per protein	Arterial	0.66	0.50 - 0.80	0.067	> 5.367	48.28	85	33.3	3.22
	Venous	0.73	0.59-0.88	0.0052	> 4.532	70.37	77.27	47.6	3.1
Total nitroso species	Arterial	0.84	0.72-0.96	<0.0001	> 59.07	75.86	85	60.9	5.057
	Venous	0.77	0.62 -0.91	0.0015	> 33.64	96.3	54.55	50.9	2.12

Sensitivity and specificity corresponding to the optimum cut-off, as estimated by the maximum Youden's statistic. LR: likelihood ratio.

5.8.9. Redox change in survivors and non survivors

There was no difference between survivors and non survivors in terms of the absolute within-subject change in any of the redox measures from the first to the second timepoint (ΔT2-T1). This was calculated as the value measured for a subject at day 3-4 minus the value for the same subject measured at < 48 hours. The percentage differences (calculated as the absolute difference between timepoints divided by their average) are displayed in Figure 54. There was also no difference between survivors and non survivors in terms of the absolute change in any of the redox measures for the first to the third timepoint (ΔT3 - T1) calculated as the value measured for a subject at day 5-7 minus the value for the same subject measured at < 48 hours.

Figure 54. Comparison of survivor and non survivor cohorts in terms of within subject change in plasma redox components from < 48 hours to day 3-4.

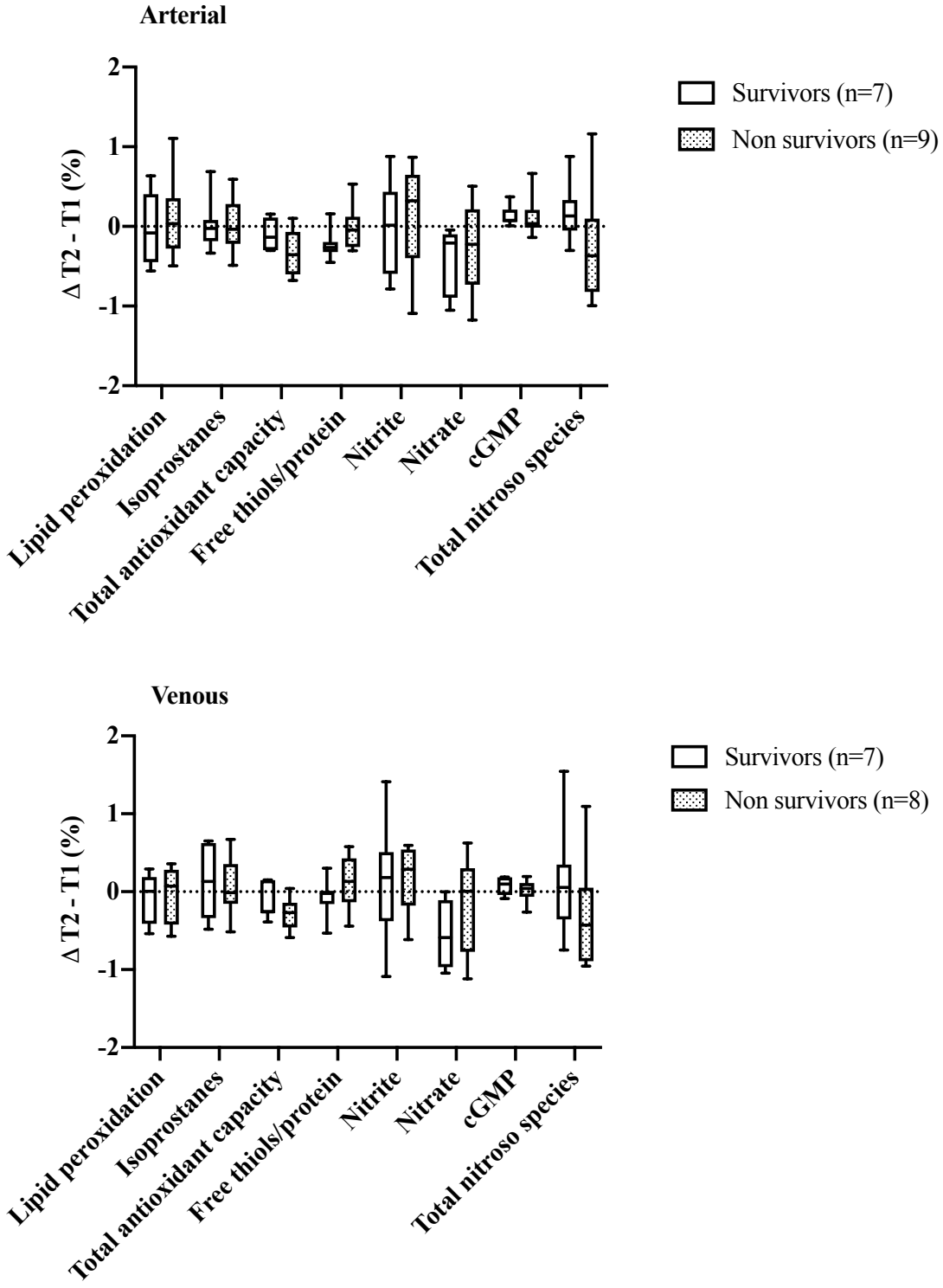

Box and whisker plots of the percentage change in plasma redox components from timepoint 1 (<48 h) to timepoint 2 (day 3-4).

Arterio-venous differences in survivors and non survivors

The medians (and IQR) of the difference between paired arterial (A) and venous (V) plasma values (expressed relative to the arterial value) for survivors and non survivors are shown in Figure 55. There were no significant differences in arterio-venous differences between survivors and non survivors for any of the redox measures.

Figure 55. Arterio-venous differences in survivors and non survivors at all three timepoints

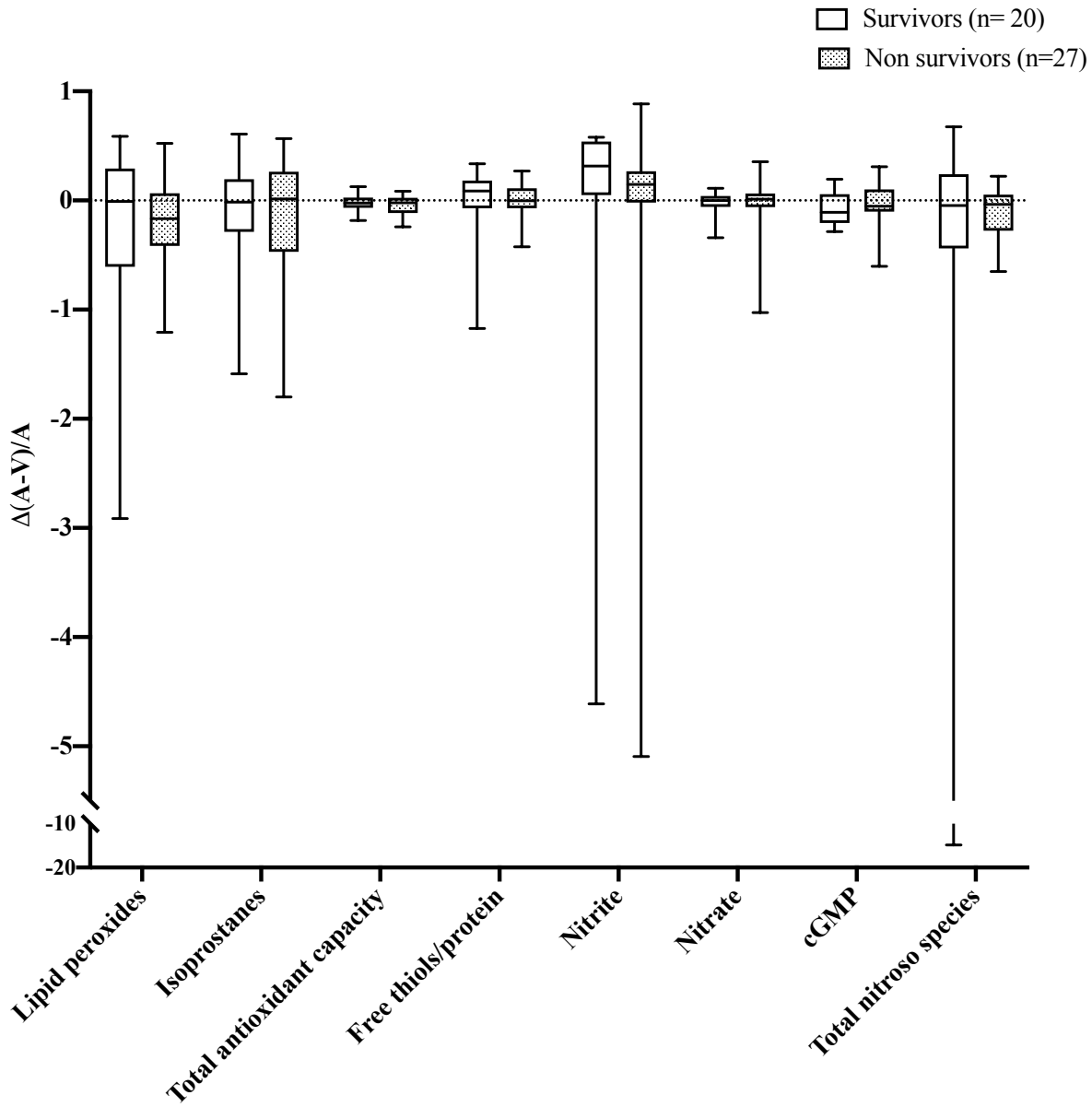

Box and whisker plot of arteriovenous differences at all three timepoints in survivors (n=20) and non survivors (n=27). AV differences expressed relative to arterial value; calculated as the arterial value (A) minus the paired venous value (V) divided by the arterial value (A).

5.8.10. Relationships between organ failure and plasma redox profile

There was significant positive correlation between APACHE II score and the contemporaneous measure of arterial plasma lipid peroxidation taken at < 48 h ($r=0.46$, $p=0.036$, Figure 56). There was moderate positive correlation between APACHE II score and total antioxidant capacity measured in both arterial plasma ($r=0.72$, $p = 0.0002$) and venous plasma ($r=0.76$, $p < 0.0001$), shown in Figure 57. Correlation was assessed between SOFA score and plasma redox measures at all three timepoints (49 pairs). There was significant positive correlation between the SOFA score and lipid peroxides in arterial ($r=0.41$, $p = 0.003$) and venous plasma ($r=0.48$, $p=0.0005$) shown in Figure 58. Higher SOFA scores were also associated with greater total antioxidant capacity in both arterial ($r=0.66$, $p < 0.0001$) and venous plasma ($r=0.65$, $p <0.0001$), shown in Figure 59. Weak positive association was also demonstrated between SOFA score and nitrate, in both arterial ($r=0.37$, $p=0.0097$) and venous plasma ($r=0.37$, $p=0.0098$) shown in Figure 60, and between SOFA scores and total nitroso species in both arterial ($r=0.42$, $p=0.0025$) and venous compartments ($r=0.37$, $p=0.0091$), shown in Figure 61. There was no relationship between organ failure and plasma nitrite concentrations.

Figure 56. Association between APACHE II scores and plasma lipid peroxides

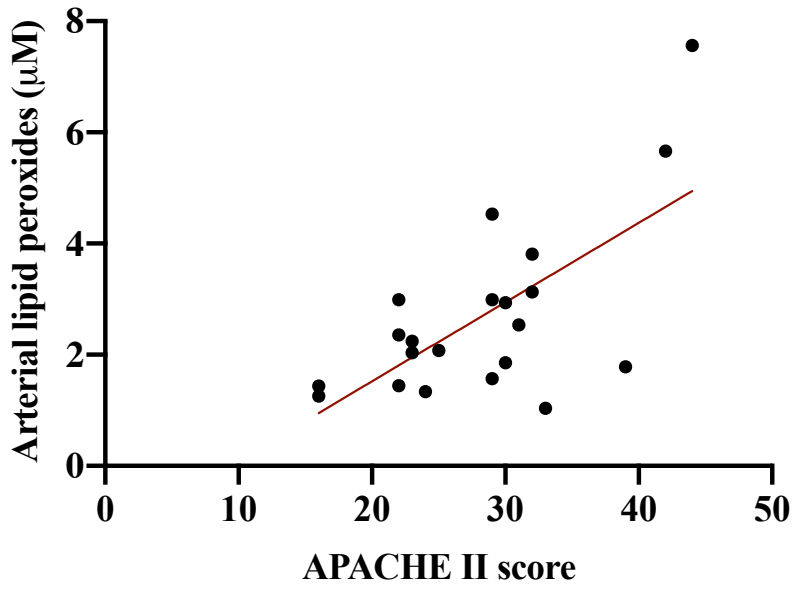

Lipid peroxides measured at < 48 h; 21 pairs.

Figure 57. Association between APACHE II scores and plasma total antioxidant capacity

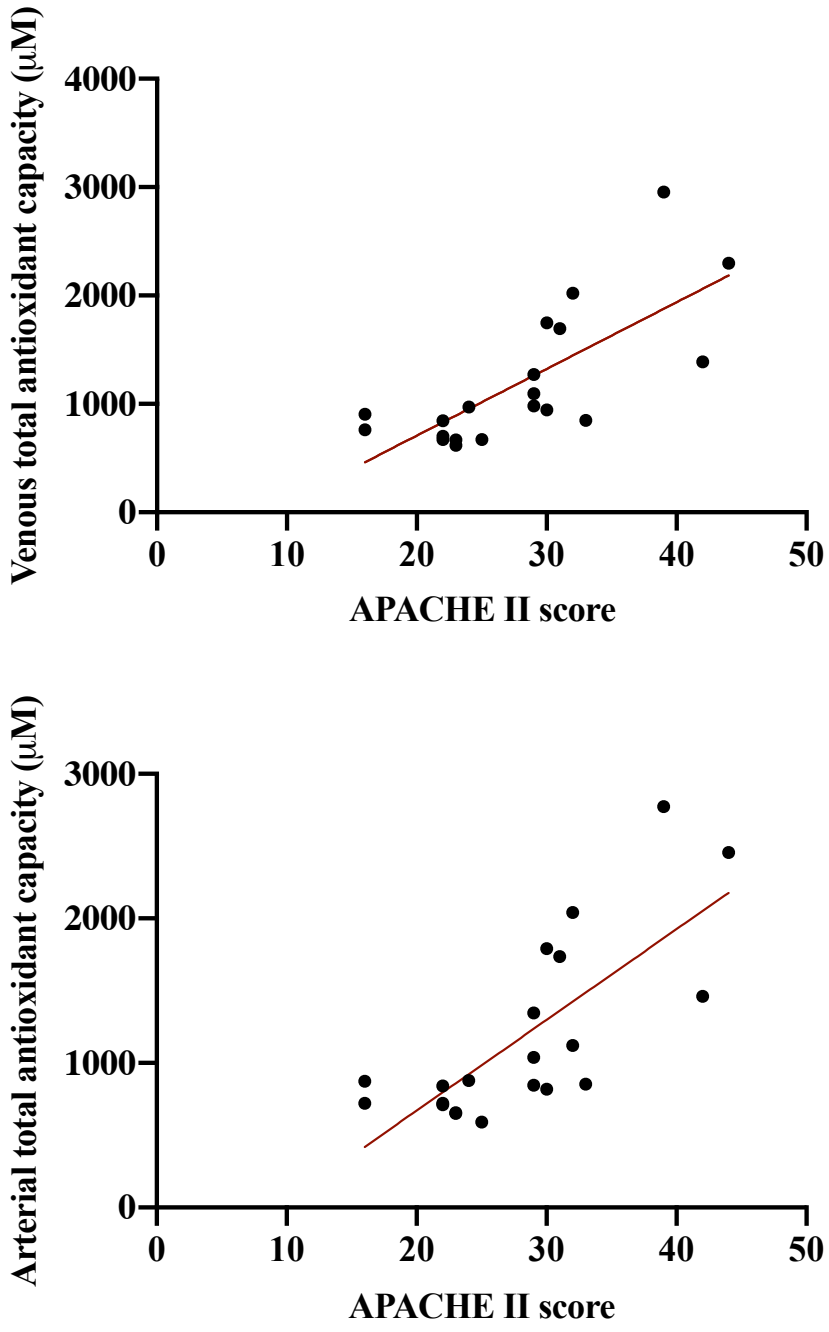

Total antioxidant capacity measured at < 48 h. 21 pairs for arterial; 20 pairs for venous plasma.

Figure 58. Associations between SOFA scores and plasma lipid peroxides

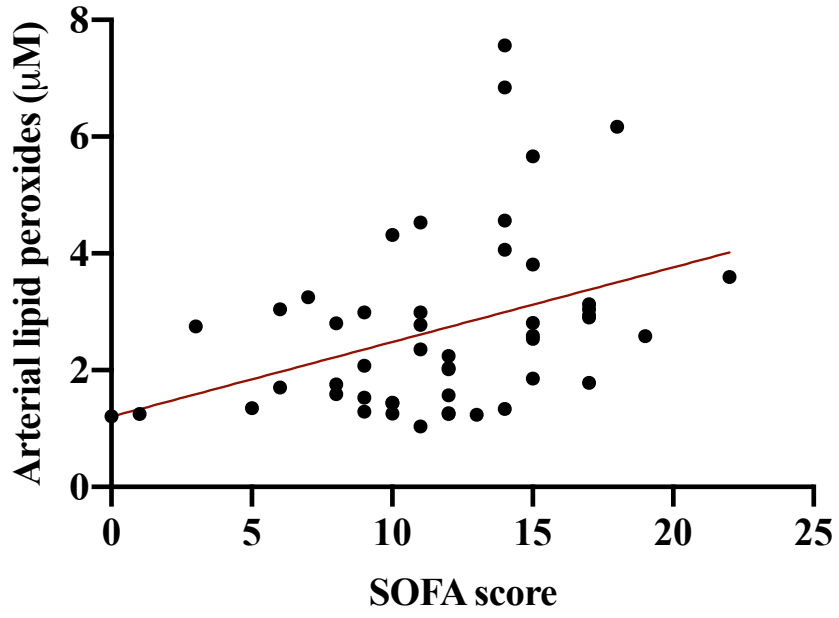

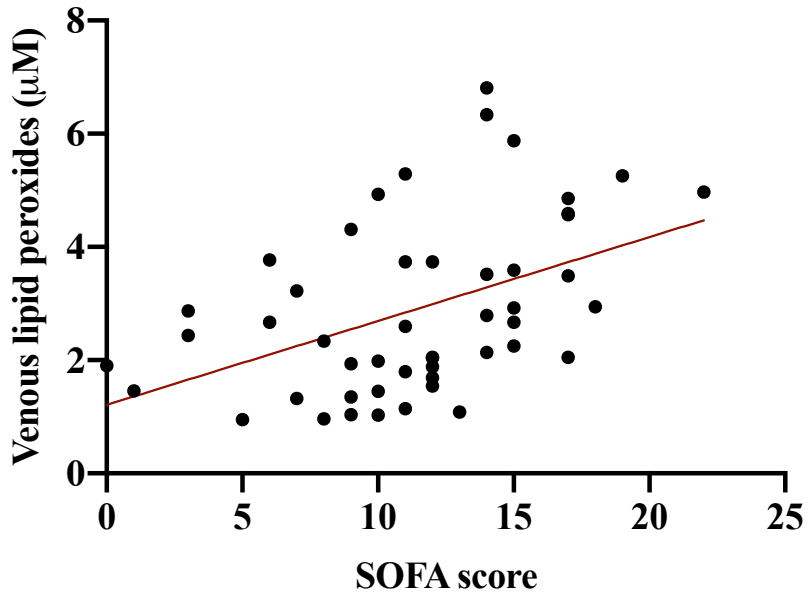

Measures taken at all three timepoints; 49 pairs.

Figure 59. Associations between SOFA scores and plasma total antioxidant capacity

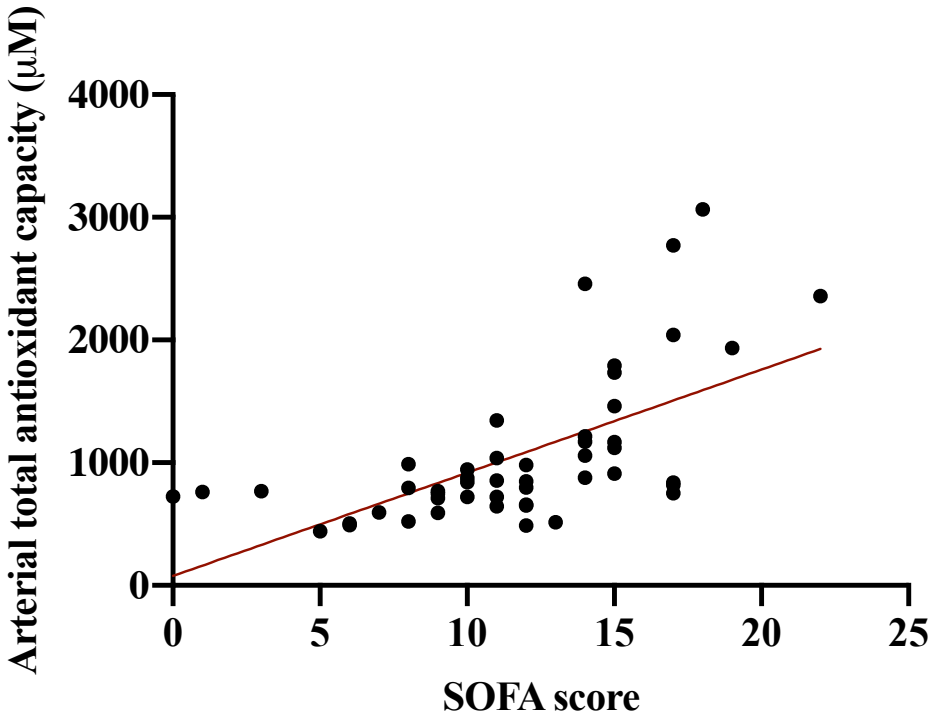

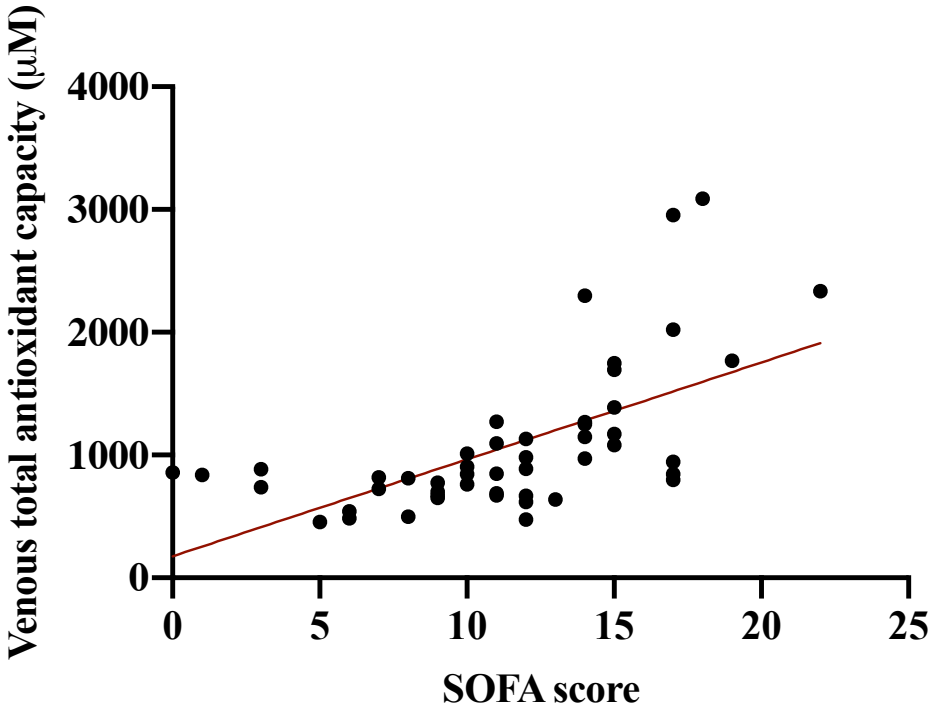

Measures at all three timepoints; 49 pairs.

Figure 60. Associations between SOFA scores and plasma nitrate

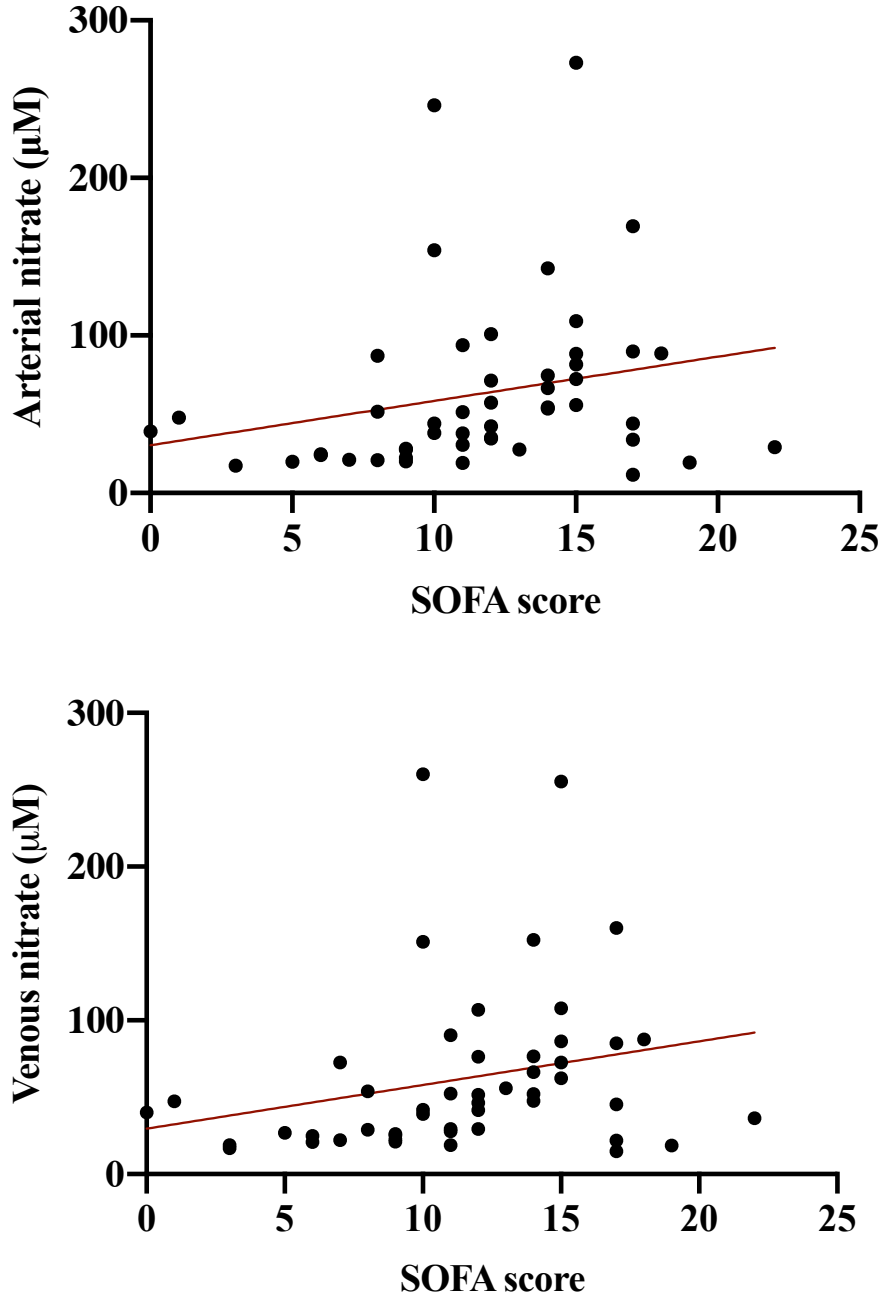

Measures at all three timepoints; 49 pairs.

Figure 61. Associations between SOFA scores and plasma total nitroso species

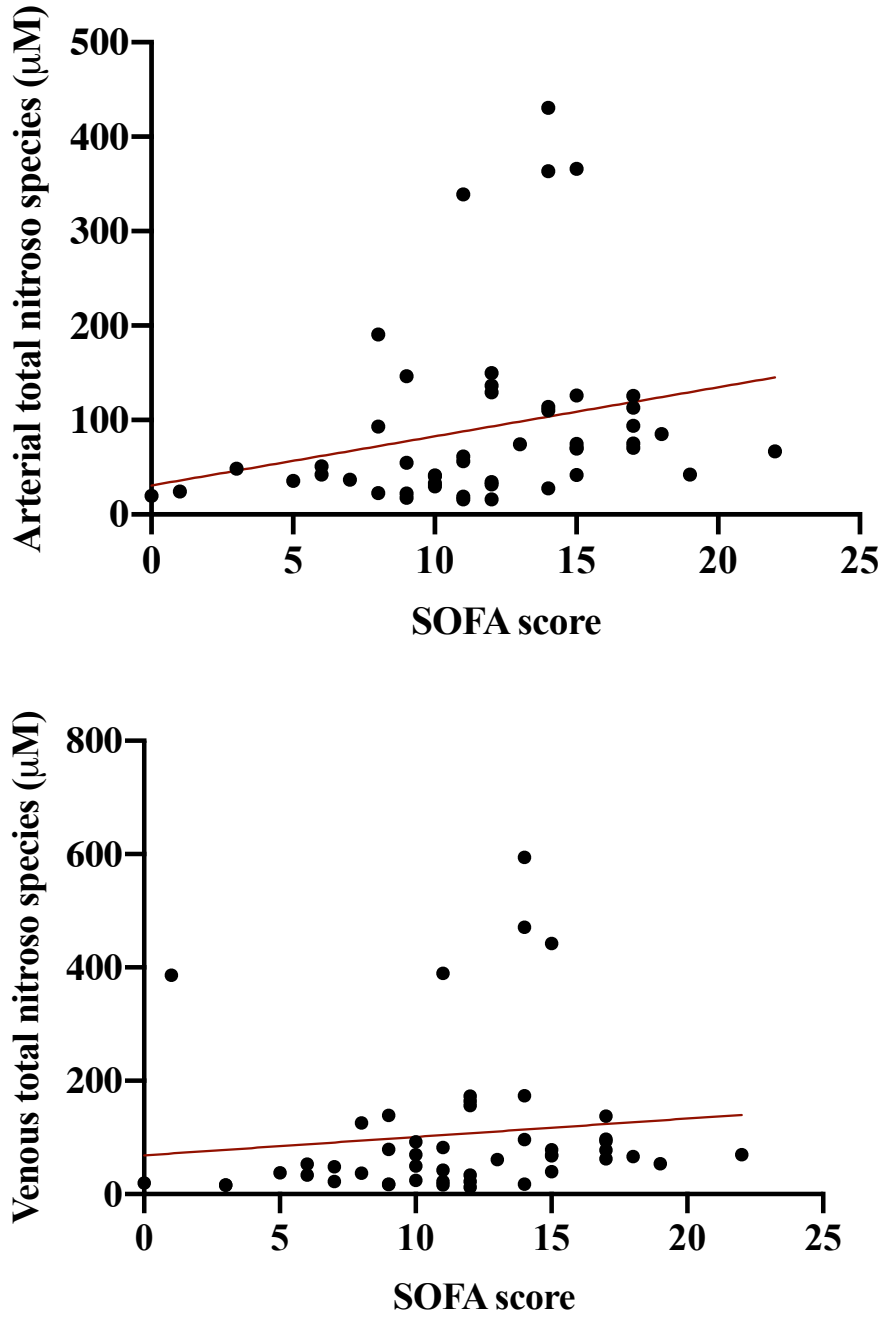

Measures at all three timepoints; 49 pairs.

5.8.11. Relationship between plasma redox markers and oxygenation

Significant associations between plasma redox components and measures of exposure to oxygen (F_IO_2), or adequacy of oxygenation (arterial lactate concentration), are summarised in Table 36. There was moderate positive correlation between arterial lactate concentrations and total antioxidant capacity, in both arterial and venous plasma ($r = 0.6$; $p < 0.0001$) shown in Figure 62. There was weak positive correlation between plasma lipid peroxides and both F_IO_2 and arterial lactate concentration; but a negative correlation with PaO_2 (Figure 63). There was weak positive correlation between plasma total antioxidant capacity and both F_IO_2 and arterial lactate concentration; but again, a negative correlation with PaO_2 (Figure 64).

Table 36. Associations between plasma redox profile and arterial oxygenation variables

Clinical measure	Plasma measure	Lipid peroxides	Total antioxidant capacity	Nitrite	Nitrate	Total nitroso species	cGMP
F_IO_2 (fraction)	Arterial	r = 0.41 p = 0.0035*	r = 0.46 p = 0.0008*	NS	r = 0.43 p = 0.002*	r = 0.35 p = 0.013*	NS
	Venous	r = 0.31* p = 0.031	r = 0.43 p = 0.0021*	r = 0.31 p = 0.027*	r = 0.39 p = 0.0051*	NS	NS
PaO_2 (kPa)	Arterial	r = -0.31 p = 0.032*	NS	NS	r = -0.38 p = 0.0068*	NS	NS
	Venous	NS	NS	NS	NS	NS	NS
Arterial lactate	Arterial	r = 0.33 p = 0.019*	r = 0.60 p < 0.0001*	NS	NS	r = 0.34 p = 0.019*	r = -0.28 p = 0.049*
	Venous	r = 0.49 p = 0.0003*	r = 0.60 p < 0.0001*	NS	NS	NS	r = -0.38 p = 0.0072*

*p < 0.05, NS: non significant.

Figure 62. Associations between arterial lactate and total antioxidant capacity

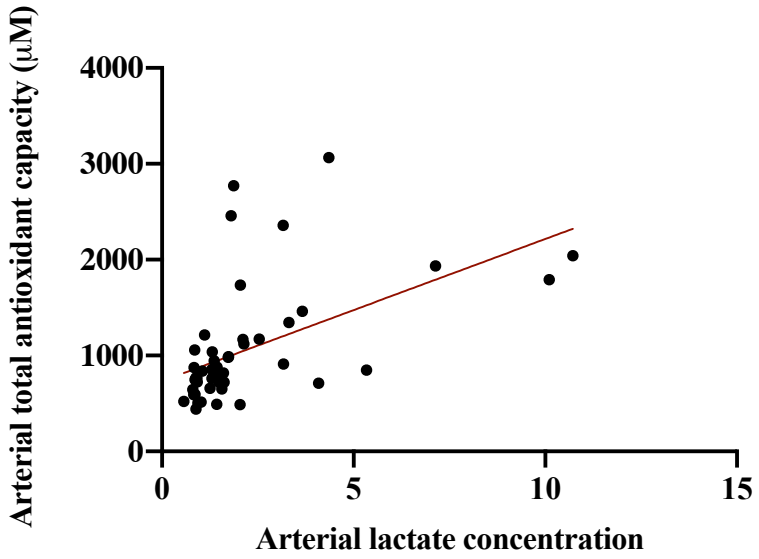

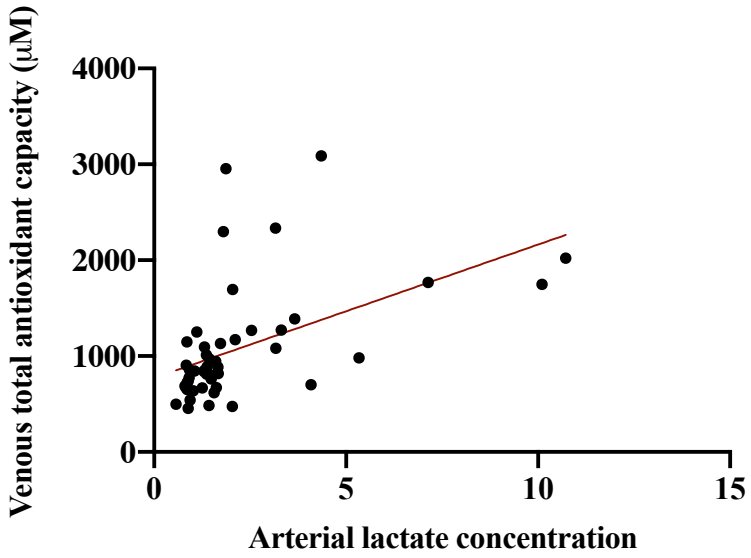

Measures at all three timepoints; 49 pairs

Figure 63. Association between arterial lipid peroxides and systemic oxygenation

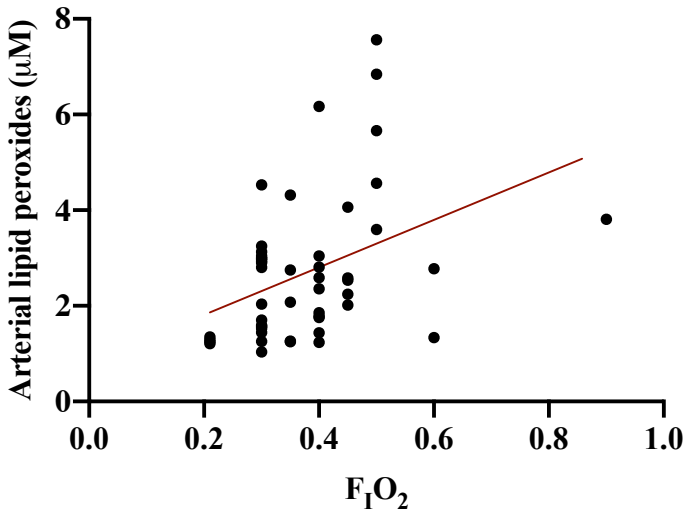

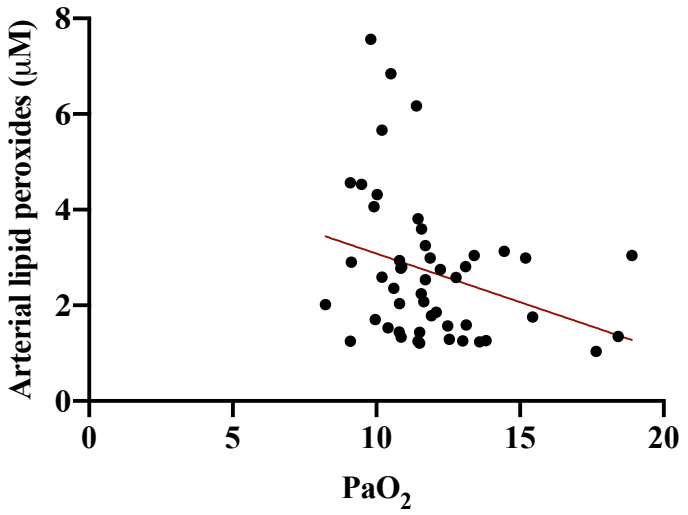

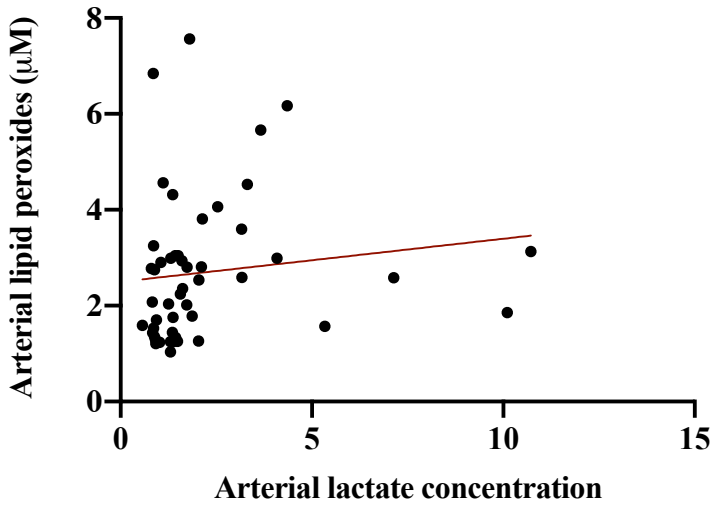

Measures at all three timepoints; 49 pairs

Figure 64. Relationship between arterial antioxidant capacity and systemic oxygenation

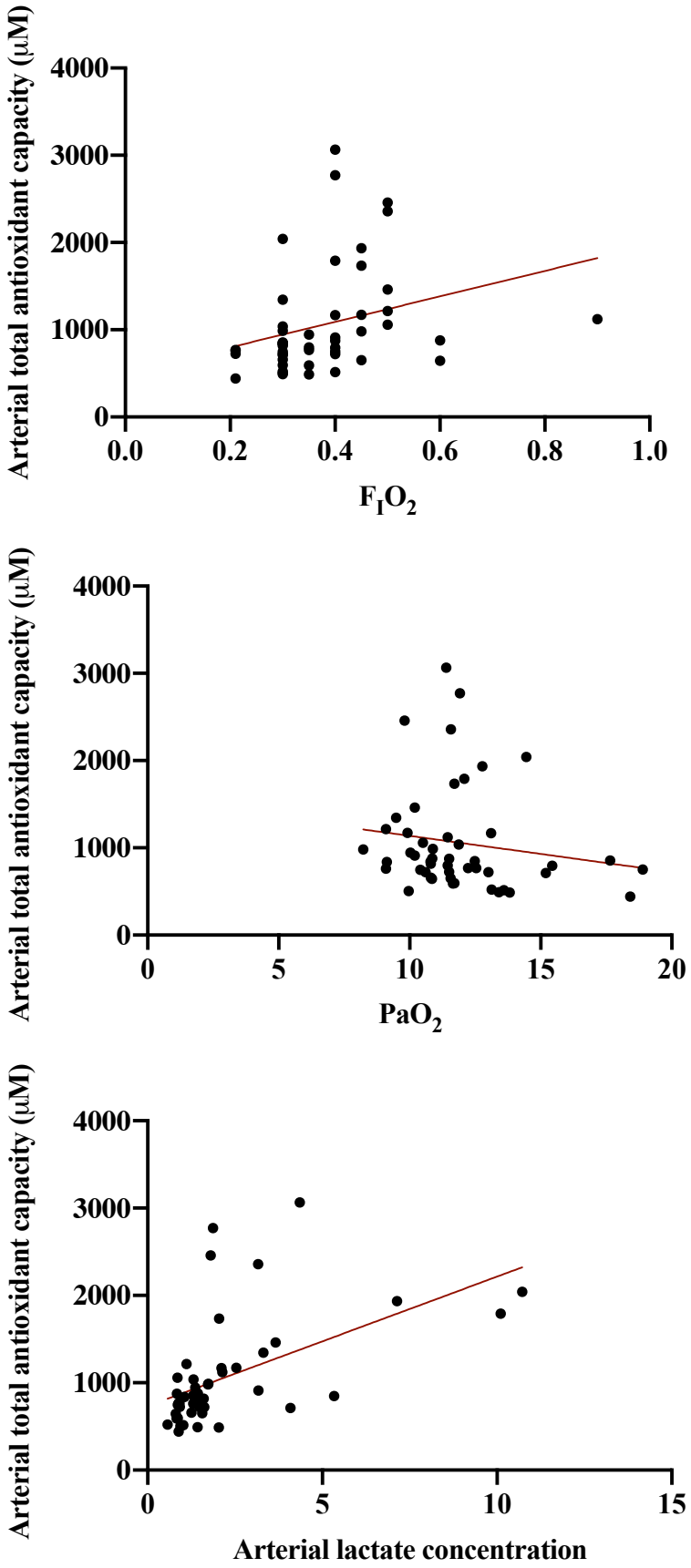

5.8.12. Relationship between plasma redox markers and inflammation

There was no relationship between venous levels of C-reactive protein (a non-specific marker of inflammation) and lipid peroxides, antioxidant capacity or measures of NO metabolism. However, there was significant negative correlation between CRP and total free thiols, in both arterial ($r = -0.53$, $p < 0.0001$) and venous plasma ($r = -0.55$, $p < 0.0001$), shown in Figure 65.

Figure 65. Association between C-reactive protein and plasma free thiols

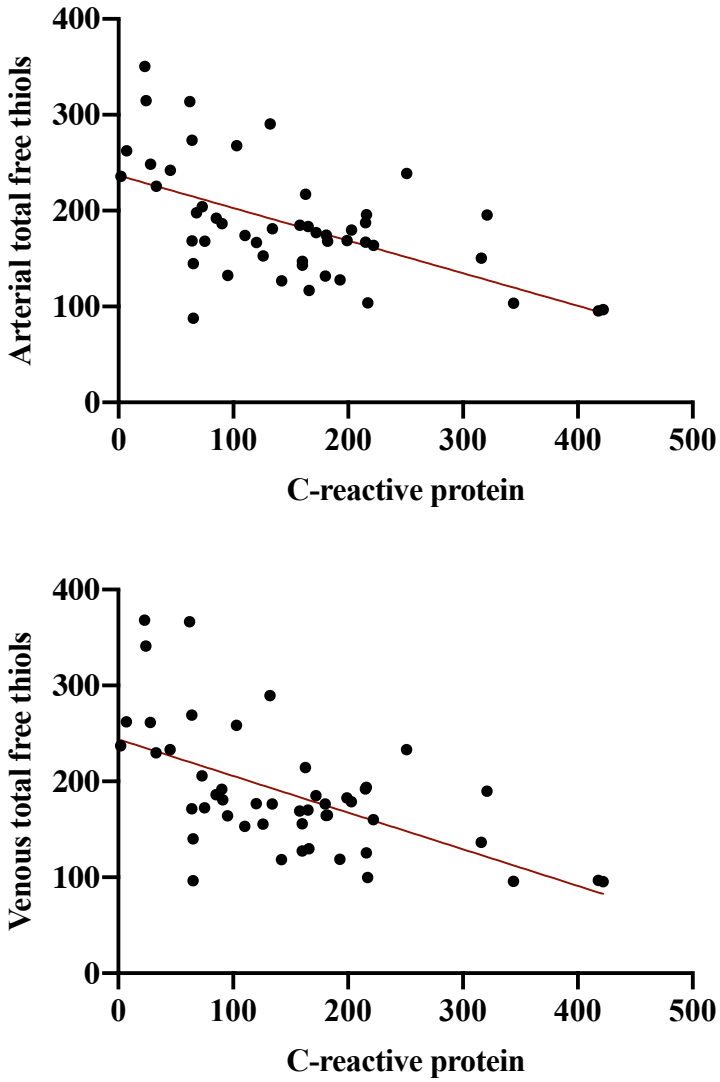

Measures at all three timepoints; 49 pairs

5.8.13. Relationship between skeletal muscle phenotype and plasma redox profile

Several respirometry variables demonstrated a significant relationship with the same plasma redox component: arterial plasma lipid peroxides. Relative capacity for leak- ($LEAK_{FAO}/ETS_{MAX}$); FAO- ($OXPHOS_{FAO}/ETS_{MAX}$) and complex I-supported respiration ($OXPHOS_{CI}/ETS_{MAX}$) were all (weakly) positively correlated with arterial concentrations of lipid peroxides (Table 37). Coupling efficiency was also negatively correlated with arterial plasma lipid peroxides ($r = 0.4$, $p = 0.02$).

Table 37. Correlations between respirometry variables and arterial plasma lipid peroxides

Skeletal muscle respiratory capacity	Correlation with arterial plasma lipid peroxides	
	Spearman's r	p value
$LEAK_{FAO}/ETS_{MAX}$	0.51	0.003
$OXPHOS_{FAO}/ETS_{MAX}$	0.54	0.0016
$OXPHOS_{CI}/ETS_{MAX}$	0.36	0.04
OXPHOS coupling efficiency	-0.41	0.02

5.8.14. Relationship between redox status in central and peripheral compartments

The relationship between redox profile in the central (plasma) compartment and that in skeletal muscle was also investigated. There was weak negative correlation between intramuscular [Met]/[MetSO] ratio and both arterial total free thiols ($r = - 0.37$; $p = 0.035$) and venous free thiols ($r = 0.- 42$, $p = 0.016$), shown in Figure 66. There was weak negative correlation between arterial lipid peroxides and the intramuscular [Met]/[MetSO] ratio ($r = - 0.37$; $p = 0.037$) shown in Figure 67. There was weak positive correlation between only the oxidised component of the methionine redox couple, MetSO, and total antioxidant capacity in both arterial ($r = 0.46$; $p = 0.0075$) and venous plasma ($r = 0.47$, $p = 0.0062$), shown in Figure 68. There were no significant relationships between any plasma indicators of NO metabolism and skeletal muscle redox status.

Figure 66. Association between skeletal muscle redox status and plasma free thiols

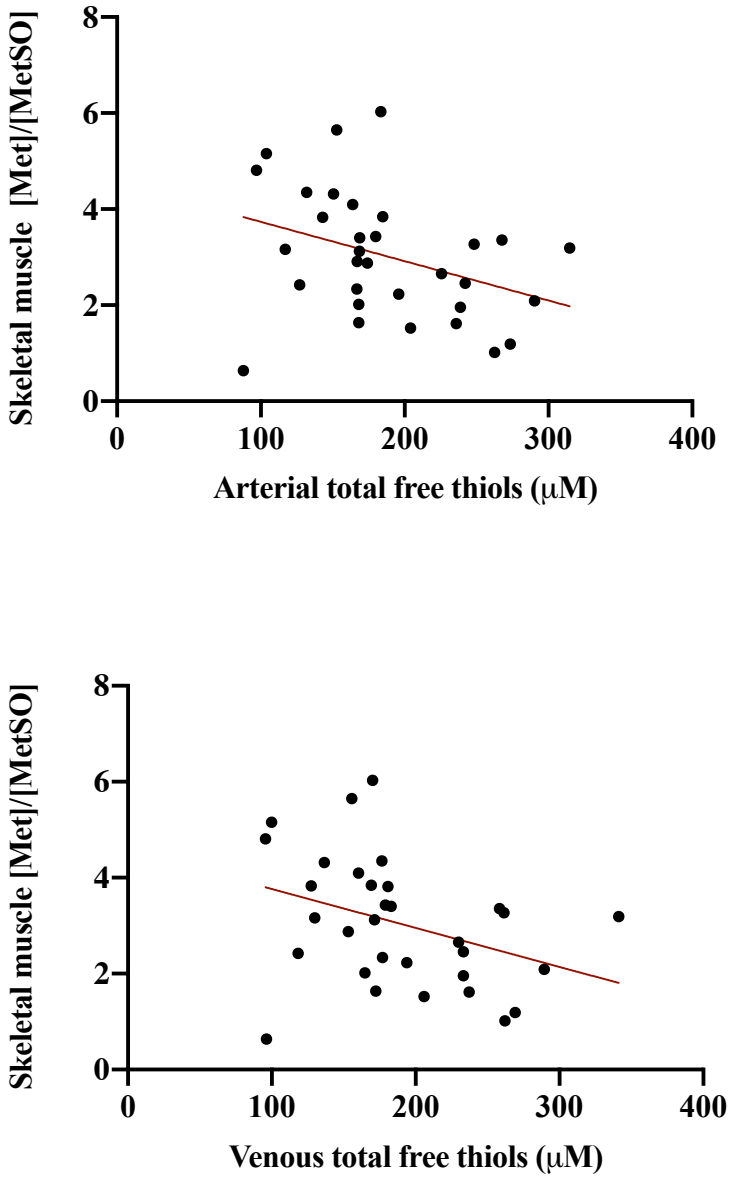

Measures at 48h and days 5-7; 33 pairs

Figure 67. Association between skeletal muscle redox status and arterial lipid peroxides

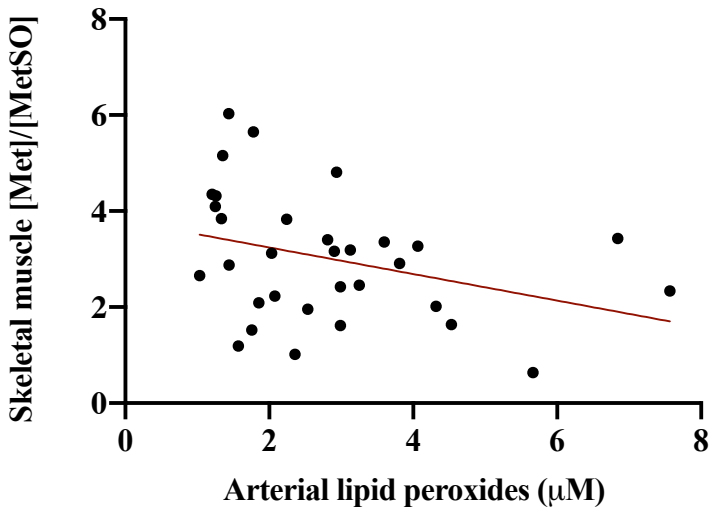

Measures at 48h and days 5-7; 33 pairs

Figure 68. Association between skeletal muscle redox status and plasma antioxidant capacity

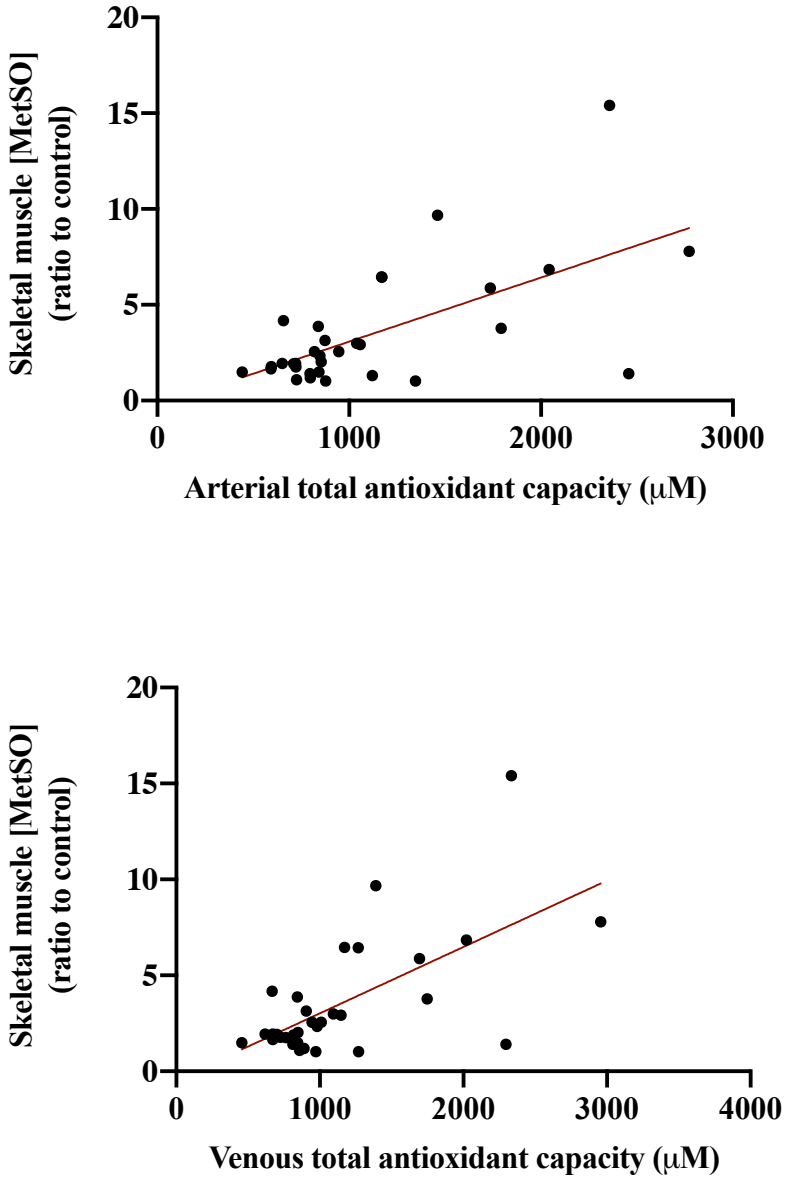

Measures at 48h and days 5-7; 33 pairs

5.9. Discussion

5.9.1. Summary of major findings

Redox differences between survivors and non survivors

Survivors and non survivors of critical illness demonstrated clearly different redox profiles, summarised in Table 38. The key features that distinguished non survivors from eventual survivors were greater levels of plasma lipid peroxidation, despite also exhibiting greater plasma total antioxidant capacity. Non survivors also exhibited greater free thiol concentrations per protein and greater levels of total nitroso species, despite no difference in plasma nitrite, nitrate or cGMP. These differences between survivors and non survivors were consistent in both the arterial and venous compartments. Differences between survivors and non-survivors were more marked in different components at particular timepoints. At < 48 hours, eventual non survivors had significantly greater total antioxidant capacity and levels of total nitroso species than survivors. By day 3-4, this difference was no longer significant, but non-survivors had greater concentrations of free thiols per protein and plasma lipid peroxides than survivors. At day 5-7, plasma lipid peroxides remained higher in the patients who died. Plasma lipid peroxides, total antioxidant capacity and total nitroso species represent potential biomarkers of death from critical illness. Total antioxidant capacity (as measured by the FRAP assay) >1138 μM predicted death with 100% specificity (52% sensitivity); while venous total nitroso species > 33.6 μM predicted death with 96% sensitivity (55% specificity).

Table 38. Summary of survivor plasma redox profile

Plasma redox profile	Survivor phenotype	Timepoint at which difference from non survivors detected
Antioxidant capacity	Lower	48 h
Total nitroso species	Lower	48 h
Free thiols per protein	Lower	Day 3-4
Lipid peroxides	Lower	Day 3-4 and 5-7

Plasma redox profile was associated with degree of organ failure and inflammation

Global organ dysfunction (as measured by the SOFA score) was associated with greater levels of plasma lipid peroxides, total antioxidant capacity and total nitroso species (as well as nitrate). These relationships were demonstrated in both arterial and venous plasma. Patients judged to have a greater severity of critical illness on admission to the ICU (as measured by the APACHE II score) also had greater plasma levels of lipid peroxides and total antioxidant capacity measured at the time of admission. Plasma lipid peroxides, total antioxidant capacity, total nitroso species and nitrate were also associated with the inspired concentration of oxygen. However, this relationship did not seem to be due to higher partial pressures of oxygen (PaO_2) in the plasma, as lipid peroxides and nitrate were actually inversely correlated with PaO_2. The fact that arterial antioxidant capacity was positively correlated with both F_IO_2 and lactate; but negatively correlated with PaO_2 may suggest that antioxidant capacity is related to tissue hypoxia rather than hyperoxia. On ICU, higher F_IO_2 is administered to hypoxaemic patients; who may also experience increased anaerobic lactate production. However, without the ability to measure actual tissue oxygenation, this relationship must be speculative. Only plasma free thiols were related to systemic markers of inflammation, with greater inflammation (CRP) associated with lower levels of free thiols in venous and arterial plasma.

Relationship between plasma redox profile and skeletal muscle phenotype

Redox status in muscle was related to redox status in plasma, with more reduced state in muscle (according to the ratios of reduced to oxidised methionine) associated with lower plasma levels of lipid peroxides and free thiols. Greater absolute levels of the oxidised version of methionine were also associated with higher plasma antioxidant capacity. Several aspects of the skeletal muscle bioenergetic profile, observed in Chapter 4 to be diminished in

the critically ill cohort; namely relative capacity for $LEAK_{FAO}$; $OXPHOS_{FAO}$ and $OXPHOS_{CI}$; were also noted to be greater in patients with higher levels of arterial lipid peroxides.

Depletion of total antioxidant capacity during critical illness

Total antioxidant capacity consistently decreased across all subjects from < 48 hours to Day 3-4, suggesting a universal depletion of antioxidant capacity following the immediate phase of critical illness.

Arterio-venous gradients in antioxidant capacity and nitrite during critical illness

Antioxidant capacity was marginally but consistently greater in the venous compartment, whilst, in contrast, nitrite was markedly higher in the arterial compared to paired venous samples.

5.9.2. Interpretation and significance

Plasma redox dysregulation is associated with organ failure and death from critical illness

In this study, death from critical illness was associated with greater plasma levels of lipid peroxidation during the first week of admission to the ICU. These findings were consistent with previous studies that have shown increased plasma lipid peroxidation during critical illness compared to healthy subjects, both in septic (251) and in non-septic patients (132), and in a manner that positively correlated with degree of organ dysfunction, and with higher concentrations associated with death (282). This study supports the finding that plasma lipid peroxidation is a general feature of critical illness, rather than sepsis alone (132).

In this study, total antioxidant capacity was also higher in in the non-survivors, and greater levels were associated with greater organ dysfunction (SOFA scores). While previous studies have demonstrated lower levels of specific antioxidants in critical illness compared to healthy controls (251), and lower total plasma antioxidant capacity in ICU patients with SIRS compared to those without, there has been some inconsistency depending upon the manner of assessing antioxidants and the time of measurement. For example, using a peroxyl trapping method, antioxidant capacity was found to be greater in patients with septic shock compared to controls, and greater in non-survivors of critical illness (290). The demonstration of decreasing total antioxidant capacity from < 48 hours to day 3-4 is consistent with a previous study in patients with septic shock (296).

The association between organ dysfunction and plasma levels of both lipid peroxides and antioxidant capacity is consistent with the existence of a dynamic redox system in human plasma, in which antioxidant capacity is acutely upregulated in response to oxidative stress. All subjects underwent a relative depletion in antioxidant capacity by day 3-4, suggesting that this compensation cannot be sustained indefinitely. The presence of higher levels of plasma lipid peroxides despite simultaneously higher plasma total antioxidant capacity in non survivors implies that, during the pathway towards multiple organ failure and death, redox regulation is stretched beyond its ability to compensate. The higher antioxidant capacity in non survivors was most marked at < 48 hours, and the higher lipid peroxidation was significant from day 3-4 to day 5-7, suggesting that this redox compensation was either exhausted or overwhelmed and outside the regulatory range in the patients who ultimately succumbed.

The availability of specific protein redox transducers increases during acute life-threatening stress

Free thiols represent important redox targets (for transducing redox changes, buffering oxidants and neutralising electrophiles). Demonstration of higher levels in non survivors implies a role for this redox-sensitive signalling system in the development of, or attempted compensation against organ failure and death. Higher free thiols in the non survivors may represent one component of the higher overall plasma antioxidant capacity that was observed in that group. Increases in plasma free thiols have been observed in humans exposed to acute stress. In healthy volunteers exposed to hypobaric hypoxia over 7 days, plasma free thiol availability increased, and was consistently higher than the corresponding sea level value at all stages during and after an exercise protocol (146). It was proposed that this increase may have been activated as an antioxidant buffer against increased ROS production. In a study of 160 patients with acute renal impairment, mortality was higher in patients with high serum protein thiols (304). The relationship between free thiols and mortality observed in these studies of humans during acute stress is the reverse of that observed in studies of chronic illness, in which lower levels of free thiols have been associated with increased mortality (176, 303). The chronicity of the stress appears to be a factor influencing the response of this redox pathway. Alternatively, it may reflect an impaired capacity of the free -SH group of albumin to scavenge reactive species, or an enhanced susceptibility to reduction elsewhere in the system.

Increased nitrosation products may reflect a dysregulated redox system operating outside its setpoint

Neither nitrite, nitrate nor cGMP differed significantly between survivors and non-survivors. Taking these species to represent stable oxidation products of NO, this suggests that NO

regulation is subject to tight controls even during extreme stress. Failure to detect significant differences in these values may imply that values outside the observed range are not compatible with life. Studies in mice have demonstrated this tight regulation of plasma nitrite and nitrate, with levels returning to within a narrow range after weeks of significant dietary nitrate supplementation (325). However, a role for the nitrosative signalling pathway during decompensated organ failure is implied by the markedly higher levels of nitroso species in the non-survivors and the positive correlation between total nitroso species and degree of organ dysfunction. Nitrosation reflects the interactions of NO with other ROS, and the resultant nitroso species are thought to modulate downstream targets, and potentially function as a buffer against excessive alterations in circulating NO. Greater activation of this pathway in the cohort who ultimately failed to survive again suggests a system stretched beyond its survivable range. The ability to detect such differences in nitroso species, in the absence of observable differences in nitrite and nitrate, highlights the importance of considering the downstream products to understand NO activity in critical illness. One explanation is that increased nitrosation may represent a pathway through which NO levels are buffered in plasma. Reducing NO during hypoxia causes cell death via increased protein carbonylation (326). Respiratory complexes, particularly complex I, are susceptible to inhibition by S-nitrosation (315). However, in the current study, at the first timepoint, when relative complex I capacity was lower in survivors; both arterial and venous RXNO were significantly lower in survivors compared to non survivors. Without the possibility to intervene, it is difficult to mechanistically distinguish between lower formation of nitroso species or increased consumption (turnover), via a putative dinitrosylation pathway.

Potential relationship between cellular modifications and plasma redox status

The fact that the specific respiratory capacities found to be lower in early critical illness compared to health (relative capacity for $LEAK_{FAO}$; $OXPHOS_{FAO}$ and $OXPHOS_{CI}$) were also related to the degree of arterial lipid peroxidation suggested the possibility of a shared mechanism, although it was not possible to map it out from these data. This finding would seem to be consistent with the notion that reactive aldehydes, the major breakdown products of lipid peroxides detected by the TBARS assay (and chemically electrophiles), are potent modulators of mitochondrial respiratory chain function (327, 328) by virtue of their reactivity with nucleophilic thiol groups (329).

Respiratory complexes are known to be producers of ROS, but also subject to inhibition by ROS. One possible explanation for the correlation could be that selective downregulation of complex I at < 48 h reduces its release of ROS, and thus survivors, with lower complex I capacities, were exposed to less oxidative stress at the later timepoints (reflected in lower levels of arterial lipid peroxides at the later timepoints). Redox status in muscle was indeed related to redox status in plasma, with more oxidised state in muscle associated with greater plasma levels of lipid peroxides, and also free thiols. An alternative explanation for the relationship could be that respiratory complexes were subject to inhibition by ROS. At < 48 h, the greater antioxidant capacity in non survivors may have initially conferred protection against inhibition of complex I, but once this excess antioxidant capacity was exhausted at day 3-4, uncompensated oxidation resulted in the observed failure of these capacities to recover, or further decline in non survivors along with a rise in arterial lipid peroxides above survivors at the later timepoints. Attempting to understand the potential interactions between compartments is hindered by the observational nature of the data, potential for confounding, and the fact that redox alterations in one compartment may result in compensatory changes in another (93). Plasma redox changes may reflect global redox changes across all cellular and

extracellular compartments or represent a compensation for localised redox changes elsewhere in the body.

Depletion of total antioxidant capacity after 48 hours of critical illness

Of all the redox components measured, only plasma total antioxidant capacity changed in a consistent manner from early (< 48 hours) to later (day 3-4) stages of critical illness, undergoing a significant decrease in all but two subjects. This decrease occurred in both venous and arterial plasma, suggesting that a relative depletion of plasma antioxidant capacity follows the early phase of critical illness. As a result of the complexity of redox interactions, little is known about their kinetics, particularly in humans with life-threatening organ dysfunction. Critical illness has been proposed as two phases: the acute phase, characterised by an inflammatory response, and a chronic phase, associated with downregulation of the immune system (330). Compared to the first timepoint, at day 3-4 the subjects had similar SOFA scores and oxygen requirement, but the most marked difference was the lower vasopressor requirement, which may reflect the lower doses of propofol-sedation administered at this timepoint, and partial resolution of their vasoplegic state at day 3-4. In the many studies investigating the effectiveness of antioxidant supplementation in critical illness, the timing of introduction may thus be one feature influencing the lack of benefit.

Physiological significance of arterio-venous gradients in critical illness

In this cohort, nitrite was consistently greater in arterial than venous plasma. This gradient is consistent with higher shear-stress induced NO release on the arterial than the venous side of the cardiovascular system and the A-V gradient previous reported for nitrite (331, 332). This arterio-venous gradient was not observed for nitrate, but nitrate has a high background

concentration and a relatively long-half-life, and together these factors may contribute to gradients not being detected. In a study of 24 healthy volunteers, it was demonstrated that alterations in nitrite, not nitrate, reflected acute changes in endothelial NOS activity (317). However, this study did not demonstrate arterio-venous differences in nitrate or nitrate. The arterio-venous gradient for the downstream markers of NO signalling in plasma, namely cGMP and total nitroso species, was in the opposite direction to that for nitrite, being consistently were greater in venous than arterial plasma. This suggests that although release of NO occurs in the arterial vasculature, considerable efflux of downstream products, such as cGMP and cellular nitroso species takes place at the tissue level, manifesting as higher levels in venous blood. This study demonstrates that different aspects of the plasma reactive species interactome, including NO, may differ between arterial and venous compartments during critical illness. The functional significance of these arterio-venous differences is not certain, but they reflect processes differentially affecting the arterial and venous compartments. Differences between the two compartments must be taken into consideration when assessing plasma redox status, and each compartment must be considered individually. The plasma concentration of each redox measure will depend on its rate of production and clearance, as well as interaction with other ROS, RNS, thiols and other constituents of the reactive species interactome.

5.9.3. Study strengths

Simultaneous assessment of multiple components of the reactive species interactome in plasma, alongside measures of redox status and bioenergetic profile in skeletal muscle, provided insight into the complexity of redox alterations during critical illness. The overall consistency in observations in the arterial and venous compartments supported the validity of the reported data. The ability to detect marked differences between survivors and non-

survivors, which were consistent across both paired venous and arterial samples, despite the heterogeneity of the cohort (outlined in general in section 2.5.10, and with reference to specific factors that may influence redox status, in section 5.9.4 below), suggests that these differences may reflect true alterations in redox physiology that are relevant to organ function and patients' ability to survive. It is not possible to say whether the observed differences in redox profile reflect a greater degree of imposed pathological stress or lower innate resilience in the non-survivors. However, the fact that they are distinguishable despite the background noise in this heterogenous cohort suggest they could represent future important plasma biomarkers for failure to cope with life-threatening stress. From assessing redox profile at multiple timepoints, evidence for time-dependent differences between survivors and non survivors emerged, adding to the complexity of what is known about redox signalling in critical illness.

5.9.4. Study limitations

Heterogeneity of the critically ill cohort

This was an observational study intended to characterise the human plasma reactive species interactome in response to life-threatening stress and multiple organ failure. The cohort under investigation was highly heterogenous, in terms of age, co-morbidity, medications, prior nutrition, as well as their primary pathologies and degree of organ dysfunction on admission. All of these factors are likely to influence our capability to accurately capture metabolic readouts of the reactive species interactome. For example, lipid peroxidation is not specific to critical illness and may be affected by comorbid conditions, diet, and lifestyle behaviours. Increased blood MDA levels occur in smokers (279) and patients with diabetes mellitus and hypertriglyceridemia (333) (334). Data related to smoking history was not specifically collected from participants, and only 4 of the 21 critically ill cohort had a history

of type II diabetes. There was no significant difference between arterial or venous TBARS concentrations in the diabetic and non diabetic critically ill patients ($p > 0.05$). TBARS has previously been shown to demonstrate age dependence (in females rather than males); but in this work, there was no significant differences in the TBARS concentrations in males and females ($p > 0.2$), and no significant correlation was demonstrated between age and either arterial or venous plasma TBARS concentration overall ($p = 0.7$ and 0.2 for venous and arterial plasma respectively); or in males ($p = 0.37$ and 0.28 respectively) or females ($p > 0.99$ and 0.85 respectively). Disease severity, organ function and intensive care medications and interventions also varied for each patient during the timecourse of the study. It is not possible to ascertain whether the universal decrease in total antioxidant capacity within subjects from the first to the second timepoint was related to any of these factors, or whether it truly reflected a time-dependent depletion of antioxidant capacity.

Incomplete data collection

This study was limited by incomplete data collection for recruited subjects at all three planned timepoints. This resulted from the high acute mortality rate, characteristic of the patients under investigation, as well as an unexpected withdrawal of recovering subjects before completion of the study and the occasional lack of pre-existing indwelling arterial and venous catheters. This resulted in only 12 of the original subjects having complete data sets at all three timepoints for both arterial and venous plasma. It was decided to use all available data to gain the maximum amount of information from this cohort of extremely sick individuals, but there was an increased risk of type II error. Limited inferences can be drawn regarding the differences observed between timepoints during this study.

Ex vivo assays of plasma redox status

All of the assays measured plasma redox status *ex vivo* and were therefore limited by the possibility of auto-oxidation during sample extraction, centrifugation and assay processing, and potential interaction between the redox systems of the plasma and blood cells prior to and during centrifugation. All sample extraction and processing were carried out in a uniform manner, according to the same time frame, in an attempt to keep the effect of these confounders as uniform as possible. Plasma redox status cannot distinguish between events in different cellular compartments. The plasma compartment is also subject to specific redox changes related to the immune response, the influence of erythrocytes (which have a much higher antioxidant capacity than plasma) as a redox scrubber (291), and the influence of infusions containing redox active substances (such as propofol or parental nutrition) administered directly into this compartment.

Assay-specific limitations

For the TBARS, FRAP and free thiols and nitroso species assays, groups of compounds react with the reagent, to produce the compound measured by the colorimetric assay. The measured end-product reflected the reactions of multiple different compounds. The alternative to this approach is to use specific measures of individual components (such as nitrate and nitrite), which are characteristic for one read-out only, but may be affected by factors other than oxidative stress, such as dietary intake (nitrate). A deliberate decision was made to use these less specific measures, to cast a wide net to detect potentially important signals, that could subsequently inform a more specific and targeted approach in later investigations.

FRAP assay

The FRAP assay measures the reduction of Fe^{3+}, which may be mediated by a number of different plasma antioxidants (for example, urate, ascorbate, glutathione or polyphenolic antioxidants), some of which may reduce Fe^{3+} better than others. Some of the individual compounds within this group are known or suspected, but the test is non-specific, and the relative contribution of each compound is not known. Some compounds within the group may be increasing or decreasing, and different antioxidants may reduce Fe^{3+} via different mechanisms. Alternative assays for measuring total antioxidant capacity have been extensively reviewed recently (335), and include total radical-trapping parameter (TRAP), enhanced chemiluminescence or by measurement of the antioxidant-mediated quenching of the absorbance of a radical cation(336). However, for the reasons stated above, the FRAP assay was selected precisely because it is non-specific and sensitive; any compound with suitable redox potential will drive the reaction. Importantly, however, the FRAP assay is known not to react with thiols, thus the information it offers is complementary to that of the other measurements.

TBARS assay

Although the TBARS assay is widely accepted as an index of oxidative stress, this method does not specifically measure lipid peroxidation. Not all TBARS, including MDA, are derived from lipid peroxidation, and the presence of other aldehydes and non lipids may confound the results (337). Also, as it measures peroxidised lipids, the TBARS assay will detect changes in both oxidative stress and lipid metabolism, which were shown in Chapter 4 to be altered in this cohort. Use of high-performance liquid chromatography to isolate MDA would improve specificity beyond the spectrophotometric measurements used in this study (338). Despite these limitations, the TBARS assay was used because it was an inexpensive and simple method, and, as such still represents one of the most widely used assays for

estimating lipid peroxidation in clinical contexts, with associations between patient plasma TBARS concentration and severity of various diseases reported, including cardiovascular disease (339, 340); neurodegenerative disease (341) and sepsis (342). It is possible that in conditions associated with increased oxidative stress, such as critical illness, the non-specific background reactions between thiobarbituric acid and products not derived from lipid peroxidation, make relatively less contribution to the overall TBARS concentration.

Variability of data

The variation between the triplicate repeats in the 8-isoprostanes $PG_{F2\alpha}$ assay was greater than desirable, with co-efficient of variation between repeats as high as 56% in one case. This may contribute to the failure of this test of lipid peroxidation to detect the same differences in survivors and non survivors as the TBARS assay.

Limitation of statistical techniques

As discussed in Chapter 4, the potential for type I error (the probability of detecting a difference between the groups when it does not exist) increases with the number of comparisons using a given data set. As discussed in that section, multiplicity was not corrected for, because the priority was to optimise sensitivity to detect potential differences in phenotype, using multiple complementary approaches, at the cost of increased type I error. Rather than being considered definitive, these data should be considered as potential signal, requiring validation in future work. However, the data also demonstrated internal consistency, through the strong agreement between concomitant arterial and venous values, and their respective relationships with relevant clinical variables. As previously discussed, the risk of type II error (the probability of failing to detect a difference between the two groups when it does exist) increases when the study sample size is small; and fewer subjects

were recruited than planned. Despite this, significant differences between the survivors and non survivors were detected in several variables; even at the third timepoint, when subject number had decreased, implying that for these variables, power was adequate. Simple comparisons of different components of redox status in an observational study fails to reveal the complexity of redox signalling. Relatively small or statistically insignificant changes in the steady-state concentration of biomarkers and signalling molecules may be associated with biological significant changes in physiology, in particular when regulating circuits are acting at their limits (93). Statistically significant changes from baseline may indicate that the system is operating at a different setpoint, which may be well within the regulatory range.

5.9.5. Unanswered questions and future work

The aim of this prospective longitudinal study was to determine whether plasma redox status, defined by a selection of measurable components could constitute a measurable "signature" of deterioration and death from critical illness. This chapter provided evidence that a plasma profile of increased lipid peroxidation, antioxidant capacity and total nitroso species was a hallmark for failure to compensate for acute life-threatening stress. High plasma concentrations of lipid peroxides, total antioxidant capacity and total nitroso species were predictors of poor outcome, but these potential biomarkers require validation in a larger cohort. It is possible that they may provide greater specificity and sensitivity in combination. Undertaking larger studies, which focus on specific subsets of critically ill patients (for example, sepsis, trauma, liver failure, cardiogenic shock), may allow us to determine whether the non survivor profile observed in this study truly represents universal features of non survival in critical illness.

This observational study also cannot provide information on whether the observed differences in survivor and non survivor redox status represent a cause or effect of the observed clinical phenotype. It is not yet clear to what extent the observed plasma measures reflect (1) redox status in tissues, (2) compensation of the plasma compartment in response to redox changes in a cellular compartment, (3) adaptive signalling, (4) harmful consequences of pathological perturbation, either from the disease or its treatment. Describing mechanisms in critically unwell human patients involving this highly complex network will continue to pose a challenge (343). Discriminating between redox signalling and indiscriminate oxidative stress may ultimately depend on the ability to measure redox changes *in vivo*, ideally in response to a pre-determined, controlled, dynamic stress. Greater understanding of the interaction between cellular and plasma compartments will require synchronous measures spanning subcellular, cellular and plasma compartments.

The first step may be to map, with greater granularity, the temporal changes during deterioration into critical illness. This is generally difficult to predict, but one possibility would be study a cohort of high risk surgical patients (elderly, with multiple co-morbidities, undergoing major surgery), with a significant risk of post-operative organ dysfunction. By undertaking frequent measures of plasma redox status, before, during and after their surgical insult, and possible ICU stay, the time course of redox changes and how they herald or contribute to the development of critical illness may be better understood. Ideally, plasma measures would be combined with contemporaneous measures of redox status in other tissues, such as muscle, skin or blood cells.

5.10. Conclusions

Specific plasma redox components during the first week of critical illness are associated with organ dysfunction and can predict mortality. Higher levels of lipid peroxidation products despite greater antioxidant capacity in non survivors suggested that loss of redox regulation may be related to poor outcome. Redox status in muscle was related to redox status in plasma, with more oxidised state in muscle associated with greater plasma levels of lipid peroxides, and also free thiols. There was also evidence for a relationship between the bioenergetic modifications in skeletal muscle which distinguish critical illness from health, and levels of arterial lipid peroxidation products. Plasma redox status is an accessible and relevant compartment for studying redox signalling, but understanding mechanisms requires tools for *in vivo* monitoring, of plasma, cellular and subcellular redox status.

6. Chapter 6. The peripheral microcirculation in critical illness

6.1. Introduction

The modifications to oxidative phosphorylation machinery and metabolic pathways in critically ill patients described in this thesis were consistent with a co-ordinated cellular response to hypoxia (52). However, they occurred in the context of normal systemic oxygenation indices (SpO_2, PaO_2 and CaO_2), which had been corrected by supplementation of inspired oxygen concentrations and mechanical ventilation. Nor was any relationship found between the critical illness cellular phenotype and systemic haemodynamic measures, such as mean arterial pressure, which are targeted in an effort to maintain end-organ perfusion, through intravascular volume expansion and administration of vasopressors and inotropes. The observed bioenergetic adjustments thus do not appear to relate to the mass flow of oxygen within the major vessels of the circulatory system. The question remains as to whether they could still represent a response to critical limitation of oxygen provision to the tissues. Increased skeletal muscle levels of HIF-1α have been demonstrated in a comparable heterogenous cohort of critically ill patients during the first week of ICU admission, in the presence of normal arterial oxygenation indices (87). As previously outlined in Chapter 1, systemic measurements give no indication of specific blood flow or oxygen delivery to individual organs, which is instead governed by the microcirculation. The microcirculation refers to the smallest vessels of the cardiovascular system (less than 100 μM in diameter, comprising arterioles, capillaries and venules), which are ultimately responsible for the transfer of oxygen to the cells (344). Factors known to influence microcirculatory blood flow were discussed in Chapter 1 (section 1.3.2).

The microcirculation in critical illness

In critical illness, it has been shown that even in the presence of normal or elevated systemic blood flow, disturbances to capillary blood flow can result in inadequate oxygen availability to several tissues (345). Using direct visualisation of the sublingual microcirculation, total vessel density and proportion of perfused vessels has consistently been shown to be lower in critically ill patients with sepsis, compared to healthy controls, with the reduction more marked in non survivors (47, 346). Together, these changes may reduce oxygen availability to some cells, by increasing the diffusion distance for oxygen transfer. The heterogeneity of capillary blood flow is also higher in patients with septic shock; capillaries with stopped or intermittent flow adjacent to well-perfused capillaries (218), causing an uneven distribution of oxygen supply (microvascular shunting) (49). The proportion of perfused small vessels is a stronger predictor of outcome than traditional haemodynamic variables in critically ill patients with sepsis (347). Lower perfused capillary density has also been associated with the development of multiple organ failure and death following acute myocardial infarction (44). Microcirculatory changes are not related to systemic haemodynamics, with reduced perfusion and increased flow heterogeneity shown to be similar in patients with normodynamic and hyperdynamic septic shock, compared to health controls (218). In fact, the current approach to increase mean arterial pressure using vasopressors such as noradrenaline have been shown to decrease perfused capillary density in patients with septic shock (121). Microcirculatory modifications appear to alter with time in critical illness. In a study of patients with septic shock, survivors and non survivors had similar small vessel perfusion at the onset of shock; but this persisted in non survivors, but recovered in survivors over time (348). Survivors from resuscitated septic shock also demonstrated greater microcirculatory vessel density and perfused vessel density than non survivors at 72 hours (349). A similar time course was demonstrated in children with septic shock: survivors increased their perfused capillary

density between day 1 and 2, whilst non survivors did not change and were significantly lower than survivors by day 2 and 3 (350).

Another particular component of microcirculatory function thought to be relevant for survival in critical illness, is the ability to respond appropriately to an ischaemic challenge, through rapid endothelial-mediated vasodilation, in response to vasoactive mediators released during a phase of tissue hypoxia and lack of nutrient supply. Endothelial dysfunction, including diminished sensitivity to vasoconstrictors and vasodilators, has been proposed as one potential mechanism underpinning the development of microcirculatory dysfunction in critical illness. Microvascular reactivity, the rapidity with which microcirculatory vessels dilate following an ischaemic challenge can be assessed using near-infrared spectroscopy with a vascular occlusion test (outlined in section 3.7.5). Microvascular reactivity is blunted in critically ill patients compared to healthy volunteers (178, 192), and this impairment is greater in patients with more severe organ dysfunction (351). Microvascular reactivity has also been shown to be lower in patients with greater severity of chronic heart failure and sepsis and, implying a common impairment of endothelial function in these conditions which can lead to critical illness (193). Another indicator of the ability of the microcirculation to respond to an ischaemic stimulus is called “vascular reserve”. It refers to the hyperaemia following an ischaemic challenge, over and above baseline, produced by vasoactive mediators released during a phase of tissue ischaemia. The reactive hyperaemia response has also been shown to be blunted in critically ill patients with sepsis (194).

There is limited understanding of how the specific microcirculatory modifications observed during critical illness may relate to the alterations described in cellular bioenergetics and redox status. The potential relationship between microcirculatory function and these

fundamental cellular survival functions, has not yet been investigated in human critical illness. In a rat model of sepsis, microcirculatory dysfunction, as defined by decreased microvascular reactivity and perfused vessel density and increased flow heterogeneity, was associated with elevated markers of oxidative stress and damage to the glycocalyx (352). In a murine sepsis model, administration of EPO, a downstream target of HIF, was shown to increase both perfused capillary density and bioenergetics (judged by a decrease in NADH fluorescence, indicating increased pyruvate metabolism and oxidative phosphorylation) in skeletal muscle (353).

6.2. Aims

The primary aim of this study was to determine if there was a survival phenotype in critically ill patients involving changes in skeletal muscle oxygenation and functional aspects of the microcirculation. The secondary aims were to investigate the putative relationship between microcirculatory function and (1) clinical indicators of organ failure, (2) global measures of oxygenation or haemodynamics, (3) the previously described cellular modifications in skeletal muscle during acute organ failure and (4) the previously described redox profile in patients with organ failure.

6.3. Hypothesis

I hypothesised that non survivors would exhibit lower tissue oxygenation and greater microcirculatory dysfunction, compared to survivors. I predicted that skeletal muscle microcirculatory dysfunction would be associated with global organ dysfunction, as well as reduced capacity for mitochondrial oxidative phosphorylation. A second hypothesis was that the mitochondrial modifications observed in critical illness (reduced respiratory capacity for $LEAK_{FAO}$, $OXPHOS_{FAO}$, $OXPHOS_{CI}$), which are common to the cellular hypoxia response,

will be associated with microcirculatory impairment and reduced tissue oxygenation. Finally, I hypothesised that microcirculatory dysfunction would also be associated with systemic redox dysregulation in the plasma compartment, indicated by levels of plasma lipid peroxides and total antioxidant capacity, or to circulating levels of the vasoactive mediator, NO.

6.4. Objectives

1. Quantify relevant aspects of skeletal muscle microcirculatory function in critically ill patients at three timepoints of critical illness and determine if differences existed between eventual survivors and non survivors.

3. Determine if aspects of microcirculatory dysfunction were associated with contemporaneous measures of organ dysfunction, the plasma reactive species interactome, or the bioenergetic profile in skeletal muscle.

6.5. Methods

6.5.1. Study design and subject selection

The study was part of the TIMELORD study, the conduct of which is outlined in detail in Chapter 2. This component of the study was a prospective longitudinal cohort study of skeletal muscle microcirculatory function and oxygenation during the first week of critical illness. Study design, ethical approval, screening, consent and enrolment were described in full in section 2.5.2.

6.5.2. Study specific measures

Following enrolment, all subjects underwent testing within 48 hours of admission to the ICU. Where possible, testing was repeated at day 3-4 and again at day 5-7. Assessment of skeletal muscle oxygenation and microcirculatory function was assessed in the thenar eminence using near infrared spectroscopy and a vascular occlusion test (NIRS-VOT), the principles of which

are outlined in section 3.7.5. The protocol, described in section 3.7.9, yielded measures for: skeletal muscle oxygenation (StO_2) at baseline, as well as the minimum, peak and recovery StO_2 measured during the VOT). It also provided values for the oxygen consumption rate of the tissue (StO_2 downslope); microvascular reactivity (StO_2 upslope); and vascular reserve (hyperaemia area and StO_2 overshoot). These simple summary statistics derived using the NIRS-VOT were chosen as they have been validated in critically ill patients, and clinically detectable differences in human volunteers in response to hypobaric hypoxia have been demonstrated by our own research group.

6.5.3. Collection of clinical, skeletal muscle bioenergetic and plasma redox data

Collection of clinical data from the critically ill cohort at three timepoints is outlined in section 2.5.6. Contemporaneous measures of skeletal muscle bioenergetic and redox profile were carried out at the first and final timepoint, as outlined in section , and assessment of plasma redox status was carried out at all three timepoints, as described in section 5.7.3.

6.5.4. Data analysis

Data analysis was carried out as outlined in section 2.5.7. Movement artefact in an awake patient led to exclusion of one value for StO_2 upslope; and software was unable to calculate the reactive hyperaemia area in 3 cases.

6.6. Results

6.6.1. Subject characteristics

The subjects are described in Chapter 2, section 2.5.8. The presenting diagnoses of the critically ill cohort are outlined in Table 4; the clinical characteristics of the cohort at the

three timepoints are summarised in Table 5. Baseline characteristics of survivors and non survivors are summarised in Table 6.

6.6.2. Changes in microcirculatory function during the first week of critical illness

As the distributions for the NIRS-VOT measurements in organ failure patients at < 48h, day 3-4 and day 5-7 were normally distributed, the mean (SD) values for these groups are shown in Table 39. During the first week of critical illness, there was no significant change in baseline, minimum, peak or recovery StO_2 values during the VOT, or StO_2 upslope or downslope. The overshoot (peak minus baseline StO_2) and hyperaemia recovery area was also similar at all three timepoints.

Table 39. NIRS-VOT values from thenar eminence skeletal muscle during the first week of critical illness

NIRS-VOT variable	< 48 h (n = 21)	Day 3-4 (n = 16)	Day 5-7 (n = 13)	p value
Baseline StO_2 (%)	83.4 (11.2)	81.5 (7.9)	82.3 (5.8)	0.57
Minimum StO_2 (%)	52.1 (21.0)	52.8 (11.9)	50.8 (11.2)	0.89
Peak StO_2 (%)	89.4 (8.3)	88.1 (6.2)	90.3 (6.7)	0.54
Recovery StO_2 (%)	84.4 (10.3)	80.6 (7.4)	83.5 (5.5)	0.19
Overshoot (Peak-Baseline StO_2) (%)	6.0 (4.5)	7.5 (4.8)	7.3 (3.8)	0.73
StO_2 downslope (%/min)	8.9 (3.9)	9.5 (2.2)	10.5 (3.8)	0.48
StO_2 upslope (%/sec)	2.0 (1.3)	2.8 (1.6)	2.7 (0.8)	0.12
Hyperaemia recovery area (%.min)	7.6 (5.9)	8.8 (4.5)	7.3 (4.9)	0.37

Mean (SD); different timepoints of critical illness compared using a mixed effects model.

6.6.3. NIRS-VOT indices in survivors and non survivors

Baseline, minimum and peak and recovery StO_2 values in survivors and non survivors at each of the three timepoints are displayed in Figure 69. The distributions of the survivor and non survivor cohorts were not normally distributed and therefore described using median (IQR). At the first timepoint, there was a consistent pattern of higher StO_2 in survivors, when measured at rest, after three minutes of complete arteriovenous occlusion, as well as at the peak and resolution of hyperaemic recovery. These differences did not meet the criteria for statistical significance. This pattern of differentiation was lost at day 3-4 and by day 5-7, survivors demonstrated significantly *lower* minimum StO_2 (median 45% IQR 36.5-51) compared to non survivors (median 54%, IQR 53-60; p = 0.023).

Microcirculatory indices at all three timepoints are compared in survivors and non survivors in Figure 70. There was a trend towards lower StO_2 upslope in non survivors at day 5-7, (median 2.22%/sec (IQR 1.6-3.27) compared to survivors (3.43 %/sec, IQR 2.76-3.6, p = 0.07), but no difference between the groups in terms of downslope, hyperaemia area or overshoot (peak – baseline StO_2).

During the first week of organ failure, trajectory of StO_2 values diverged in survivors and non survivors (Figure 71), although these differences did not meet the criteria for statistical significance. In non survivors, baseline, minimum, peak and recovery StO_2 all increased after 48 h; whilst in survivors, StO_2 values generally decreased after 48 h, particularly at day 3-4. Different trajectories in microcirculatory indices were also observed in survivors and non survivors; though again differences did not meet the criteria for statistical significance (Figure 72). In survivors, there was a trend towards increasing StO_2 upslope from 48 h to day 5-7 (median increase 0.45 %/sec, IQR 0.32-1.14, p = 0.06), and in non-survivors there

was a sharper increase by day 3-4 (median 0.9%/sec, IQR 0.06-2.73, p =0.07), which then declined by day 5-7. Similarly, hyperaemia area and overshoot tended to decrease in non survivors by the final timepoint (median decrease in hyperaemia area 5.33 %.min, IQR 0.15-7.7, p = 0.09); whilst in survivors they were maintained or increased.

Figure 69. Tissue oxygenation values measured using NIRS-VOT in survivors and non survivors

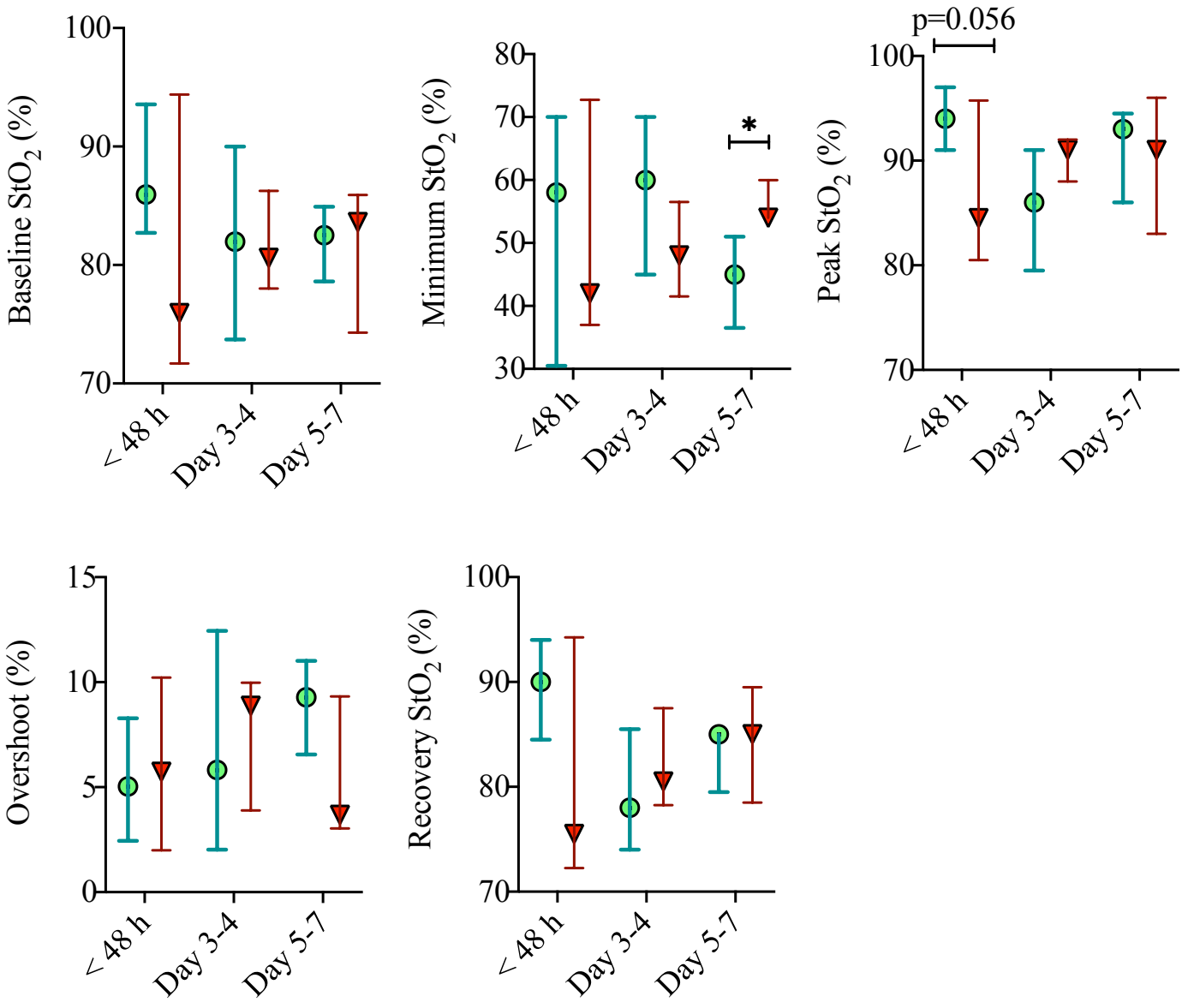

StO_2 values measured during NIRS-VOT protocol: baseline, minimum, peak and recovery. Survivors shown as green circles (n = 9 at < 48 h, 7 at day 3-4 and 6 at day 5-7); non survivors as red triangles (n=12 at < 48 h, 9 at day 3-4 and 7 at day 5-7). Median (IQR); * $p < 0.05$, survivors *vs* non survivors.

Figure 70. Microcirculatory indices in survivors and non survivors

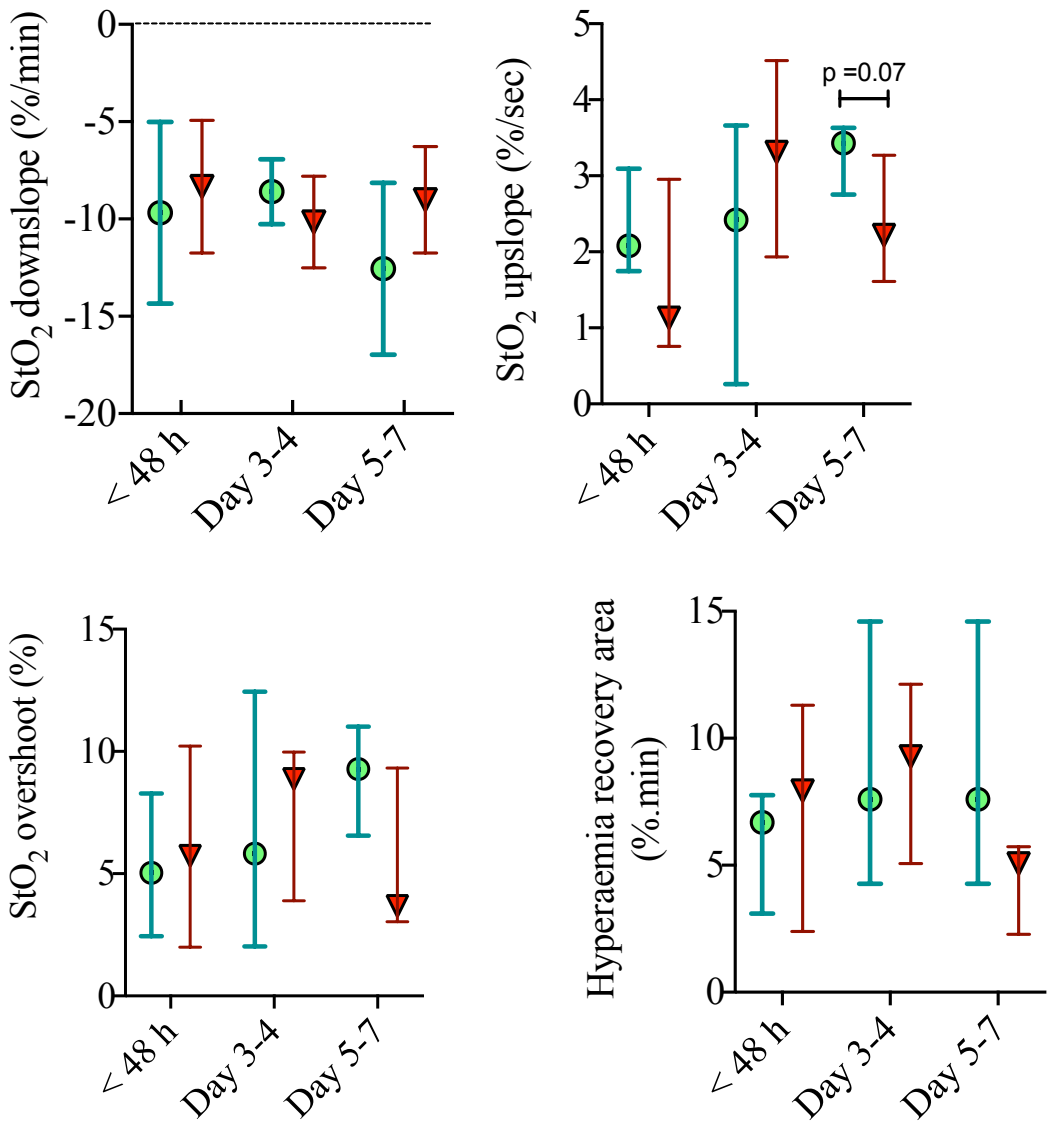

Derived microcirculatory variables using NIRS-VOT protocol: StO_2 downslope, upslope, overshoot and hyperaemia recovery area. Survivors shown as green circles (n = 9 at < 48 h, 7 at day 3-4 and 6 at day 5-7); non survivors as red triangles (n=12 at < 48 h, 9 at day 3-4 and 7 at day 5-7). Median (IQR); *p < 0.05, survivors *vs* non survivors.

Figure 71. Trajectory of StO_2 values in survivors and non survivors

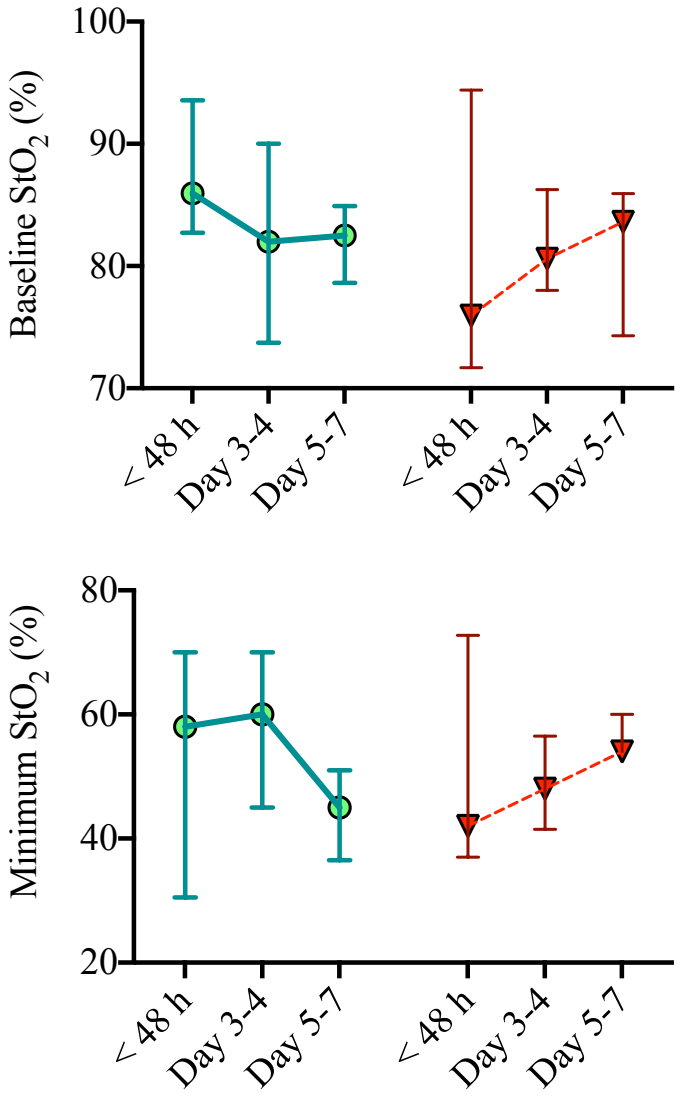

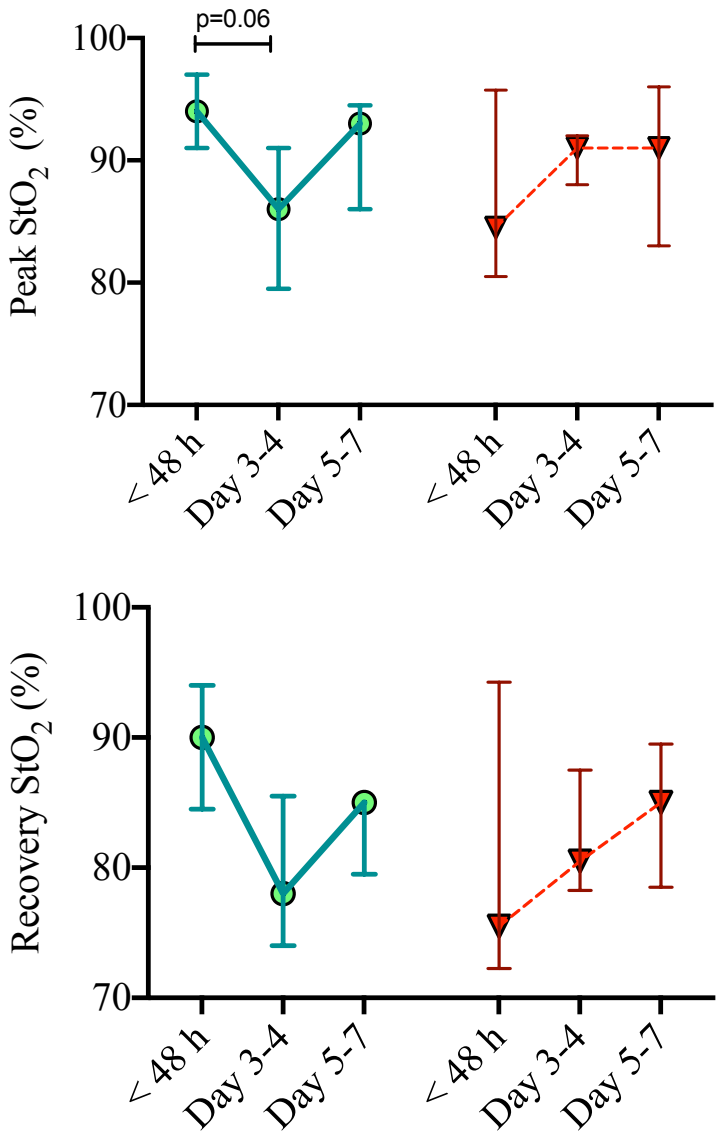

Trajectories of StO_2 values measured during NIRS-VOT protocol: baseline, minimum, peak and recovery. Survivors shown as green circles (n = 9 at < 48 h, 7 at day 3-4 and 6 at day 5-7); non survivors as red triangles (n=12 at < 48 h, 9 at day 3-4 and 7 at day 5-7). Median (IQR); * $p < 0.05$, survivors *vs* non survivors.

Figure 72. Trajectory of microcirculatory indices in survivors and non survivors

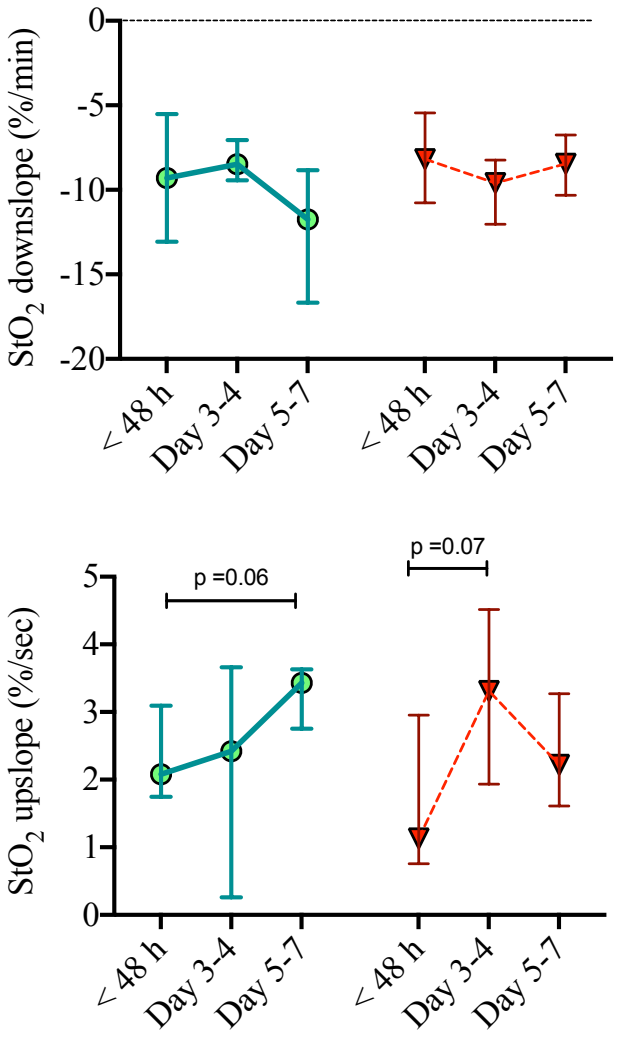

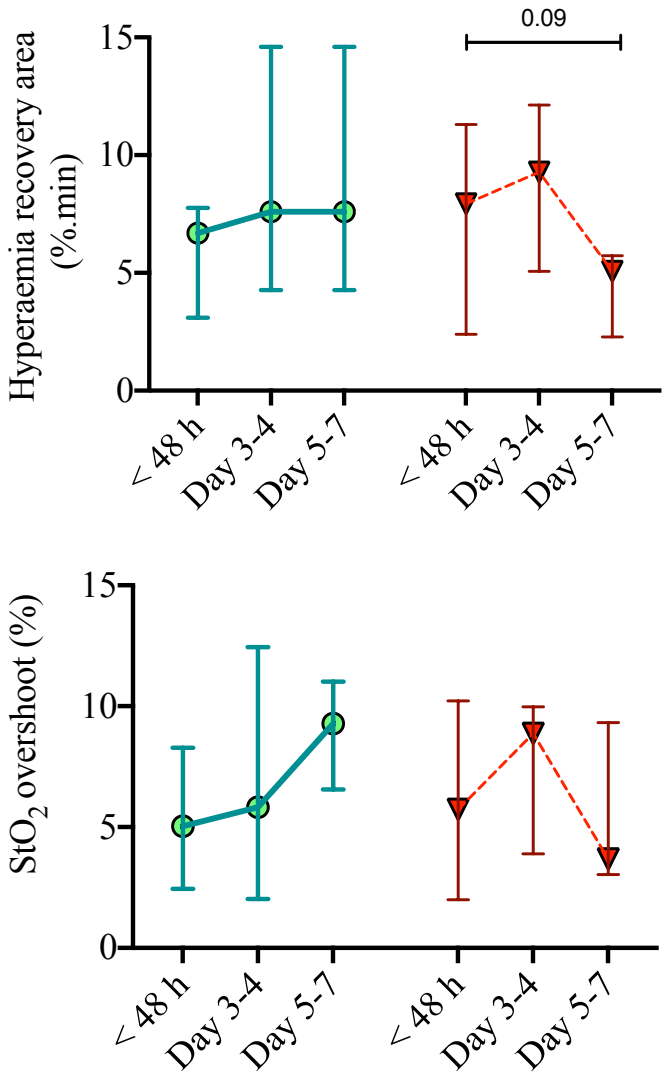

Trajectories of derived microcirculatory variables using NIRS-VOT protocol: StO_2 downslope, upslope, overshoot and hyperaemia recovery area. Survivors shown as green circles (n = 9 at < 48 h, 7 at day 3-4 and 6 at day 5-7); non survivors as red triangles (n=12 at < 48 h, 9 at day 3-4 and 7 at day 5-7). Median (IQR); *p < 0.05, survivors *vs* non survivors.

6.6.4. Correlations with clinical variables

There was moderate negative association between the StO_2 upslope and degree of organ dysfunction, whether determined by APACHE II score on admission ($r = -0.68$, $p = 0.0007$) or SOFA score at all three timepoints ($r = -0.42$, $p = 0.0024$) as shown in Figure 73. StO_2 upslope was also negatively correlated with vasopressor dose ($r= -0.38$, $p =0.007$); Figure 74. Organ dysfunction (as measured by the SOFA score at all three timepoints) as also negatively correlated with hyperaemia recovery area ($r = -0.37$, $p =0.012$), as was another putative marker of vascular reserve, StO_2 overshoot ($r = -0.40$, $p = 0.0067$), demonstrated in Figure 75. There was no relationship between thenar muscle StO_2 or microcirculatory indices (StO_2 upslope, downslope, hyperaemia area or overshoot) and systemic measures of oxygenation, such as SpO_2, PaO_2 or CaO_2, or mean arterial pressure or arterial lactate concentration. There was no relationship between any NIRS-VOT measurement and traditional markers of inflammatory state (such as white cell count, or C-reactive protein concentration).

Figure 73. Correlations between StO_2 upslope and organ dysfunction

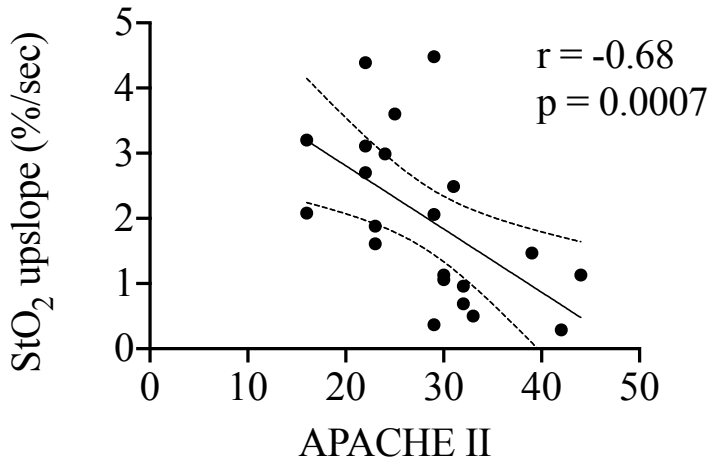

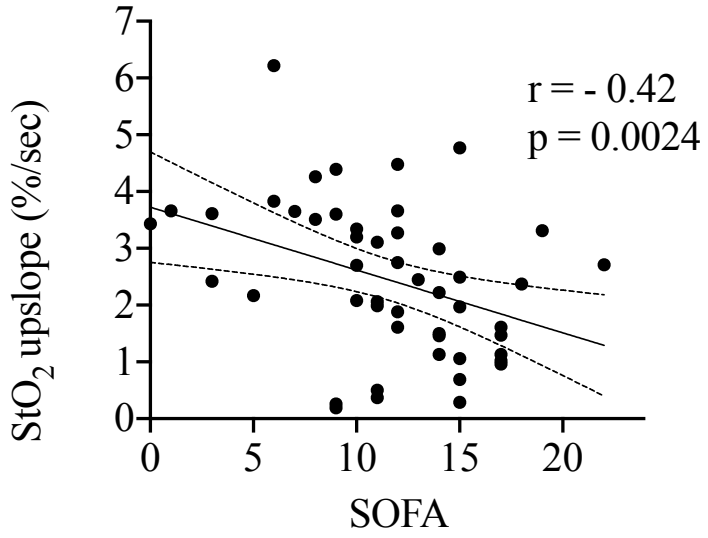

Solid line indicates line of best fit; dashed lines 95% CI.

Figure 74. Correlation between StO_2 upslope and vasopressor dose

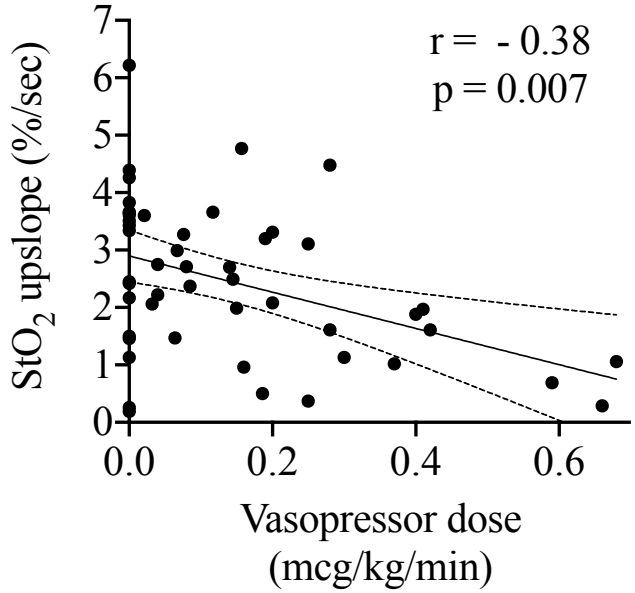

Solid line indicates line of best fit; dashed lines 95% CI.

Figure 75. Correlation between degree of organ dysfunction and vascular reserve

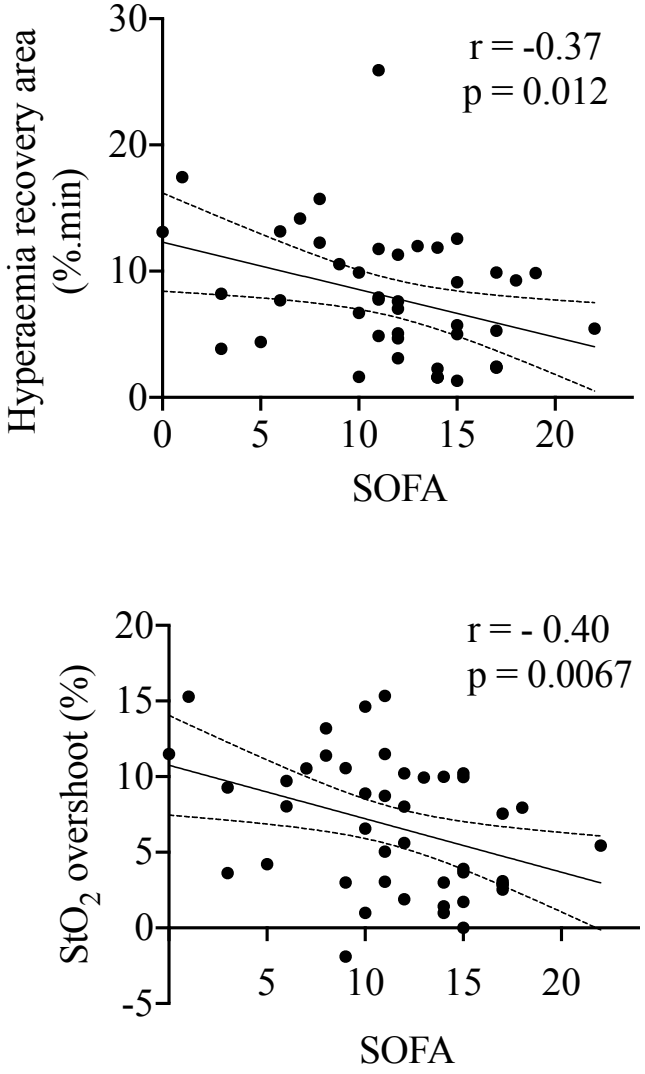

Solid line indicates line of best fit; dashed lines 95% CI.

6.6.5. Relationship between tissue microcirculatory function and bioenergetic profile

There was no relationship between thenar muscle StO_2 and any aspect of intact mitochondrial respiration measured in *vastus lateralis* using high resolution respirometry. However, the StO_2 upslope demonstrated weak negative correlation with specific respiratory capacities, demonstrated in Figure 76, namely relative capacity for leak respiration ($r = - 0.37$, $p = 0.039$), relative capacity for FAO-supported oxidative phosphorylation ($r = -0.38$, $p =0.03$), and relative capacity for complex II-supported respiration ($r = -0.43$, $p=0.014$).

Figure 76. Correlations between StO_2 upslope and specific respiratory capacities

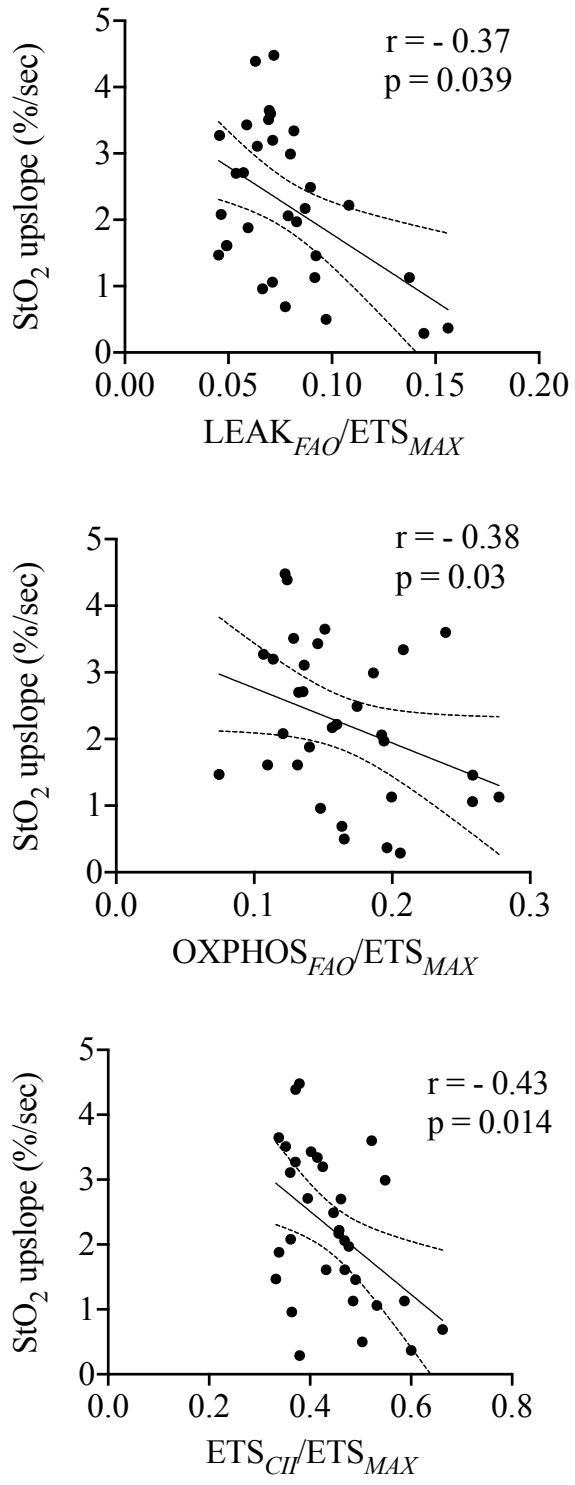

Specific respiratory capacities measured in *vastus lateralis* muscle and expressed relative to maximum uncoupled capacity. $LEAK_{FAO}/ETS_{MAX}$: capacity for leak supported respiration; $OXPHOS_{FAO}/ETS_{MAX}$: capacity for FAO-supported oxidative phosphorylation; ETS_{CII}/ETS_{MAX}: capacity for complex II supported respiration. Solid line indicates line of best fit; dashed lines 95% CI.

6.6.6. Relationship between microcirculatory function and plasma redox profile

All StO_2 measurements (baseline, minimum, peak and recovery) were positively correlated with arterial plasma levels of cGMP (Figure 77). A similar relationship was observed between StO_2 and venous cGMP (r=0.34, p=0.18 for baseline StO_2; r=0.31, p=0.036 for recovery StO_2). There was no relationship between the StO_2 downslope and any aspect of plasma redox profile measured in this study. However, the StO_2 upslope, indicative of microvascular reactivity (reperfusion rate of the tissue depending upon endothelial-dependent vasodilatation) was negatively associated with both venous isoprostanes (r = -0.29, p = 0.049) and arterial total antioxidant capacity as measured by the FRAP assay (r = 0.29, p = 0.045), shown in Figure 78.

Hyperaemia recovery area, an indicator of vascular reserve, was negatively correlated with arterial lipid peroxidation products as measured by the TBARS assay (r = -0.38, p = 0.014) as shown in Figure 79. These correlations with hyperaemia recovery area were consistent in venous plasma (lipid peroxides: r = -0.32, p = 0.041). This relationship was supported by the fact that a second indicator of vascular reserve, StO_2 overshoot, demonstrated the same associations with venous lipid peroxidation (r = -0.35, p = 0.022) as shown in

Figure 80.

Figure 77. Correlation between StO_2 values and plasma concentrations of cGMP

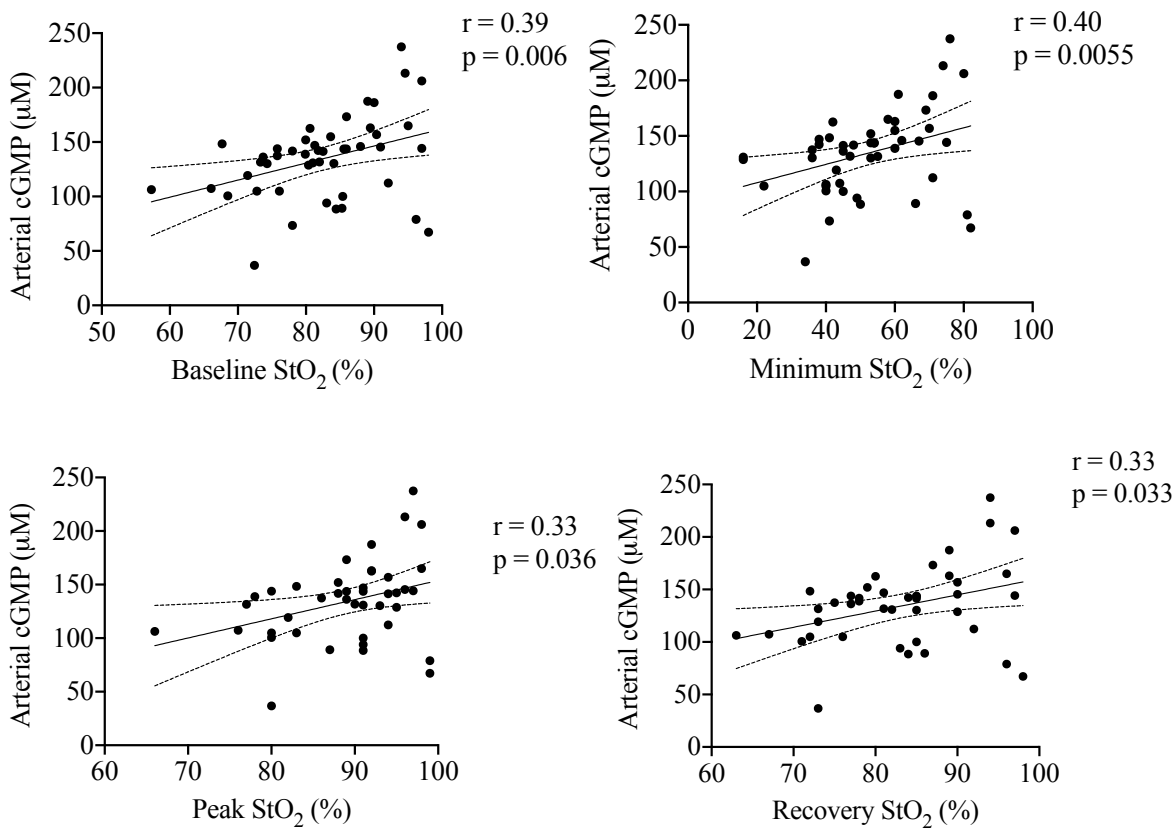

Solid line indicates line of best fit; dashed lines 95% CI.

Figure 78. Associations between StO_2 upslope and plasma redox profile

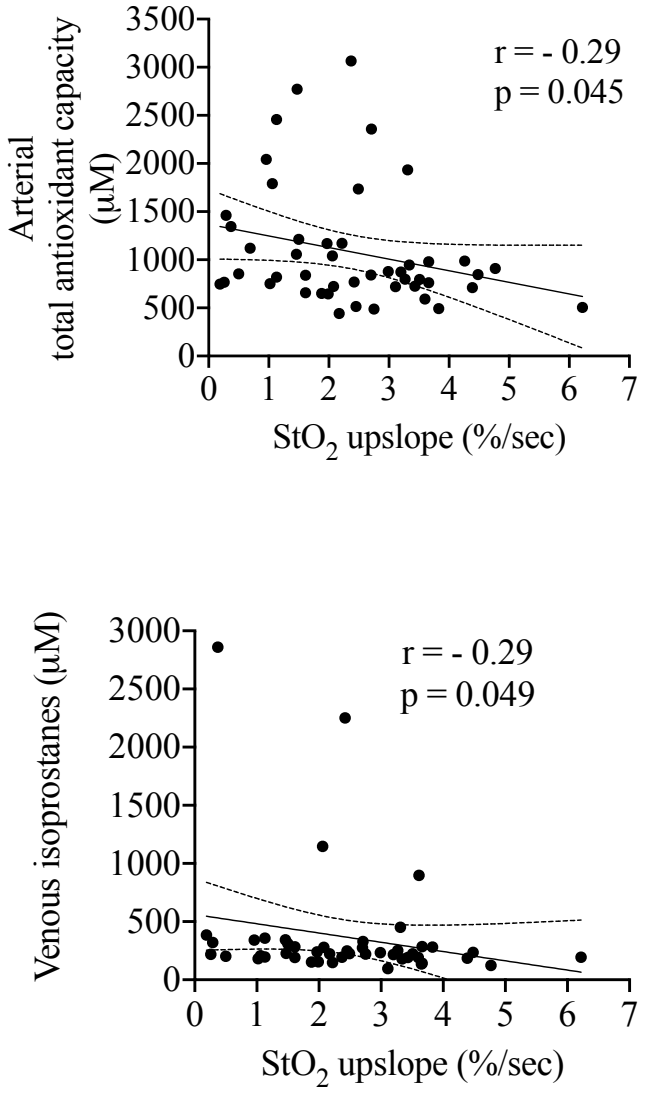

Solid line indicates line of best fit; dashed lines 95% CI.

Figure 79. Correlation between hyperaemia recovery area and plasma redox profile

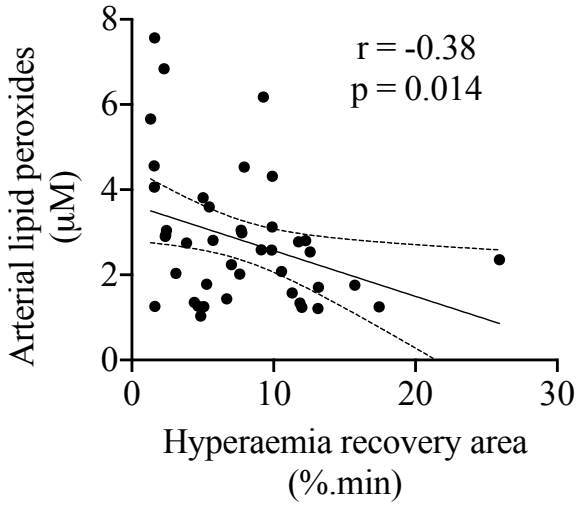

Solid line indicates line of best fit; dashed lines 95% CI.

Figure 80. Associations between StO_2 overshoot and plasma redox profile

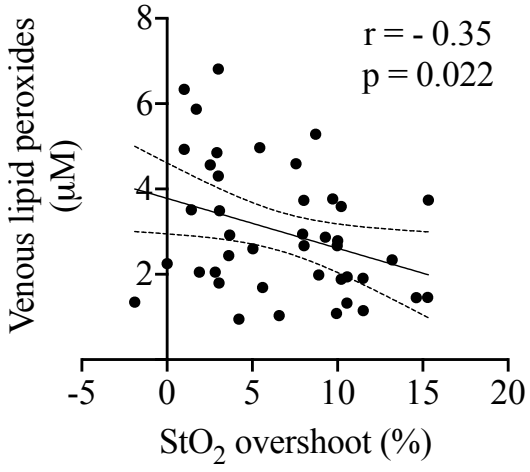

Solid line indicates line of best fit; dashed lines 95% CI.

6.7. Discussion

6.7.1. Summary of major findings

Thenar muscle microcirculatory profile in survivors and non survivors

Minimum StO_2 was lower in eventual survivors at day 5-7, but no other differences between the groups was statistically significant. A summary of the (non significant) pattern of differences between survivors and non survivors is outlined in Table 40.

Table 40. Summary of NIRS-VOT survival phenotype

Survival phenotype (compared to non survivors)				
Microcirculatory function	<48 h	Day 3-4	Day 5-7	Direction of change from < 48 h today 5-7
Skeletal muscle oxygenation	Greater (baseline, min, peak and recovery)	=	*Lower min StO_2	Decreasing *(Non survivors: increasing)*
Microvascular reactivity	=	=	Greater	Increasing *(Non survivors: decreasing)*
Vascular reserve	=	=	Greater	Increasing *(Non survivors: decreasing)*

*Only statistically significant difference was lower minimum StO_2 in survivors at day 5-7; other trends reported were not statistically significant. Microvascular reactivity indicated by StO_2 upslope; vascular reserve indicated by hyperaemia recovery area and StO_2 overshoot.

Microcirculatory dysfunction was related to organ dysfunction, skeletal muscle bioenergetic alterations and plasma redox markers

Organ dysfunction (as estimated by the SOFA score) was associated with lower microvascular reactivity (StO_2 upslope) and vascular reserve (hyperaemia recovery area or overshoot). Thenar muscle microvascular reactivity was also related to *vastus lateralis* respiratory capacity, with lower microvascular reactivity associated with greater relative capacity for leak respiration and FAO-supported respiration. Lower microvascular reactivity and vascular reserve were also associated with greater plasma levels of oxidative stress (venous isoprostanes and lipid peroxidation products) and antioxidant capacity.

No relationship between systemic and tissue oxygenation

There was no relationship between skeletal muscle absolute StO_2 values and arterial oxygenation indices (SpO_2, PaO_2, CaO_2) or mean arterial pressure. One explanation for this is that these systemic variables were corrected through resuscitation measures on the ICU (mechanical ventilation, supplemental inspired oxygen concentrations and vasopressor/inotropic therapy). However, all StO_2 values were positively correlated with circulating levels of cGMP. No relationship was demonstrated between absolute StO_2 values measured in thenar eminence muscle and maximum respiratory capacity measured in intact mitochondria from *vastus lateralis* muscle.

6.7.2. Interpretation and significance

Failure to detect clear differences in survivors and non survivors

I hypothesised that non survivors of critical illness would have impaired skeletal muscle oxygenation and microcirculatory function compared to survivors, consistent with the previous findings in critically ill patients (178, 347). However, differences in the

microcirculatory measures between survivors and non survivors in this study were not statistically significant. This may have reflected small number of subjects, with heterogenous diagnoses, and the degree of attrition at later timepoints, discussed in section 2.5.10. There was, however, a consistent trend of higher muscle StO_2 values in survivors at 48 h, which disappeared by day 3-4, and even reversed by day 5-7. The time frame roughly corresponds to the findings of a previous study of critically ill patients, which demonstrated no difference between eventual survivors and non survivors in skeletal muscle StO_2 on admission to ICU (i.e. earlier than the first time point of testing in the current study), but higher StO_2 values in survivors at day 3(192). Different StO_2 trajectories in survivors and non survivors, with StO_2 values consistently increasing in non survivors during the first 7 days, while survivors tended to decrease their StO_2, implies that the processes determining tissue oxygenation during critical illness are dynamic, and the direction of change is relevant to clinical outcome. Greater tissue oxygenation may confer survival advantage during the first 48 h of organ failure but increasing StO_2 after this point is not. This echoes the temporal specificity of bioenergetic and redox differentiation between survivors and non survivors reported in previous chapters.

Microcirculatory dysfunction unrelated to systemic blood flow and oxygenation

This absence of a relationship between any muscle StO_2 value and arterial oxygenation indices (SpO_2, PaO_2 or CaO_2) or mean arterial pressure is consistent with the concept that microcirculatory function becomes dissociated from microcirculatory haemodynamics in critical illness (121, 347). Lack of correlation between systemic and tissue oxygenation in critically ill patients has been shown in previous studies (189), and direct imaging of the sublingual microcirculation showed non survivors of multiple organ failure to have a smaller percentage of perfused small vessels than survivors, despite similar haemodynamic and oxygenation profiles (348). In the current study, a potential role for local microvascular

recruitment in regulating tissue oxygenation in patients with organ failure, via cGMP-mediated vasodilation, was suggested by finding that plasma cGMP was consistently correlated with all StO_2 values. This mediator is involved in the relaxation of vascular smooth muscle, via initiation of calcium extrusion, and representing the distal end of the pathway of nitric oxide (NO)-induced vasodilation (354). As outlined in previous chapters, NO is an important endogenous regulator of vascular tone (355) and its circulating levels are elevated in multiple organ failure, inflammatory and septic shock, and acute respiratory distress syndrome (306), resulting in vasoplegia (uncontrolled vasodilatation) and hypotension. Although it is not possible to establish any mechanism, the results of the current study are consistent with the view that the downstream actions of NO influences the local delivery of oxygen to distal tissues by the microcirculation.

Association of organ failure with skeletal muscle endothelial dysfunction

The results of this study supported the hypothesis that skeletal muscle microcirculatory dysfunction would be associated with global organ dysfunction and suggested a role for local endothelial dysfunction in the development of organ failure, with higher SOFA scores associated with lower StO_2 upslopes and lower hyperaemia recovery areas. The StO_2 upslope represents the removal of deoxyhaemoglobin from the ischaemic skeletal muscle by a rapid influx of oxyhaemoglobin, when arterial influx returns. During this period of reoxygenation, there is intense vasodilatation within the skeletal muscle microcirculation, recruiting previously dormant capillaries to maximise oxygen flux to the ischaemic muscle, and reflects the so-called “microvascular reactivity” of the tissue whilst the “hyperaemia recovery area” represents the vascular reserve(356). The endothelium plays a dominant role in this vasodilatation-mediated reoxygenation, and endothelial dysfunction results in slower reperfusion rates (357). The trend towards greater StO_2 upslope in survivors at day 5-7 also

suggests that recovery of microvascular reactivity may represent a hallmark of good outcome. Impaired microvascular reactivity associated with greater vasopressor doses in the critically ill patients. Vasopressors are used to augment perfusion pressure in a vasoplegic states, by stimulating arteriolar vasoconstriction, to increase mean arterial pressure and thus peripheral perfusion pressure gradient at the tissues. One explanation for this relationship is that vasopressor-induced arteriolar constriction impairs endothelial-dependent microvascular reactivity, at least in skeletal muscle and actually reduces local blood flow (358). An alternative explanation is that patients with more severe endothelial dysfunction may require higher vasopressor doses to maintain their mean arterial pressure at the targets set by intensive care physicians. Either way, it seems that targeting mean arterial pressure with vasopressors fails to improve microcirculatory function. This conclusion is in line with a recent randomised controlled trial of 2600 ICU patients aged 65 and older receiving vasopressors for vasodilatory hypotension, which showed that targeting a lower mean arterial pressure (60-65 mmHg) resulted in a similar 90-day mortality compared to the "usual standard of care" in which the average mean arterial pressure recorded was > 70 mmHg(118).

Microvascular reactivity was associated with mitochondrial and redox changes.

The results of this study supported the hypothesis that cellular bioenergetic function in critical illness would be related to microcirculatory function. The downslope represents tissue oxygen consumption rate, and as such, may have been expected to be associated with ex vivo measures of mitochondrial oxygen consumption. No such relationship was found, but instead, in the critically ill cohort, lower StO_2 upslopes were associated greater capacity for leak and FAO-supported oxidation, which theoretically reduce the efficiency of respiration. Lower StO_2 upslopes were also associated with a less favourable plasma redox status, represented by greater levels of both venous isoprostanes and plasma reductive

capacity. The link between endothelial dysfunction and systemic oxidative stress was strengthened by the finding that lower vascular reserve was also associated with elevated plasma lipid peroxidation products, which in previous chapters were shown to be associated with disease severity and death. These findings strengthen the proposed relationship between microcirculatory dysfunction, organ dysfunction and redox profile. The signature of organ failure at a microscopic level may include impaired microvascular endothelial function, increased plasma oxidative stress and compensatory antioxidant upregulation, and less efficient respiration. It is not clear from this work how these aspects of biology are related. In a murine sepsis model, administration of erythropoietin (EPO), a downstream target of HIF, was shown to increase perfused capillary density and bioenergetics (judged by a decrease in NADH fluorescence, indicating improved pyruvate metabolism and oxidative phosphorylation) in skeletal muscle (353). In a rat model of sepsis, injection of LPS resulted in increased myocardial diffusion distances, tissue hypoxia and upregulation of HIF-1 alpha and its downstream targets VEGF and the glucose transporter, GLUT1 and the latter was positively correlated with organ function (indicated by left ventricular contractility) (48).

6.7.3. Study limitations

The strengths and limitations related to subject selection for the critically ill cohort was discussed previously in Chapter 2 (section 2.5.9) to avoid repetition. Strengths and limitations specific to the techniques used in this study are discussed below.

Technological factors

The validity of NIRS-VOT measurements has been demonstrated previously (359). There can be a considerable degree of inter-individual variability related to subcutaneous adipose tissue depth. The InSpectra NIR spectrometer measures StO_2 at three second intervals, and

curves are generated by the software by extrapolating between the measurement intervals. During periods of rapid reoxygenation, accuracy of values may be reduced. The response of skeletal muscle to ischaemia is dependent on its duration; and it is important that the ischaemic time was uniform for all tests. In this study, a manual cuff was used, which may contribute to inconsistencies in the rapidity of cuff manipulation. Three minutes of arterial occlusion was chosen to allow adequate time for ischaemia to develop, without causing undue pain in unstable patients. Movement of the arm or hand during the measurements will increase muscle oxygen consumption, and all measurements. All measurements were taken at rest, but some inadvertent clenching of the hand could not be prevented in patients who were not completely awake and co-operative.

Patient factors

The development of tissue oedema, common in critical illness, in response to resuscitation with fluid, and increased capillary permeability can deteriorate the NIRS signal. By measuring the StO_2 at the thenar eminence, this possible source of error was minimised, as the thenar eminence is an uncommon site for the accumulation of interstitial oedema (180). A reduction in skin temperature can cause vasoconstriction that may reduce blood flow within the skeletal muscle. All testing was carried out within the same ICU, but ambient temperature was not measured.

Generalisability

Characteristics of the microcirculation vary according to the function of the tissue it supplies (360). In this chapter, skeletal muscle of the thenar eminence was investigated, as a proxy for skeletal muscle microcirculatory function, as it was accessible and represented the same tissue type in which bioenergetic phenotype was contemporaneously described in these

patients (albeit in *vastus lateralis* muscle). Ideally, these investigations would have been performed in the same muscle bed, but the NIRS-VOT was not technically feasible in these patients. It is not known if the pattern of differences observed here also occurs in other vital organs such as the brain, liver and heart.

6.7.4. Future work and unanswered questions

The pattern of differences in the microcirculatory profile of survivors and non survivors did not meet the criteria for statistical significance but represent a signal to be investigated further in a larger cohort of patients. An alternative approach to assessing the microcirculation is to directly visualise the network of vessels, and use semi-quantitative methods to determine vessel density, red blood cell flow and heterogeneity. This approach was attempted in this thesis, but the quality of films did not meet the criteria for quality control, and thus were not included.

6.8. Conclusion

This study demonstrated the existence of a microcirculatory phenotype associated with organ dysfunction, involving impaired microvascular reactivity and vascular reserve. Although these features were independent of mean arterial pressure and systemic oxygenation, they were related to increasing dose of vasopressor administration. This study also provides some preliminary information about potential relationships between microcirculatory function and mitochondrial alterations thought to improve respiratory efficiency and the systemic redox profile thought to be relevant to clinical outcome. This study provided additional support for the growing body of evidence that the function of the peripheral microcirculation represents a more important therapeutic target in critical illness than current measures, which focus on the global function of the macrovascular cardiovascular and respiratory systems.

7. Chapter 7. General Discussion

7.1. Summary of findings

The aim of this thesis was to further our understanding of the molecular changes that underpin multiple organ failure and the ability to recover from it. The first hypothesis was that cells operate differently during critical illness than in health, particularly in terms of interrelated functions thought to be fundamental to survival, namely: bioenergetic capacity, substrate metabolism and redox status. Following on from that, the aim was to determine if differences in these intracellular functions, systemic redox status or local microvascular function could explain the ability of some patients to recover from multiple organ failure.

This work showed that, at an intracellular level in a representative end-organ, the extreme pathophysiological stress of critical illness manifests as selective modifications to bioenergetic efficiency, metabolic compensation and redox balance, which share many similarities to the cellular response to oxygen limitation. These changes were not related to the traditional clinical measures of systemic oxygenation or mean arterial pressure targeted by intensive care physicians but were instead associated with elements of the plasma reactive species interactome and endothelial-dependent aspects of microcirculatory function. Eventual survivors demonstrated a bioenergetic-redox profile and trajectory that was distinct from that of non survivors.

In Chapter 4, skeletal muscle taken from patients in the first 48 hours of critical illness diagnosis had more efficient mitochondrial oxidative phosphorylation with respect to oxygen consumption, achieved by reduced capacity for proton leak and a switch in substrate preference away from FAO. These bioenergetic alterations were accompanied by compensations in intermediary metabolism, including higher glycolytic flux and lower early

TCA cycle flux to support oxygen-independent ATP production, and diminished FAO. Maximum oxidative phosphorylation capacity and alternative measures of tissue energetics were preserved in critical illness, despite a relative decrease in complex I capacity. Higher intramuscular levels of both oxidised and reduced versions of the redox couple, methionine/methionine sulfoxide, suggested both increased production of ROS and active upregulation of cellular reducing machinery in critical illness. The skeletal muscle profile in critical illness shared many features of the HIF-response to hypoxia in cell models and in humans acclimatising to hypobaric hypoxia.

In Chapters 4 and 5, a survival phenotype was identified, which included specific and dynamic modifications to skeletal muscle bioenergetics and the plasma reactive species interactome. Two of the skeletal bioenergetic modifications noted in the first 48 h of critical illness: lower capacity for complex I-supported respiration and the trend towards lower FAO-supported respiration were initially more marked in eventual survivors, indicating that these modifications may have served a protective function. At the same timepoint, survivors also displayed lower plasma concentrations of lipid peroxidation products and total nitroso species (RXNO), in the context of lower plasma total antioxidant capacity, compared to non survivors. There was evidence that the putative benefit from these modifications was time-specific, as survivors and non survivors also differed in the direction of change in these variables over time. By day 5-7, the initially lower respiratory capacities showed signs of increasing towards healthy values in survivors, but in non survivors they either did not change (complex I capacity) or declined further (FAO capacity). Differences in the plasma redox profile were also time-specific; by day 3-4, the survivors had shifted to lower plasma free thiols and lower lipid peroxidation products than non survivors; and at day 5-7 only the lipid peroxidation products remained higher in survivors. Several of the specific components

of bioenergetics and redox profile shown to be modified in critical illness (including capacity for leak and FAO-supported respiration, plasma lipid peroxidation products and total antioxidant capacity) were correlated with the severity of multiple organ dysfunction, suggesting a shared pathway.

In Chapter 6, although trajectories of skeletal muscle oxygenation and microcirculatory function appeared to diverge in survivors and non survivors, differences did not reach the criteria for statistical significance. Blunted endothelial-dependent microvascular reactivity and vascular reserve were associated with greater degrees of organ failure. Skeletal muscle microcirculatory function did not relate to systemic haemodynamics or oxygen transport, but microvascular reactivity was lower in patients receiving higher doses of vasopressor. Furthermore, lower microvascular reactivity and vascular reserve were also associated with greater plasma levels of oxidative stress (venous isoprostanes and lipid peroxidation products) and antioxidant capacity, and greater relative capacity for leak respiration and FAO-supported respiration in skeletal muscle.

7.2. Interpretation, implications and recommendations

7.2.1. The need to re-evaluate assumptions underlying supportive therapy in critical illness

Limitations of augmenting global oxygen transport in critical illness

The findings of this work call into question two assumptions that underpin much of supportive therapy on the ICU. The first is the assumption is that organ dysfunction in critical illness results from a cellular bioenergetic impairment; and the second is that this putative cellular bioenergetic impairment can be improved by increasing systemic oxygen transport. The findings of this thesis were in conflict with both assumptions. First, intramuscular energetic ratios and theoretical maximum oxidative phosphorylation capacity were preserved in multiple organ failure, and similar in survivors and non survivors. Second, there was no evidence that higher systemic oxygen transport translated into increased oxygen availability to the cells in the critically ill cohort. Skeletal muscle StO_2 was unrelated to indices targeted by intensive care physicians, such as PaO_2, SpO_2 or mean arterial pressure, and increasing vasopressor doses were actually associated with lower endothelial-dependent microcirculatory function. Vasopressors are administered under the assumption that vasoconstriction will improve tissue perfusion when mean arterial pressure is diminished by pathological vasodilation. However, vasoconstriction may also impair local tissue blood flow, and indiscriminate pharmacological vasoconstriction may disrupt the microscopic coupling between tissue demand and local supply, which differs between organs in different contexts (361, 362). Finally, there was no relationship between the measures of skeletal muscle bioenergetic capacity undertaken in this thesis and measures of either arterial or skeletal muscle oxygenation. As outlined in Chapter 1, ATP synthesis via chemiosmosis depends on a multitude of factors in addition to the continuous supply of oxygen as the final electron acceptor. These include: the capacity of the electron transfer system (which couples

electron flow to the generation of an electrochemical gradient), the continuous supply of electrons via metabolic pathways (such as the TCA cycle and FAO) which extract electrons from substrates and donate them to the electron transfer system. Each of these components depends upon a multitude of enzyme catalysed steps, which may also be influenced by substrate availability and product inhibition, and alteration to any one of these components may have an impact on the ability of the system to produce ATP. By demonstrating deviation from health in several of these components during organ failure (lower complex I capacity, increased coupling efficiency of oxidative phosphorylation, reduced FAO and increased glycolysis), this thesis also provides a plausible explanation for why increasing global oxygen delivery fails to increase bioenergetic capacity. If cells have adopted a different phenotype, which preserves bioenergetic capacity through increased efficiency of oxidative phosphorylation and upregulation of oxygen-independent ATP production, it may explain why increases in oxygen availability in this context do not translate into increased bioenergetic capacity. Collectively, these findings question the biological basis of current systemic physiological targets in intensive care medicine and are in keeping with the well-recognised phenomenon that normalising global oxygen transport in patients with multiple organ failure does not improve their survival (363). The implication is that we can no longer rely on systemic values as proxies for cellular end points, or assume that the range of values for systemic oxygen transport or global haemodynamics reported in healthy, non-stressed adults, under typical environmental conditions, necessarily represent the most beneficial targets during the extreme stress of critical illness. The advancement of supportive therapy may thus require the development of accessible biomarkers which reflect true cellular end points, in order to judge the success of intensive care interventions to achieve their biological goals (364).

Failure to consider the concept of cellular hypoxia adaptation in critical illness

The limitations of current supportive therapy may also reflect the failure to consider the unintended impact of interventions to change systemic oxygen transport on putative innate cellular survival responses. Thus far, supportive therapy on ICU has neglected to consider the fundamental processes of cellular adaptation to hypoxia, which are known to be vital for the survival of all complex organisms, including humans (364). The fact that survivors showed the greatest deviation from health in two of the bioenergetic modifications, with lower complex I capacity and a trend towards lower FAO capacity compared to non survivors, emphasises the potentially protective nature of the intracellular modifications observed in early critical illness. The features shared by the HIF response and the critically ill skeletal muscle phenotype described in this thesis include: implementation of oxygen-independent ATP production (365), alteration of metabolic fuel preference (217) and "tuning" down mitochondrial proton leak to increase the efficiency of oxidative phosphorylation (56), and inhibition of complex I (232). The fact that these modifications were demonstrated together is consistent with the existence of a highly regulated response to cellular oxygen limitation in the critically ill patients and suggests a potential role for the HIF pathway in co-ordinating this putative adaptive phenotype. It must be emphasised, however, that neither tissue PO_2 nor HIF levels were measured in this work. The potential ability of human cells to adapt to hypoxia, or other forms of physiological stress in critical illness, by reprogramming cellular bioenergetic pathways, in the context of critical illness opens up a new avenue of potential therapeutic strategies to investigate. Review of the mechanisms involved in hypoxic adaptation, in other fields of medicine and biology, provides suggestions of how this pathway could be targeted. For example, it may be possible to support the expression of the entire cellular suite of adaptations in a co-ordinated manner, through activation of the HIF pathway itself (366). Pharmacological stabilisation of HIF, through

administration of prolyl hydroxylase inhibitors had been trialled in patients, although concerns have been raised about the risk of supporting tumour growth (367). In animal models, activation of HIF1 has shown to reduce inflammation in periodontal infection and suppress LPS-stimulated macrophage differentiation (368). Supporting the HIF pathway by other means could also be investigated, such as altering the composition of substrate supply by increasing the ratio of carbohydrate to fat in feeding regimens, in recognition that mitochondria are less able to use fat, and accumulation of unused byproducts of incomplete FAO may be toxic (73). In recent network analysis of a heterogenous group of critically ill patients, it was shown that skeletal muscle bioenergetic capacity was unrelated to the quantity of fatty acids delivered (87) and the authors argued that this may contribute to the failure of increasing the delivery of nutrition to improve outcomes on ICU (119), as lipids contribute 29-43% of the energy content in enteral, and 50% of parenteral nutrition (369). Authors have also suggested the potential utility of supporting rather than suppressing the catabolic response to critical illness and trialling exogenous administration of ketones and amino acids (370, 371). The potential clinical benefit of selectively augmenting individual components of the survival phenotype should be investigated. Pharmacological agents exist which inhibit mitochondrial ROS production by a specific site in complex I without reducing its oxidative phosphorylation capacity (372). One such agent, OP2113 (5-(4-methoxyphenyl)- 3H-1,2-dithiole-3-thione), has been used safely in humans for hundreds of years, and has been shown to protect heart function in rat model of myocardial infarction (372).

Another implication of the theory that cells may undergo adaptive modification to hypoxia during critical illness, is that current supportive therapy may cause harm by inadvertently suppressing it. It is possible that the indiscriminate provision of oxygen and substrate may obscure beneficial hypoxic adaptive signalling, or that excessive oxygenation superimposed

upon adapting cells may cause a new form of stress. Evidence is solidifying for harm associated with supraphysiological levels of arterial oxygenation in large data sets of critically ill patients (373)and the therapeutic benefit of targeting so-called "permissive hypoxaemia" is currently under investigation (374). This is part of a growing challenge to the dogma of "correcting" deranged physiology in critically ill patients, with an increasing number of randomised controlled trials demonstrating benefit from "permissive" targets, which minimise intervention and tolerate abnormal physiology (358). These trials include permissive targets for oxygenation and ventilation (375), haemoglobin concentration (376), systemic haemodynamics (118), nutrition (120) and glycaemic control (377). However, a greater understanding of the relationship between systemic physiological variables and cellular endpoints, in the context of human critical illness, is required to develop better therapeutic targets (271).

7.2.2. Inter-related bioenergetic, redox and microcirculatory modifications

The findings of this thesis were consistent with the concept that bioenergetic pathways lie at the intersection between two processes fundamental to cell survival: energy metabolism and redox signalling. Several of the microscopic features found to be related to the degree of organ dysfunction (illustrated in Figure 81) including blunted microvascular endothelial function (microvascular reactivity and vascular reserve), increased plasma lipid peroxidation and elevated antioxidant capacity, and relative capacity for leak and FAO-supported respiration, were also related to each other. This may represent the effect of confounding, and it is not possible to infer biological relationships between these components, due to the observational nature of the study. However, adequately powered future studies may investigate the existence of a signature of multiple organ failure involving these components, and a shared mechanism that may link them. Such understanding will be necessary in the

development of a more cell-based approach to human life support. It is difficult to distinguish cause from effect, and signalling from pathology, when it comes to the relationship between bioenergetic function and ROS generation. From experimental models in the literature, suggestions regarding the biological basis for several of these relationships have been demonstrated.

Figure 81. Microscopic features associated with organ dysfunction in critical illness

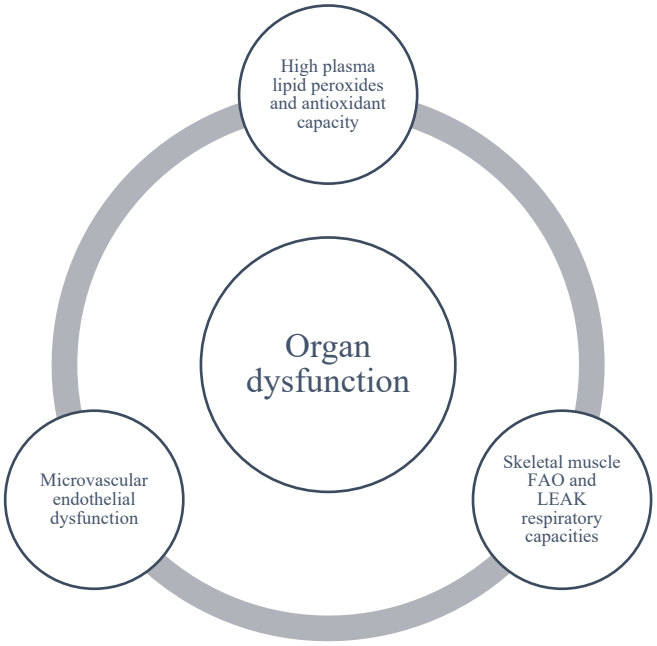

Relationship between uncoupling, superoxide production and complex I activity

A review of ROS generation outlines 11 different sites in mammalian mitochondria, involved in substrate oxidation and oxidative phosphorylation, from which electrons may leak (378). Two of these sites exist within complex I, which release superoxide into the matrix, including the site with maximum capacity for superoxide production (the ubiquinone binding site). The generation and the biological effects of mitochondrially generated ROS are thought to depend on the site of their generation, the substrates present and the antioxidant systems in both the

mitochondria and the cytosol(379), and inhibition of complex I has differential effects on superoxide production in these different contexts. For example, in isolated mitochondria, substrates that stimulate forward electron flow through complex I (malate and pyruvate) give low rates of superoxide production (380). In this condition, application of the inhibitor rotenone, which blocks the ubiquinone binding site of complex I, causes electrons back up and reduce the redox centres upstream, increasing production of superoxide several fold. In contrast, substrates that stimulate reverse electron flow through complex I, such as succinate, produce the maximum rate of superoxide production, which is diminished by the application of rotenone (380). Superoxide production is highly sensitive to the proton gradient across the inner membrane, which is in turn influenced by the degree of proton leak (381). Uncoupling of mitochondria has been shown to reduce superoxide production (31). Therefore, the more efficient mitochondrial phenotype in critically ill skeletal muscle shown in this work may come at the cost of increased ROS production by complex I. The concomitant downregulation of complex I capacity in early critical illness may represent a consequence of this, or an attempt to compensate for this. The latter concept is consistent with the lower complex I capacity and lower levels of plasma lipid peroxidation products seen in survivors in this thesis. A HIF-1 target gene, called mitochondrial NADH dehydrogenase ubiquinone 1 alpha subcomplex 4-lik2 2 (NDUFA4L2) has been shown to inhibit complex I activity and reduce exposure to complex I-generated superoxide (232). Inhibition of complex I has also been shown to activate ROS sensors, while not altering cell viability, in a cell model, suggesting a role for this form of ROS generation in redox signalling (382).

FAO capacity, lipid peroxidation and uncoupling

The correlation between plasma levels of lipid peroxidation products and skeletal muscle capacities for leak- and FAO-supported respiration highlighted another pathway which may

be relevant in critical illness. Mitochondria can be uncoupled by fatty acids and reactive aldehydes. The mechanism involves direct activation of uncoupling proteins by fatty acids (383), particularly long-chain fatty acids (384). In a mouse model, the uncoupling protein, UCP3, was not only subject to activation by lipid hydroperoxides, mediating mitochondrial uncoupling, but was also involved in the translocation of lipid hydroperoxides across the mitochondrial inner membrane, with the effect of protecting the mitochondrial matrix from interaction with these highly reactive species (385). It is possible that the alterations to the FAO pathway seen in critically ill skeletal muscle, characterised by reduced mitochondrial preference for FAO to drive oxidative phosphorylation and reduced FAO enzyme capacity, has secondary effects on mitochondrial coupling and oxidative stress. Accumulation of medium and long chain carnitines may react with mitochondrially generated ROS, forming fatty acyl radicals (102), which may through UCP3, subsequently uncouple mitochondria and translocate the reactive species away from the matrix. There is evidence that mitochondrial uncoupling by complex I generated superoxide depends on the presence of free fatty acids (386).

Nitric oxide, complex I and microcirculatory function

NO has long been considered to play a central role in mediating physiological alterations seen in critical illness, as it is known to influence both local microcirculatory blood flow, through the actions of its downstream mediator, cGMP, and to inhibit mitochondrial respiration through diverse mechanisms (387). High circulating levels of NO and peroxynitrite are responsible for vasoplegia but the fact that non-selective inhibition of NO production in septic patients led to an increased mortality, despite an improvement in systemic haemodynamics (388), hints at a potentially critical signalling role. By focusing only on deranged systemic variables, we may miss cellular alterations which are more vital

for survival. In a rat model of sepsis, increased microvascular dysfunction (heterogenous flow) was associated with reduced tissue oxygen partial pressure and reduced cell function (contractility of the left ventricle) (48). However, the same study also demonstrated increased tissue expression of HIF1α, and its downstream targets, including VEGF and the glucose transporter, GLUT 1, and that left ventricular contractility was associated with increased GLUT1 expression. NO signalling represents an important potential mechanism for complex I inhibition in survivors of critical illness, as complex I is known to be subject to inhibition by NO, and its derivatives peroxynitrite and S-nitrosothiols, by a number of different mechanisms, including nitrosation and nitration (389). However, in this work, no differences were observed between survivors and non survivors in terms of plasma nitrate or nitrite, and total nitroso species were consistently lower in survivors.

7.2.3. The relevance of timing in critical illness interventions

The profile of bioenergetic, redox and microcirculatory differences between eventual survivors and non survivors were time-specific, with different trajectories in the two groups. One explanation for this recurring theme is that survivors are characterised not only by their ability to launch more robust deviations from health, argued here to represent potentially protective modifications, but also by their ability to reverse these changes faster, whilst non-survivors undergo persistent or progressive deviation over time. This may reflect the potential cost of adaptation, in which excessive or prolonged deviation from normal may be incompatible with life. Stress resilience may rely on both the ability to launch an appropriate adaptive response at the onset of a critical insult as well as the ability to switch it off in a timely manner, to allow metabolic recovery and minimise harmful consequences of bioenergetic and redox compensation. One implication of the temporal specificity of the differences between the groups is that intensive care interventions should also be time-

specific (390). For example, during the precipitating phase of critical illness, preventing hypoxia may circumvent deterioration into critical illness, but once organ dysfunction is underway, it may be more appropriate to support a more efficient cellular use of oxygen, until the triggering disease process can be resolved. The temporal specificity of interventions is an area of increasing interest in medicine, including critical illness (391). Currently the manner in which cellular metabolism and mitochondrial function alter during different phases of critical illness, and how this influences clinical outcomes, is not adequately understood. Exploring the role of time in the relationship between cellular hypoxia, bioenergetic capacity and redox signalling will be required to effectively harness potential adaptive strategies in critical illness.

7.2.4. The need for an integrated approach to understand bioenergetic and redox function in critical illness

The interpretation of the bioenergetic changes is at variance with previous work in this field, which used ATP concentrations as a surrogate marker for bioenergetic capacity. Regulation of complex systems involved in bioenergetic capacity and redox architecture cannot be adequately captured or understood by measuring shifts in steady-state concentration of a single biomarker at a single timepoint. The new insights into the complex and dynamic nature of human survival processes, bioenergetics and redox signalling, described in this thesis have been gained by simultaneous measurement of interrelated pathways, in several compartments, at multiple timepoints. Only by combining functional analyses of intact mitochondria with metabolomic analyses in cellular and systemic compartments a coherent picture emerges, which attests to altered mitochondrial substrate utilisation and reduced metabolic flexibility associated with intracellular and whole-body lipid accumulation consistent with a co-ordinated adaptation to hypoxia. Similarly, a more comprehensive

analysis of redox components in multiple compartments revealed that, in conjunction with increased oxidative stress, the cellular reducing machinery was working at an increased rate. Future studies should consider this approach in trying to map out the co-ordinated, multi-level responses of the body to stress, which may enable local demands to be met, whilst mitigating potential damage to the body as whole (392).

7.3. Limitations

The bioenergetic-metabolic phenotype in multiple organ failure was described in skeletal muscle, and may not be generalisable to other tissues, such as brain, cardiac muscle or liver, whose function is arguably more relevant to survival in critical illness than inactive skeletal muscle. Although skeletal muscle represents a relevant end-organ, subject to microcirculatory changes, it is possible that microcirculatory flow differs according to the specific tissue, and that supply to other tissues may be prioritised over skeletal during life-threatening stress. Due to lack of data, the results cannot confirm if the phenotype described in multiple organ failure was associated with cell hypoxia, as there was inadequate tissue remaining to answer this question, once the bioenergetic, metabolic and redox pathways had been characterised. The study cannot show that cellular adaptation to hypoxia occurs in multiple organ failure. Interpretation of the observed differences in the critically ill phenotype (in comparison to reference subjects) and the survivor phenotype (in comparison to non survivors) must be made with caution. The definitiveness of these phenotypes is limited by the fact that this is a single study, in a small group of highly heterogenous patients, with a high attrition rate, which increases the risk of type II error. There was a high potential for confounding: although no relationship was demonstrated between the bioenergetic changes and nutritional intake or medications, it is impossible to rule out that the combination of differences between the reference cohort undergoing surgery and organ failure cohort,

apart from acute organ failure, may have contributed to some or all aspects of the consistent pattern of differences between the groups. The multiple statistical tests and correlations tested within this dataset increases the risk of a type I error. Due to all these reasons, ultimately this data set can thus only act as a spring board, which raises many important questions to be definitively answered in future studies.

7.4. Unanswered questions and future work

This thesis identified a signature of bioenergetic, metabolic and redox modifications in critically ill skeletal muscle, which bore many similarities to the universal cellular response to hypoxia. However, further work is required to confirm whether or not the skeletal muscle modifications observed in critical illness are actually associated with tissue hypoxia and to explore the mechanism by which they may be triggered. The cell phenotype observed in this thesis call for further exploration of the potential role of the HIF pathway, and in particular, the expression and activity of one the HIF downstream targets, PPARα; the master regulator of fat metabolism; and the expression and activation of UCPs and respiratory complex I. Genetic variation in HIF subunits and downstream targets, including PPAR genotypes have been linked to human hypoxia adaptation in high altitude populations (68, 249). Mapping out the potential relationship between genotype, biological phenotype and clinical outcomes could inform the prediction of which patients are at greatest risk from multiple organ failure and enable the development of personalised approaches to support the expression of a survival phenotype.

This thesis also provided evidence that a plasma profile of increased lipid peroxidation, antioxidant capacity and total nitroso species was a hallmark for failure to compensate for acute life-threatening stress. High plasma concentrations of lipid peroxides, total antioxidant

capacity and total nitroso species were predictors of poor outcome, but these potential biomarkers require validation in a larger cohort. It is possible that they may provide greater specificity and sensitivity in combination. Undertaking larger studies, which focus on specific subsets of critically ill patients (for example, sepsis, trauma, liver failure, cardiogenic shock), may allow us to determine whether the non survivor profile observed in this cohort truly represents universal features of poor outcome in critical illness.

Describing mechanisms in critically unwell human patients involving this highly complex network will continue to pose a challenge (343). As an observational study, this work could not provide insight on whether the observed differences in survivor and non survivors represent a cause or effect. For example, it is not yet clear to what extent the observed plasma measures reflected (1) redox status in specific tissues, (2) compensation of the plasma compartment in response to redox changes in a cellular compartment, (3) adaptive signalling, (4) harmful consequences of pathological perturbation, either from the disease or its treatment. Discriminating between redox signalling and indiscriminate oxidative stress may ultimately depend on the ability to measure redox changes *in vivo*, ideally in response to a pre-determined, controlled, dynamic stress. Greater understanding of the interaction between cellular and plasma compartments will require synchronous measures spanning subcellular, cellular and plasma compartments.

The first step may be to map, with greater granularity, the temporal changes during deterioration into critical illness. This is generally difficult to predict, but one possibility would be study a cohort of high risk surgical patients (elderly, with multiple co-morbidities, undergoing major surgery), with a significant risk of post operative organ dysfunction. By undertaking frequent measures of plasma redox status, before, during and after their surgical

insult, and possible ICU stay, the time course of redox changes and how they herald or contribute to the development of critical illness may be better understood. Ideally, plasma measures would be combined with contemporaneous measures of redox status in other tissues, such as muscle, skin or blood cells.

7.5. Conclusion

The difference between life and death may lie in the complex co-ordination of cell energy production, and interrelated pathways of substrate metabolism and redox status, and their modification to compensate for life-threatening stress. The work in this thesis revealed novel aspects of cellular bioenergetic, metabolic and redox responses to critical illness, in real patients, which may contribute to survival. These findings have the potential to change the focus of life-support strategies in multiple organ failure, away from global oxygen delivery, towards manipulation of relevant intracellular processes. When the fundamental processes underlying survival in multiple organ failure have been mapped out, we may be able to offer a more sophisticated and personalised approach to supporting energy production and cell integrity in critically ill patients.

8. Peer reviewed manuscripts related to this submission

8.1. Primary manuscripts

McKenna H, O'Brien K, Fernandez B, Minnion M, Tod A, McNally B, West J, Griffin J, Grocott M, Mythen M, Feelisch M, Murray A, Martin D. An emergent phenotype of resilience in life-threatening human illness. *In submission to Cell Metabolism, April 2020.*

Morkane H, **McKenna H**, Cumpstey A, Oldman A, Grocott M, Martin D, Pan London Perioperative Audit and Research Network (PLAN). Intraoperative oxygenation in adult patients undergoing surgery (iOPS): a retrospective observational study across 29 UK hospitals. Perioperative Medicine (2018). Vol 7 (1), 17.

8.2. Review articles

McKenna H and Murray AJ. Reconsidering critical illness as an uncharacterised acquired mitochondrial disorder. Journal of the Intensive Care Society; published online October 2019.

McKenna H and Martin DS. High altitude research and its relevance to critical illness. ICU Management & Practice (2017): Vol 17 (2).

Martin D, **McKenna H** and Livina V. The human physiological impact of global deoxygenation. The Journal of Physiological Sciences (2017). Vol 67 (1) 97-106.

McKenna H and Martin D. Surviving physiological stress: can insights into human adaptation to austere environments be applied to the critical care unit? Trends in anaesthesia and Critical Care (2016). Vol 11. p 6-13.

Martin D, **McKenna H** and Morkane C. Intraoperative hyperoxaemia: an unnecessary evil? Anaesthesia and Analgesia. Vol 123 (6). p 1643.

8.3. Published Abstracts

McKenna H, Murray AJ and Martin DS. Direct measurement of intracellular mitochondrial respiration in skeletal muscle taken from critically ill patients demonstrates functional alterations with potential adaptive implications. Journal of the Intensive Care Society. Vol 20 (2). State of the Art 2018 Abstracts Supplement p 252. 2019.

Stevens J, **McKenna H**, Gurusamy K, Jell G, Guliyeva M, Martin D. Perioperative antioxidants for adults undergoing elective non-cardiac surgery. Cochrane Database of Systematic Reviews. Nov 2018.

Stevens J, **McKenna H**, Murray AJ, Jell G, Guliyeva M, Martin D. Effects of major hepato-pancreatico-biliary surgery and general anaesthesia on skeletal muscle mitochondrial respiration: a pilot study. British Journal of Anaesthesia, Vol 121 (2) p 28. 2018.

Appendix 1: Media for assays

Biopsy preservation medium (BIOPS)

The following was dissolved in distilled water to give the final concentration stated:

CaK_2EGTA	2.77 mM
K_2EGTA	7.23 mM
$MgCl_2.6H20$	6.56 mM
Taurine	20 mM
Phosphocreatine	15 mM
Dithiothreitol	0.5 mM
MES	50 mM
Na_2ATP	5.77 mM

The pH of the medium was altered to 7.10 with dropwise addition of KOH. The medium was filtered, divided into 30 ml aliquots and stored at -40 °C until use to prevent bacterial growth.

Mitochondrial respiration medium (MIRO5)

The following was dissolved in distilled water to give the final concentration stated:

EGTA	0.5 mM
$MgCl_2.6H20$	3 mM
K-lactobionate	60 mM
Taurine	20 mM
KH_2PO4	10 mM
HEPES	20 mM

Sucrose	110 mM
Defatted	BSA 1g/L

The pH of the medium was altered to 7.40 with dropwise addition of HCl and/or KOH. The medium was filtered, divided into 30 m aliquots and stored at -40 °C until use.

Media for enzyme activity assays

Process/Assay	Solution	Compound	Concentration	Amount added	pH	Code	Storage
Tissue homogenisation	Homogenisation buffer	HEPES EDTA Triton X-100 dH2O	20mM 1 mM 0.1%	238mg 18.6mg 50µl 100ml	7.2 (10N KOH)	Sigma H3375 Sigma E5134	4°C
Citrate synthase	Citrate synthase assay buffer	Tris Base DTNB (added on experiment day)	20 mM	242.3mg 1mg/25ml	8.0 (10N HCL)	Fisher BP152-1	4°C for
	TEA-HCL buffer	Triethanolamine EDTA dH2O	0.5M 5mM	242.3mg 50ml	8.0 (10N HCL)	Sigma 90279 Sigma ES134	4°C for
	Oxaloacetate	Oxaloacetate 0.5M TEA-HCl buffer dH2O	10mM 0.1M	6.6mg 1ml 4ml		Sigma 4126	Make fresh
	Acetyl CoA	Acetyl CoA dH2O	12mM	9.7mg 1ml		Sigma A2056	200µl aliquots at -20°C
HADH	HADH assay buffer	Imidazole Triton X-100 dH2O	50Mm 0.1%	170.2mg 50µL 50ml	7.4 (10N HCL)	Fluka S6750	4°C for
	NADH	NADH dH_2O	15mM	10.64mg 1ml		Sigma N8129	Make fresh
	Acetoacetyl CoA	Acetoacetyl CoA dH_2O	10mM	25mg 2.9256ml		Sigma A1625	200µl aliquots at -20°C

Final buffer for assay

Assay	Compound	Concentration
Citrate synthase	Tris-Base	20 mM
	DTNB	0.1mM
	Acetyl CoA	0.3 mM
	Oxaloacetate	0.5 mM
HADH	Imidazole	50 mM
	NADH	0.15 mM
	Triton X-100	0.1%
	Acetoacetyl CoA	0.1 mM

Appendix 2. Detected analytes in mass spectrometry

HILIC metabolites

ANALYTE	IONIZATION MODE	PARENT ION (m/z)	PRODUCT ION (m/z)	RETENTION TIME (min)
Pyr	neg	87.0	43.0	0.47
cAMP	pos	330.1	136.0	0.56
MeCyt	pos	126.1	109.1	0.65
Glu IS	pos	154.1	89.0	1.00
Glu IS	neg	152.1	134.1	1.00
ACoA	pos	810.1	303.2	1.44
F6P	neg	259.0	97.0	1.68
ADP	pos	428.0	136.2	1.72
PEP	neg	167.0	79.0	1.74
G6P	neg	259.0	97.0	2.04
UDP	pos	405.0	97.0	2.00
CDP	pos	404.0	112.1	2.24
ATP	pos	508.0	136.2	2.32
GDP	pos	444.0	152.0	2.33
UTP	neg	483.0	159.0	2.56
FBP	neg	339.0	97.1	2.68
CTP	pos	484.0	112.2	2.69
GTP	pos	524.0	152.1	2.74

Aqueous phase metabolites

ANALYTE	IONISATION MODE	PARENT ION (m/z)	PRODUCT ION (m/z)	RETENTION TIME (min)
Oxal	neg	131	87.083	0.73
Orn	pos	133.2	70.167	0.76
Asn	pos	133.1	116.048	0.77
Lys	pos	147.1	84.168	0.77
Gly	pos	76.1	76.099	0.85
Ser	pos	106.075	60.119	0.85
Arg	pos	175.15	70.199	0.86
Carn	pos	227.25	110.199	0.86
His	pos	156.1	110. 149	0.86
Taur	pos	126.1	44.099	0.86
Asp	pos	134.175	74.174	0.87
Ala	pos	90.1	44.274	0.88
Gln	pos	147.1	84.168	0.88
PrOH	pos	132.025	86.199	0.88
Ribu5P	neg	229	97.099	0.88
Thr	pos	120.1	74.124	0.88
C-C	pos	241.05	74.151	0.89
MeHis	pos	170.2	95.159	0.89
2PG/3PG	neg	185	97.064	0.9
Ans	pos	241.15	170.099	0.9
Glu	pos	148	84.149	0.9
GluIS	neg	152.1	134.101	0.9
GluIS	pos	154.1	89.093	0.9
Citl	pos	176.15	159.085	0.93
MetSO	pos	166	149.108	0.93
Bet	pos	118.1	58.224	0.98
Ch	pos	104.1	60.099	0.98
CDP	pos	404	112.131	0.99
DHAP	neg	169	97.142	0.99
PCr	neg	210	79.027	1
Pro	pos	115.975	10.174	1.01
SAM	pos	399.1	250.146	1.04
CDP-ch	pos	489.1	184.11	1.05
Sar	pos	90.1	40.274	1.05
AAA	pos	162.124	116.149	1.06
Crn	pos	114.1	86.14	1.08
AIBA	pos	104.05	85.974	1.09
Glucosamine6P	neg	258	97.099	1.1
UDP-glcNAC	neg	606.1	158.999	1.1
Pyr	neg	87	42.999	1.17
ADP	pos	428	136.173	1.21
Mal	neg	133	115.08	1.26
Icit	neg	191	110.999	1.31
Val	pos	118.1	72.199	1.34
UMP	pos	325	97.178	1.38
AKG	neg	145	101.122	1.49
CMP	pos	324.1	112.193	1.49
Met	pos	150.05	61.159	1.67
AMP	pos	248.1	136.122	1.78
Cyd	pos	244.1	112.124	1.8
GSH	pos	308.1	233.103	1.84
NADP	neg	742.1	408.122	1.93
GMP	pos	364.1	152.196	2.02

Cit	neg	191	110.999	2.14
Fum	neg	115	71.171	2.39
Suc	neg	117	72.999	2.67
Ile	pos	132.025	86.199	2.7
Aco	neg	173.05	85.128	2.75
Leu	pos	132.024	85.199	3.09
Urd	pos	245.1	112.916	3.19
NAD	pos	664.1	136.236	3.43
GSSG	pos	613.2	355.16	3.66
Guas	pos	248.1	152.101	3.66
SAH	pos	385.1	136.131	3.66
Tyr	pos	182.075	136.124	3.66
TyrOH	pos	198.1	152.099	3.66
Phe	pos	166.1	120.149	3.76
FAD	pos	786.2	348.152	3.77
Ad	pos	136.1	119.191	3.82
Trp	pos	205.2	188.092	3.92

Acyl carnitine metabolites

ANALYTE	PRECURSOR ION (m/z)	RETENTION TIME (min)	ANALYTE	PRECURSOR ION (m/z)	RETENTION TIME (min)
Carnitine d9	227.2	0.32	C12:1	398.3	2.59
Carnitine	218.2	0.37	C16:1-OH	470.4	2.69
C2	260.2	0.52	C12	400.3	2.73
C2 d3	260.2	0.54	C6-DC	402.3	2.73
C5-OH	318.2	0.54	C14:2	424.3	2.78
C3 d3	263.2	0.74	C16-OH	472.4	2.90
C3	274.2	0.77	C18:1-OH	498.4	2.90
C4	288.2	1.03	C14:1	426.4	3.00
C4 d3	291.2	1.03	C16:2	452.4	3.00
C5:1	300.2	1.13	C18:2-OH	496.4	3.00
C5	302.3	1.25	C18-OH	500.4	3.20
C5 d9	311.3	1.25	C14	428.4	3.22
C4-DC	374.3	1.50	C16:1	454.4	3.50
C5-DC	388.3	1.50	C15	442.4	3.70
C8-OH	361.3	1.50	C16	456.4	4.00
C6	316.3	1.58	C18:2	480.4	4.00
C8:1	342.3	1.82	C16_d3	459.4	4.20
C8	344.3	2.00	C20:4	504.4	4.20
C8 d3	347.3	2.02	C18:1	482.4	4.65
C10:2	368.3	2.05	C17	470.4	4.69
C10:1	370.3	2.22	C20:2	508.4	4.94
C10	372.3	2.40	C18	484.4	5.02
C8-DC	430.4	2.40	C20:1	510.4	5.26
C14-OH	444.4	2.54	C20	512.4	5.51

References

1. ICNARC. Key statistics from the Case Mix Programme - adult, general critical care units 1 April 2017 to 31 March 2018. Case Mix Programme. 2017
2. Ridley S, Morris S. Cost effectiveness of adult intensive care in the UK. Anaesthesia. 2007;62:547-554.
3. Parker A, Wyatt R, Ridley S. Intensive care services; a crisis of increasing expressed demand. Anaesthesia. 1998;53:113-120.
4. Cannon WB. Organization for physiological homeostasis. Physiological reviews. 1929;IX:399-433.
5. Modell H, Cliff W, Michael J, McFarland J, Wenderoth MP, Wright A. A physiologist's view of homeostasis. Adv Physiol Educ. 2015;39:259-266.
6. Tan SY, Yip A. Hans Selye (1907-1982): Founder of the stress theory. Singapore Med J. 2018;59:170-171.
7. Koolhaas JM, Bartolomucci A, Buwalda B et al. Stress revisited: a critical evaluation of the stress concept. Neurosci Biobehav Rev. 2011;35:1291-1301.
8. Marshall JC. SIRS and MODS: what is their relevance to the science and practice of intensive care. Shock. 2000;14:586-589.
9. Baue AE. Multiple organ failure, multiple organ dysfunction syndrome, and systemic inflammatory response syndrome. Why no magic bullets. Arch Surg. 1997;132:703-707.
10. Moreno R, Vincent JL, Matos R et al. The use of maximum SOFA score to quantify organ dysfunction/failure in intensive care. Results of a prospective, multicentre study. Working Group on Sepsis related Problems of the ESICM. Intensive Care Med. 1999;25:686-696.
11. Lone NI, Walsh TS. Impact of intensive care unit organ failures on mortality during the five years after a critical illness. Am J Respir Crit Care Med. 2012;186:640-647.
12. Schenck EJ, Ma KC, Murthy SB, Choi AMK. Danger Signals in the ICU. Crit Care Med. 2018;46:791-798.
13. Zhang Q, Raoof M, Chen Y et al. Circulating mitochondrial DAMPs cause inflammatory responses to injury. Nature. 2010;464:104-107.
14. Li Y, Yang X, He Y et al. Negative regulation of NLRP3 inflammasome by SIRT1 in vascular endothelial cells. Immunobiology. 2017;222:552-561.
15. Lord JM, Midwinter MJ, Chen YF et al. The systemic immune response to trauma: an overview of pathophysiology and treatment. Lancet. 2014;384:1455-1465.
16. Singer M, Deutschman CS, Seymour CW et al. The Third International Consensus Definitions for Sepsis and Septic Shock (Sepsis-3). JAMA. 2016;315:801-810.
17. Singer M. Critical illness and flat batteries. Crit Care. 2017;21:309.
18. Bar-Or D, Carrick MM, Mains CW, Rael LT, Slone D, Brody EN. Sepsis, oxidative stress, and hypoxia: Are there clues to better treatment. Redox Rep. 2015;20:193-197.
19. Acuña-Castroviejo D, Martín M, Macías M et al. Melatonin, mitochondria, and cellular bioenergetics. J Pineal Res. 2001;30:65-74.

20. Brealey D, Brand M, Hargreaves I et al. Association between mitochondrial dysfunction and severity and outcome of septic shock. Lancet. 2002;360:219-223.
21. Carre JE, Orban JC, Re L et al. Survival in critical illness is associated with early activation of mitochondrial biogenesis. Am J Respir Crit Care Med. 2010;182:745-751.
22. Singer M, Brealey D. Mitochondrial dysfunction in sepsis. Biochem Soc Symp. 1999;66:149-166.
23. Pereira RS, Bertoncheli CM, Adefegha SA et al. Sepsis induced by cecal ligation and perforation (CLP) alters nucleotidase activities in platelets of rats. Microb Pathog. 2017;111:345-351.
24. Balaban RS, Kantor HL, Katz LA, Briggs RW. Relation between work and phosphate metabolite in the in vivo paced mammalian heart. Science. 1986;232:1121-1123.
25. Nsiah-Sefaa A, McKenzie M. Combined defects in oxidative phosphorylation and fatty acid β-oxidation in mitochondrial disease. Biosci Rep. 2016;36
26. Kim JW, Tchernyshyov I, Semenza GL, Dang CV. HIF-1-mediated expression of pyruvate dehydrogenase kinase: a metabolic switch required for cellular adaptation to hypoxia. Cell Metab. 2006;3:177-185.
27. van Hall G, Strømstad M, Rasmussen P et al. Blood lactate is an important energy source for the human brain. J Cereb Blood Flow Metab. 2009;29:1121-1129.
28. Mitchell P. Coupling of phosphorylation to electron and hydrogen transfer by a chemi-osmotic type of mechanism. Nature. 1961;191:144-148.
29. Nobes CD, Brown GC, Olive PN, Brand MD. Non-ohmic proton conductance of the mitochondrial inner membrane in hepatocytes. J Biol Chem. 1990;265:12903-12909.
30. Brand MD. The efficiency and plasticity of mitochondrial energy transduction. Biochem Soc Trans. 2005;33:897-904.
31. Jastroch M, Divakaruni AS, Mookerjee S, Treberg JR, Brand MD. Mitochondrial proton and electron leaks. Essays Biochem. 2010;47:53-67.
32. Bouillaud F, Alves-Guerra MC, Ricquier D. UCPs, at the interface between bioenergetics and metabolism. Biochim Biophys Acta. 2016;1863:2443-2456.
33. Polymeropoulos ET, Oelkrug R, Jastroch M. Mitochondrial Proton Leak Compensates for Reduced Oxidative Power during Frequent Hypothermic Events in a Protoendothermic Mammal, Echinops telfairi. Front Physiol. 2017;8:909.
34. Boveris A, Chance B. The mitochondrial generation of hydrogen peroxide. General properties and effect of hyperbaric oxygen. Biochem J. 1973;134:707-716.
35. Walter EJ, Hanna-Jumma S, Carraretto M, Forni L. The pathophysiological basis and consequences of fever. Crit Care. 2016;20:200.
36. Schumacker PT. Cellular and Molecular Mechanisms of O2 sensing. In: Bartsch ERSAP, editor. Human adaptation to hypoxia. New York: Springer Science and Business Media; 2014. p. 1-18.
37. Vallet B, Tavernier B, Lund N. Assessment of tissue oxygenation in the critically-ill. Eur J Anaesthesiol. 2000;17:221-229.
38. Hotchkiss RS, Karl IE. Reevaluation of the role of cellular hypoxia and bioenergetic failure in sepsis. JAMA. 1992;267:1503-1510.

39. Andersen LW, Mackenhauer J, Roberts JC, Berg KM, Cocchi MN, Donnino MW. Etiology and therapeutic approach to elevated lactate levels. Mayo Clin Proc. 2013;88:1127-1140.
40. Cutts S, Talboys R, Paspula C, Prempeh EM, Fanous R, Ail D. Adult respiratory distress syndrome. Ann R Coll Surg Engl. 2017;99:12-16.
41. Parker MM, Shelhamer JH, Bacharach SL et al. Profound but reversible myocardial depression in patients with septic shock. Ann Intern Med. 1984;100:483-490.
42. Levy B, Fritz C, Tahon E, Jacquot A, Auchet T, Kimmoun A. Vasoplegia treatments: the past, the present, and the future. Crit Care. 2018;22:52.
43. Kara A, Akin S, Ince C. Monitoring microcirculation in critical illness. Curr Opin Crit Care. 2016;22:444-452.
44. den Uil CA, Lagrand WK, van der Ent M et al. Impaired microcirculation predicts poor outcome of patients with acute myocardial infarction complicated by cardiogenic shock. Eur Heart J. 2010;31:3032-3039.
45. Ruokonen E, Takala J, Kari A, Saxén H, Mertsola J, Hansen EJ. Regional blood flow and oxygen transport in septic shock. Crit Care Med. 1993;21:1296-1303.
46. Beerthuizen GI, Goris RJ, Kreuzer FJ. Skeletal muscle Po2 during imminent shock. Arch Emerg Med. 1989;6:172-182.
47. De Backer D, Creteur J, Preiser JC, Dubois MJ, Vincent JL. Microvascular blood flow is altered in patients with sepsis. Am J Respir Crit Care Med. 2002;166:98-104.
48. Bateman RM, Tokunaga C, Kareco T, Dorscheid DR, Walley KR. Myocardial hypoxia-inducible HIF-1alpha, VEGF, and GLUT1 gene expression is associated with microvascular and ICAM-1 heterogeneity during endotoxemia. Am J Physiol Heart Circ Physiol. 2007;293:H448-56.
49. De Backer D, Orbegozo Cortes D, Donadello K, Vincent JL. Pathophysiology of microcirculatory dysfunction and the pathogenesis of septic shock. Virulence. 2014;5:73-79.
50. Ince C. The microcirculation is the motor of sepsis. Crit Care. 2005;9 Suppl 4:S13-9.
51. Kaelin WG, Ratcliffe PJ. Oxygen sensing by metazoans: the central role of the HIF hydroxylase pathway. Mol Cell. 2008;30:393-402.
52. Semenza GL. Hypoxia-inducible factor 1: oxygen homeostasis and disease pathophysiology. Trends Mol Med. 2001;7:345-350.
53. Haase VH. Regulation of erythropoiesis by hypoxia-inducible factors. Blood Rev. 2013;27:41-53.
54. Krock BL, Skuli N, Simon MC. Hypoxia-induced angiogenesis: good and evil. Genes Cancer. 2011;2:1117-1133.
55. Palmer LA, Semenza GL, Stoler MH, Johns RA. Hypoxia induces type II NOS gene expression in pulmonary artery endothelial cells via HIF-1. Am J Physiol. 1998;274:L212-9.
56. Fukuda R, Zhang H, Kim JW, Shimoda L, Dang CV, Semenza GL. HIF-1 regulates cytochrome oxidase subunits to optimize efficiency of respiration in hypoxic cells. Cell. 2007;129:111-122.

57. Papandreou I, Cairns RA, Fontana L, Lim AL, Denko NC. HIF-1 mediates adaptation to hypoxia by actively downregulating mitochondrial oxygen consumption. Cell Metab. 2006;3:187-197.
58. Semenza GL, Roth PH, Fang HM, Wang GL. Transcriptional regulation of genes encoding glycolytic enzymes by hypoxia-inducible factor 1. J Biol Chem. 1994;269:23757-23763.
59. Welch KC, Altshuler DL, Suarez RK. Oxygen consumption rates in hovering hummingbirds reflect substrate-dependent differences in P/O ratios: carbohydrate as a 'premium fuel'. J Exp Biol. 2007;210:2146-2153.
60. Stanley WC, Recchia FA, Lopaschuk GD. Myocardial substrate metabolism in the normal and failing heart. Physiol Rev. 2005;85:1093-1129.
61. Narravula S, Colgan SP. Hypoxia-inducible factor 1-mediated inhibition of peroxisome proliferator-activated receptor alpha expression during hypoxia. J Immunol. 2001;166:7543-7548.
62. Villarroya F, Iglesias R, Giralt M. PPARs in the Control of Uncoupling Proteins Gene Expression. PPAR Res. 2007;2007:74364.
63. Hochachka PW, Buck LT, Doll CJ, Land SC. Unifying theory of hypoxia tolerance: molecular/metabolic defense and rescue mechanisms for surviving oxygen lack. Proc Natl Acad Sci U S A. 1996;93:9493-9498.
64. Zhang H, Bosch-Marce M, Shimoda LA et al. Mitochondrial autophagy is an HIF-1-dependent adaptive metabolic response to hypoxia. J Biol Chem. 2008;283:10892-10903.
65. Semenza GL. Hypoxia-inducible factors in physiology and medicine. Cell. 2012;148:399-408.
66. Formenti F, Constantin-Teodosiu D, Emmanuel Y et al. Regulation of human metabolism by hypoxia-inducible factor. Proc Natl Acad Sci U S A. 2010;107:12722-12727.
67. Levett DZ, Viganò A, Capitanio D et al. Changes in muscle proteomics in the course of the Caudwell Research Expedition to Mt. Everest. Proteomics. 2015;15:160-171.
68. Horscroft JA, Kotwica AO, Laner V et al. Metabolic basis to Sherpa altitude adaptation. Proc Natl Acad Sci U S A. 2017;114:6382-6387.
69. Levett DZ, Radford EJ, Menassa DA et al. Acclimatization of skeletal muscle mitochondria to high-altitude hypoxia during an ascent of Everest. FASEB J. 2012;26:1431-1441.
70. Clanton TL. Hypoxia-induced reactive oxygen species formation in skeletal muscle. J Appl Physiol (1985). 2007;102:2379-2388.
71. Jacobs RA, Siebenmann C, Hug M, Toigo M, Meinild AK, Lundby C. Twenty-eight days at 3454-m altitude diminishes respiratory capacity but enhances efficiency in human skeletal muscle mitochondria. FASEB J. 2012;26:5192-5200.
72. Gilbert-Kawai ET, Milledge JS, Grocott MP, Martin DS. King of the mountains: Tibetan and Sherpa physiological adaptations for life at high altitude. Physiology (Bethesda). 2014;29:388-402.

73. Koves TR, Ussher JR, Noland RC et al. Mitochondrial overload and incomplete fatty acid oxidation contribute to skeletal muscle insulin resistance. Cell Metab. 2008;7:45-56.
74. Bigham A, Bauchet M, Pinto D et al. Identifying signatures of natural selection in Tibetan and Andean populations using dense genome scan data. PLoS Genet. 2010;6:e1001116.
75. Wanders RJ, Komen J, Kemp S. Fatty acid omega-oxidation as a rescue pathway for fatty acid oxidation disorders in humans. FEBS J. 2011;278:182-194.
76. Rajabi M, Kassiotis C, Razeghi P, Taegtmeyer H. Return to the fetal gene program protects the stressed heart: a strong hypothesis. Heart Fail Rev. 2007;12:331-343.
77. Breckenridge RA, Piotrowska I, Ng KE et al. Hypoxic regulation of hand1 controls the fetal-neonatal switch in cardiac metabolism. PLoS Biol. 2013;11:e1001666.
78. Neary MT, Ng KE, Ludtmann MH et al. Hypoxia signaling controls postnatal changes in cardiac mitochondrial morphology and function. J Mol Cell Cardiol. 2014;74:340-352.
79. Barger PM, Kelly DP. PPAR signaling in the control of cardiac energy metabolism. Trends Cardiovasc Med. 2000;10:238-245.
80. Olenchock BA, Moslehi J, Baik AH et al. EGLN1 Inhibition and Rerouting of α-Ketoglutarate Suffice for Remote Ischemic Protection. Cell. 2016;164:884-895.
81. Razeghi P, Young ME, Cockrill TC, Frazier OH, Taegtmeyer H. Downregulation of myocardial myocyte enhancer factor 2C and myocyte enhancer factor 2C-regulated gene expression in diabetic patients with nonischemic heart failure. Circulation. 2002;106:407-411.
82. Liao R, Jain M, Cui L et al. Cardiac-specific overexpression of GLUT1 prevents the development of heart failure attributable to pressure overload in mice. Circulation. 2002;106:2125-2131.
83. Pereira RO, Wende AR, Olsen C et al. Inducible overexpression of GLUT1 prevents mitochondrial dysfunction and attenuates structural remodeling in pressure overload but does not prevent left ventricular dysfunction. J Am Heart Assoc. 2013;2:e000301.
84. Cabrera JA, Butterick TA, Long EK et al. Reduced expression of mitochondrial electron transport chain proteins from hibernating hearts relative to ischemic preconditioned hearts in the second window of protection. J Mol Cell Cardiol. 2013;60:90-96.
85. Frangogiannis NG. The inflammatory response in myocardial injury, repair, and remodelling. Nat Rev Cardiol. 2014;11:255-265.
86. Chen Q, Camara AK, Stowe DF, Hoppel CL, Lesnefsky EJ. Modulation of electron transport protects cardiac mitochondria and decreases myocardial injury during ischemia and reperfusion. Am J Physiol Cell Physiol. 2007;292:C137-47.
87. Puthucheary ZA, Astin R, Mcphail MJW et al. Metabolic phenotype of skeletal muscle in early critical illness. Thorax. 2018;73:926-935.
88. Kreymann G, Grosser S, Buggisch P, Gottschall C, Matthaei S, Greten H. Oxygen consumption and resting metabolic rate in sepsis, sepsis syndrome, and septic shock. Crit Care Med. 1993;21:1012-1019.

89. Garrabou G, Morén C, López S et al. The effects of sepsis on mitochondria. J Infect Dis. 2012;205:392-400.
90. Puthucheary ZA, Rawal J, McPhail M et al. Acute skeletal muscle wasting in critical illness. JAMA. 2013;310:1591-1600.
91. Calvo SE, Pagliarini DJ, Mootha VK. Upstream open reading frames cause widespread reduction of protein expression and are polymorphic among humans. Proc Natl Acad Sci U S A. 2009;106:7507-7512.
92. Edwards LM, Murray AJ, Tyler DJ et al. The effect of high-altitude on human skeletal muscle energetics: P-MRS results from the Caudwell Xtreme Everest expedition. PLoS One. 2010;5:e10681.
93. Santolini J WS, Jackson A, Feelisch M. The Redox Architecture of physiological function. Current Opinion in Physiology. 2019;9:34-47.
94. Ballatori N, Krance SM, Notenboom S, Shi S, Tieu K, Hammond CL. Glutathione dysregulation and the etiology and progression of human diseases. Biol Chem. 2009;390:191-214.
95. Giles GI, Nasim MJ, Ali W, Jacob C. The Reactive Sulfur Species Concept: 15 Years On. Antioxidants (Basel). 2017;6
96. Cortese-Krott MM, Koning A, Kuhnle GGC et al. The Reactive Species Interactome: Evolutionary Emergence, Biological Significance, and Opportunities for Redox Metabolomics and Personalized Medicine. Antioxid Redox Signal. 2017;27:684-712.
97. Waypa GB, Smith KA, Schumacker PT. O2 sensing, mitochondria and ROS signaling: The fog is lifting. Mol Aspects Med. 2016;47-48:76-89.
98. Movafagh S, Crook S, Vo K. Regulation of hypoxia-inducible factor-1a by reactive oxygen species: new developments in an old debate. J Cell Biochem. 2015;116:696-703.
99. Chandel NS, McClintock DS, Feliciano CE et al. Reactive oxygen species generated at mitochondrial complex III stabilize hypoxia-inducible factor-1alpha during hypoxia: a mechanism of O2 sensing. J Biol Chem. 2000;275:25130-25138.
100. Janssen-Heininger YM, Mossman BT, Heintz NH et al. Redox-based regulation of signal transduction: principles, pitfalls, and promises. Free Radic Biol Med. 2008;45:1-17.
101. Radi R. Oxygen radicals, nitric oxide, and peroxynitrite: Redox pathways in molecular medicine. Proc Natl Acad Sci U S A. 2018;115:5839-5848.
102. Murphy MP. How mitochondria produce reactive oxygen species. Biochem J. 2009;417:1-13.
103. Kansanen E, Kuosmanen SM, Leinonen H, Levonen AL. The Keap1-Nrf2 pathway: Mechanisms of activation and dysregulation in cancer. Redox Biol. 2013;1:45-49.
104. Thimmulappa RK, Lee H, Rangasamy T et al. Nrf2 is a critical regulator of the innate immune response and survival during experimental sepsis. J Clin Invest. 2006;116:984-995.
105. Vinogradov AD, Grivennikova VG. Oxidation of NADH and ROS production by respiratory complex I. Biochim Biophys Acta. 2016;1857:863-871.

106. Rius-Pérez S, Torres-Cuevas I, Millán I, Ortega ÁL, Pérez S. PGC-1α, Inflammation, and Oxidative Stress: An Integrative View in Metabolism. Oxid Med Cell Longev. 2020;2020:1452696.
107. Handschin C, Spiegelman BM. Peroxisome proliferator-activated receptor gamma coactivator 1 coactivators, energy homeostasis, and metabolism. Endocr Rev. 2006;27:728-735.
108. Lin J, Handschin C, Spiegelman BM. Metabolic control through the PGC-1 family of transcription coactivators. Cell Metab. 2005;1:361-370.
109. Rodgers JT, Lerin C, Gerhart-Hines Z, Puigserver P. Metabolic adaptations through the PGC-1 alpha and SIRT1 pathways. FEBS Lett. 2008;582:46-53.
110. Hatazawa Y, Senoo N, Tadaishi M et al. Metabolomic Analysis of the Skeletal Muscle of Mice Overexpressing PGC-1α. PLoS One. 2015;10:e0129084.
111. Dioum EM, Chen R, Alexander MS et al. Regulation of hypoxia-inducible factor 2alpha signaling by the stress-responsive deacetylase sirtuin 1. Science. 2009;324:1289-1293.
112. O'Hagan KA, Cocchiglia S, Zhdanov AV et al. PGC-1alpha is coupled to HIF-1alpha-dependent gene expression by increasing mitochondrial oxygen consumption in skeletal muscle cells. Proc Natl Acad Sci U S A. 2009;106:2188-2193.
113. ARISE I, ANZICS CTG, Peake SL et al. Goal-directed resuscitation for patients with early septic shock. N Engl J Med. 2014;371:1496-1506.
114. Mouncey PR, Osborn TM, Power GS et al. Trial of early, goal-directed resuscitation for septic shock. N Engl J Med. 2015;372:1301-1311.
115. ProCESS I, Yealy DM, Kellum JA et al. A randomized trial of protocol-based care for early septic shock. N Engl J Med. 2014;370:1683-1693.
116. Hayes MA, Timmins AC, Yau EH, Palazzo M, Hinds CJ, Watson D. Elevation of systemic oxygen delivery in the treatment of critically ill patients. N Engl J Med. 1994;330:1717-1722.
117. Maitland K, George EC, Evans JA et al. Exploring mechanisms of excess mortality with early fluid resuscitation: insights from the FEAST trial. BMC Med. 2013;11:68.
118. Lamontagne F, Richards-Belle A, Thomas K et al. Effect of Reduced Exposure to Vasopressors on 90-Day Mortality in Older Critically Ill Patients With Vasodilatory Hypotension: A Randomized Clinical Trial. JAMA. 2020
119. TARGET Investigators FTANZICSCTG, Chapman M, Peake SL et al. Energy-Dense versus Routine Enteral Nutrition in the Critically Ill. N Engl J Med. 2018;379:1823-1834.
120. Arabi YM, Aldawood AS, Al-Dorzi HM et al. Permissive Underfeeding or Standard Enteral Feeding in High- and Low-Nutritional-Risk Critically Ill Adults. Post Hoc Analysis of the PermiT Trial. Am J Respir Crit Care Med. 2017;195:652-662.
121. Dubin A, Pozo MO, Casabella CA et al. Increasing arterial blood pressure with norepinephrine does not improve microcirculatory blood flow: a prospective study. Crit Care. 2009;13:R92.
122. Crouser ED, Julian MW, Huff JE, Struck J, Cook CH. Carbamoyl phosphate synthase-1: a marker of mitochondrial damage and depletion in the liver during sepsis. Crit Care Med. 2006;34:2439-2446.

123. Akimoto T, Pohnert SC, Li P et al. Exercise stimulates Pgc-1alpha transcription in skeletal muscle through activation of the p38 MAPK pathway. J Biol Chem. 2005;280:19587-19593.
124. Less is more in critical care is supported by evidence-based medicine. [editorial]. Intensive Care Med 2019;45(12):1806.
125. Morkane CM, McKenna H, Cumpstey AF et al. Intraoperative oxygenation in adult patients undergoing surgery (iOPS): a retrospective observational study across 29 UK hospitals. Perioper Med (Lond). 2018;7:17.
126. VijayGanapathy S, Karthikeyan VS, Sreenivas J, Mallya A, Keshavamurthy R. Validation of APACHE II scoring system at 24 hours after admission as a prognostic tool in urosepsis: A prospective observational study. Investig Clin Urol. 2017;58:453-459.
127. Raith EP, Udy AA, Bailey M et al. Prognostic Accuracy of the SOFA Score, SIRS Criteria, and qSOFA Score for In-Hospital Mortality Among Adults With Suspected Infection Admitted to the Intensive Care Unit. JAMA. 2017;317:290-300.
128. Mercer S, Guha A, Ramesh V. The P-POSSUM scoring systems for predicting the mortality of neurosurgical patients undergoing craniotomy: Further validation of usefulness and application across healthcare systems. Indian J Anaesth. 2013;57:587-591.
129. ARDS DTF, Ranieri VM, Rubenfeld GD et al. Acute respiratory distress syndrome: the Berlin Definition. JAMA. 2012;307:2526-2533.
130. Filho RR, Rocha LL, Corrêa TD, Pessoa CM, Colombo G, Assuncao MS. Blood Lactate Levels Cutoff and Mortality Prediction in Sepsis-Time for a Reappraisal? a Retrospective Cohort Study. Shock. 2016;46:480-485.
131. Jiroutková K, Krajčová A, Ziak J et al. Mitochondrial function in skeletal muscle of patients with protracted critical illness and ICU-acquired weakness. Crit Care. 2015;19:448.
132. Galley HF, Davies MJ, Webster NR. Xanthine oxidase activity and free radical generation in patients with sepsis syndrome. Crit Care Med. 1996;24:1649-1653.
133. Patsopoulos NA. A pragmatic view on pragmatic trials. Dialogues Clin Neurosci. 2011;13:217-224.
134. Chistiakov DA, Sobenin IA, Revin VV, Orekhov AN, Bobryshev YV. Mitochondrial aging and age-related dysfunction of mitochondria. Biomed Res Int. 2014;2014:238463.
135. Seo DY, Lee SR, Kim N, Ko KS, Rhee BD, Han J. Age-related changes in skeletal muscle mitochondria: the role of exercise. Integr Med Res. 2016;5:182-186.
136. Gan Z, Fu T, Kelly DP, Vega RB. Skeletal muscle mitochondrial remodeling in exercise and diseases. Cell Res. 2018;28:969-980.
137. Buso A, Comelli M, Picco R et al. Mitochondrial Adaptations in Elderly and Young Men Skeletal Muscle Following 2 Weeks of Bed Rest and Rehabilitation. Front Physiol. 2019;10:474.
138. Cockcroft DW, Gault MH. Prediction of creatinine clearance from serum creatinine. Nephron. 1976;16:31-41.

139. Brown DL, Masselink AJ, Lalla CD. Functional range of creatinine clearance for renal drug dosing: a practical solution to the controversy of which weight to use in the Cockcroft-Gault equation. Ann Pharmacother. 2013;47:1039-1044.
140. Winter MA, Guhr KN, Berg GM. Impact of various body weights and serum creatinine concentrations on the bias and accuracy of the Cockcroft-Gault equation. Pharmacotherapy. 2012;32:604-612.
141. Warnke C, Bollmann T, Ittermann T et al. [Reference values for arterial oxygen content]. Pneumologie. 2014;68:788-792.
142. Chesher D. Evaluating assay precision. Clin Biochem Rev. 2008;29 Suppl 1:S23-6.
143. Ziak J, Krajcova A, Jiroutkova K, Nemcova V, Dzupa V, Duska F. Assessing the function of mitochondria in cytosolic context in human skeletal muscle: adopting high-resolution respirometry to homogenate of needle biopsy tissue samples. Mitochondrion. 2015;21:106-112.
144. Scheiber D, Jelenik T, Zweck E et al. High-resolution respirometry in human endomyocardial biopsies shows reduced ventricular oxidative capacity related to heart failure. Exp Mol Med. 2019;51:1-10.
145. Perrotta S, Roberti D, Bencivenga D et al. Effects of Germline VHL Deficiency on Growth, Metabolism, and Mitochondria. N Engl J Med. 2020;382:835-844.
146. Cumpstey AF, Minnion M, Fernandez BO et al. Pushing arterial-venous plasma biomarkers to new heights: A model for personalised redox metabolomics. Redox Biol. 2019;21:101113.
147. Martin DS, Levett DZ, Bezemer R, Montgomery HE, Grocott MP, Caudwell XERG. The use of skeletal muscle near infrared spectroscopy and a vascular occlusion test at high altitude. High Alt Med Biol. 2013;14:256-262.
148. Djafarzadeh S, Jakob SM. High-resolution Respirometry to Assess Mitochondrial Function in Permeabilized and Intact Cells. J Vis Exp. 2017
149. Pesta D, Gnaiger E. High-resolution respirometry: OXPHOS protocols for human cells and permeabilized fibers from small biopsies of human muscle. Methods Mol Biol. 2012;810:25-58.
150. Vial G, Guigas B. Assessing Mitochondrial Bioenergetics by Respirometry in Cells or Isolated Organelles. Methods Mol Biol. 2018;1732:273-287.
151. Puchowicz MA, Varnes ME, Cohen BH, Friedman NR, Kerr DS, Hoppel CL. Oxidative phosphorylation analysis: assessing the integrated functional activity of human skeletal muscle mitochondria--case studies. Mitochondrion. 2004;4:377-385.
152. Monaco CMF, Hughes MC, Ramos SV et al. Altered mitochondrial bioenergetics and ultrastructure in the skeletal muscle of young adults with type 1 diabetes. Diabetologia. 2018;61:1411-1423.
153. Kuznetsov AV, Veksler V, Gellerich FN, Saks V, Margreiter R, Kunz WS. Analysis of mitochondrial function in situ in permeabilized muscle fibers, tissues and cells. Nat Protoc. 2008;3:965-976.
154. Doerrier Carolina G-PP, Distefano G, Pesta D, Soendergaard SD, Chroeis KM, Gonzalez-Franquesa A, Goodpaster BH, Coen P, Larsen S, Gnaiger E, Garcia-Roves PM. Inter-laboratory harmonization of respiratory protocols in permeabilized human muscle fibers

. MitoFIt Preprint Arch. 2019;MiP/MitoEAGLE School Coimbra
155. Chabi B OM, Gama-Perez P, Dahdah N, Lemieux H, Holody CD, Carpenter RG, Tepp K, Puurand M, Kaambre T, Dubouchaud H, Cortade F, Pesta D, Calabria E, Casado M, Fernandez-Ortiz M, Acuña-Castroviejo D, Villena JA, Grefte S, Keijer J, O'Brien K, Sowton A, Murray AJ, Campbell MD, Marcinek DJ, Nollet E, Wüst R, Dayanidhi S, Gnaiger E, Doerrier C, Garcia-Roves PM. Generating reference values on mitochondrial respiration in permeabilized muscle fibers
. MitoFit Preprint Arch. 2019;MitoEAGLE Belgrade
156. Gnaiger E, Boushel R, Søndergaard H et al. Mitochondrial coupling and capacity of oxidative phosphorylation in skeletal muscle of Inuit and Caucasians in the arctic winter. Scand J Med Sci Sports. 2015;25 Suppl 4:126-134.
157. Sheafor BA. Metabolic enzyme activities across an altitudinal gradient: an examination of pikas (genus Ochotona). J Exp Biol. 2003;206:1241-1249.
158. Holloszy JO, Oscai LB, Don IJ, Molé PA. Mitochondrial citric acid cycle and related enzymes: adaptive response to exercise. Biochem Biophys Res Commun. 1970;40:1368-1373.
159. Renner K, Amberger A, Konwalinka G, Kofler R, Gnaiger E. Changes of mitochondrial respiration, mitochondrial content and cell size after induction of apoptosis in leukemia cells. Biochim Biophys Acta. 2003;1642:115-123.
160. Pesta D, Hoppel F, Macek C et al. Similar qualitative and quantitative changes of mitochondrial respiration following strength and endurance training in normoxia and hypoxia in sedentary humans. Am J Physiol Regul Integr Comp Physiol. 2011;301:R1078-87.
161. Lemieux H, Semsroth S, Antretter H, Höfer D, Gnaiger E. Mitochondrial respiratory control and early defects of oxidative phosphorylation in the failing human heart. Int J Biochem Cell Biol. 2011;43:1729-1738.
162. Marin-Garcia J, Ananthakrishnan R, Goldenthal MJ. Human mitochondrial function during cardiac growth and development. Mol Cell Biochem. 1998;179:21-26.
163. Kuznetsov AV, Strobl D, Ruttmann E, Königsrainer A, Margreiter R, Gnaiger E. Evaluation of mitochondrial respiratory function in small biopsies of liver. Anal Biochem. 2002;305:186-194.
164. Hutter E, Renner K, Pfister G, Stöckl P, Jansen-Dürr P, Gnaiger E. Senescence-associated changes in respiration and oxidative phosphorylation in primary human fibroblasts. Biochem J. 2004;380:919-928.
165. Wakil SJ, Grenn D, Mii S, Mahler HR. Studies on the fatty acid oxidizing system of animal tissues. VI. beta-Hydroxyacyl coenzyme A dehydrogenase. J Biol Chem. 1954;207:631-638.
166. Houle-Leroy P, Garland T, Swallow JG, Guderley H. Effects of voluntary activity and genetic selection on muscle metabolic capacities in house mice Mus domesticus. J Appl Physiol (1985). 2000;89:1608-1616.
167. Thébault MT, Raffin JP, Picado AM, Mendonça E, Skorkowski EF, Le Gal Y. Coordinated changes of adenylate energy charge and ATP/ADP: use in ecotoxicological studies. Ecotoxicol Environ Saf. 2000;46:23-28.

168. Murgia A, Hinz C, Liggi S et al. Italian cohort of patients affected by inflammatory bowel disease is characterised by variation in glycerophospholipid, free fatty acids and amino acid levels. Metabolomics. 2018;14:140.
169. West JA, Beqqali A, Ament Z et al. A targeted metabolomics assay for cardiac metabolism and demonstration using a mouse model of dilated cardiomyopathy. Metabolomics. 2016;12:59.
170. Folch J, Lees M, Sloane Stanley GH. A simple method for the isolation and purification of total lipides from animal tissues. J Biol Chem. 1957;226:497-509.
171. Benzie IF, Strain JJ. The ferric reducing ability of plasma (FRAP) as a measure of "antioxidant power": the FRAP assay. Anal Biochem. 1996;239:70-76.
172. Lefèvre G, Beljean-Leymarie M, Beyerle F et al. [Evaluation of lipid peroxidation by measuring thiobarbituric acid reactive substances]. Ann Biol Clin (Paris). 1998;56:305-319.
173. Koliakos GG, Konstas AG, Schlötzer-Schrehardt U et al. 8-Isoprostaglandin F2a and ascorbic acid concentration in the aqueous humour of patients with exfoliation syndrome. Br J Ophthalmol. 2003;87:353-356.
174. Roberts LD, Murray AJ, Menassa D, Ashmore T, Nicholls AW, Griffin JL. The contrasting roles of PPARδ and PPARγ in regulating the metabolic switch between oxidation and storage of fats in white adipose tissue. Genome Biol. 2011;12:R75.
175. Samouilov A, Zweier JL. Development of chemiluminescence-based methods for specific quantitation of nitrosylated thiols. Anal Biochem. 1998;258:322-330.
176. Koning AM, Meijers WC, Pasch A et al. Serum free thiols in chronic heart failure. Pharmacol Res. 2016;111:452-458.
177. Pareznik R, Knezevic R, Voga G, Podbregar M. Changes in muscle tissue oxygenation during stagnant ischemia in septic patients. Intensive Care Med. 2006;32:87-92.
178. Creteur J, Carollo T, Soldati G, Buchele G, De Backer D, Vincent JL. The prognostic value of muscle StO2 in septic patients. Intensive Care Med. 2007;33:1549-1556.
179. Miura H, McCulley, Chance B. application of multiple NIRS imaging device to the exercising muscle metabolism. Spectroscopy. 2003;17:549-558.
180. Mancini DM, Bolinger L, Li H, Kendrick K, Chance B, Wilson JR. Validation of near-infrared spectroscopy in humans. J Appl Physiol (1985). 1994;77:2740-2747.
181. Ward KR, Ivatury RR, Barbee RW et al. Near infrared spectroscopy for evaluation of the trauma patient: a technology review. Resuscitation. 2006;68:27-44.
182. Boushel R, Langberg H, Olesen J, Gonzales-Alonzo J, Bülow J, Kjaer M. Monitoring tissue oxygen availability with near infrared spectroscopy (NIRS) in health and disease. Scand J Med Sci Sports. 2001;11:213-222.
183. Neto AS, Pereira VG, Manetta JA, Espósito DC, Schultz MJ. Association between static and dynamic thenar near-infrared spectroscopy and mortality in patients with sepsis: a systematic review and meta-analysis. J Trauma Acute Care Surg. 2014;76:226-233.
184. Shapiro NI, Arnold R, Sherwin R et al. The association of near-infrared spectroscopy-derived tissue oxygenation measurements with sepsis syndromes, organ dysfunction and mortality in emergency department patients with sepsis. Crit Care. 2011;15:R223.

185. Cohn SM, Nathens AB, Moore FA et al. Tissue oxygen saturation predicts the development of organ dysfunction during traumatic shock resuscitation. J Trauma. 2007;62:44-54; discussion 54.
186. Bazerbashi H, Merriman KW, Toale KM et al. Low tissue oxygen saturation at emergency center triage is predictive of intensive care unit admission. J Crit Care. 2014;29:775-779.
187. Iyegha UP, Conway T, Pokorney K, Mulier KE, Nelson TR, Beilman GJ. Low StO2 measurements in surgical intensive care unit patients is associated with poor outcomes. J Trauma Acute Care Surg. 2014;76:809-816.
188. Lima A, van Bommel J, Jansen TC, Ince C, Bakker J. Low tissue oxygen saturation at the end of early goal-directed therapy is associated with worse outcome in critically ill patients. Crit Care. 2009;13 Suppl 5:S13.
189. Leone M, Blidi S, Antonini F et al. Oxygen tissue saturation is lower in nonsurvivors than in survivors after early resuscitation of septic shock. Anesthesiology. 2009;111:366-371.
190. Myers D, McGraw M, George M, Mulier K, Beilman G. Tissue hemoglobin index: a non-invasive optical measure of total tissue hemoglobin. Crit Care. 2009;13 Suppl 5:S2.
191. De Blasi RA, Ferrari M, Natali A, Conti G, Mega A, Gasparetto A. Noninvasive measurement of forearm blood flow and oxygen consumption by near-infrared spectroscopy. J Appl Physiol (1985). 1994;76:1388-1393.
192. Donati A, Damiani E, Domizi R et al. Near-infrared spectroscopy for assessing tissue oxygenation and microvascular reactivity in critically ill patients: a prospective observational study. Crit Care. 2016;20:311.
193. Skarda DE, Mulier KE, Myers DE, Taylor JH, Beilman GJ. Dynamic near-infrared spectroscopy measurements in patients with severe sepsis. Shock. 2007;27:348-353.
194. Nanas S, Gerovasili V, Dimopoulos S et al. Inotropic agents improve the peripheral microcirculation of patients with end-stage chronic heart failure. J Card Fail. 2008;14:400-406.
195. Kragelj R, Jarm T, Miklavcic D. Reproducibility of parameters of postocclusive reactive hyperemia measured by near infrared spectroscopy and transcutaneous oximetry. Ann Biomed Eng. 2000;28:168-173.
196. Shoemaker WC, Montgomery ES, Kaplan E, Elwyn DH. Physiologic patterns in surviving and nonsurviving shock patients. Use of sequential cardiorespiratory variables in defining criteria for therapeutic goals and early warning of death. Arch Surg. 1973;106:630-636.
197. Wandrag L, Brett SJ, Frost GS, Bountziouka V, Hickson M. Exploration of muscle loss and metabolic state during prolonged critical illness: Implications for intervention. PLoS One. 2019;14:e0224565.
198. Tappy L, Chioléro R. Substrate utilization in sepsis and multiple organ failure. Crit Care Med. 2007;35:S531-4.
199. Wolfe RR. Substrate utilization/insulin resistance in sepsis/trauma. Baillieres Clin Endocrinol Metab. 1997;11:645-657.
200. Brooks GA. Cell-cell and intracellular lactate shuttles. J Physiol. 2009;587:5591-5600.

201. De Jonghe B, Cook D, Sharshar T, Lefaucheur JP, Carlet J, Outin H. Acquired neuromuscular disorders in critically ill patients: a systematic review. Groupe de Reflexion et d'Etude sur les Neuromyopathies En Reanimation. Intensive Care Med. 1998;24:1242-1250.
202. Lodeserto F, Yende S. Understanding skeletal muscle wasting in critically ill patients. Crit Care. 2014;18:617.
203. Fletcher SN, Kennedy DD, Ghosh IR et al. Persistent neuromuscular and neurophysiologic abnormalities in long-term survivors of prolonged critical illness. Crit Care Med. 2003;31:1012-1016.
204. Hermans G, De Jonghe B, Bruyninckx F, Van den Berghe G. Clinical review: Critical illness polyneuropathy and myopathy. Crit Care. 2008;12:238.
205. Fredriksson K, Hammarqvist F, Strigård K et al. Derangements in mitochondrial metabolism in intercostal and leg muscle of critically ill patients with sepsis-induced multiple organ failure. Am J Physiol Endocrinol Metab. 2006;291:E1044-50.
206. Puigserver P, Rhee J, Lin J et al. Cytokine stimulation of energy expenditure through p38 MAP kinase activation of PPARgamma coactivator-1. Mol Cell. 2001;8:971-982.
207. Hammarqvist F, Luo JL, Cotgreave IA, Andersson K, Wernerman J. Skeletal muscle glutathione is depleted in critically ill patients. Crit Care Med. 1997;25:78-84.
208. Takasu O, Gaut JP, Watanabe E et al. Mechanisms of cardiac and renal dysfunction in patients dying of sepsis. Am J Respir Crit Care Med. 2013;187:509-517.
209. Puskarich MA, Kline JA, Watts JA, Shirey K, Hosler J, Jones AE. Early alterations in platelet mitochondrial function are associated with survival and organ failure in patients with septic shock. J Crit Care. 2016;31:63-67.
210. Sjövall F, Morota S, Hansson MJ, Friberg H, Gnaiger E, Elmér E. Temporal increase of platelet mitochondrial respiration is negatively associated with clinical outcome in patients with sepsis. Crit Care. 2010;14:R214.
211. Sjövall F, Morota S, Persson J, Hansson MJ, Elmér E. Patients with sepsis exhibit increased mitochondrial respiratory capacity in peripheral blood immune cells. Crit Care. 2013;17:R152.
212. Belikova I, Lukaszewicz AC, Faivre V, Damoisel C, Singer M, Payen D. Oxygen consumption of human peripheral blood mononuclear cells in severe human sepsis. Crit Care Med. 2007;35:2702-2708.
213. Japiassú AM, Santiago AP, d'Avila JC et al. Bioenergetic failure of human peripheral blood monocytes in patients with septic shock is mediated by reduced F1Fo adenosine-5'-triphosphate synthase activity. Crit Care Med. 2011;39:1056-1063.
214. Jagannathan L, Cuddapah S, Costa M. Oxidative stress under ambient and physiological oxygen tension in tissue culture. Curr Pharmacol Rep. 2016;2:64-72.
215. Wojtczak L, Schönfeld P. Effect of fatty acids on energy coupling processes in mitochondria. Biochim Biophys Acta. 1993;1183:41-57.
216. Katz J, Tayek JA. Gluconeogenesis and the Cori cycle in 12-, 20-, and 40-h-fasted humans. Am J Physiol. 1998;275:E537-42.
217. Huang, Li T, Li X et al. HIF-1-mediated suppression of acyl-CoA dehydrogenases and fatty acid oxidation is critical for cancer progression. Cell Rep. 2014;8:1930-1942.

218. Edul VS, Ince C, Vazquez AR et al. Similar Microcirculatory Alterations in Patients with Normodynamic and Hyperdynamic Septic Shock. Ann Am Thorac Soc. 2016;13:240-247.
219. Mullen AR, Wheaton WW, Jin ES et al. Reductive carboxylation supports growth in tumour cells with defective mitochondria. Nature. 2011;481:385-388.
220. Wu N, Yang M, Gaur U, Xu H, Yao Y, Li D. Alpha-Ketoglutarate: Physiological Functions and Applications. Biomol Ther (Seoul). 2016;24:1-8.
221. Lopaschuk GD, Ussher JR, Folmes CD, Jaswal JS, Stanley WC. Myocardial fatty acid metabolism in health and disease. Physiol Rev. 2010;90:207-258.
222. Morino K, Petersen KF, Shulman GI. Molecular mechanisms of insulin resistance in humans and their potential links with mitochondrial dysfunction. Diabetes. 2006;55 Suppl 2:S9-S15.
223. Hoeks J, Mensink M, Hesselink MK, Ekroos K, Schrauwen P. Long- and medium-chain fatty acids induce insulin resistance to a similar extent in humans despite marked differences in muscle fat accumulation. J Clin Endocrinol Metab. 2012;97:208-216.
224. Wolfe RR, Shaw JH, Durkot MJ. Energy metabolism in trauma and sepsis: the role of fat. Prog Clin Biol Res. 1983;111:89-109.
225. Krogh-Madsen R, Plomgaard P, Akerstrom T, Møller K, Schmitz O, Pedersen BK. Effect of short-term intralipid infusion on the immune response during low-dose endotoxemia in humans. Am J Physiol Endocrinol Metab. 2008;294:E371-9.
226. Smiseth OA, Mjøs OD. Haemodynamic and metabolic consequences of elevated plasma free fatty acids during acute ischaemic left ventricular failure in dogs. Scand J Clin Lab Invest. 1985;45:515-520.
227. Lerin C, Goldfine AB, Boes T et al. Defects in muscle branched-chain amino acid oxidation contribute to impaired lipid metabolism. Mol Metab. 2016;5:926-936.
228. Newgard CB, An J, Bain JR et al. A branched-chain amino acid-related metabolic signature that differentiates obese and lean humans and contributes to insulin resistance. Cell Metab. 2009;9:311-326.
229. Diabetes and branched-chain amino acids: What is the link [editorial]. J Diabetes 2018;10(5):350.
230. Adam-Vizi V, Chinopoulos C. Bioenergetics and the formation of mitochondrial reactive oxygen species. Trends Pharmacol Sci. 2006;27:639-645.
231. Starkov AA, Fiskum G. Regulation of brain mitochondrial H2O2 production by membrane potential and NAD(P)H redox state. J Neurochem. 2003;86:1101-1107.
232. Tello D, Balsa E, Acosta-Iborra B et al. Induction of the mitochondrial NDUFA4L2 protein by HIF-1α decreases oxygen consumption by inhibiting Complex I activity. Cell Metab. 2011;14:768-779.
233. Chauvin C, De Oliveira F, Ronot X, Mousseau M, Leverve X, Fontaine E. Rotenone inhibits the mitochondrial permeability transition-induced cell death in U937 and KB cells. J Biol Chem. 2001;276:41394-41398.
234. Colleoni F, Padmanabhan N, Yung HW et al. Suppression of mitochondrial electron transport chain function in the hypoxic human placenta: a role for miRNA-210 and protein synthesis inhibition. PLoS One. 2013;8:e55194.

235. Hernansanz-Agustín P, Ramos E, Navarro E et al. Mitochondrial complex I deactivation is related to superoxide production in acute hypoxia. Redox Biol. 2017;12:1040-1051.
236. Hernansanz-Agustín P, Izquierdo-Álvarez A, Sánchez-Gómez FJ et al. Acute hypoxia produces a superoxide burst in cells. Free Radic Biol Med. 2014;71:146-156.
237. Alonso de Vega JM, Díaz J, Serrano E, Carbonell LF. Oxidative stress in critically ill patients with systemic inflammatory response syndrome. Crit Care Med. 2002;30:1782-1786.
238. Cowley HC, Bacon PJ, Goode HF, Webster NR, Jones JG, Menon DK. Plasma antioxidant potential in severe sepsis: a comparison of survivors and nonsurvivors. Crit Care Med. 1996;24:1179-1183.
239. Parry SM, El-Ansary D, Cartwright MS et al. Ultrasonography in the intensive care setting can be used to detect changes in the quality and quantity of muscle and is related to muscle strength and function. J Crit Care. 2015;30:1151.e9-14.
240. Miró O, Barrientos A, Alonso JR et al. Effects of general anaesthetic procedures on mitochondrial function of human skeletal muscle. Eur J Clin Pharmacol. 1999;55:35-41.
241. Hoeks J, van Herpen NA, Mensink M et al. Prolonged fasting identifies skeletal muscle mitochondrial dysfunction as consequence rather than cause of human insulin resistance. Diabetes. 2010;59:2117-2125.
242. Perneger TV. What's wrong with Bonferroni adjustments. BMJ. 1998;316:1236-1238.
243. Amrhein V, Korner-Nievergelt F, Roth T. The earth is flat ($p > 0.05$): significance thresholds and the crisis of unreplicable research. PeerJ. 2017;5:e3544.
244. Gonzalez-Freire M, Scalzo P, D'Agostino J et al. Skeletal muscle ex vivo mitochondrial respiration parallels decline in vivo oxidative capacity, cardiorespiratory fitness, and muscle strength: The Baltimore Longitudinal Study of Aging. Aging Cell. 2018;17
245. Larsen S, Lundby AM, Dandanell S et al. Four days of bed rest increases intrinsic mitochondrial respiratory capacity in young healthy males. Physiol Rep. 2018;6:e13793.
246. De Jonghe B, Sharshar T, Lefaucheur JP et al. Paresis acquired in the intensive care unit: a prospective multicenter study. JAMA. 2002;288:2859-2867.
247. De Jonghe B, Bastuji-Garin S, Sharshar T, Outin H, Brochard L. Does ICU-acquired paresis lengthen weaning from mechanical ventilation. Intensive Care Med. 2004;30:1117-1121.
248. Ali NA, O'Brien JM, Hoffmann SP et al. Acquired weakness, handgrip strength, and mortality in critically ill patients. Am J Respir Crit Care Med. 2008;178:261-268.
249. Bigham A, Bauchet M, Pinto D et al. Identifying signatures of natural selection in Tibetan and Andean populations using dense genome scan data. PLoS Genet. 2010;6:e1001116.
250. Bryan NS, Rassaf T, Maloney RE et al. Cellular targets and mechanisms of nitros(yl)ation: an insight into their nature and kinetics in vivo. Proc Natl Acad Sci U S A. 2004;101:4308-4313.

251. Goode HF, Cowley HC, Walker BE, Howdle PD, Webster NR. Decreased antioxidant status and increased lipid peroxidation in patients with septic shock and secondary organ dysfunction. Crit Care Med. 1995;23:646-651.
252. Cross CE, Forte T, Stocker R et al. Oxidative stress and abnormal cholesterol metabolism in patients with adult respiratory distress syndrome. J Lab Clin Med. 1990;115:396-404.
253. Bowler RP, Velsor LW, Duda B et al. Pulmonary edema fluid antioxidants are depressed in acute lung injury. Crit Care Med. 2003;31:2309-2315.
254. Baldwin SR, Simon RH, Grum CM, Ketai LH, Boxer LA, Devall LJ. Oxidant activity in expired breath of patients with adult respiratory distress syndrome. Lancet. 1986;1:11-14.
255. Sznajder JI, Fraiman A, Hall JB et al. Increased hydrogen peroxide in the expired breath of patients with acute hypoxemic respiratory failure. Chest. 1989;96:606-612.
256. Chuang CC, Shiesh SC, Chi CH et al. Serum total antioxidant capacity reflects severity of illness in patients with severe sepsis. Crit Care. 2006;10:R36.
257. Winkler MS, Kluge S, Holzmann M et al. Markers of nitric oxide are associated with sepsis severity: an observational study. Crit Care. 2017;21:189.
258. McClintock DE, Ware LB, Eisner MD et al. Higher urine nitric oxide is associated with improved outcomes in patients with acute lung injury. Am J Respir Crit Care Med. 2007;175:256-262.
259. Adhikari N, Burns KE, Meade MO. Pharmacologic therapies for adults with acute lung injury and acute respiratory distress syndrome. Cochrane Database Syst Rev. 2004CD004477.
260. Szakmany T, Hauser B, Radermacher P. N-acetylcysteine for sepsis and systemic inflammatory response in adults. Cochrane Database Syst Rev. 2012CD006616.
261. Heyland D, Muscedere J, Wischmeyer PE et al. A randomized trial of glutamine and antioxidants in critically ill patients. N Engl J Med. 2013;368:1489-1497.
262. Bjelakovic G, Nikolova D, Gluud LL, Simonetti RG, Gluud C. Mortality in randomized trials of antioxidant supplements for primary and secondary prevention: systematic review and meta-analysis. JAMA. 2007;297:842-857.
263. Jain M, Chandel NS. Rethinking antioxidants in the intensive care unit. Am J Respir Crit Care Med. 2013;188:1283-1285.
264. Broome SC, Woodhead JST, Merry TL. Mitochondria-Targeted Antioxidants and Skeletal Muscle Function. Antioxidants (Basel). 2018;7
265. Galley HF. Bench-to-bedside review: Targeting antioxidants to mitochondria in sepsis. Crit Care. 2010;14:230.
266. Godbout JP, Berg BM, Kelley KW, Johnson RW. alpha-Tocopherol reduces lipopolysaccharide-induced peroxide radical formation and interleukin-6 secretion in primary murine microglia and in brain. J Neuroimmunol. 2004;149:101-109.
267. Ng LT, Ko HJ. Comparative effects of tocotrienol-rich fraction, α-tocopherol and α-tocopheryl acetate on inflammatory mediators and nuclear factor kappa B expression in mouse peritoneal macrophages. Food Chem. 2012;134:920-925.
268. Lowes DA, Webster NR, Murphy MP, Galley HF. Antioxidants that protect mitochondria reduce interleukin-6 and oxidative stress, improve mitochondrial function,

and reduce biochemical markers of organ dysfunction in a rat model of acute sepsis. Br J Anaesth. 2013;110:472-480.
269. Merry TL, Ristow M. Do antioxidant supplements interfere with skeletal muscle adaptation to exercise training. J Physiol. 2016;594:5135-5147.
270. Bellamy MC. Wet, dry or something else. Br J Anaesth. 2006;97:755-757.
271. Martin DS, Grocott MP. Oxygen therapy in critical illness: precise control of arterial oxygenation and permissive hypoxemia. Crit Care Med. 2013;41:423-432.
272. Martin DS, Grocott MP. Oxygen therapy and anaesthesia: too much of a good thing. Anaesthesia. 2015;70:522-527.
273. Kim JM, Kim HG, Son CG. Tissue-Specific Profiling of Oxidative Stress-Associated Transcriptome in a Healthy Mouse Model. Int J Mol Sci. 2018;19
274. van 't Erve TJ, Kadiiska MB, London SJ, Mason RP. Classifying oxidative stress by F_2-isoprostane levels across human diseases: A meta-analysis. Redox Biol. 2017;12:582-599.
275. Loiseaux-Meunier MN, Bedu M, Gentou C, Pepin D, Coudert J, Caillaud D. Oxygen toxicity: simultaneous measure of pentane and malondialdehyde in humans exposed to hyperoxia. Biomed Pharmacother. 2001;55:163-169.
276. Walter MF, Jacob RF, Bjork RE et al. Circulating lipid hydroperoxides predict cardiovascular events in patients with stable coronary artery disease: the PREVENT study. J Am Coll Cardiol. 2008;51:1196-1202.
277. Markesbery WR. Oxidative stress hypothesis in Alzheimer's disease. Free Radic Biol Med. 1997;23:134-147.
278. Reis GS, Augusto VS, Silveira AP et al. Oxidative-stress biomarkers in patients with pulmonary hypertension. Pulm Circ. 2013;3:856-861.
279. Nielsen F, Mikkelsen BB, Nielsen JB, Andersen HR, Grandjean P. Plasma malondialdehyde as biomarker for oxidative stress: reference interval and effects of life-style factors. Clin Chem. 1997;43:1209-1214.
280. Slatter DA, Paul RG, Murray M, Bailey AJ. Reactions of lipid-derived malondialdehyde with collagen. J Biol Chem. 1999;274:19661-19669.
281. Levonen AL, Landar A, Ramachandran A et al. Cellular mechanisms of redox cell signalling: role of cysteine modification in controlling antioxidant defences in response to electrophilic lipid oxidation products. Biochem J. 2004;378:373-382.
282. Lorente L, Martín MM, Abreu-González P et al. Sustained high serum malondialdehyde levels are associated with severity and mortality in septic patients. Crit Care. 2013;17:R290.
283. Motoyama T, Okamoto K, Kukita I, Hamaguchi M, Kinoshita Y, Ogawa H. Possible role of increased oxidant stress in multiple organ failure after systemic inflammatory response syndrome. Crit Care Med. 2003;31:1048-1052.
284. Roberts LJ, Morrow JD. Measurement of F(2)-isoprostanes as an index of oxidative stress in vivo. Free Radic Biol Med. 2000;28:505-513.
285. Morrow JD, Roberts LJ. The isoprostanes: unique bioactive products of lipid peroxidation. Prog Lipid Res. 1997;36:1-21.
286. Montuschi P, Barnes PJ, Roberts LJ. Isoprostanes: markers and mediators of oxidative stress. FASEB J. 2004;18:1791-1800.

287. Ware LB, Fessel JP, May AK, Roberts LJ. Plasma biomarkers of oxidant stress and development of organ failure in severe sepsis. Shock. 2011;36:12-17.
288. Van't Erve TJ, Lih FB, Jelsema C et al. Reinterpreting the best biomarker of oxidative stress: The 8-iso-prostaglandin F2α/prostaglandin F2α ratio shows complex origins of lipid peroxidation biomarkers in animal models. Free Radic Biol Med. 2016;95:65-73.
289. Montuschi P, Corradi M, Ciabattoni G, Nightingale J, Kharitonov SA, Barnes PJ. Increased 8-isoprostane, a marker of oxidative stress, in exhaled condensate of asthma patients. Am J Respir Crit Care Med. 1999;160:216-220.
290. MacKinnon KL, Molnar Z, Lowe D, Watson ID, Shearer E. Measures of total free radical activity in critically ill patients. Clin Biochem. 1999;32:263-268.
291. Turell L, Radi R, Alvarez B. The thiol pool in human plasma: the central contribution of albumin to redox processes. Free Radic Biol Med. 2013;65:244-253.
292. Ghiselli A, Serafini M, Natella F, Scaccini C. Total antioxidant capacity as a tool to assess redox status: critical view and experimental data. Free Radic Biol Med. 2000;29:1106-1114.
293. Alonso de Vega JM, Díaz J, Serrano E, Carbonell LF. Plasma redox status relates to severity in critically ill patients. Crit Care Med. 2000;28:1812-1814.
294. Pascual C, Karzai W, Meier-Hellmann A et al. Total plasma antioxidant capacity is not always decreased in sepsis. Crit Care Med. 1998;26:705-709.
295. Tsai K, Hsu T, Kong C, Lin K, Lu F. Is the endogenous peroxyl-radical scavenging capacity of plasma protective in systemic inflammatory disorders in humans. Free Radic Biol Med. 2000;28:926-933.
296. Doise JM, Aho LS, Quenot JP et al. Plasma antioxidant status in septic critically ill patients: a decrease over time. Fundam Clin Pharmacol. 2008;22:203-209.
297. Cooper CE, Patel RP, Brookes PS, Darley-Usmar VM. Nanotransducers in cellular redox signaling: modification of thiols by reactive oxygen and nitrogen species. Trends Biochem Sci. 2002;27:489-492.
298. Jones DP, Sies H. The Redox Code. Antioxid Redox Signal. 2015;23:734-746.
299. Hansen RE, Roth D, Winther JR. Quantifying the global cellular thiol-disulfide status. Proc Natl Acad Sci U S A. 2009;106:422-427.
300. Go YM, Jones DP. Cysteine/cystine redox signaling in cardiovascular disease. Free Radic Biol Med. 2011;50:495-509.
301. Banne AF, Amiri A, Pero RW. Reduced level of serum thiols in patients with a diagnosis of active disease. J Anti Aging Med. 2003;6:327-334.
302. Patel RS, Ghasemzadeh N, Eapen DJ et al. Novel Biomarker of Oxidative Stress Is Associated With Risk of Death in Patients With Coronary Artery Disease. Circulation. 2016;133:361-369.
303. Frenay AS, de Borst MH, Bachtler M et al. Serum free sulfhydryl status is associated with patient and graft survival in renal transplant recipients. Free Radic Biol Med. 2016;99:345-351.
304. Qian J, Fang J, Zhu Q et al. Serum Protein Thiol Levels in Patients with Hospital-Acquired Acute Kidney Injury. Kidney Blood Press Res. 2015;40:623-629.
305. Ueland PM, Mansoor MA, Guttormsen AB et al. Reduced, oxidized and protein-bound forms of homocysteine and other aminothiols in plasma comprise the redox thiol status-

-a possible element of the extracellular antioxidant defense system. J Nutr. 1996;126:1281S-4S.
306. Hollenberg SM, Cinel I. Bench-to-bedside review: nitric oxide in critical illness--update 2008. Crit Care. 2009;13:218.
307. Trzeciak S, Cinel I, Phillip Dellinger R et al. Resuscitating the microcirculation in sepsis: the central role of nitric oxide, emerging concepts for novel therapies, and challenges for clinical trials. Acad Emerg Med. 2008;15:399-413.
308. Lundberg JO, Weitzberg E, Gladwin MT. The nitrate-nitrite-nitric oxide pathway in physiology and therapeutics. Nat Rev Drug Discov. 2008;7:156-167.
309. Stamler JS, Lamas S, Fang FC. Nitrosylation. the prototypic redox-based signaling mechanism. Cell. 2001;106:675-683.
310. Foster MW, McMahon TJ, Stamler JS. S-nitrosylation in health and disease. Trends Mol Med. 2003;9:160-168.
311. Rassaf T, Feelisch M, Kelm M. Circulating NO pool: assessment of nitrite and nitroso species in blood and tissues. Free Radic Biol Med. 2004;36:413-422.
312. Thomas DD, Ridnour LA, Isenberg JS et al. The chemical biology of nitric oxide: implications in cellular signaling. Free Radic Biol Med. 2008;45:18-31.
313. Pacher P, Beckman JS, Liaudet L. Nitric oxide and peroxynitrite in health and disease. Physiol Rev. 2007;87:315-424.
314. Erusalimsky JD, Moncada S. Nitric oxide and mitochondrial signaling: from physiology to pathophysiology. Arterioscler Thromb Vasc Biol. 2007;27:2524-2531.
315. Clementi E, Brown GC, Feelisch M, Moncada S. Persistent inhibition of cell respiration by nitric oxide: crucial role of S-nitrosylation of mitochondrial complex I and protective action of glutathione. Proc Natl Acad Sci U S A. 1998;95:7631-7636.
316. Heiss C, Lauer T, Dejam A et al. Plasma nitroso compounds are decreased in patients with endothelial dysfunction. J Am Coll Cardiol. 2006;47:573-579.
317. Lauer T, Preik M, Rassaf T et al. Plasma nitrite rather than nitrate reflects regional endothelial nitric oxide synthase activity but lacks intrinsic vasodilator action. Proc Natl Acad Sci U S A. 2001;98:12814-12819.
318. Weitzberg E, Hezel M, Lundberg JO. Nitrate-nitrite-nitric oxide pathway: implications for anesthesiology and intensive care. Anesthesiology. 2010;113:1460-1475.
319. MacKenzie IM, Garrard CS, Young JD. Indices of nitric oxide synthesis and outcome in critically ill patients. Anaesthesia. 2001;56:326-330.
320. Matejovic M, Krouzecky A, Martinkova V et al. Selective inducible nitric oxide synthase inhibition during long-term hyperdynamic porcine bacteremia. Shock. 2004;21:458-465.
321. López A, Lorente JA, Steingrub J et al. Multiple-center, randomized, placebo-controlled, double-blind study of the nitric oxide synthase inhibitor 546C88: effect on survival in patients with septic shock. Crit Care Med. 2004;32:21-30.
322. Investigators, TRIUMPH, Alexander JH et al. Effect of tilarginine acetate in patients with acute myocardial infarction and cardiogenic shock: the TRIUMPH randomized controlled trial. JAMA. 2007;297:1657-1666.
323. Ivanisevic J, Elias D, Deguchi H et al. Arteriovenous Blood Metabolomics: A Readout of Intra-Tissue Metabostasis. Sci Rep. 2015;5:12757.

324. Boekstegers P, Weidenhöfer S, Pilz G, Werdan K. Peripheral oxygen availability within skeletal muscle in sepsis and septic shock: comparison to limited infection and cardiogenic shock. Infection. 1991;19:317-323.
325. Marsch E, Theelen TL, Janssen BJ et al. The effect of prolonged dietary nitrate supplementation on atherosclerosis development. Atherosclerosis. 2016;245:212-221.
326. Gangwar A, Paul S, Ahmad Y, Bhargava K. Competing trends of ROS and RNS-mediated protein modifications during hypoxia as an alternate mechanism of NO benefits. Biochimie. 2018;148:127-138.
327. Anderson EJ, Katunga LA, Willis MS. Mitochondria as a source and target of lipid peroxidation products in healthy and diseased heart. Clin Exp Pharmacol Physiol. 2012;39:179-193.
328. Gomes KM, Campos JC, Bechara LR et al. Aldehyde dehydrogenase 2 activation in heart failure restores mitochondrial function and improves ventricular function and remodelling. Cardiovasc Res. 2014;103:498-508.
329. LoPachin RM, Gavin T. Reactions of electrophiles with nucleophilic thiolate sites: relevance to pathophysiological mechanisms and remediation. Free Radic Res. 2016;50:195-205.
330. Ward NS, Casserly B, Ayala A. The compensatory anti-inflammatory response syndrome (CARS) in critically ill patients. Clin Chest Med. 2008;29:617-25, viii.
331. Cosby K, Partovi KS, Crawford JH et al. Nitrite reduction to nitric oxide by deoxyhemoglobin vasodilates the human circulation. Nat Med. 2003;9:1498-1505.
332. Gladwin MT, Shelhamer JH, Schechter AN et al. Role of circulating nitrite and S-nitrosohemoglobin in the regulation of regional blood flow in humans. Proc Natl Acad Sci U S A. 2000;97:11482-11487.
333. Slatter DA, Bolton CH, Bailey AJ. The importance of lipid-derived malondialdehyde in diabetes mellitus. Diabetologia. 2000;43:550-557.
334. Trevisan M, Browne R, Ram M et al. Correlates of markers of oxidative status in the general population. Am J Epidemiol. 2001;154:348-356.
335. Gulcin İ. Antioxidants and antioxidant methods: an updated overview. Arch Toxicol. 2020;94:651-715.
336. Goode HF, Richardson N, Myers DS, Howdle PD, Walker BE, Webster NR. The effect of anticoagulant choice on apparent total antioxidant capacity using three different methods. Ann Clin Biochem. 1995;32:413-416.
337. Dalle-Donne I, Rossi R, Colombo R, Giustarini D, Milzani A. Biomarkers of oxidative damage in human disease. Clin Chem. 2006;52:601-623.
338. Halliwell B, Whiteman M. Measuring reactive species and oxidative damage in vivo and in cell culture: how should you do it and what do the results mean. Br J Pharmacol. 2004;142:231-255.
339. Tanaka S, Miki T, Sha S, Hirata K, Ishikawa Y, Yokoyama M. Serum levels of thiobarbituric acid-reactive substances are associated with risk of coronary heart disease. J Atheroscler Thromb. 2011;18:584-591.
340. Walter MF, Jacob RF, Jeffers B et al. Serum levels of thiobarbituric acid reactive substances predict cardiovascular events in patients with stable coronary artery disease: a longitudinal analysis of the PREVENT study. J Am Coll Cardiol. 2004;44:1996-2002.

341. Lovell MA, Ehmann WD, Butler SM, Markesbery WR. Elevated thiobarbituric acid-reactive substances and antioxidant enzyme activity in the brain in Alzheimer's disease. Neurology. 1995;45:1594-1601.
342. Hsiao SY, Kung CT, Su CM et al. Impact of oxidative stress on treatment outcomes in adult patients with sepsis: A prospective study. Medicine (Baltimore). 2020;99:e20872.
343. Ghezzi P, Davies K, Delaney A, Floridi L. Theory of signs and statistical approach to big data in assessing the relevance of clinical biomarkers of inflammation and oxidative stress. Proc Natl Acad Sci U S A. 2018;115:2473-2477.
344. De Backer D, Durand A. Monitoring the microcirculation in critically ill patients. Best Pract Res Clin Anaesthesiol. 2014;28:441-451.
345. Østergaard L, Granfeldt A, Secher N et al. Microcirculatory dysfunction and tissue oxygenation in critical illness. Acta Anaesthesiol Scand. 2015;59:1246-1259.
346. Edul VS, Enrico C, Laviolle B, Vazquez AR, Ince C, Dubin A. Quantitative assessment of the microcirculation in healthy volunteers and in patients with septic shock. Crit Care Med. 2012;40:1443-1448.
347. De Backer D, Donadello K, Sakr Y et al. Microcirculatory alterations in patients with severe sepsis: impact of time of assessment and relationship with outcome. Crit Care Med. 2013;41:791-799.
348. Sakr Y, Dubois MJ, De Backer D, Creteur J, Vincent JL. Persistent microcirculatory alterations are associated with organ failure and death in patients with septic shock. Crit Care Med. 2004;32:1825-1831.
349. Massey MJ, Hou PC, Filbin M et al. Microcirculatory perfusion disturbances in septic shock: results from the ProCESS trial. Crit Care. 2018;22:308.
350. Top AP, Ince C, de Meij N, van Dijk M, Tibboel D. Persistent low microcirculatory vessel density in nonsurvivors of sepsis in pediatric intensive care. Crit Care Med. 2011;39:8-13.
351. Doerschug KC, Delsing AS, Schmidt GA, Haynes WG. Impairments in microvascular reactivity are related to organ failure in human sepsis. Am J Physiol Heart Circ Physiol. 2007;293:H1065-71.
352. Marechal X, Favory R, Joulin O et al. Endothelial glycocalyx damage during endotoxemia coincides with microcirculatory dysfunction and vascular oxidative stress. Shock. 2008;29:572-576.
353. Kao R, Xenocostas A, Rui T et al. Erythropoietin improves skeletal muscle microcirculation and tissue bioenergetics in a mouse sepsis model. Crit Care. 2007;11:R58.
354. Kukovetz WR, Holzmann S, Romanin C. Mechanism of vasodilation by nitrates: role of cyclic GMP. Cardiology. 1987;74 Suppl 1:12-19.
355. Palmer RM, Ferrige AG, Moncada S. Nitric oxide release accounts for the biological activity of endothelium-derived relaxing factor. Nature. 1987;327:524-526.
356. Neviere R, Mathieu D, Chagnon JL, Lebleu N, Millien JP, Wattel F. Skeletal muscle microvascular blood flow and oxygen transport in patients with severe sepsis. Am J Respir Crit Care Med. 1996;153:191-195.
357. Gerovasili V DS, Tzanis G, Anastasiou-Nana M, Nanas S. Utilizing the vascular occlusion technique with NIRS technology. Intl J Indust Ergonom. 2010;40:218-222.

358. Lamontagne F, Marshall JC, Adhikari NKJ. Permissive hypotension during shock resuscitation: equipoise in all patients. Intensive Care Med. 2018;44:87-90.
359. Kragelj R, Jarm T, Miklavcic D. Reproducibility of parameters of postocclusive reactive hyperemia measured by near infrared spectroscopy and transcutaneous oximetry. Ann Biomed Eng. 2000;28:168-173.
360. Klijn E, Den Uil CA, Bakker J, Ince C. The heterogeneity of the microcirculation in critical illness. Clin Chest Med. 2008;29:643-54, viii.
361. Dünser MW, Mayr AJ, Tür A et al. Ischemic skin lesions as a complication of continuous vasopressin infusion in catecholamine-resistant vasodilatory shock: incidence and risk factors. Crit Care Med. 2003;31:1394-1398.
362. Schmittinger CA, Torgersen C, Luckner G, Schröder DC, Lorenz I, Dünser MW. Adverse cardiac events during catecholamine vasopressor therapy: a prospective observational study. Intensive Care Med. 2012;38:950-958.
363. PRISM I, Rowan KM, Angus DC et al. Early, Goal-Directed Therapy for Septic Shock - A Patient-Level Meta-Analysis. N Engl J Med. 2017;376:2223-2234.
364. Horscroft JA, Murray AJ. Skeletal muscle energy metabolism in environmental hypoxia: climbing towards consensus. Extrem Physiol Med. 2014;3:19.
365. Belanger AJ, Luo Z, Vincent KA et al. Hypoxia-inducible factor 1 mediates hypoxia-induced cardiomyocyte lipid accumulation by reducing the DNA binding activity of peroxisome proliferator-activated receptor alpha/retinoid X receptor. Biochem Biophys Res Commun. 2007;364:567-572.
366. Bogdanovski DA, DiFazio LT, Bogdanovski AK et al. Hypoxia-inducible-factor-1 in trauma and critical care. J Crit Care. 2017;42:207-212.
367. Joharapurkar AA, Pandya VB, Patel VJ, Desai RC, Jain MR. Prolyl Hydroxylase Inhibitors: A Breakthrough in the Therapy of Anemia Associated with Chronic Diseases. J Med Chem. 2018;61:6964-6982.
368. Hirai K, Furusho H, Hirota K, Sasaki H. Activation of hypoxia-inducible factor 1 attenuates periapical inflammation and bone loss. Int J Oral Sci. 2018;10:12.
369. Kabiven. http://www.kabivenusa.com/pdf/Kabiven_PI.pdf. 2014
370. Cox PJ, Kirk T, Ashmore T et al. Nutritional Ketosis Alters Fuel Preference and Thereby Endurance Performance in Athletes. Cell Metab. 2016;24:256-268.
371. Murray AJ, Montgomery HE. How wasting is saving: weight loss at altitude might result from an evolutionary adaptation. Bioessays. 2014;36:721-729.
372. Detaille D, Pasdois P, Sémont A, Dos Santos P, Diolez P. An old medicine as a new drug to prevent mitochondrial complex I from producing oxygen radicals. PLoS One. 2019;14:e0216385.
373. Palmer E, Post B, Klapaukh R et al. The Association between Supraphysiologic Arterial Oxygen Levels and Mortality in Critically Ill Patients. A Multicenter Observational Cohort Study. Am J Respir Crit Care Med. 2019;200:1373-1380.
374. ICU-ROX IATAANZICSCTG, Mackle D, Bellomo R et al. Conservative Oxygen Therapy during Mechanical Ventilation in the ICU. N Engl J Med. 2020;382:989-998.
375. Acute RDSN, Brower RG, Matthay MA et al. Ventilation with lower tidal volumes as compared with traditional tidal volumes for acute lung injury and the acute respiratory distress syndrome. N Engl J Med. 2000;342:1301-1308.

376. Holst LB, Haase N, Wetterslev J et al. Lower versus higher hemoglobin threshold for transfusion in septic shock. N Engl J Med. 2014;371:1381-1391.
377. Ling Y, Li X, Gao X. Intensive versus conventional glucose control in critically ill patients: a meta-analysis of randomized controlled trials. Eur J Intern Med. 2012;23:564-574.
378. Brand MD. Mitochondrial generation of superoxide and hydrogen peroxide as the source of mitochondrial redox signaling. Free Radic Biol Med. 2016;100:14-31.
379. Quinlan CL, Perevoshchikova IV, Hey-Mogensen M, Orr AL, Brand MD. Sites of reactive oxygen species generation by mitochondria oxidizing different substrates. Redox Biol. 2013;1:304-312.
380. Gyulkhandanyan AV, Pennefather PS. Shift in the localization of sites of hydrogen peroxide production in brain mitochondria by mitochondrial stress. J Neurochem. 2004;90:405-421.
381. Brand MD, Brindle KM, Buckingham JA, Harper JA, Rolfe DF, Stuart JA. The significance and mechanism of mitochondrial proton conductance. Int J Obes Relat Metab Disord. 1999;23 Suppl 6:S4-11.
382. Forkink M, Basit F, Teixeira J, Swarts HG, Koopman WJH, Willems PHGM. Complex I and complex III inhibition specifically increase cytosolic hydrogen peroxide levels without inducing oxidative stress in HEK293 cells. Redox Biol. 2015;6:607-616.
383. Parker N, Vidal-Puig A, Brand MD. Stimulation of mitochondrial proton conductance by hydroxynonenal requires a high membrane potential. Biosci Rep. 2008;28:83-88.
384. Fedorenko A, Lishko PV, Kirichok Y. Mechanism of fatty-acid-dependent UCP1 uncoupling in brown fat mitochondria. Cell. 2012;151:400-413.
385. Lombardi A, Busiello RA, Napolitano L et al. UCP3 translocates lipid hydroperoxide and mediates lipid hydroperoxide-dependent mitochondrial uncoupling. J Biol Chem. 2010;285:16599-16605.
386. Lombardi A, Grasso P, Moreno M et al. Interrelated influence of superoxides and free fatty acids over mitochondrial uncoupling in skeletal muscle. Biochim Biophys Acta. 2008;1777:826-833.
387. Carreras MC, Poderoso JJ. Mitochondrial nitric oxide in the signaling of cell integrated responses. Am J Physiol Cell Physiol. 2007;292:C1569-80.
388. Hauser B, Bracht H, Matejovic M, Radermacher P, Venkatesh B. Nitric oxide synthase inhibition in sepsis? Lessons learned from large-animal studies. Anesth Analg. 2005;101:488-498.
389. Brown GC, Borutaite V. Inhibition of mitochondrial respiratory complex I by nitric oxide, peroxynitrite and S-nitrosothiols. Biochim Biophys Acta. 2004;1658:44-49.
390. Marini JJ. Time-sensitive therapeutics. Crit Care. 2017;21:317.
391. McKenna HT, Reiss IK, Martin DS. The significance of circadian rhythms and dysrhythmias in critical illness. J Intensive Care Soc. 2017;18:121-129.
392. McKenna HT, Murray AJ. Reconsidering critical illness as an uncharacterised acquired mitochondrial disorder. Journal of the Intensive Care Society. 2019